SEDIMENTOLOGY AND TECTONIC IMPLICATIONS OF THE LATE PROTEROZOIC TO EARLY CAMBRIAN CHILHOWEE GROUP IN SOUTHERN AND CENTRAL VIRGINIA

by

Edward Leonard Simpson

Dissertation submitted to the Faculty of the
Virginia Polytechnic Institute and State University
in partial fulfillment of the requirements for the degree of
DOCTOR OF PHILOSOPHY
in
Geology

APPROVED:

K. A. Eriksson

R. K. Bambach

J. F. Read

C. Simpson

Lynn Glover III

June, 1987
Blacksburg, VIrginia

ABSTRACT

Few detailed facies analyses of rift to passive-margin transitions have been undertaken in exhumed orogenic belts. In the central Appalachians, the Chilhowee Group records such an evolution. The Unicoi and basal Hampton Formations record the transition from rifting to initial opening of the Iapetus Ocean. The majority of the Hampton Formation and the overlying Erwin Formation represent an overall regressive sequence punctuated by five progradational packages that accumulated along a passive margin. The rift to passive-margin phases of sedimentation in the central Appalachians reflect a continuum from fault-influenced to thermotectonic subsidence.

Alluvial sediments and intercalated basalts of the lower Unicoi Formation developed in a rift setting. Paleontological data indicate that rifting continued into lower Cambrian time. The upper Unicoi Formation represents the incipient phase of passive-margin sedimentation related to a first-order, sea level rise. Differences in degree of crustal attenuation controlled the distribution of sedimentary environments during transgression. On the most attenuated crust to the east, initial transgressive facies consist of tidal sandwave and sandridge deposits intercalated with proximal and medial braid-plain deposits. As transgression progressed cratonwards onto less attenuated crust, tidal sedimentation was supplanted by tide- and wave-influenced sedimentation characterized by sandwave complexes, tidal inlets and longshore bedforms. Drowning at the top of the Unicoi Formation is indicated by outer-shelf black mudstones. Deepening may have been enhanced by continued movement along listric faults throughout the incipient phase of passive-margin development.

Examination of outcrops of the Hampton and Erwin Formations on different thrust sheets has permitted an across-strike reconstruction of the Early Cambrian Chilhowee shelf in space and time. Progradational packages developed under storm- and fair-weather wave conditions. Coarsening- and thickening-upward sequences on westerly thrust sheets were generated during progradation of shoreface, inner-shelf and outer-shelf environments. Outer-shelf facies predominate on easterly thrust sheets. Intertidal-flat deposits on the most westerly thrust sheet erosively overlie progradational shoreface sediments and developed during transgression in an embayment in which the tidal wave was amplified. More distal transgressive deposits consist of fining- and thinning-upward sequences with glauconitic horizons, and condensed sections in mudstones.

ACKNOWLEDGEMENTS

I would like to thank Dr. Kenneth A. Eriksson for suggesting this project, assisting in all stages of the work and guiding it to completion. Dr. Richard Bambach spent several days in the field discussing interpretations and stratigraphy and acted as a committee member. Dr.'s Lynn Glover III, Fred Read, and Carol Simpson acted as committee members and generously shared their expertise.

Special thanks are extended to for many disscussions concerning science and philosophy, for frank and insightful observations and consultations in the field and for critically reading portions of these papers. gave freely of his drafting expertise, which greatly improved the figures. spent many days in the field generously sharing his knowledge, identifed the trace fossils discussed, and found the hyolithid? within the first two minutes of stepping onto the outcrop. was extremely patient in teaching me to repell in order to work on outcrops of the Unicoi Formation and spent several days hanging off the end of a rope above the James River examining sedimentary structures under less than ideal conditions.

of the University of Tennessee visited many of the outcrops and openly disscussed their findings on the Chilhowee Group in Tennessee. Many graduate and undergraduate students have visted exposures of Chilhowee Group over the past several years and discussed and helped refine my interpetations; they include:

and of the Virginia Division of Mineral Resources freely dicussed

their observations on the Chilhowee Group. aided in measuring stratigraphic sections during the second field season. and the students of the second summer session field camp of 1986 visted several of the outcrops and crtically discussed many of my interpretations.

and gave much needed emotional support and friendship throughout my tenure at Virginia Tech; also reviewed several drafts of paper 1. lent emotional support, helped measure a Unicoi section and visted all section localities.

made my tenure at Virginia Tech very tolerable.

gave emotional support during final stages of completing the dissertation and I am very grateful to her.

I would like to thank for helping at all stages of the photographic work from taking photographs of outcrops to final printing of plates.

Funding for this project was provided by the Appalachian Basin Industrial Associates, the Geological Society of America, and Sigma XI, the Scientific Research Society. Permission was granted by the United States Department of Interior to work in Shenandoah National Park and Jefferson National Forest and on the Blue Ridge Parkway. Park service employees were most gracious and understanding; special note is given to

and and the rest of the permanent and summer staff.

Without support from my family,

, this project would not have been completed and I dedicate this Dissertation to them.

TABLE OF CONTENTS

LIST OF ILLUSTRATIONS

EARLY CAMBRIAN AGE FOR SYNRIFT DEPOSITS OF THE CHILHOWEE GROUP OF SOUTHWESTERN VIRGINIA

ABSTRACT

A newly discovered shelly fossil (hyolithid?) and trace fossil (*Rusophycus*) were found within synrift and post rift sediments of the Chilhowee Group in southwestern Virginia. These specimens indicate that the Chilhowee Group may be entirely of Cambrian age and that rifting in the central and southern Appalachians extended into the Early Cambrian.

INTRODUCTION

The Chilhowee Group has been interpreted as being deposited in late Precambrian to Early Cambrian rift and postrift tectonic settings on the basis of subsidence curves, lithology, and megafossil remains (Bond *et al.*, 1984). Bond *et al.* (1984) stated that the Proto-Atlantic Ocean opened at about 600±15 Ma. Williams *et al.* (1985) proposed that the opening of the Proto-Atlantic was diachronous and that rifting developed in North Carolina at 820 Ma and propagated northward to Newfoundland by 602 Ma. Fichter and Diecchio (1986) derived a stratigraphic model for the opening of the Proto-Atlantic in northern Virginia on the basis of theoretical rift models of Bott (1979) and Kinsman (1975). The Fichter and Diecchio model assigned absolute ages to unfossiliferous formations and determines the time of opening to be 610-630 Ma.

The age of the Chilhowee Group has been poorly established; Cambrian fossils have been reported only from the upper part of the group. The Chilhowee Group has been referred to as entirely Early Cambrian (King, 1949), the upper part Early

Cambrian and the lower part Early Cambrian (?) (Rankin, 1967) or Early Cambrian and late Precambrian (Schwab, 1972; Bond *et al.*, 1984, Fichter and Diecchio, 1986). The lack of fossil remains below the uppermost Chilhowee Group has made the age assignment of the lower part speculative.

In this study, newly discovered trace and body fossils from southern Virginia (Fig. 1) indicate that the Chilhowee Group may be entirely Early Cambrian in age. The Early Cambrian fossils in the synrift and postrift deposits of the central and southern Appalachians extend the upper limit of the rifting event into the earliest Cambrian, as proposed by Bond *et al.* (1984). The final phase of rifting in the southern Appalachians is synchronous with rifting in Newfoundland. Absolute ages proposed by Fichter and Diecchio (1986) for the lower formations of the Chilhowee Group are not substantiated by these discoveries.

STRATIGRAPHY

The Chilhowee Group is subdivided into three formations in southern Virginia; from oldest to youngest they are (1) Unicoi, (2) Hampton, and (3) Erwin (Fig. 2). These units are equivalent to the (1) Weaverton, (2) Harpers, and (3) Antietam Formations (Schwab, 1972) in northern Virginia. Underlying the Chilhowee Group are late Precambrian glacial sediments and volcanics of the Mount Rogers Group (Schwab, 1976). The type of contact between the Mount Rogers and the Chilhowee Groups is uncertain and is interpreted as conformable (Rankin, 1967), unconformable (Stose and Stose, 1957; King and Ferguson, 1960), or structural. The Chilhowee Group is conformably overlain by Shady Dolomite (Schwab, 1972).

Figure 1. Location of fossil occurrences in southern Virginia. Locality is given in Rankin (1967, Stop 1); A is *Rusophycus* locality and B is hyolithid occurrence.

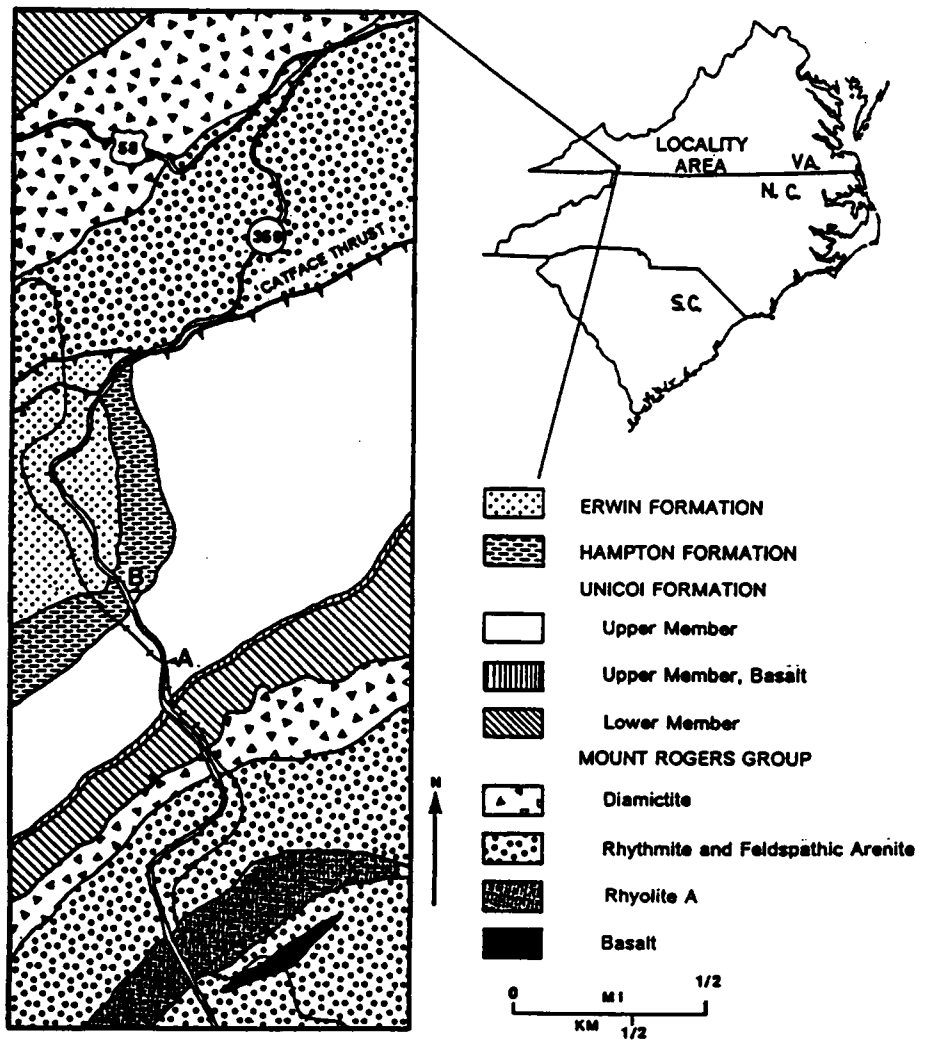
58
36
CATFACE THRUST
B
A
LOCALITY AREA
VA
N. C.
S.C.
N
ERWIN FORMATION
HAMPTON FORMATION
UNICOI FORMATION
Upper Member
Upper Member, Basalt
Lower Member
MOUNT ROGERS GROUP
Diamictite
Rhythmite and Feldspathic Arenite
Rhyolite A
Basalt
0
MI
1/2
KM
1/2

Figure 2. Generalized stratigraphic section of Chilhowee Group on Catface thrust sheet and biostratigraphy. Fossil occurrences were projected into stratigraphic section from other localities (Laurence and Palmer, 1963; Walcott, 1981; Wood and Clendening, 1982; Stose and Stose, 1957). Chronostratigraphic units reflect maximum possible ages.

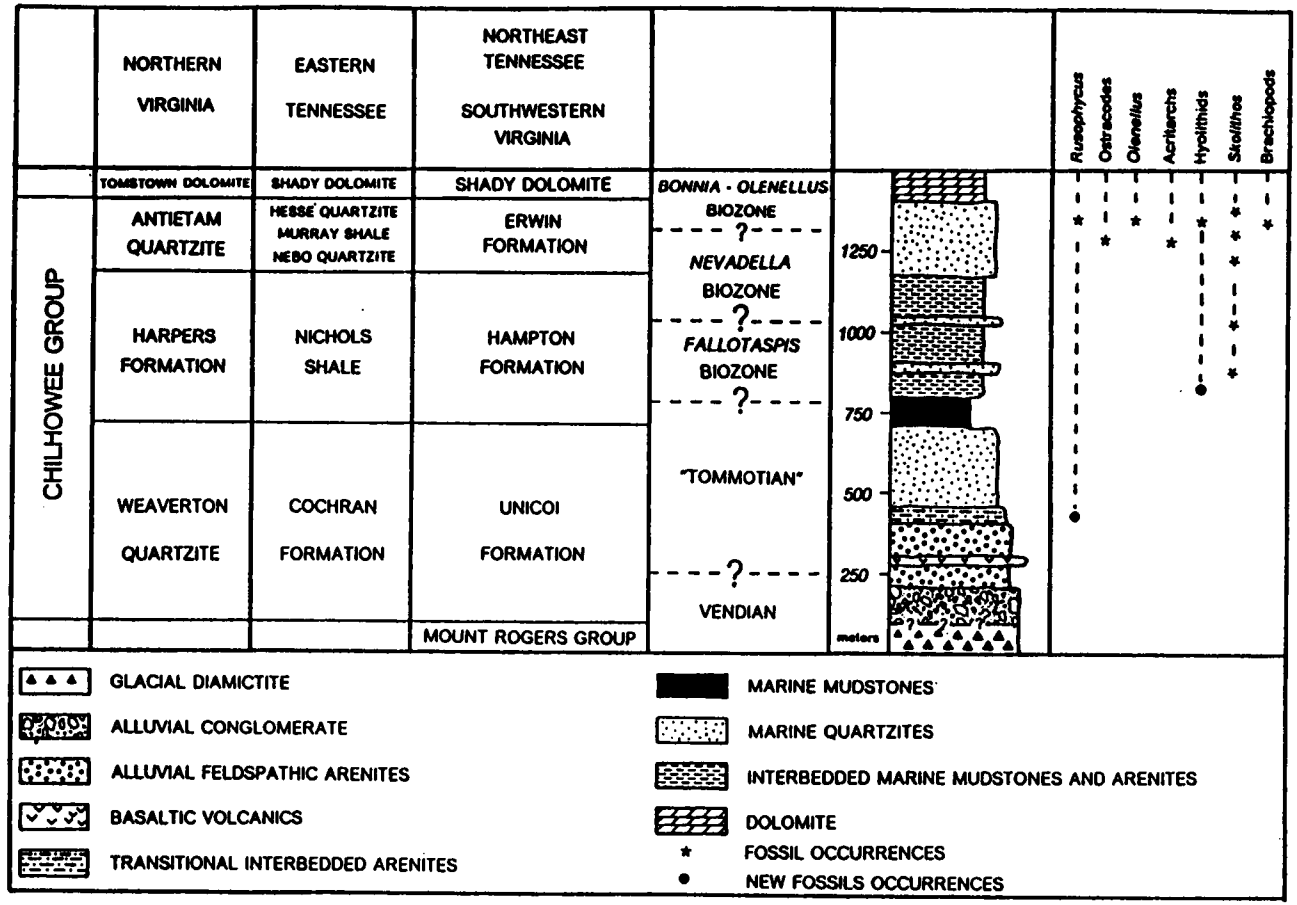
NORTHERN VIRGINIA
EASTERN TENNESSEE
NORTHEAST TENNESSEE
SOUTHWESTERN VIRGINIA
Rusophycus
Ostracodes
Olenellus
Acritarchs
Hyolithids
Stolithos
Brachiopods
CHILHOWEE GROUP
TOMSTOWN DOLOMITE
SHADY DOLOMITE
SHADY DOLOMITE
BONNIA - OLENELLUS BIOZONE
ANTIETAM QUARTZITE
HESSE QUARTZITE
MURRAY SHALE
NEBO QUARTZITE
ERWIN FORMATION
NEVADELLA BIOZONE
HARPERS FORMATION
NICHOLS SHALE
HAMPTON FORMATION
FALLOTASPIS BIOZONE
"TOMMOTIAN"
WEAVERTON QUARTZITE
COCHRAN FORMATION
UNICOI FORMATION
VENDIAN
MOUNT ROGERS GROUP
1250
1000
750
500
250
meters
GLACIAL DIAMICTITE
ALLUVIAL CONGLOMERATE
ALLUVIAL FELDSPATHIC ARENITES
BASALTIC VOLCANICS
TRANSITIONAL INTERBEDDED ARENITES
MARINE MUDSTONES
MARINE QUARTZITES
INTERBEDDED MARINE MUDSTONES AND ARENITES
DOLOMITE
FOSSIL OCCURRENCES
NEW FOSSILS OCCURRENCES

Overall, the Chilhowee is a transgressive to regressive clastic package deposited in nonmarine environments. The Unicoi Formation is subdivided into two members (Rankin, 1967) interpreted by us as (1) a lower member of alluvial quartz-pebble conglomerates and feldspathic arenites and (2) an upper transgressive member of alluvial plain to shelf sediments containing basalts, feldspathic arenites, and quartz arenites. The Hampton Formation is composed of two outer-shelf to nearshore regressive sequences of interbedded muds and arenites (Simpson, in prep). The Erwin Formation is composed of quartz arenites and subordinate mudstones and represents nearshore environments affected by wave and storm processes (Simpson and Eriksson, 1986).

These formations were deposited in sedimentary basins that formed as a result of the opening of the Proto-Atlantic Ocean (Bond *et al.*, 1984). Bond *et al.* (1984) considered the Unicoi Formation to be synrift stage and the Erwin and Hampton Formations to be a basal, postrift clastic wedge.

FOSSIL LOCALITIES AND DESCRIPTIONS

Fossil specimens were collected in southwestern Virginia (Fig. 1) on the Catface thrust sheet within the Hampton (long 81deg. 41 min. 09.9 sec W, lat 36 deg. 38 min. 16.5 sec N) and Unicoi (long 81 deg. 40 min. 03.5 sec. W, lat 36 deg. 38 min. 06.0 sec. N) Formations, between road-log 26.7 mi and Stop 1 on County Road 600 (Rankin, 1967, p. 25).

Hampton Formation

The trace fossil *Planolites* occurs in turbidite beds throughout the formation. A fragment of a shelly fossil (Fig. 3 A, B) was found 20 m below the base of the lowest quartzite member of the Hampton Formation. This specimen is in intercalated parallel-laminated, fine-grained arenite and siltstone within a turbidite bed. The turbidites containing the body fossil form a fining- and thinning-upward cycle interpreted to be the product of storm-induced sedimentation on an inner- to outer-shelf setting (Simpson and Eriksson, 1986).

The shelly fossil is a phosphatic (?) (did not effervesce in dilute HCL), laminated (?), single-walled shell. It is relatively large (8.2 mm long and 3.4 mm in maximum width), cone-shaped, and relatively coarse ribbed (2 to 3 ribs per millimetre at larger end). The specimen is possibly a hyolithid. It is similar in ornamentation, size and shape to the hyolithid *Tuojdochithes* ? *biconvexus* (Cobbold) from the upper Tommotian or early Adtabanian of England (Brasier, 1984).

Unicoi Formation

Rusophycus and *Planolites* were collected 347 m above the base of the Unicoi Formation. They occur in the base of a coarse-grained, trough-cross-bedded, feldspathic arenite. This facies is interpreted as having been deposited in a transitional alluvial to nearshore environment (middle part of the upper member).

The *Rusophycus* specimen is preserved in hyporelief on an arenite bed (Fig. 3, C and D). The heart-shaped morphology typical of *Rusophycus* is present. The left lobe (viewed from the bottom surface) has an additional lobe that slopes upward to the

Figure 3. Lower Cambrian fossils from lower Chilhowee Group. Specimens are whitened with ammonium chloride sublimate. A and B: Shelly fossil (hyolithid?) from lower Hampton Formation; B is drawing of shell showing ribs and cone-shaped outline. C and D: *Rusophycus* specimen from upper Unicoi Formation; C is laterial view of trace showing bilobed nature of burrow, and D is ventral view (hyporelief).

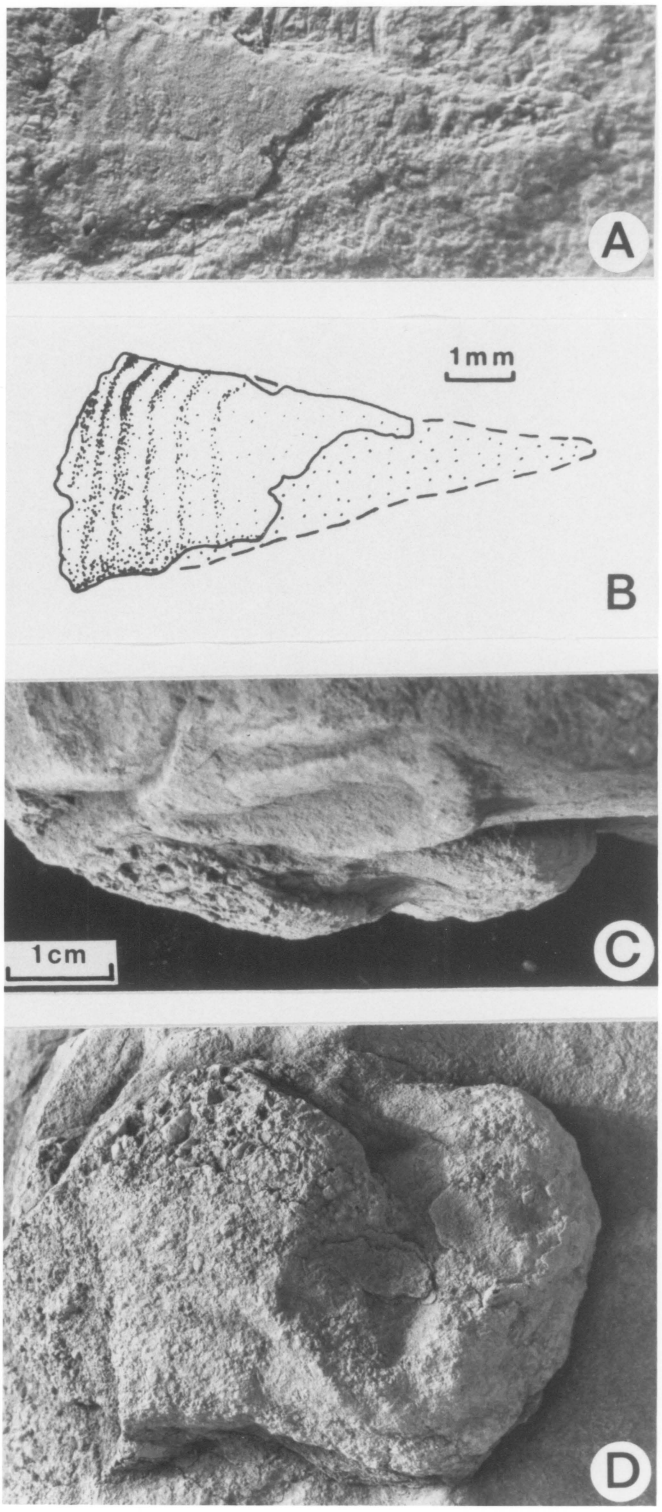
A
1mm
B
1cm
C
D

bedding plane of the bed. The right lobe, in contrast, undercuts the contact between the arenite and the underlying mudstone to form an overlap of 1 to 2 mm.

Rusophycus is regarded as a resting trace (cubichnia) of an arthropod (Hantzchel, 1975). The lobe morphology of the specimen is probably the result of the arthropod initially moving laterally while excavating sediment. While still excavating sediment, the arthropod then moved downward with no lateral movement, whichproduced the equal-lobed, heart-shaped burrow. *Planolites* is associated with the *Rusophycus* specimen.

BIOSTRATIGRAPHY

Figure 2 illustrates the known fossil occurrences in the Chilhowee Group in Tennesseee and Virginia. The only age-diagnostic fossils previously reported are the inarticulate brachiopod *Obolella,* the trilobite *Olenellus* sp., and ostracodes and hyolithids from strata correlative to the Erwin Formation (Walcott, 1981; Stose and Stose, 1957; Laurence and Palmer, 1963). The genus *Olenellus* is diagnostic of the upper Lower Cambrian *Bonnia-Olenellus* Biozone (Fritz, 1972; Palmer, 1981). *Olenellus* ranges up to the Lower/Middle Cambrian boundary (540 Ma) (Palmer, 1983) and may range from 550 (?) to 540 Ma. The assignment of *Olenellus*-bearing to a maximum age of 570 Ma by Fichter and Diecchio (1986) is incorrect. Hyolithids and inarticulate brachiopods are associated with the *Olenellus* specimens (Walcott, 1891; Stose and Stose, 1957; Laurence and Palmer, 1963). Cambrian acritarchs and ostracodes have been recognized in the middle part of the Erwin Formation (Wood and Clendening, 1982). Precambrian acritarchs (Vendian age) also reported in an older

stratigraphic unit (Ocoee Supergroup; Knoll and Keller, 1979). *Rusophycus* and *Skolithos* also occur in the Erwin Formation (Schwab, 1972; Cudzil, 1985).

There are no published reports of body fossils from the Hampton Formation. The trace fossil *Skolithos* occurs in quartzites of the Hampton Formation (King and Ferguson, 1960). Our shelly fossil (possible hyolithid) and *Planolites* were discovered below the lowest quartzite bed in the formation. Neither *Skolithos* (or *Skolithos-like* burrows) nor *Planolites* are age-diagnostic trace fossils because they occur in both Cambrian and Vendian deposits (Cloud *et al.*, 1976; Alpert, 1977; Glaessner, 1984; Kumar *et al.*, 1984; Fritz and Crimes, 1985). However, shelly fossils are generally indicative of Cambrian and younger ages (560 to 570 Ma or younger; Sepkoski and Knoll, 1983). *Cloudina* (Germs, 1972) from the Nama Group of South Africa in an exception to the above rule; it is derived from supposed Vendian-age deposits (Glaessner, 1984). *Cloudina* is unlike the shell fragment from the Hampton because it is composed of several walls. The similarity of the possible hyolithid to forms in England may indicate a late Tommotian or Adtabanian (=*Fallotaspis* biozone) age (Fig. 2).

The Unicoi Formation has no published reports of fossil remains. *Paleophycus* is reported by Cudzil (1985) from the upper Unicoi in Tennessee. We report here the occurrence of *Rusophycus* and *Planolites* from the middle part of the upper Unicoi Formation. Neither *Planolites*, as discussed above, nor *Paleophycus* (Hantzchel, 1975) is age diagnostic. However, *Rusophycus* is age diagnostic. *Rusophycus* or other arthropod trace fossils have been reported to be as old as medial to early Tommotian from different geographic regions, but not as old as Vendian (Alpert, 1977; Brasier *et al.*, 1978; Bergstrom, 1981; Fedonkin, 1981; Jiang, 1981; Xing and Luo, 1984; Nowlan *et al.*, 1985). Therefore, the upper Unicoi is no older than early

Tommotian (Early Cambrian), and the Precambrian boundary is no higher than the middle Unicoi.

CONCLUSIONS

A newly discovered shelly fossil in the Hampton Formation and a trace fossil in the Unicoi Formation confirm the idea that most of the Chilhowee Group is Early Cambrian in age (560 to 570 Ma or younger; Sepkoski and Knoll, 1983). These fossil discoveries place the known occurrence of Cambrian fossils from the Chilhowee Group 850 m below previously reported stratigraphically datable fossil remains. This narrows the potential placement of the Precambrian/ Cambrian boundary in the central and southern Appalachians to the middle or lower part of the Unicoi Formation or lower.

The establishment of synrift sediments as Early Cambrian in age suggests that the rifting episode continued into the earliest Cambrian in the central and southern Appalachians, as suggested by Bond *et al.* (1984), These findings decrease the age of onset of the filling of rift basins (youthful stage) to approximately the beginning of the Cambrian in the stratigraphic model proposed by Fichter and Diecchio (1986).

RIFT TO INCIPIENT PASSIVE-MARGIN SEDIMENTATION WITHIN THE LATE PROTEROZOIC TO EARLY CAMBRIAN UNICOI FORMATION, SOUTHERN AND CENTRAL VIRGINIA

ABSTRACT

Few detailed facies analyses of the rift to passive-margin transition have been undertaken in exhumed orogenic belts. The Unicoi and lower Hampton Formations in the central and southern Appalachians records the transition from rifting to initial opening of the Iapetus Ocean. The lower Unicoi Formation consists of feldspathic sandstones, conglomerates and basalts. Sandstones and conglomerates were deposited from hyperconcentrated flows and tractional currents in alluvial-fan and proximal and medial braid-plain environments. Extrusion of basalts was associated with influx of coarser-grained siliciclastics. The alluvial sediments and intercalated basalts developed in a rift setting. Paleontological data indicate that rifting continued into lower Cambrian time. The upper Unicoi Formation is composed predominantly of transgressive, quartzose sandstones which represent the incipient phase of passive-margin sedimentation related to a first-order, sea level rise. Differences in degree of crustal attenuation controlled the distribution of sedimentary environments during transgression. On most attenuated crust to the east, initial transgressive facies consist of tidal sandwave and sandridge deposits intercalated with proximal and medial braid-plain deposits. As transgression progressed cratonwards onto less attenuated crust, tidal sedimentation was supplanted by tide- and wave-influenced sedimentation characterized by sandwave complexes, tidal inlets and longshore bedforms. Drowning at the top of the Unicoi Formation is indicated by outer-shelf black mudstones containing Tabc, Tbc and Tc beds and gravity flow deposits at the base of the Hampton Formation. Deepening may have been enhanced by continued movement along listric faults throughout the incipient phase of passive-margin development. The majority of the Hampton Formation and the overlying Erwin Formation and Shady Dolomite record progradation of the passive margin which culminated in the

development of a carbonate rimmed shelf. The rift to passive-margin phases of sedimentation in the central Appalachians reflect a continuum from fault-influenced to thermotectonic subsidence.

INTRODUCTION

In the central and southern Appalachian orogen, rifting associated with the initial phase of development of the Iapetus Ocean, commenced at approximately 690 Ma (Odom and Fullagar, 1984). The transition from rifting to the onset of passive-margin development is constrained poorly both stratigraphically and temporally; estimated ages of onset of ocean floor spreading vary from between 660 to 570 Ma (Bond *et al.*, 1984; Odom and Fullagar, 1984; Fichter and Diecchio, 1986).

In southern and central Virginia, the rift-to-passive margin transition is well developed. Thick volcanic, volcaniclastic and sedimentary successions of late Proterozoic age Swift Run Formation, Mount Rogers Group, Catoctin Formation and Lynchburg Group accumulated in rift basins related to the initial extension (Fig. 4; Odom and Fullagar, 1973; Rankin, 1975; Miller, 1986; Schwab, 1986; Wehr, 1985; 1986). Each of these rift-related sequences, with the exception of the Lynchburg Group and Swift Run Formation, is overlain by the late Proterozoic to lower Cambrian Chilhowee Group (Fig. 5; Schwab, 1972; 1975; 1976; 1986; Miller, 1986; Rast and Koles, 1986, Wehr, 1986). Temporally equivalent distal-shelf and slope-rise deposits of the Evington Group and Alligator Back Formation outcrop on the eastern limb of the Blue Ridge anticlinorium (Fig. 4; Wehr and Glover, 1985; Schwab, 1986; Patterson, 1987). In southern and central Virginia and northeast Tennessee, the Chilhowee Group is subdivided into the Unicoi, Hampton and Erwin Formations (Fig. 5). The Unicoi Formation bridges the transition from rift to passive-margin

Figure 4: Geologic map of the Blue Ridge Province in southern and central Virginia showing location of stratigraphic sections through the Unicoi Formation: 1) Virginia Creeper Trail; 2) Elk Creek; and 3) Balcony Falls.

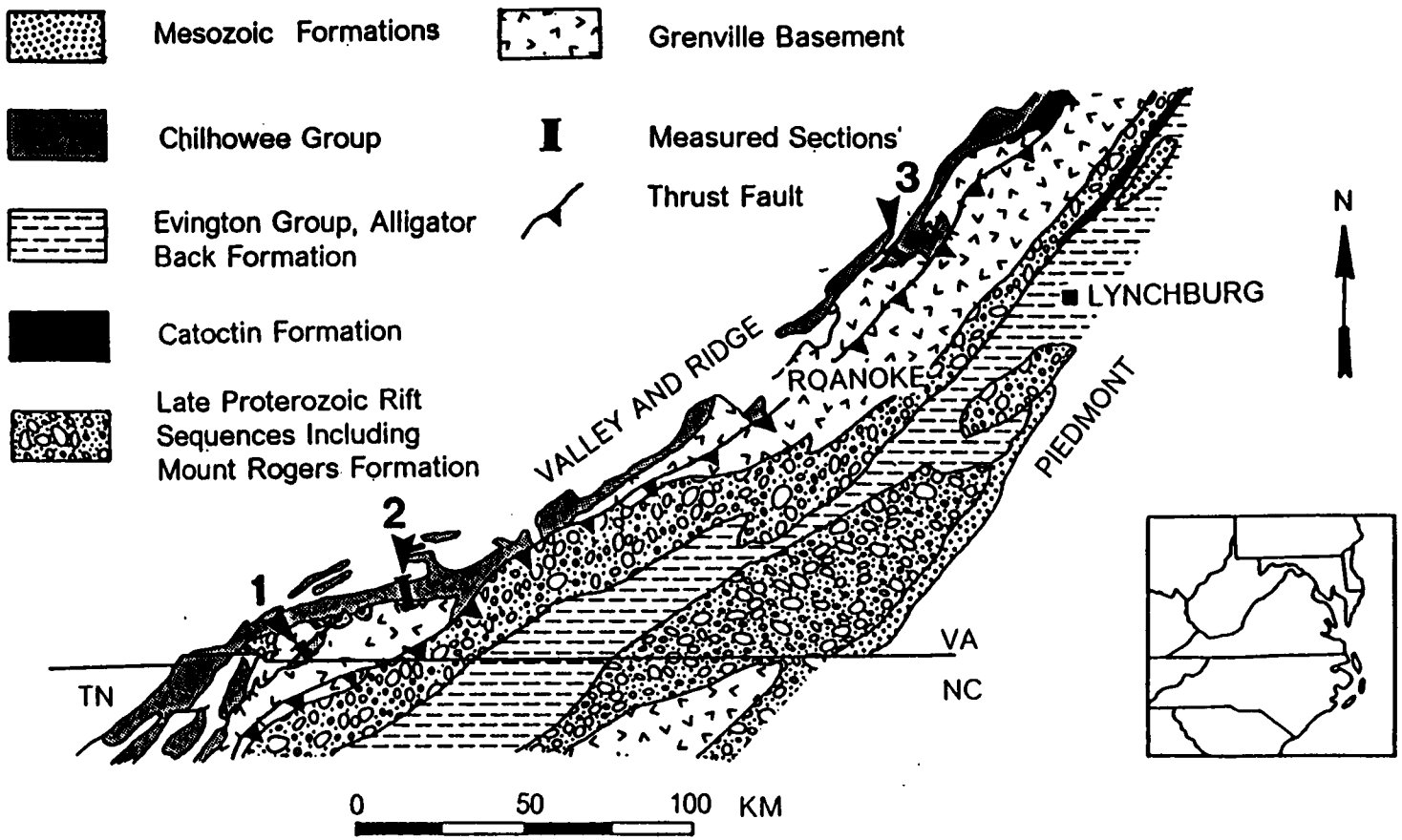
Mesozoic Formations
Grenville Basement
Chilhowee Group
Measured Sections
Thrust Fault
Evington Group, Alligator Back Formation
Catoctin Formation
Late Proterozoic Rift Sequences Including Mount Rogers Formation
1
2
3
VALLEY AND RIDGE
ROANOKE
LYNCHBURG
PIEDMONT
N
TN
VA
NC
0
50
100 KM

Figure 5: Correlation chart for the Chilhowee Group

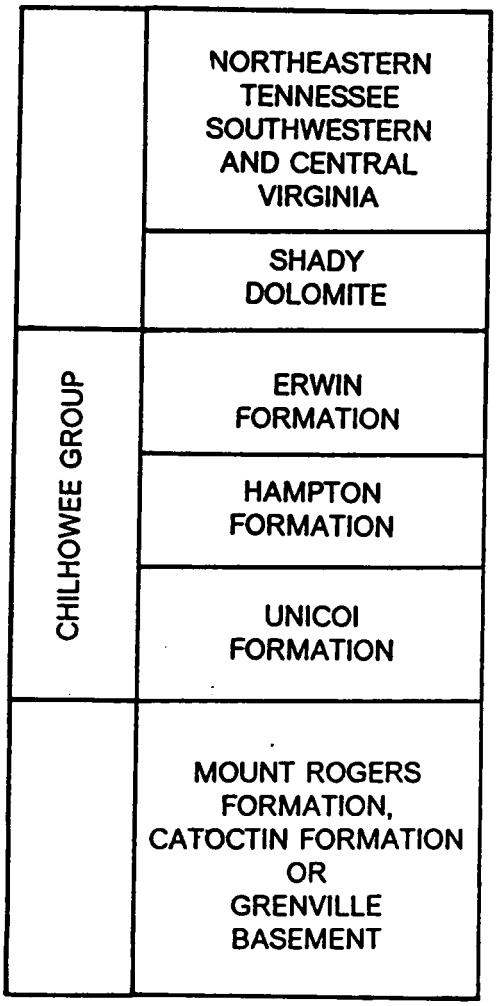
NORTHEASTERN TENNESSEE SOUTHWESTERN AND CENTRAL VIRGINIA
SHADY DOLOMITE
CHILHOWEE GROUP
ERWIN FORMATION
HAMPTON FORMATION
UNICOI FORMATION
MOUNT ROGERS FORMATION, CATOCTIN FORMATION OR GRENVILLE BASEMENT

sedimentation. Overlying Hampton and Erwin Formations record the construction of an east-facing, wave- and storm-dominated, siliciclastic ramp and represent the basal portion of the passive-margin prism (Simpson and Eriksson, 1986; submitted). A carbonate ramp to rimmed-shelf sequence of the Shady Dolomite conformably overlies the Erwin Formation (Barnaby and Simpson, 1987; Read, in press).

In view of the critical stratigraphic position in the rift-to-drift transition, an understanding of the Unicoi Formation is important to the development of tectonic models for the early evolution of the Iapetus margin in the southern Appalachians. Past studies of the Unicoi Formation and its lateral equivalents have concentrated on petrology, paleocurrent analysis, stratigraphic complexities and broad paleoenvironmental reconstruction (Schwab, 1972; Whisonant, 1970; 1974; Mack, 1980; Nunan, 1980). Based on mineralogical and textural immaturity, the Unicoi Formation has been assigned to alluvial and transitional marine settings. Imprecise knowledge of depositional environments and their temporal and spatial distribution has led to conflicting assignment of the Unicoi Formation to rift (Bond *et al.*, 1984), passive-margin (Wehr and Glover, 1985) or youthful passive-margin setting (Fichter and Diecchio, 1986). Using back-stripping techniques, Bond *et al.* (1984) proposed that the onset of ocean floor spreading and thermal subsidence occurred at the base of the Hampton Formation, with fault-controlled subsidence influencing sedimentation during Unicoi time. Wehr and Glover (1985) inferred the presence of a break-up unconformity, generated by domal uplift at the base of the Unicoi Formation. Fichter and Diecchio (1986) developed a stratigraphic model that placed the Weaverton Formation, a northern equivalent of the Unicoi Formation, into the thermally subsiding youthful stage of Bott (1979) and thermal subsidence and submergence stage of Kinsman (1975).

This study documents facies and interprets depositional environments within the

Unicoi and lower Hampton Formations. The results are used to demonstrate that active rifting influenced deposition of alluvial sediments, and that tidal- and wave-produced deposits resulted from the initial transgression associated with mid-ocean ridge development. Few detailed stratigraphic analyses have been undertaken across this critical transition (*cf.* Miller, 1987); this study thus provides insights into how a rift to incipient passive-margin transition will be manifested in other exhumed orogenic belts.

AGE CONSTRAINTS

In southern Virginia the Unicoi Formation either nonconformably overlies Grenville basement or overlies Mount Rogers Formation (Fig. 5). The transition from the upper sedimentary member of the Mount Rogers Formation into the overlying Unicoi Formation has been interpreted as conformable (Rankin, 1967) and nonconformable (Stose and Stose, 1957; King and Ferguson, 1960); the contact may also be structural. In central Virginia the Unicoi Formation overlies Grenville basement or Catoctin Formation greenstones.

A maximum age for the Unicoi Formation is provided by basement rocks. Mount Rogers volcanics and Crossnore plutons have been demonstrated to be consanguineous (Rankin, 1969; 1970; 1975; 1976; Rankin *et al.*, 1969). Crossnore plutons were dated as *ca.* 820 Ma (U-Pb zircon; Davis *et al.*, 1962; Rankin *et al.*, 1969). This age was questioned initially because it necessitated the presence of a significant unconformity at the Mount Rogers to Chilhowee Group transition (Rogers, 1972; Rankin *et al.*, 1972; Odom and Fullagar, 1984) and because it was at variance with preliminary Rb-Sr dating (Odom, 1971; Odom and Fullagar, 1971). More recently, Odom and Fullagar (1984) have demonstrated the existence of different age

populations of zircons, one inherited from Grenville basement and the other representing the crystallization age of the Crossnore magma. The younger zircons yield ages of 690±10 Ma. (Odom and Fullagar, 1984). The age of the Catoctin Formation has been established as Precambrian/Cambrian, because feeder dikes for the Catoctin cross-cut the Robertson River Pluton dated at 570±15 Ma old (Mose and Nagel, 1984; Rb-Sr whole rock). Fichter and Diecchio (1986) questioned this age date as being too young, based on their stratigraphic model and assigned a 610 to 630 Ma age to the Catoctin Formation. Glacial deposits are present in the upper sedimentary member of the Mount Rogers Formation (Rankin, 1967; Blondeau and Lowe, 1972; Schwab, 1976; 1981; Miller, 1986) and in the Rockfish Conglomerate of the Lynchburg Group (Wehr, 1986). In many parts of the world two late Proterozoic glaciogenic episodes are recognized (Crittenden *et al.*, 1983; Harland, 1983) and are considered to be 650 and 600 Ma-old, respectively (Harland, 1983). It is, however, not possible to assign the glacial deposits in the central Appalachians to either of these events. The Catoctin Formation (less than 570±15 Ma old) provides a maximum age for the Unicoi Formation in central Virginia. However, evidence will be presented later for the Catoctin Formation being correlative with alluvial sediments in the lower Unicoi Formation in southern Virginia, implying that Unicoi sedimentation in this area commenced in the late Proterozoic

Biostratigraphic control within the Chilhowee Group is limited. Early Cambrian fossils are known from the Erwin Formation and its correlatives (Walcott, 1891; Stose and Stose, 1957; Laurence and Palmer, 1963; Wood and Clendening, 1982). Recently a fragment of a hyolithid was recovered from the Hampton and *Rusophycus*, a resting trace of a trilobite, was discovered in marine strata from the upper Unicoi Formation (Simpson and Sundberg, 1987). These fossils indicate a Tommotian or younger age implying that the majority of the Chilhowee Group is of Cambrian age

(Simpson and Sundberg, 1987).

METHODS

In central and southern Virginia, the Unicoi and lower Hampton Formations are exposed on a number of thrust sheets within the Blue Ridge Province (Fig. 4). At three localities on different thrust sheets, complete stratigraphic sections were measured on a cm by cm scale recording grainsize, mineralogy, sedimentary structures and bedding morphology. Representative samples were collected for slabbing and thin-sectioning. Photo mosaics were constructed of critical exposures. Depositional processes were reconstructed at the facies level (see Table I). Facies were grouped into facies associations at which level depositional environments could be interpreted.

The limited outcrop does not permit architectural element analysis necessary for detailed interpretation of ancient fluvial systems (Miall, 1985). However, vertical changes in facies and facies associations in the Unicoi and lower Hampton Formations permit generalized depositional environments to be reconstructed, from which pertinent information can be gleaned concerning the tectonic history of the early Iapetian margin.

Six facies associations make up the Unicoi and lower Hampton Formations in measured sections. The stratigraphic relationships of the facies associations are illustrated in Figure 6.

FACIES ASSOCIATION A: DISTAL ALLUVIAL FAN

Description

TABLE 1: FACIES ABBREVIATIONS

Abbreviation	Facies
Gms	Massive Conglomerate
Sms	Massive Sandstone
Sh	Horizontally Stratified Sandstone
St	Trough Cross-bedded Sandstone
Gm	Massive, Clast-supported, Pebble Conglomerate
Sp	Tabular-planar, Cross-bedded Sandstone
Sr	Ripple Cross-laminated Sandstone
Fl	Graded, Finely Laminated Siltsone and Mudstone
Fm	Mudstone
Smc	Channelized, Massive Sandstone
Stc	Channelized, Trough Cross-bedded Sandstone
Smr	Megarippled Sandstone
Sr	Symmetrical-rippled Sandstone
Scp	Compound, Cross-stratified Sandstone

Figure 6: Generalized stratigraphy of the Unicoi and lower Hampton Formations for the three measured sections. See figure 1 for locations of sections.

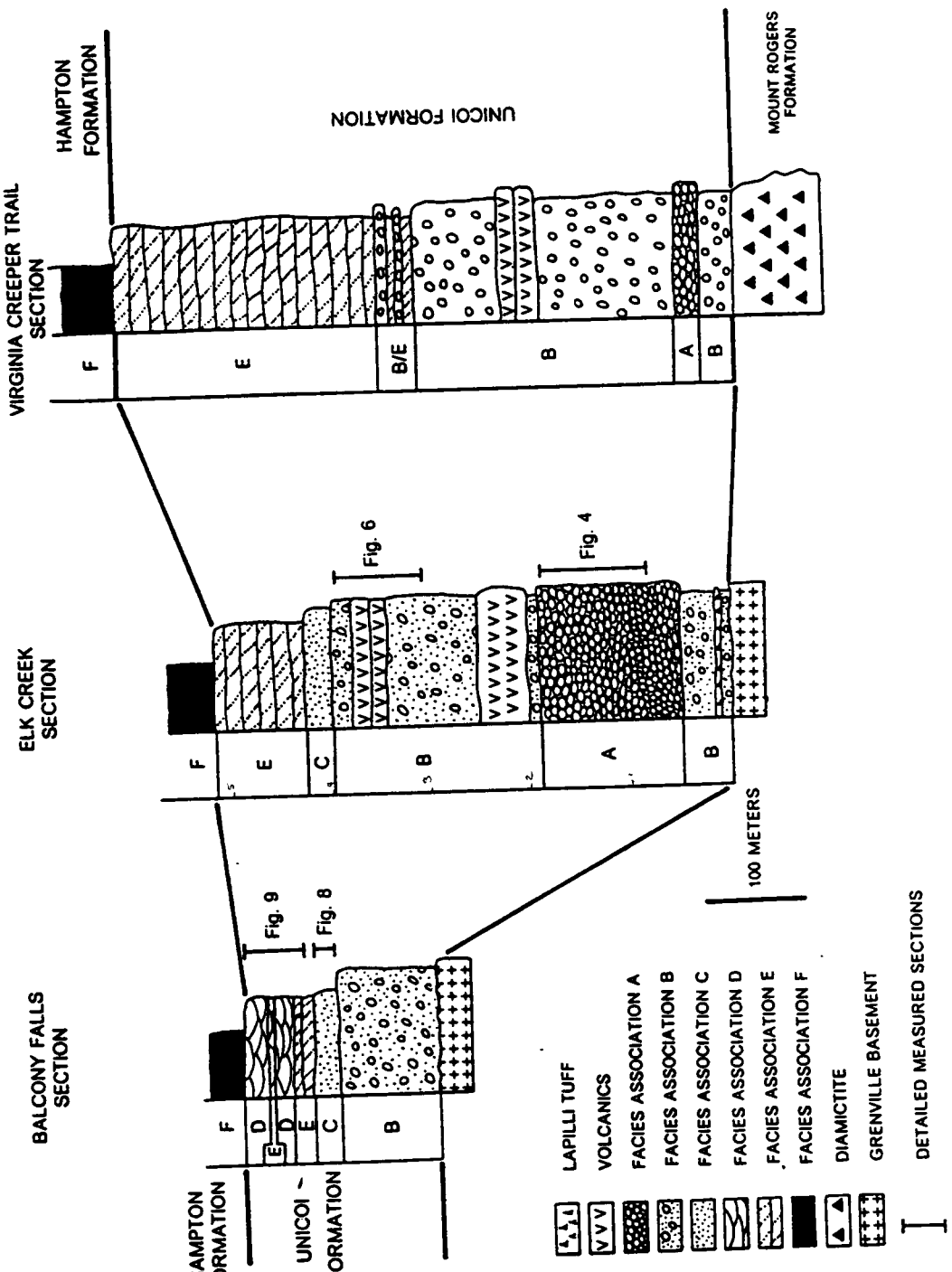
BALCONY FALLS SECTION
ELK CREEK SECTION
VIRGINIA CREEPER TRAIL SECTION
HAMPTON FORMATION
UNICOI FORMATION
MOUNT ROGERS FORMATION
Fig. 9
Fig. 8
Fig. 6
Fig. 4
100 METERS
LAPILLI TUFF
VOLCANICS
FACIES ASSOCIATION A
FACIES ASSOCIATION B
FACIES ASSOCIATION C
FACIES ASSOCIATION D
FACIES ASSOCIATION E
FACIES ASSOCIATION F
DIAMICTITE
GRENVILLE BASEMENT
DETAILED MEASURED SECTIONS

Facies association A is confined to the Elk Creek and Virginia Creeper sections (Fig. 6). Four facies are recognized in this association: 1) massive conglomerate (Gms); 2) massive sandstone (Sms); 3) horizontally stratified sandstone (Sh); and trough cross-bedded sandstone (St).

Massive conglomerates are poorly sorted and matrix supported and contain clasts of granite, potassium feldspar and subordinate volcanics and intraformational mudstones. Clasts range from granules to small pebbles. Matrix ranges from upper very fine to upper very coarse sand with minor silt- and clay-sized detritus also present. The sand-size fraction is composed of potassium feldspar, quartz and subordinate lithic constituents. Plagioclase is restricted to the finer grain-size fraction in the lower portions of the stratigraphic section. The proportion of granite clasts and potassium feldspar decrease upsection whereas quartz increases in abundance.

Massive conglomerates (Gms) are present in beds with sharp, flat to slightly undulatory and rarely channelized bases. Beds are tabular and range in thickness from 0.4 to 6.0 m. Beds are structureless but display distributive normal grading which is best observed in the coarser fraction, as well as inverse-to-normal grading and non-graded base overlain by normally graded top (Fig. 7). Crude horizontal stratification may be present within beds and is manifest as weak normal grading from small-pebble conglomerate to upper medium-grained sandstone. Clast-supported pebbles define the lower boundary of 4 to 16 mm-thick horizontal stratification The massive conglomerate beds resemble the Gms facies of Miall (1977, 1981) but differ in that the matrix is predominately sand- rather than mud-sized and clasts are smaller.

Massive conglomerate beds are capped by 5 to 50 cm-thick sandstone intervals (Fig. 7) which are massive (Sm), horizontally stratified (Sh) or trough cross bedded (St). The proportion of stratified to massive sandstone increases upward in the facies association (Fig. 7). Massive sandstone intervals typically display normal grading

Figure 7: Measured section through facies association A at Elk Creek. Insets illustrate bed types present in this association. See figure 3 for location of section.

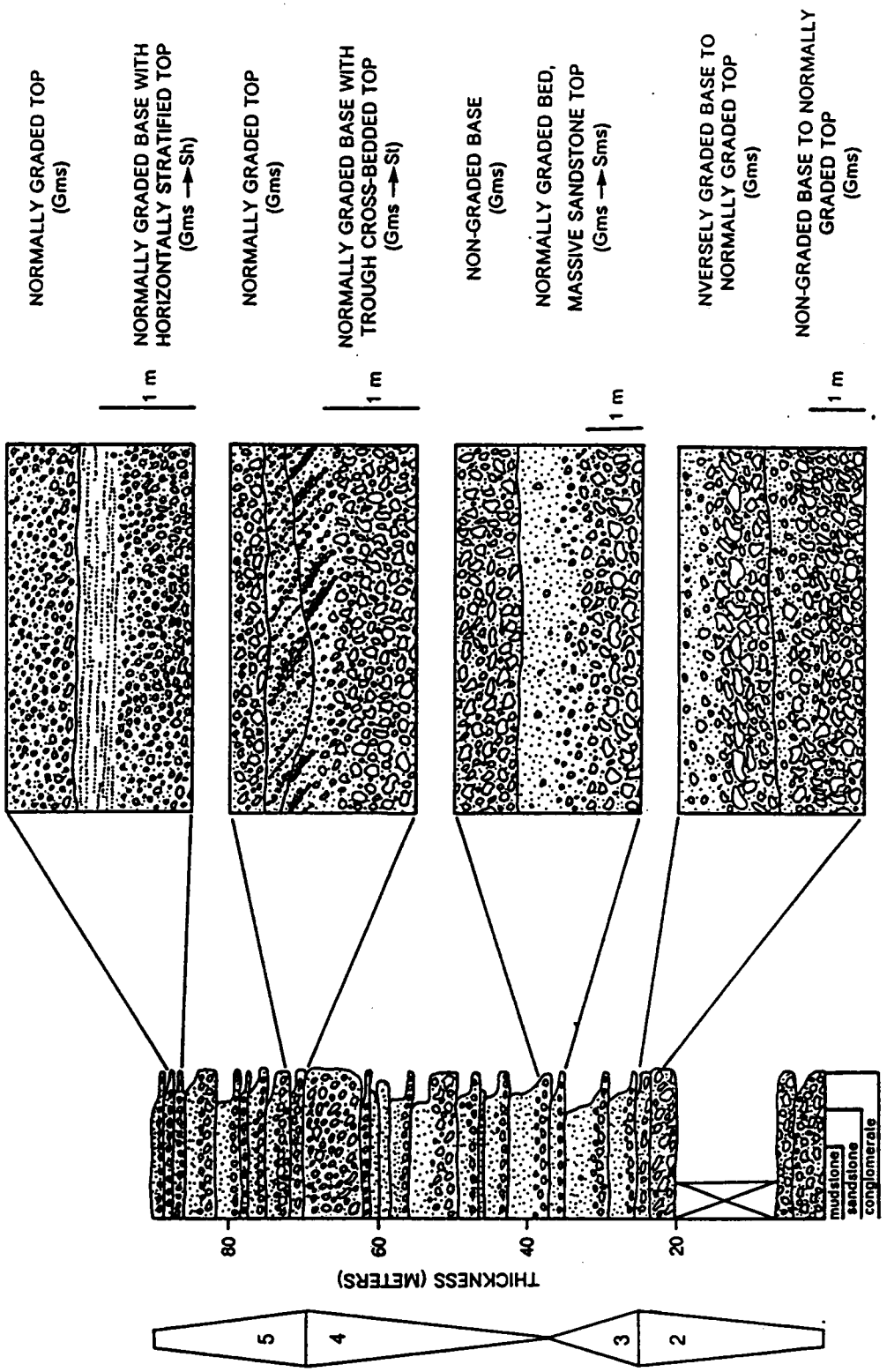
NORMALLY GRADED TOP (Gms)
NORMALLY GRADED BASE WITH HORIZONTALLY STRATIFIED TOP (Gms → Sh)
NORMALLY GRADED TOP (Gms)
NORMALLY GRADED BASE WITH TROUGH CROSS-BEDDED TOP (Gms → St)
NON-GRADED BASE (Gms)
NORMALLY GRADED BED, MASSIVE SANDSTONE TOP (Gms → Sms)
NVERSELY GRADED BASE TO NORMALLY GRADED TOP (Gms)
NON-GRADED BASE TO NORMALLY GRADED TOP (Gms)
1 m
1 m
1 m
1 m
THICKNESS (METERS)
80
60
40
20
5
4
3
2
mudstone
sandstone
conglomerate

from upper very coarse to upper fine sand. Horizontal stratification consists of 5 to 11 mm-thick, normally graded coarse to upper fine sand. Trough cross-bedded sandstones range in grain size from lower coarse to upper fine sand. Troughs are mutually cross-cutting and range from 15 to 35 cm in width and 10 to 15 cm in depth. Foresets are normally graded.

Beds in facies association A are arranged in sequences and megasequences. Sequences consist of cyclic vertical changes in bedding thickness and facies, whereas megasequences represent larger-scale vertical changes (Heward, 1978). Coarsening- and thickening-upward sequences are 5 to 15 m-thick and are superimposed on 10 to 70 m-thick megasequences that either coarsen and thicken or fine and thin upward. Four megasequences are present in the Elk Creek section (Fig. 7). These are developed above a single megasequence in facies association B. Megasequence two coarsens and thickens upward. Sequences at the base of megasequence two consist of stacked beds of Gms overlain by Sh or St. Higher sequences are characterized by beds of Gms overlain by Sms. Stacked Gms facies dominate the top of the megasequence. Megasequence three consists of upward-fining and thinning sequences of beds of Gms overlain by Sms. Megasequence four is finer-grained (Sms rather than Gms) and more quartzose than megasequence two. Sequences in the basal portion of megasequence four are dominated by bedss of Sms overlain by Hs whereas sequences at the top of the megasequence are composed of beds of Sms or Gms overlain by St. Megasequence five consists of upward-fining and thinning sequences of beds of Gms overalin by Sh or St grading into Sms overlain by Sh or St

Interpretation

Beds present in this facies association resemble hyperconcentrated-flow deposits

described from Holocene and ancient alluvial sequences (Hubert and Hyde, 1982; Nemec and Muszynski, 1982; Wells, 1984). Hyperconcentrated flows belong to a continuum based on the concentration of sediment in the flow (Beverage and Culbertson, 1964; Bull, 1972; Wasson, 1977). Mudflows contain greater than 80 percent by weight sediment whereas hyperconcentrated flows contain from 80 percent to approximately 40 percent sediment. Low concentration flows fall below the 40 percent range. Rheology and flow mechanisms vary for different water:sediment ratios and hence distinctive bed types are produced that permit separation of flow mechanisms (Hampton, 1975; Nemec and Muszynski, 1982). Mass-flows are psuedolaminar (Nemec and Muszynski, 1982) whereas low-concentration flows are characterized by tractional processes which produce distinctive sedimentary structures. Turbulent suspension is the predominant process within hyperconcentrated flows; these flows may be generated by dilution of debris flows or the addition of sediment to low-density flows (Lowe, 1976; Lawson, 1981).

Nonstratified, normally-graded beds in this facies association are interpreted to have been deposited by turbulent suspension currents which permitted normal grading to develop (*cf.* Middleton, 1970; Middleton and Hampton, 1976; Cas, 1979; Nemec and Muszynski, 1982). Normally graded beds with rare internal parallel stratification are envisioned to have developed when turbulent suspension processes yielded to upper flow regime bedload processes (Nemec and Muszynski, 1982), or by variation in flow intensity in the turbulent suspension flow (*cf.* Hampton, 1975). A non-graded, basal layer overlain by a graded, unstratified top indicates at minimum that the top was deposited from turbulent suspension (Nemec and Muszynski, 1982) with dispersive pressure and buoyancy probably dominating sedimentation within the basal portion. Nemec and Muszynski (1982) have attributed a similar non-graded, basal sequence to deposition by psuedolaminar flow. Dispersive pressure was

probably dominant because of the low mud concentration present in the Gms beds.

Beds which are normally graded with either a horizontally stratified or trough cross-bedded cap indicate a transition within a single flow from turbulent suspension to tractional processes (Nemec and Muszynski, 1982). The gradational change from the two types of sedimentary structures indicates deposition from a single event. Expulsion of water as sediment was being deposited may have been responsible for the dilution of a hyperconcentrated flow to a point where tractive flow processes became dominant. Water expulsion during deposition has been observed within modern flows of coarse-grained sediments (Lowe, 1976; Lawson, 1981). The traction-produced structures on top of the massive beds indicate relatively high current velocities. Current velocities of greater than 0.80 m/sec and 0.25 m/sec, respectively, are required to produce horizontal stratification and trough cross bedding.

The predominance of structures generated by turbulent flow followed by tractional processes, allow facies in this association to be interpreted as sheet-flood deposits (*cf.* Nemec and Muszynki, 1982). Sheet floods are low-viscosity, short-duration flows that occur below the intersection point on the distal reaches of alluvial fans (Bull, 1972; Wasson, 1977; 1979). In contrast, proximal reaches of alluvial fans are characterized by abundant mass-movement, debris-flow sedimentation (Bull, 1972). Sheet floods are characterized by thin, wide sheets of sediment-rich water that moves under upper flow regime conditions. Sedimentation takes place in response to slope angle changes, water infiltration into the basal surface or fluid migration to the flow top.

Before the Silurian Period, the absence of land plants permitted greater amounts of sediment flux, increased erosion rates and limited climatic effects on the delivery of detritus to a catchment area (Schumm, 1968). Hyperconcentrated sediment flows may have been easier to generate under these conditions and debris may have been subject

to more extensive reworking, thus destroying primary sequences of debris-flows deposits (Heward, 1978).

FACIES ASSOCIATION B: PROXIMAL TO MEDIAL BRAIDPLAIN

Description

This facies association is developed in each of the measured sections (Fig. 6). Seven facies are recognized: 1) massive, clast-supported, pebble conglomerate (Gm); 2) horizontally stratified sandstone (Sh); 3) tabular-planar, cross-bedded sandstone (Sp); 4) trough cross-bedded sandstone (St); 5) ripple cross-laminated sandstone (Sr); 6) graded, finely laminated siltstone and mudstone (Fl); and 7) mudstone (Fm);. In addition, lapilli tuffs and basalt flows are present within this facies association B (Fig. 6).

Pebble conglomerate (Gm) contains well-rounded clasts of (in decreasing abundance) vein quartz, granite, basalt, rhyolite, quartzite, porphyritic rhyolite and gneiss. The percentage of vein quartz varies from a minimum of 50 percent to a maximum of 95 percent with lower percentages of vein quartz present in proximity to basalt flows (Fig. 6). Basal surfaces of this facies are erosional with a maximum relief of 30 cm. Pebbles are clast supported with a coarse-sand matrix and are present either in tabular beds up to 2 m-thick or a 5 to 15 cm-thick lags. Apart from a crude clast imbrication beds are internally massive (Fig. 8A).

Sandstones in this facies association are feldspathic. The quartz:feldspar ratio increases upward with the exception that sandstones in proximity to basalt flows are more feldspathic. The horizontally stratified facies (Sh) is composed of upper fine- to upper medium-grained sandstone. Stratification is normally graded with fine sand

Figure 8: Photographs of facies association B. A) Massive, clast-supported, pebble conglomerate facies. B) Tabular-planar, cross-bedded sandstone and horizontally stratified sandstone facies. C) Contact between basalt flow and overlying sandstone bed showing corrugated contact. Dark spots are amygdules. D) Contact of basalt flow with overlying laminated siltstone cap. Note pipes of sediment shown by arrow 1. Sand lenses shown by arrow 2.

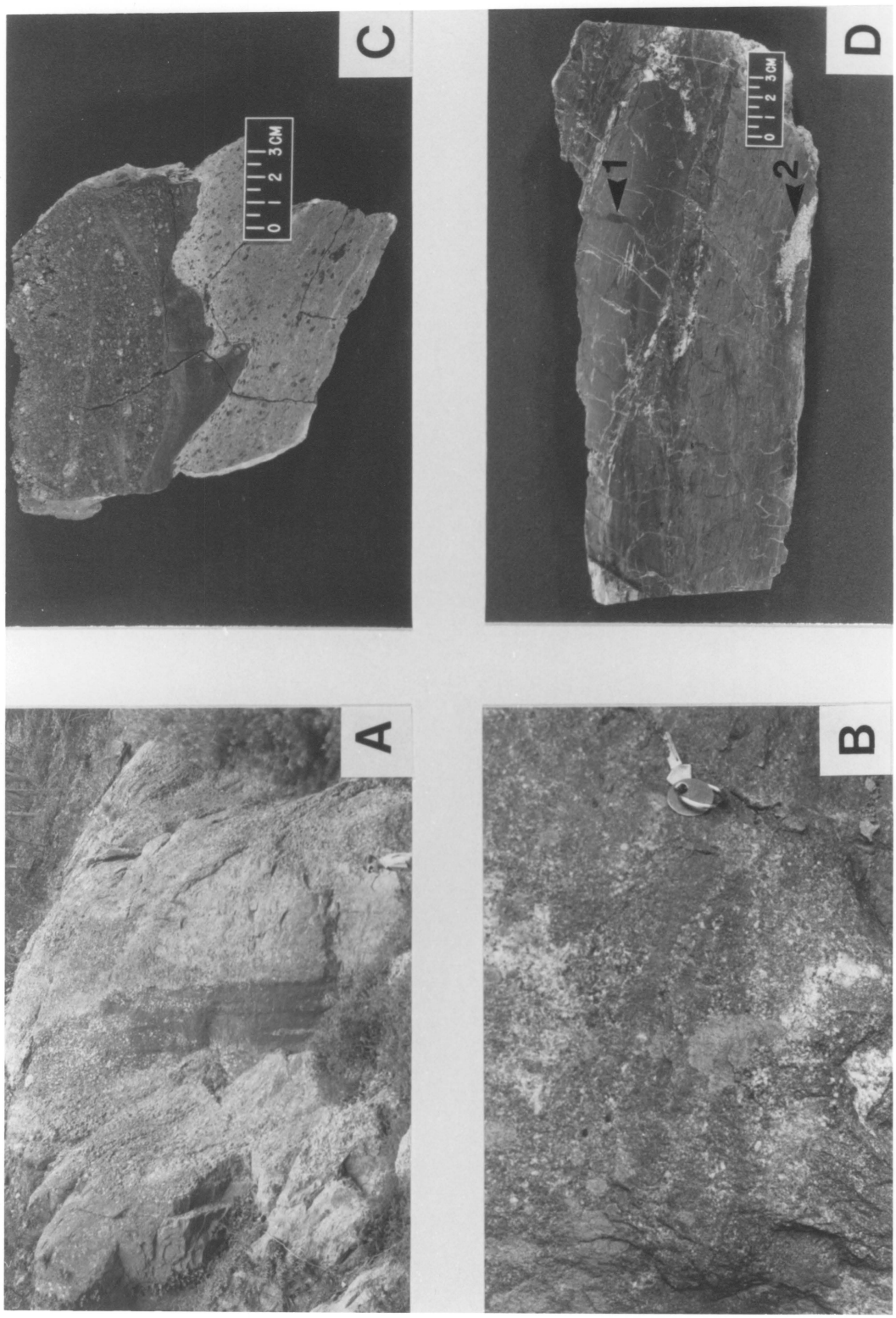
A
B
C
0 1 2 3CM
D
1
2
0 1 2 3CM

delimiting the top of 1 to 4 mm-thick laminations (Fig. 8B). The stratification may be defined by granules or pebbles. Bed thickness varies from 5 to 40 cm. The tabular planar cross-bedded facies (Sp) is composed of sets of planar stratification which are tabular to slightly wedge shaped on the outcrop scale (Fig. 8B). Set thickness varies from 10 to 45 cm. A maximum of five sets are superimposed to form cosets. Foresets vary in thickness from 0.6 to 4.0 cm and are delimited by normal grading from granule to medium sand. Foresets dip at a maximum of 28 degrees. Basal surfaces of beds resting on mudstone (Fm) or siltstones (Fl) contain flute casts. Trough cross-bedded facies (St) consist of medium-scale troughs which are present in cosets up to 65 cm thick. Foresets are normally graded. Ripple cross-laminated sandstones (Sr) range in grainsize from lower very fine to lower medium. Ripples are preserved typically as isolated form sets.

Siltstones in this facies association contain quartz, potassium feldspar and up to 15 percent biotite. Graded, finely laminated siltstone and mudstone facies (Fl) consists of a basal layer of siltstone from a minimum of several grains to a maximum of 6 cm in thickness that grades upward into mudstone. Mudstone layers may be laminated or massive. Couplet thicknesses range from 1 to 15 cm. Small syndepositional faults are present. Mudstone facies (Fm) is laminated. Laminations consist of basal mm-scale alternations of siltsize quartz and biotite overlain by mudstone.

Erosional scours at bases of beds are either broad and shallow or narrow and deep. Broad, shallow scours vary from 2 to 3 cm deep and 20 to 56 cm wide and are overlain by Fl, which thickens into depressions. Mudstone clasts may be present at the base of scours. Narrow, deep scours have maximum depths of 8 cm and are up to of 22 cm wide. Walls dip from 75 degrees to near vertical. Fill is normally graded upper fine sand to mud; complete mudstone fills also are present. These scours occur within the Sr and Fl facies.

Lapilli tuffs are exposed poorly and possess a mixed population of clast types that contain a small percentage of quartz and potassium feldspar. The dominant clasts are felsic in composition and range up to 2 cm in diameter.

Basalt flows are present in the Elk Creek and Virginia Creeper Trail sections but not in the Balcony Falls section (Fig. 6). Previous analysis by Rankin (1969) report the Unicoi basalts to be tholeiitic in composition. Basalts display varying degrees of metamorphism from near pristine condition to fine-grained chlorite/biotite schists. More intensely metamorphosed flows show strong cleavage development. Thicknesses of flows range from 9.5 to 50.0 m. Basal contacts are sharp and rest on coarse-grained sandstone. Some bases of flows are silicified. Euhedral, relict plagioclase microlites displaying hyalopilitic texture are present throughout the flows. Amygdules are common near flow tops. Tops of flows are either corrugated (Fig. 8C) or defined by overhangs filled with sediment. Corrugated tops of flows may be remnant ropy flow tops that were accentuated by cleavage development. Laminated siltstone caps display some relict basalt textures and may represent a immature soil horizon (Fig. 8D). Pipes of sediment penetrate down from overlying beds and are common in soil horizons (Fig. 8D). The uppermost flows are separated by thin beds of St facies. These interflow sandstones contain abraded detrital grains of basalt.

The facies in this association occur in four repetitive groupings: 1) Gm, Sh, Sp; 2) Gm, St; 3) Sh, Sp; and 4) subordinate Sr, Fl, Fm (Fig. 9). Broad, shallow scours are associated with the first three groups whereas narrow, deep scours are confined to the last group of facies. Paleocurrent data from facies association B below the basalt show a general southwesterly trend whereas above the basalt paleocurrents are to the south (Fig. 10).

Megasequences in facies association B are located at the base of the Unicoi Formation within the Elk Creek and Virginia Creeper sections (Fig. 6). Megasequence

Figure 9: Measured section through facies association B at Elk Creek. Insets show the most common groupings of facies. See figure 3 for location of section.

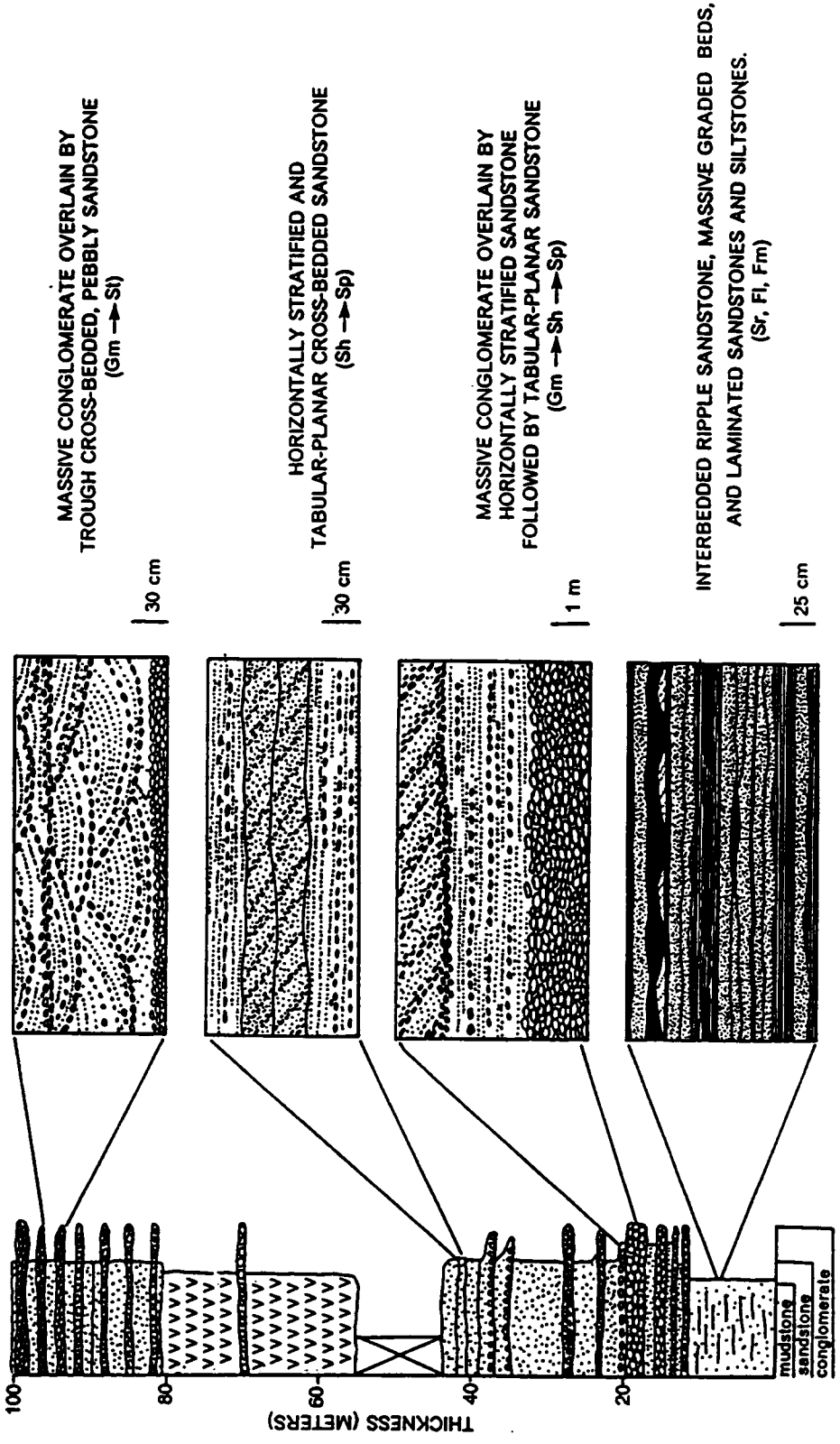
MASSIVE CONGLOMERATE OVERLAIN BY
TROUGH CROSS-BEDDED, PEBBLY SANDSTONE
(Gm → St)
30 cm
HORIZONTALLY STRATIFIED AND
TABULAR-PLANAR CROSS-BEDDED SANDSTONE
(Sh → Sp)
30 cm
MASSIVE CONGLOMERATE OVERLAIN BY
HORIZONTALLY STRATIFIED SANDSTONE
FOLLOWED BY TABULAR-PLANAR SANDSTONE
(Gm → Sh → Sp)
1 m
INTERBEDDED RIPPLE SANDSTONE, MASSIVE GRADED BEDS,
AND LAMINATED SANDSTONES AND SILTSTONES.
(Sr, Fl, Fm)
25 cm
THICKNESS (METERS)
100
80
60
40
20
mudstone
sandstone
conglomerate

Figure 10: Paleocurrent rose diagram for facies association B. N = number of observations; Vm = vector mean; Sd = standard deviation.

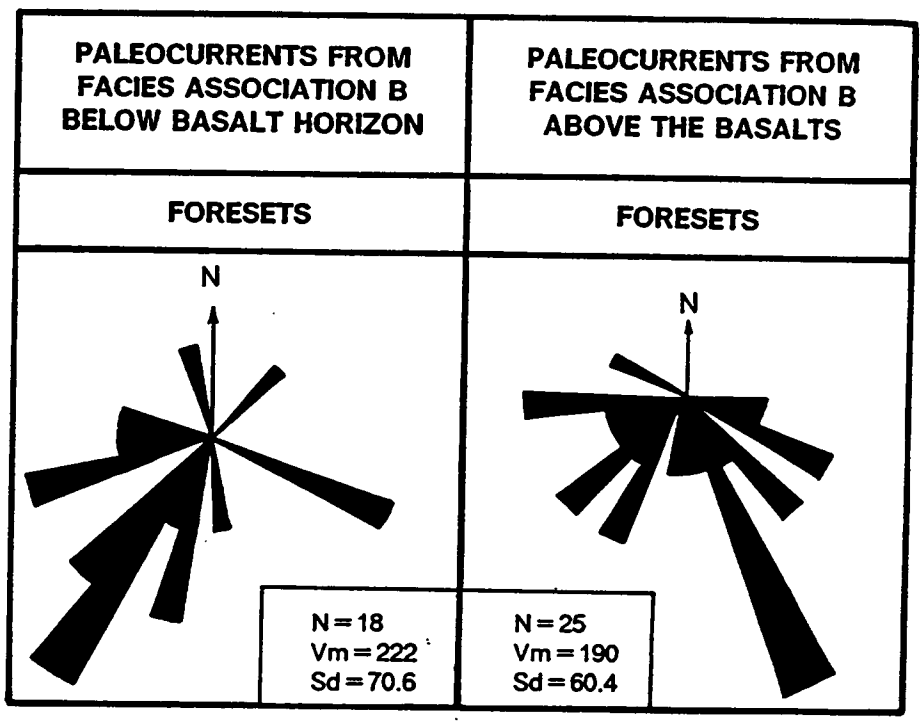
PALEOCURRENTS FROM FACIES ASSOCIATION B BELOW BASALT HORIZON
PALEOCURRENTS FROM FACIES ASSOCIATION B ABOVE THE BASALTS
FORESETS
FORESETS
N
N
N=18
Vm=222
Sd=70.6
N=25
Vm=190
Sd=60.4

one in the Elk Creek section is characterized by lapilli tuffs which pass vertically into sequences dominated by Sr, Fl and Fm facies. Isolated channels of Gm appear near the top of the megasequence. Gms beds of facies association A cap the megasequence. The basal Virginia Creeper Trail section is composed of only one megasequence. Gm, Sh, St sequences of facies association B are overlain by a sequence of Gms capped by Sms, Sh or St of facies association A.

Interpretation

The facies in this association were deposited from low-density, mostly tractive flows. Groups of facies are comparable to those documented from Holocene proximal to medial braidplains (*cf.* Bradley *et al.*, 1972; Boothroyd and Ashley, 1975; Desloges and Church, 1987) and reflect both channel and overbank sedimentation.

Gm, Sh and St represent the most proximal environment of deposition and reflect growth of longitudinal bars. Massive gravels (Gm) form the cores of bars which grow from a diffuse gravel sheet as the river loses competence (D. G. Smith, 1973; Boothroyd and Ashley, 1975; Hein and Walker, 1977). Flow velocities measured during accumulations of Gm facies in Holocene settings range from 1 to 3 m/sec (Boothroyd and Ashley, 1975). Sand-sized matrix is interpreted to have filtered into void spaces after deposition of the gravel bars or to have been trapped in interstices sheltered from currents. With a further decline in flow velocities horizontally stratified sandstones (Sh) accumulated on bar tops whereas trough cross-bedded sandstones (St) formed from migration of megaripples at low stage in channels adjacent to bars (*cf.* Boothroyd and Ashley, 1975).

Massive gravels (Gm) and trough cross-bedded sandstones (St) occur in stacked 0.6 to 3.0 m-thick upward-fining intervals (Fig. 9). By analogy with Holocene rivers

such as the Donjek, South Saskatchewan and Brahmaputra (Coleman, 1969; Williams and Rust, 1969; Hein and Walker, 1977), the gravels are interpreted as channel lag and the cross-bedded sandstones as mid-channel bar deposits. Each upward-fining sequence reflects a single flood cycle.

Horizontally stratified sandstones in the Sh -Sp grouping may reflect either upper or lower flow regime conditions. The occurrence of this facies below tabular-planar cross-beds (Fig. 9) suggests that it developed in the upper flow regime. This grouping of facies reflects deposition on transverse or linguoid bars. During floodstage, bar growth was initiated by deposition of Sh whereas Sp reflects bar migration during the waning stage (Hein and Walker, 1977). Sh may also form on the top of Sp as bars become emergent.

Interlayered Sr, Sl and Fm facies represent overbank deposits. Cross-laminated sandstone lenses (Sr) resulted from migration of isolated ripple trains. Graded siltstone and mudstone (Fl) and mudstone (Fm) laminations (Fig. 9) reflect separate overbank floods which also produced the narrow, deep scours.

FACIES ASSOCIATION C: EPHEMERAL BRAIDPLAIN

Description

This facies association is confined to the Elk Creek and Balcony Falls sections (Fig. 6). Six facies are developed: 1) horizontally stratified sandstone (Sh); 2) trough cross-bedded sandstone (St); 3) tabular-planar, cross-bedded sandstone (Sp); 4) ripple cross-laminated sandstone (Sr); 5) graded, finely laminated siltstone and mudstone (Fl); and 6) mudstone (Fm). The sandstones vary from medium- to very fine-grained, feldspathic to quartz arenites with subordinate quartz wackes.

Horizontally stratified facies (Sh) is composed of 1 to 3 mm-thick laminations

which make up beds ranging in thickness from 3.0 cm to a 3.2 m. Successive beds are separated by erosional surfaces. Trough cross-bedded facies (St) consists of mutually cross-cutting troughs which vary from 12 to 75 cm wide and 2 to 15 cm thick. Bedding-plane exposures are rare and, as a result, paleocurrent measurements are sparse. Normal grading is rarely preserved in foresets. Cosets of trough cross beds are erosional into horizontally stratified sandstone intervals.

Tabular-planar cross-bedded facies (Sp) contain 10 to 25 cm-thick sets with normally graded foresets. Beds typically consist of a single set of cross strata. Bases of beds are sharp to slightly undulatory. The ripple cross-laminated sandstone facies (Sr) ranges in thickness from 1 to 15 cm and occurs as isolated beds or as caps on tabular-planar cross-bed sets. The thicker cross-laminated sets display normal grading.

Graded, finely laminated siltstone and mudstone (Fl) contain 0.1 to a maximum of 2.0 cm-thick laminations with an average thickness of 0.2 cm. Laminations consist of a poorly developed basal siltstone layer overlain by mudstone. Mudstone facies (Fm) are massive with rare siltstone to fine-grained sandstone laminations.

The facies in this association occur in three repetitive groupings: 1) Sh; 2) Sh, St; and 3) Sp, Sr, Fl, Fm (Fig. 11). Each of these groupings of facies is present in the Balcony Falls section; Sh predominates over Sr whereas Sp, Sr, Fl, Fm grouping is subordinate. In the Elk Creek section Sp, Sr, Fl, Fm are absent and Sh, St predominate.

Interpretation

The predominance of horizontal stratification indicates that sheetflooding was the major depositional process responsible for facies association C. Sheetfloods are

Figure 11: Measured section through facies association C at Balcony Falls. Insets show the most common groupings of facies. See figure 3 for location of section.

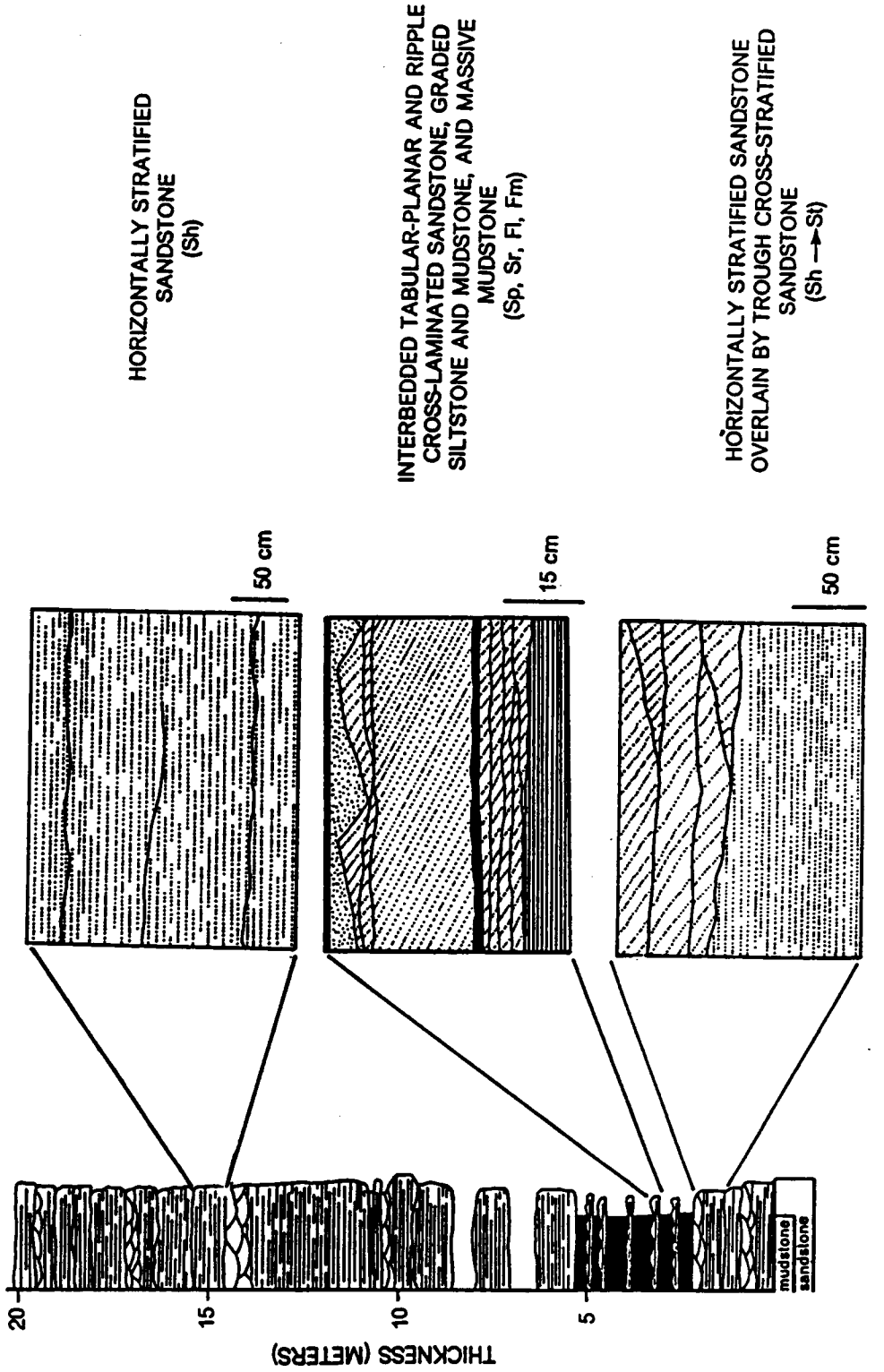
HORIZONTALLY STRATIFIED SANDSTONE (Sh)
INTERBEDDED TABULAR-PLANAR AND RIPPLE CROSS-LAMINATED SANDSTONE, GRADED SILTSTONE AND MUDSTONE, AND MASSIVE MUDSTONE (Sp, Sr, Fl, Fm)
HORIZONTALLY STRATIFIED SANDSTONE OVERLAIN BY TROUGH CROSS-STRATIFIED SANDSTONE (Sh → St)
50 cm
15 cm
50 cm
THICKNESS (METERS)
20
15
10
5
mudstone
sandstone

characteristic of ephemeral-river systems and represent unconfined flows out of channels. At Bijou Creek, Colorado, a lenticular sandstone body up to 4 m thick and consisting mostly of horizontal stratification was deposited during a single flood (McKee *et al.*, 1967). Associated trough cross-bedded sandstones probably developed at lower flow stages in channels incised into the sheetflood deposits; stream-channel deposits in ephemeral river systems are typically trough cross-bedded (Williams, 1981; Sneh, 1983). The Sp, Sr, Fl, Fm group of facies are considered to reflect deposition on distal margins of sheetfloods. Tabular-planar, cross-bedded sandstones probably were produced during peak flood stage at the same time that horizontal stratification developed more proximal to the channel. The Sr, Fl and Fm facies reflect progressively lower flow velocities.

FACIES ASSOCIATION D: UPPER SHOREFACE

Description

This facies association is confined to the Balcony Falls section (Figs. 6 and 12). Four facies are developed: 1) channelized, massive sandstone (Smc); 2) channelized, trough cross-bedded sandstone (Stc); 3) megarippled sandstone (Smr); and 4) feldspathic, trough cross-bedded sandstone (St). The latter facies demarcates the transition from the Unicoi Formation into the Hampton Formation.

Channelized, massive sandstone facies (Sm) is composed of upper medium- to coarse-grained quartzose sand. The base of the facies is channelized and truncates underlying beds of facies association E with a maximum relief of 0.80 m (Fig. 12; inset D). Grainsize decreases from the base to the top of the 0.5 to 4.6 m-thick bed. The bed is massive apart from rare troughs towards the top. The channelized, trough cross-bedded sandstone facies (Stc) is dominated by upper fine- to lower

Figure 12: Measured section through facies associations D and E at Balcony Falls. Insets illustrate details of facies. See figure 3 for location of section.

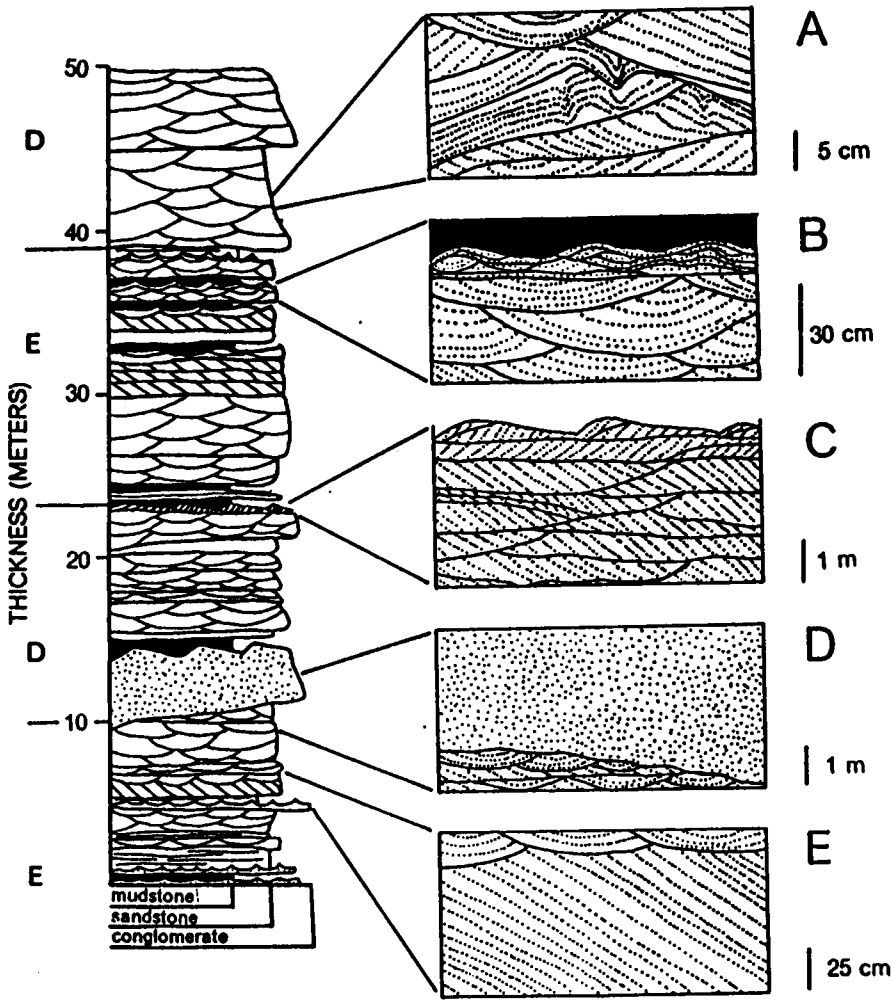

TROUGH CROSS-BEDDED SANDSTONE WITH *SKOLITHOS*(?) BURROWS (St)

TROUGH CROSS-BEDDED SANDSTONE CAPPED BY SYMMETRICAL WAVE-RIPPLED SANDSTONE (St → Swr)

TROUGH CROSS-BEDDED SANDSTONES WITH REACTIVATION SURFACES OVERLAIN BY STRAIGHT-CRESTED MEGARIPPLES WITH REACTIVATION SURFACES Stc → Smr

TRUNCATION SURFACE OVERLAIN BY MASSIVE SANDSTONE AND UNDERLAIN BY TROUGH CROSS-BEDDED SANDSTONE (St → Smc)

TABULAR-PLANAR SANDSTONE OVERLAIN BY TROUGH CROSS-BEDDED SANDSTONE (Sp → St)

coarse-grained, quartzose sand. Trough cross-beds vary in size from 0.25 m wide and 0.05 m deep to 1.25 m wide to 0.25 m deep. Trough cross-bed set size and grainsize decrease vertically in 0.5 to 3.8 m-thick cosets. Tabular-planar cross-beds are interspersed with the troughs and display reactivation surfaces (Fig. 12C; inset C). Trough axes are oriented in general to the southeast. Megaripples (Smr) are developed in medium-grained quartzose sandstone above the massive and trough cross-bedded sandstone intervals (Fig. 12). The megaripples capping the trough cross-bedded sandstones are exposed on bedding planes; bedforms are straight-crested megaripples with a northwest orientation and more sinuous-crested megaripples with a southeast orientation (Figs. 13A and 13A). The northwest-oriented megaripples have wavelengths of 0.89 m to 1.85 m and amplitudes of 3 to 17 cm. Ripple indices range from 8.5 to 30.7. Megaripples decrease in amplitude and wavelength to the southeast. Cross sections through megaripples display tabular-planar cross beds with reactivation surfaces (Fig. 12; inset C). Southeast-oriented megaripples have amplitudes of 3 to 4 cm and wavelengths of 40 to 50 cm. The Smc, Stc and Smr facies are stacked in a 13 m-thick vertical sequence (Fig. 12).

Feldspathic, trough cross-bedded sandstone facies (St) is composed of quartz with subordinate potassium feldspar and heavy minerals. Grainsize varies from granule to fine sand with potassium feldspar most abundant in the coarser fraction. Coarse sand and granules are restricted to the lower portion of the facies which fines upward through 5.6 to 4.8 m intervals. Trough cross beds are mostly medium scale (Fig. 13B) with both set and foreset thicknesses decreasing vertically in upward-fining intervals. *Skolithos* burrows disrupt laminations (Fig. 12; inset A). Trough axes give a southwesterly paleocurrent mode (Fig. 14B). This facies overlies the Sm, St, Smr vertical sequence (Fig. 12).

Figure 13: Photographs of facies association D. A) Megaripple facies. Photograph shows train of straight-crested megaripples. Amplitude of megaripples decreases towards top of photograph. Note hardhat for scale. B) Feldspathic, trough cross-bedded sandstone facies.

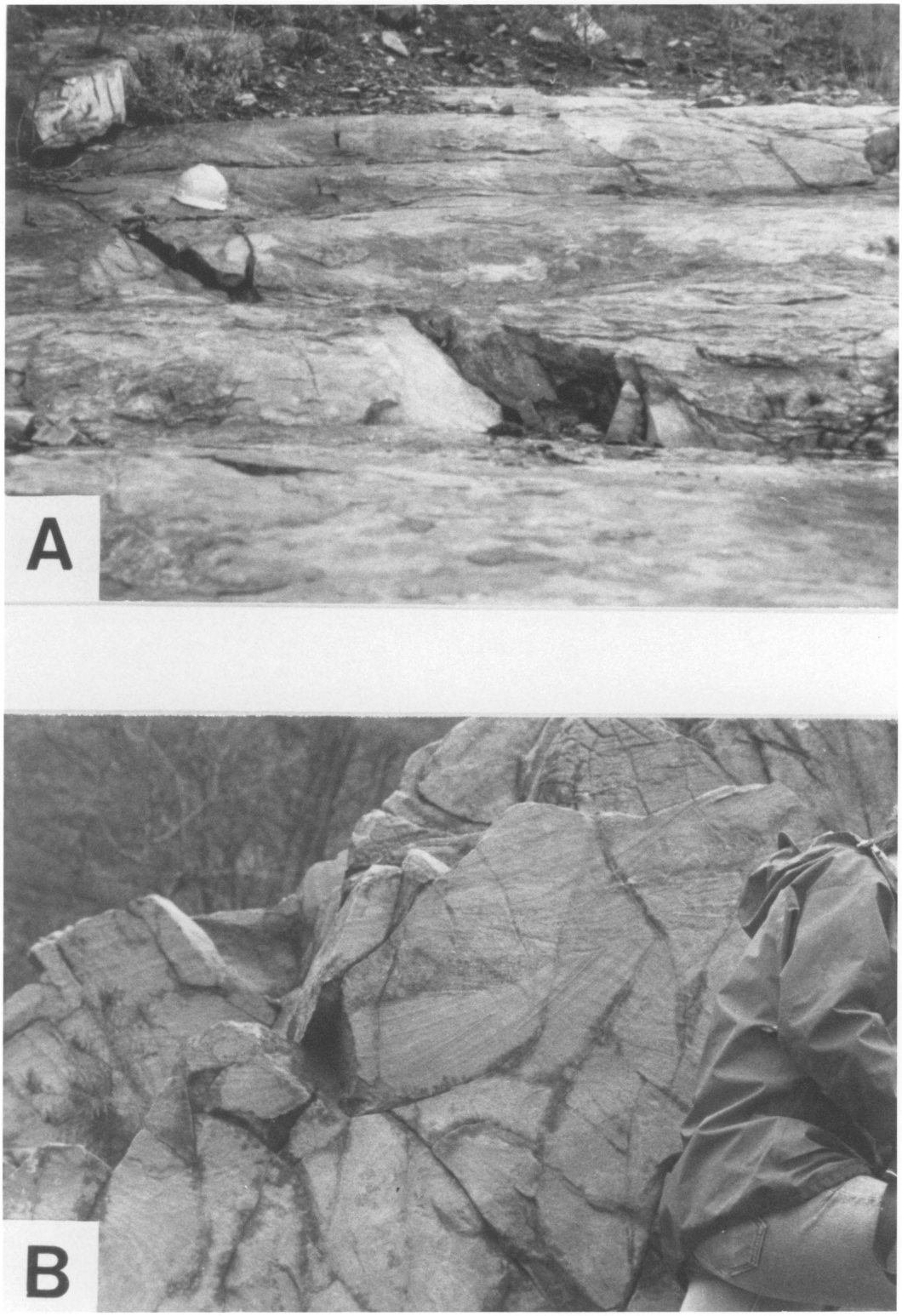
A
B

Figure 14: Paleocurrent diagram for facies associations D and E. N = number of observation; Vm = vector mean; Sd = standard deviation.

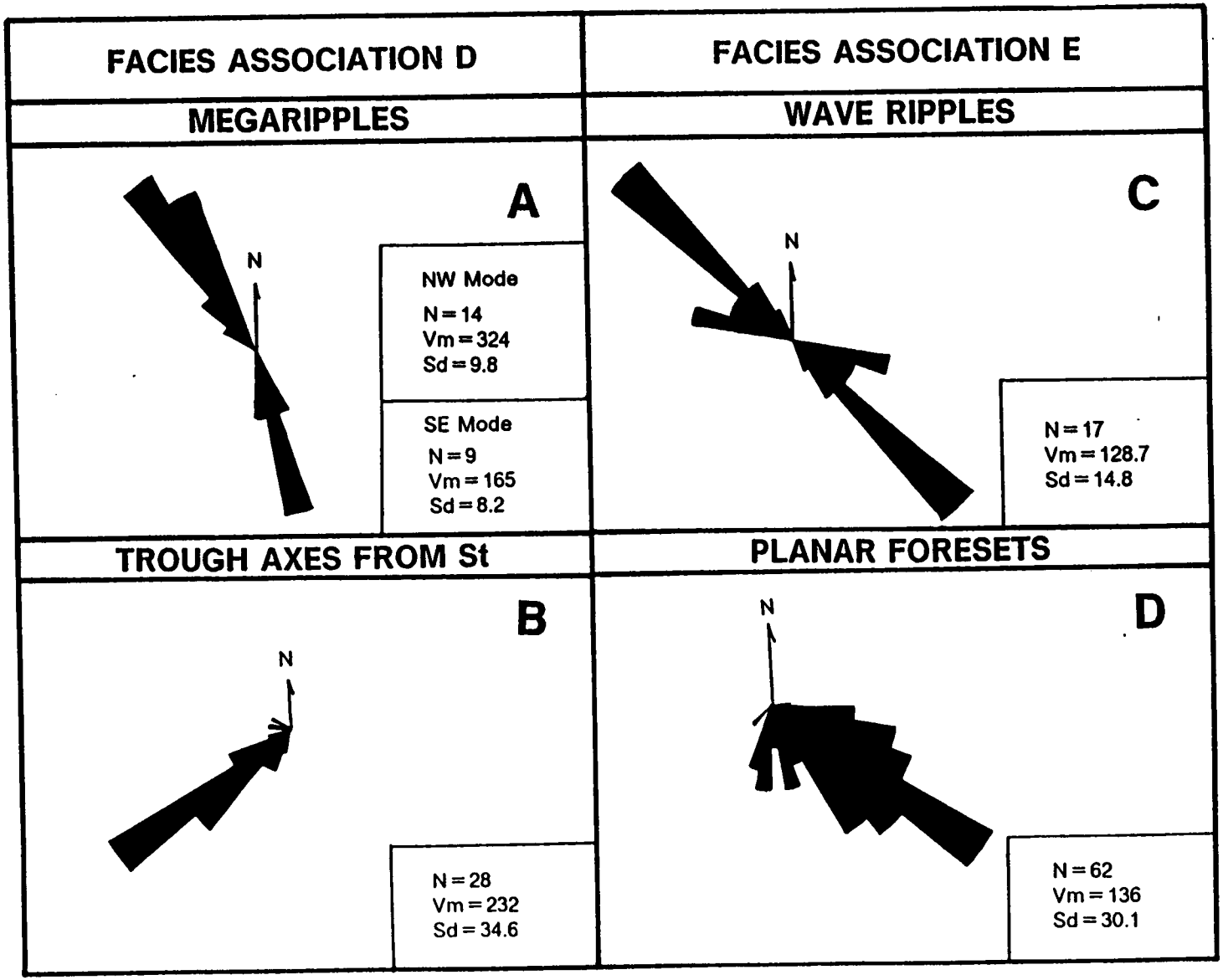
FACIES ASSOCIATION D
FACIES ASSOCIATION E
MEGARIPPLES
WAVE RIPPLES
A
N
NW Mode
N = 14
Vm = 324
Sd = 9.8
SE Mode
N = 9
Vm = 165
Sd = 8.2
C
N
N = 17
Vm = 128.7
Sd = 14.8
TROUGH AXES FROM St
PLANAR FORESETS
B
N
N = 28
Vm = 232
Sd = 34.6
D
N
N = 62
Vm = 136
Sd = 30.1

Interpretation

The geometry of the sediment body and the vertical sequence of structures exhibited by the channelized massive to trough cross-bedded to megarippled sandstone facies (Fig. 12) are comparable to that documented from tidal inlets (*cf.* Land, 1972; Kumar and Sanders, 1974; Hayes, 1980). As inlets migrate a basal scour surface results from erosion into underlying units. Truncation angles may be very slight over short distances (Moslow, 1984) and would resemble that at the base of facies association E (Fig. 12). Holocene tidal-inlet deposits characteristically display an upward-fining trend commencing with a basal lag of coarse pebbly sand or shell debris (Kumar and Sanders, 1974). The absence of a basal lag in this facies association is probably due to the lack of coarse-grained material in the system. Deeper parts of tidal inlets are generally dominated by offshore flow whereas shallow realms frequently contain bidirectional currents related to ebb and flood flow (Van Beeck and Koster, 1972). The relative position in vertical sequence, coupled with the paleocurrent data, are compatible with the trough and megarippled sandstone facies representing deep- and shallow-channel deposits, respectively. Associated reactivation surfaces reflect modification by subordinate currents of ebb-oriented bedforms in the deep channel, and flood-oriented bedforms in the shallow channel.

The depositional environment of the feldspathic, trough cross-bedded sandstone facies is problematical. Trough cross beds were produced by the migration of sinuous-crested megaripples at flow velocities greater than 0.5 m/sec (Harms *et al.*, 1982). *Skolithos* (?) burrows indicate a high-energy marine environment of deposition with mobile substrates (Seilacher, 1969). Paleocurrent data from this facies (Fig. 14B) indicate a shoreline-parallel transport direction. The barred high-energy shoreline of the Oregon coast is characterized by oblique and shore-parallel bars

(Hunter *et al.*, 1979). Longshore channels behind the bars contain megaripples migrating parallel to the shoreline. The feldspathic, trough cross-bedded facies probably formed in similar longshore channels or in a belt landward of the breaker zone but lacking bars. Heavy minerals concentrated in a swash zone were incorporated into the zone of longshore currents.

The recognition of tidal-inlet deposits and deposits produced by longshore currents establishes that this facies association accumulated in an upper-shoreface setting influenced by tides and waves. Shoreface, including tidal-inlet sequences typically are capped by swash deposits. Indirect evidence for a swash zone is provided by the heavy mineral concentrates but no swash laminations are present. Swash deposits have a low preservation potential along transgressive coastlines (Davis and Clifton, 1984) and evidence will be presented later for rapid drowning above facies association D.

FACIES ASSOCIATION E: INNER SHELF

Description

Facies association E is present in each of the measured sections (Fig. 6) and consists exclusively of quartzose sandstones. Four facies are recognized: 1) trough cross-bedded sandstone (St); 2) symmetrical-rippled sandstone (Sr); 3) tabular-planar, cross-bedded sandstone (Sp); and 4) compound, cross-stratified sandstone (Scp). The St, Sp and Sr facies are interbedded in each of the measured sections; they are erosionally overlain by facies association D at Balcony Falls and reoccur higher in the section (Fig. 12). Each of the facies are present in the Virginia Creeper section where facies associations B and E are interbedded in a transitional interval (Fig. 6).

The trough cross-bedded facies (St) consists of lower medium- to upper coarse-grained sandstone. Medium-scale, trough cross-bedding is the predominant

stratification type; a few isolated sets of tabular-planar cross beds are present. Beds are sharp based and tabular and vary from 0.75 m to 2.2 m in thickness. Paleocurrents are highly variable. In the Virginia Creeper Trail section, *Rusophycus* and *Paleophycus* were found on the basal bedding plane. Beds are often capped by symmetrical ripples (Swr) in medium-grained sandstone (Figs. 12; inset B and 15 A). Ripples are straight crested with wavelengths varying from 20 to 50 cm and amplitudes from 2 to 4 cm. Ripples are form discordant to internal cross stratification. Crest orientations indicate southeast-northwest oscillatory flow (Fig. 14C). Symmetrical ripples may be overlain by parallel-laminated and current-rippled sandstones.

The tabular-planar cross-bedded facies (Sp) is composed of medium- to lower coarse-grained sandstone. Beds consist of single, 0.15 to 1.00 m-thick cross-bed sets which are tabular and in rare exposures may be traced laterally for over 55 m. Foresets are normally graded and reactivation surfaces are present within some sets (Fig. 12B). Paleocurrents are to the southeast (Fig. 14D). Tabular-planar, cross-bed sets are often capped by small-scale, trough cross beds oriented orthogonal to the underlying set (Figs. 12; inset E and 15 C).

The compound cross-stratified facies (Scp) consists of granule conglomerate to medium-grained sandstone. Tabular-planar cross-bed sets are 2 to 35 cm thick and contain reactivation surfaces. Foresets display normal grading. Cross-bed sets are stacked in 0.8 to 1.5 m-thick cosets which are defined by bounding surfaces inclined at 3 to 4 degrees to bedding (Fig. 16). Megaripples which produced the internal cross stratification climbed up the bounding surfaces. Coset boundaries are demarcated by concentrations of coarse-grained sandstone or granule-to-pebble conglomerate (Fig. 15D). Rarely asymmetrical ripples in fine- to medium-grained sandstone define contacts between cosets. Cross beds within cosets yield southeasterly paleocurrent

Figure 15: Photographs of facies association E. A) Symmetrical-ripples. B) Tabular-planar cross bed with reactivation surface. C) Tabular-planar cross-bedded set capping small-scale trough cross beds oriented orthogonal to the underlying set. D) Coset boundary of compound cross-bedded sandstone facies demarcated by upper coarse-grained sandstone and granule-to-pebble conglomerate.

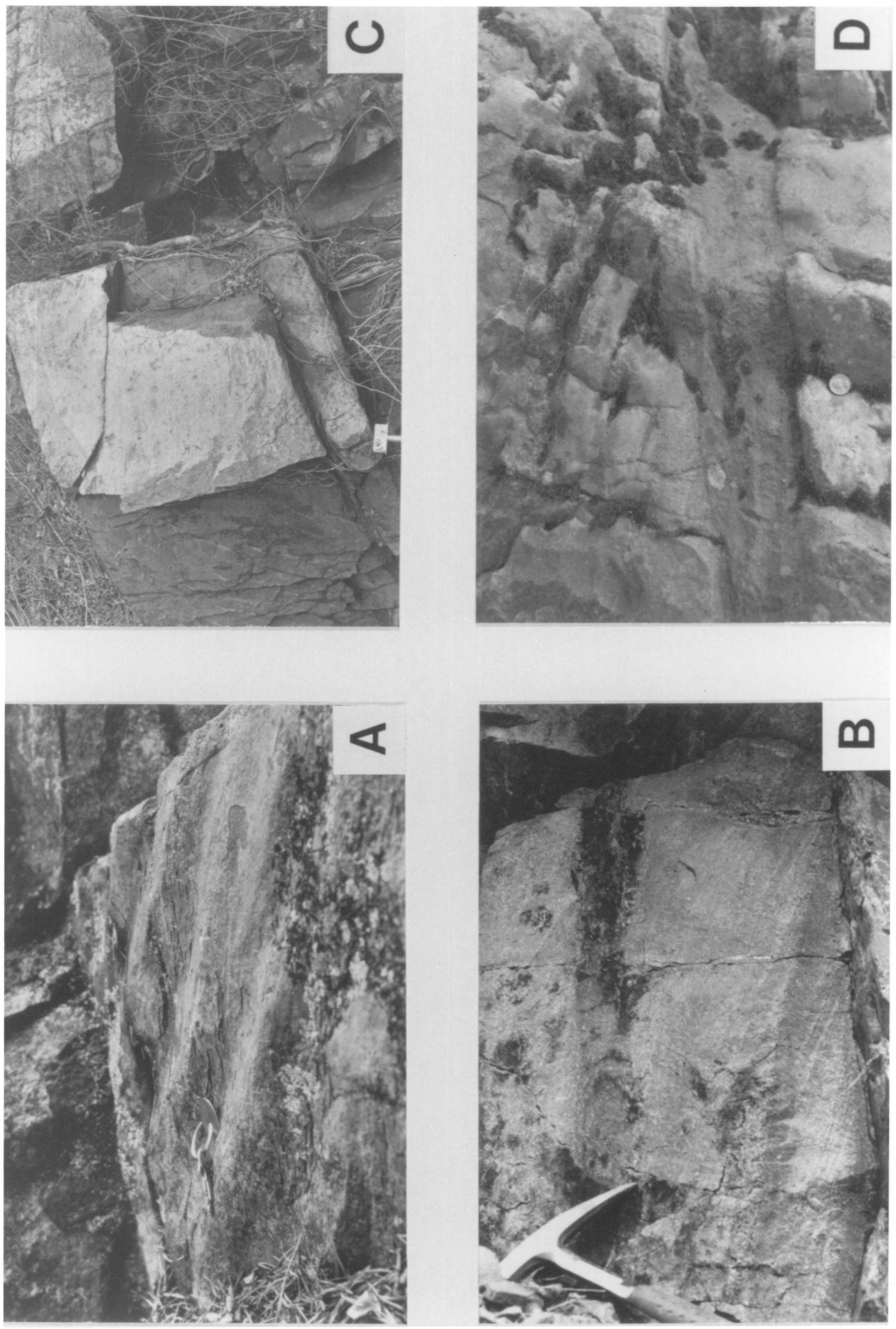
A
B
C
D

Figure 16: Schematic illustration of compound cross-stratified sandstone facies in facies association D from Virginia Creeper section.

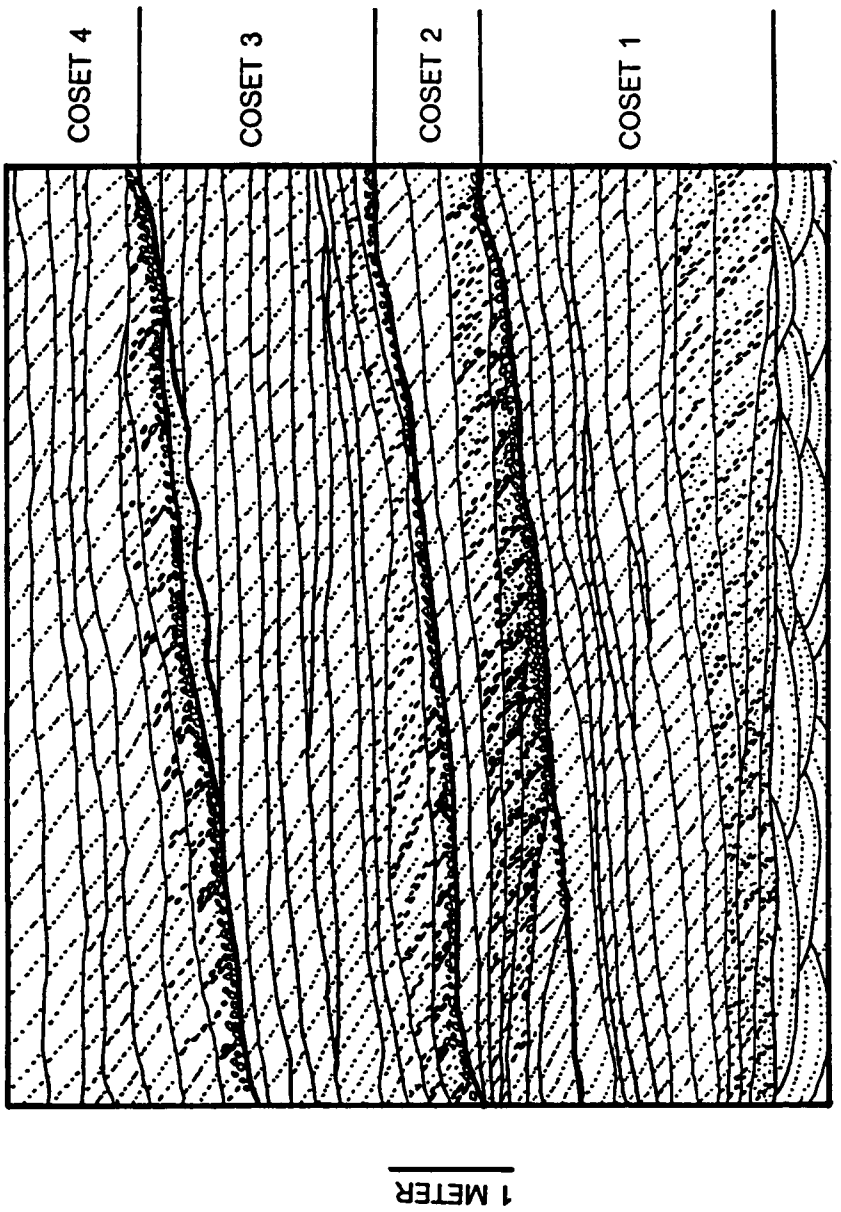
COSET 4
COSET 3
COSET 2
COSET 1
1 METER

directions (Fig. 14 D).

Interpretation

Compound cross-stratified sandstones reflect migration of a complex hierarchy of bedforms. Tabular-planar cross-bed sets were generated by migration of straight-crested megaripples or sandwaves up gently inclined surfaces of larger scale bedforms such as sandridges (Houbolt, 1968; Belderson *et al.*, 1982). The coset boundaries are comparable to E2 surfaces of Allen (1980); these are considered to form by erosion in the front of advancing sandridges with concentration of coarse debris. Crests of sandridges typically are aligned oblique to the strongest tidal current (Kenyon *et al.*, 1981), whereas superimposed sandwaves migrate in the direction of ebb or flood flow. Paleocurrent data for this facies indicate offshore or ebb flow; associated reactivation surfaces may have been generated by subordinate flood currents. The tabular-planar, cross-bedded facies resulted from migration of straight-crested megaripples in an offshore direction. Reactivation surfaces are best related to modification of megaripple crests by subordinate currents implying a tidal environment with time-velocity asymmetric flow (Klein, 1971). Nested troughs, orthogonal to the planar foresets indicate reworking by longshore currents.

The trough cross-bedded sandstone facies is more difficult to reconcile with a tidal regime but its close association with the other two facies suggests a similar depositional setting. Cosets of trough cross beds have been related to migration of sinuous-crested megaripples in a time-velocity symmetrical flow regime (Allen, 1980). Cessation of sediment supply was followed by deflation of the megaripple filed to produce the tabular cost geometries. Symmetrical ripples capping cosets were generated by fair-weather or storm reworking (*cf.* Rubin and Hunter, 1982; Harris and

Eriksson, in prep).

Sandwave and sandridge complexes typically are developed on tidal shelves (Allen, 1980; Walker, 1984; Baldwin and Johnson, 1985). Evidence of fair-weather or storm wave reworking places this facies association in an inner-shelf setting. *Rusophycus* and *Paleophycus* ichnofossils on bedding planes in the trough cross-bedded sandstones support this interpretation; both develop below fair-weather but above storm wave base (Seilacher, 1967; Frey and Seilacher, 1980).

FACIES ASSOCIATION F: OUTER SHELF

Description

This facies association makes up the base of the Hampton Formation and is present in each of the measured sections (Fig. 6). It conformably overlies facies association D or E. Facies association F consists of mudstones which typically contain siltstone laminations, and Tabc, Tbc and Tc Bouma sequences. A 15 m-thick interval made up of normally graded conglomerate beds and intercalated mudstones is present at the base of the Hampton Formation in the Virginia Creeper Trail section (Fig. 17A).

Tabc beds range in thickness from 0.5 to 6.0 cm and are graded from medium and rarely granule, to lower fine sandstone or siltstone. Tbc beds attain a maximum thickness of 3 cm and are graded from lower medium to lower fine sandstone or siltstone. Tc beds consist of starved ripples in mudstones; ripples reach 1.5 cm in height and consist of upper fine sandstone to siltstone. Cross laminations characteristically are graded.

Normally graded, clast-supported, conglomerate beds possess erosional bases with a few cm relief. Bed thicknesses range from 1.5 to 4.8 m and decrease in

Figure 17: Photographs of facies association F from Elk Creek. A) Erosional contact (arrow 1) between facies association E and conglomerate at base of facies association F. Large mudstone clast located at arrow (2). B) Conglomerate at base of debris flow. Clasts are vein quartz (1), medium-grained sandstone (2), and mudstone (3). Note compaction textures in the mudstones (arrow).

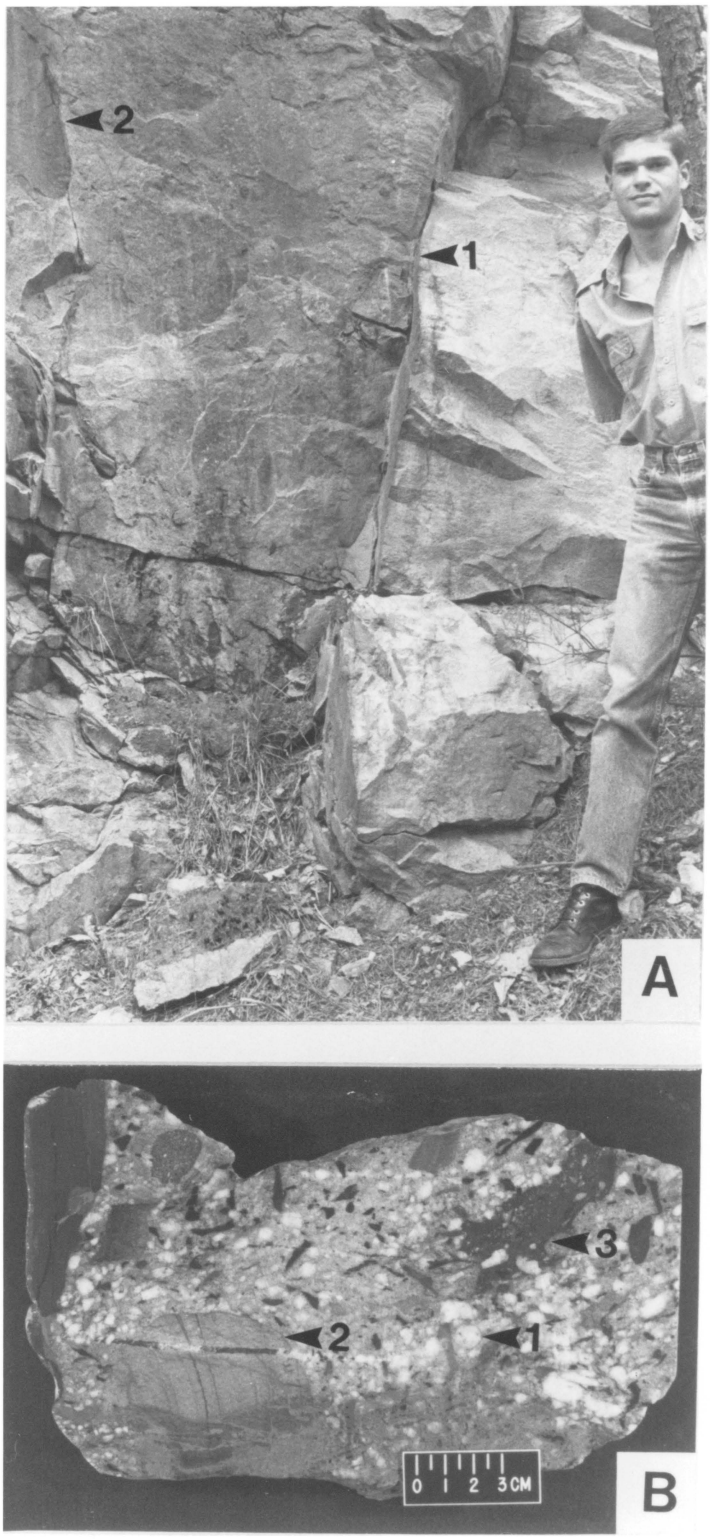
2
1
A
3
2
1
0 1 2 3CM
B

thickness upward. Groove casts are common on basal erosional surfaces. Conglomerates contain clasts of well-rounded vein quartz, medium-grained sandstone, siltstone and mudstone (Fig. 17B). Quartz clasts range in size from fine sand to pebbles with diameters 2 to 4 cm-diameters. Long axes of mudstone clasts are from 1.0 cm to 2.1m in length and display soft-sediment deformation. Beds may be capped by horizontally laminated siltstone containing small-scale load and dewatering structures.

Black pyritic mudstones without bioturbation are present above the conglomeratic interval in the Virginia Creeper Trail section and sharply overlie facies association E in the Elk Creek section. Green, bioturbated mudstones occur at the base of the Hampton Formation at Balcony Falls. The proportion and thickness of Tabc, Tbc and Tc beds increase upward in the Hampton Formation at each locality and is accompanied by an increase in bioturbation of intercalated mudstone with siltstone laminations.

Interpretation

The lack of wave-produced structures in facies association F indicate that sedimentation took place exclusively below wave base. On the basis of an upward transition into wave-produced facies, Simpson and Eriksson (submitted) argue that facies association F accumulated in an outer-shelf setting. Tabc, Tbc and Tc beds are interpreted as turbidites and the associated, predominant mudstone facies as suspension deposits. Intensity of bioturbation is a function of oxygen content at the sediment-water interface.

Normally graded, clast-supported conglomerates in association with the other gravity-flow deposits are interpreted as the product of high concentration turbidity

currents (Walker, 1978). Such currents may be generated by slope failures, seismic shock, sediment creep or rivers in flood (Stow, 1985). The turbidity currents had sufficient velocity and strength to erode underlying sedimentary layers and derives mudstone and sandstone clasts. Vein-quartz clasts are exotic to the stratigraphic section and were introduced from outside the depositional environment. The stratigraphically closest quartz pebble conglomerates are in the Unicoi Formation.

DEPOSITIONAL AND TECTONIC MODEL

The Unicoi Formation and the basal portion of the Hampton Formation record the late stages of rifting and the inception of an east-facing passive margin that bordered the Iapetus Ocean. Stratigraphic thicknesses of the Unicoi and lower Hampton Formation in conjunction with the distribution of underlying stratigraphic sequences (Fig. 18), indicate that the Virginia Creeper Trail section developed on more attenuated continental crust than the Elk Creek section. The Balcony Falls sequence accumulated on the least attenuated crust. Difference in degree of attenuation controlled the distribution of sedimentary environments within the various stratigraphic sections.

The initial stage of rifting related to the opening of the Iapetus Ocean is recorded in the Crossnore plutonic suite (690±10 Ma; Odom and Fullgar, 1984) and in sedimentary and volcanic strata of the Swift Run and Mount Rogers Formations and Lynchburg Group (Odom and Fullagar, 1973; Rankin, 1975; Wehr, 1985; 1986; Wehr and Glover, 1985; Miller, 1986). Rift-related Catoctin basalts were extruded at *ca.* 570 Ma ago onto the Lynchburg Group and Swift Run Formation (Wehr and Glover, 1985).

The contact between the Unicoi Formation and the Mount Rogers Formation in the Virginia Creeper Trail section may be unconformable (Fig. 18; T1), but time

Figure 18: Diagrammatic reconstruction of the late Precambrian-Cambrian rift to passive-margin transition in central and southern Virginia; time lines T3, T4, and T5 are interpretive. Contacts between the Grenville basement and Unicoi Formation are demonstrably autochthonous. Palinspastic restoration of the three sections based on Boyer and Elliott (1982) gives an approximate North-South transect of the continental margin. The three sections are related in this figure in an interpretive cross section orthogonal to the inferred strike of the continental margin.

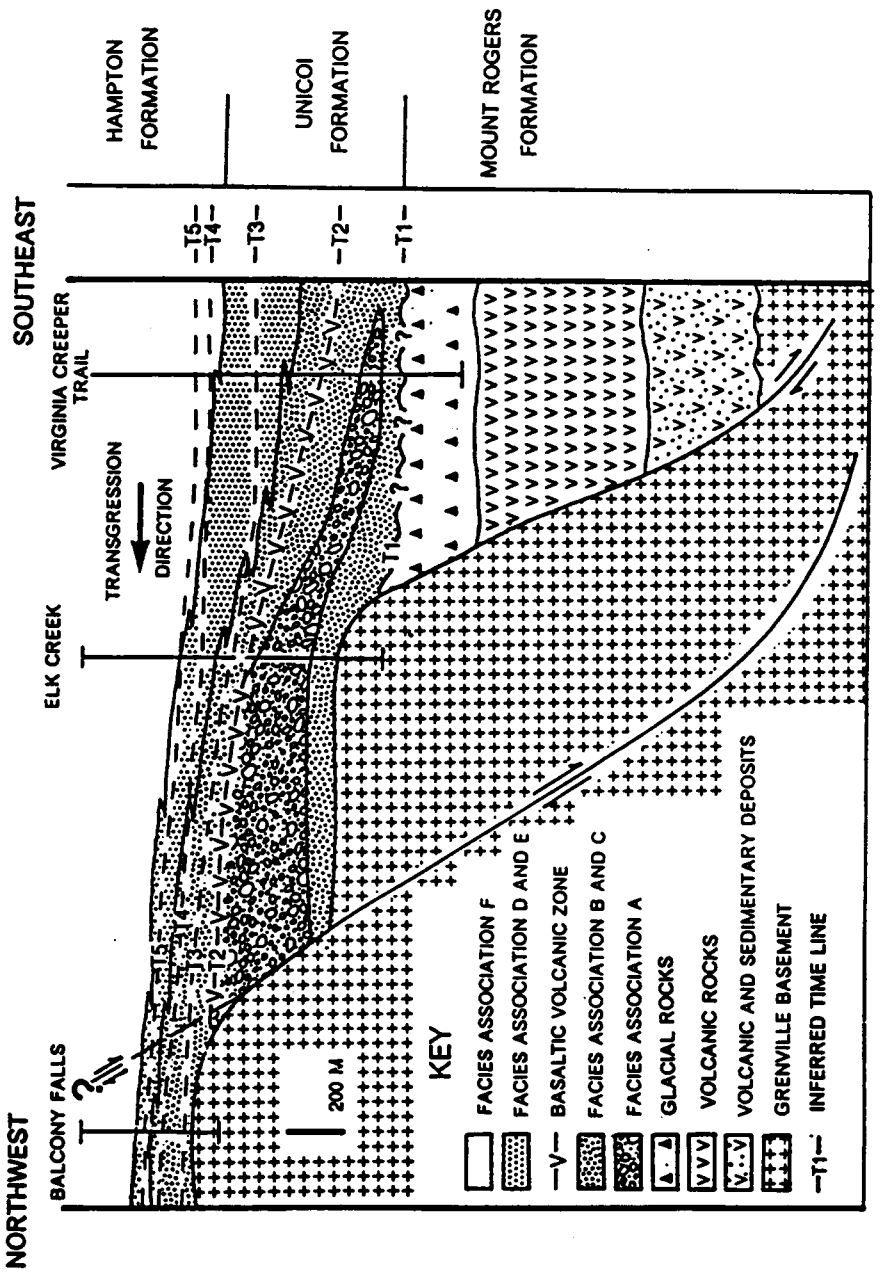
NORTHWEST
SOUTHEAST
BALCONY FALLS
ELK CREEK
VIRGINIA CREEPER TRAIL
TRANSGRESSION DIRECTION
HAMPTON FORMATION
UNICOI FORMATION
MOUNT ROGERS FORMATION
T5
T4
T3
T2
T1
200 M
KEY
FACIES ASSOCIATION F
FACIES ASSOCIATION D AND E
BASALTIC VOLCANIC ZONE
FACIES ASSOCIATION B AND C
FACIES ASSOCIATION A
GLACIAL ROCKS
VOLCANIC ROCKS
VOLCANIC AND SEDIMENTARY DEPOSITS
GRENVILLE BASEMENT
INFERRED TIME LINE

represented by or the areal extent of this surface are unknown. The unconformity may not be a break-up unconformity as proposed by Wehr and Glover (1985), but could be genetically related to the Mount Rogers glacial event. Detailed mapping of a similar type of unconformable contact between the Proterozoic Wildrose diamictite of the Kingston Peak Formation and the passive-margin Noonday Dolomite in the Panamount range of California has demonstrated the local extent of the unconformity previously thought to be a break-up unconformity (Miller, 1987). In areas a conformable transition from rift to passive-margin sediments is apparent.

Rifting continued to influence sedimentation into Unicoi time and extended beyond the limits of the basin in which the Mount Rogers Group accumulated (Fig. 18). Evidence for this faulting is reflected in thick distal alluvial-fan sediments of facies association A in the Elk Creek section and coeval proximal-to-medial braidplain deposits of facies association B in the Virginia Creeper Trail section (Fig. 18). Alluvial fans are most common adjacent to fault scarps and coarse-grained sheet-flood deposits thus are restricted to tectonically active areas. Settings from which coarse-grained, sheet-flood deposits have been reported include alluvial aprons sourced by rift-related volcanoes (Nemec and Muszynki, 1982) and grabens (Hubert and Hyde, 1982; Wells, 1984).

In facies associations A and B in the Elk Creek section, sequences of facies may be attributed to channel switching (*cf.* Heward 1978, Hubert and Hyde, 1983). Coarsening- and thickening-upward megasequences probably reflect renewed movement along faults whereas thinning- and fining-upward sequences are the product of denudation of the source area (*cf.* Hubert and Hyde, 1983). Megasequences are not developed in facies association A and B in the Virginia Creeper Trail section probably because sedimentation occurred distal to an active fault; this hypothesis is supported by thin alluvial-fan deposits in the Virginia Creeper Trail section (Fig. 18).

The overall upward decrease in grain size in facies associations A and B records long-term retreat and denudation of the source area (*cf.* Heward, 1978). Progressive infilling of the basin and resultant decrease in slope would account for the upward increase in tractional structures in megasequences. Widely dispersed paleocurrents in facies association B (Fig. 10A) are a reflection of the tectonically active nature of the basin during accumulation of facies associations A and B prior to T2 (Fig. 18).

Continued rifting is reflected by volcanic rocks in the Unicoi Formation (Fig. 6); basaltic volcanics are common in many rift settings (Crosely, 1979; Burke and Kidd, 1980). Fossils recovered from the alluvial to marine transition in the Virginia Creeper Trail section (facies association B to E; Fig. 6), suggest that rifting may have extended into the Cambrian in the central Appalachians. Basalts and associated braidplain sediments in the Elk Creek and Virginia Creeper Trail section represent a crude time line (Fig. 18, T2), and may be coeval with the Catoctin Formation to the north of the study area (Fig. 4). Catoctin volcanics and intercalated alluvial sediments are overlain by a thin equivalent of the Unicoi Formation comparable to that in the Balcony Falls section (Fig. 18). Volcanics are not present in the Balcony Falls section but evidence for their previous existence at or in close proximity to that locality is present in the form of volcanic debris in the basal Unicoi Formation.

Braided-alluvial sedimentation continued following basalt extrusion. Paleocurrents above the basalts display a shift towards a more consistent southerly mode (Fig. 10B) which reflects elimination of topography produced by active faulting. Facies associations D and E developed during east-to-west transgression of the braidplain (Fig. 18; T3 to T5). The intertounging braided alluvial and tidal inner-shelf deposits in the Virginia Creeper Trail section (Fig. 6) represents an environment analogous to a braid delta (McGowen, 1970; McPherson, *et al.*, 1986). Intercalation of sediments from the two environments may be a result of small-scale, sea-level

fluctuations or channel avulsion followed by subsidence. No such intercalation of alluvial and marine sediments is developed in the Elk Creek and Balcony Falls sections where facies association C is abruptly overlain by inner-shelf and shoreface, as well as tidal inlet deposits at Balcony Falls. The feldspathic shoreface arenites capping the Unicoi Formation at Balcony Falls may reflect renewed faulting or proximity to a fluvial source to the west.

As transgression continued, faults may have been reactivated to produce the conglomeratic, gravity-flow deposits at the base of the Hampton Formation in the Elk Creek section (Fig. 18). The thinning-upward sequence of beds in the conglomeratic interval may be related to fault-scarp retreat or reduction in fault-scarp relief. Overlying outer-shelf black mudstones at this locality as well as those which abruptly overlie inner-shelf arenites in the Virginia Creeper Trail section indicate anoxic conditions related to rapid drowning which may have been enhanced by continued movement on listric faults. In the Balcony Falls section, bioturbated, outer-shelf facies resting on shoreface deposits may reflect higher oxygen contents related to shallower water depths than to the east.

The transgression recorded in the upper Unicoi and Hampton Formations represents the initial stage of the Cambrian to Mississippian first-order, sea-level rise of Vail *et al.* (1977). This transgression has been related to the generation of mid-ocean ridges (Pittman, 1977) associated with break-up of the Eocambrian supercontinent (Matthews and Cowie, 1979; Donovan and Jones, 1979; Bond *et al.* 1983). The initial transgression occurred on more attenuated continental crust and advanced landward. This diachronous transgression represents the incipient phase of passive-margin development. The majority of the Hampton and the Erwin Formation and Shady Dolomite (Fig. 5) record progradation of the passive margin with superimposed, smaller-scale sea level fluctuations (Simpson and Eriksson, submitted).

CONCLUSIONS

1) The Unicoi and lower Hampton Formations in the central Appalachians record the transition from rift to passive margin sedimentation associated with opening of the Iapetus Ocean.

2) Alluvial-fan and proximal and medial braid-plain deposits, and basalts in the Unicoi Formation reflect rifting of the continental margin which continued possibly into lower Cambrian time.

3) The incipient phase of passive-margin sedimentation is represented by transgressive deposits at the top of the Unicoi Formation and is related to a first-order sea level rise. On most attenuated crust to the east, initial transgressive facies consisted of tidal sandwave and sandridge deposits. As transgression progressed cratonwards tidal sedimentation was supplanted by tide- and wave-influenced sedimentation.

4) Drowning at the top of the Unicoi Formation is indicated by outer-shelf black mudstones containing Tabc, Tbc and Tc beds and gravity flow deposits at the base of the Hampton Formation. Deepening may have been enhanced by continued movement along listric faults throughout the incipient phase of passive-margin development.

5) The majority of the Hampton Formation and the overlying Erwin Formation and Shady Dolomite record progradation of the passive margin.

INTERTIDAL TO OUTER-SHELF SEDIMENTATION ON A WAVE- AND STORM-DOMINATED SHELF: THE LOWER CAMBRIAN ERWIN AND HAMPTON FORMATIONS IN THE CENTRAL APPALACHIANS, VIRGINIA

ABSTRACT

Examination of outcrops of the Hampton and Erwin Formations on different thrust sheets has permitted an across-strike reconstruction of the Early Cambrian Chilhowee shelf in space and time. The Hampton and Erwin Formations represent an overall regressive sequence punctuated by five progradational packages. These packages exhibit a systematic vertical variation in depositional environments across different thrust sheets with replacement of shallower- by deeper-water environments from west to east.

Five environmental settings are reflected in facies associations within the Hampton and Erwin Formations. Intertidal flat sedimentation was dominated by flood-currents and late-stage ebb runoff. Upper shoreface sediments display evidence of reworking by longshore currents generated by shoaling fair-weather or waning storm waves. Lower shoreface and proximal inner-shelf facies consist of detritus transported from the nearshore and reworked *in situ* by the complex interaction of storm-surge ebb-return flow and waning storm waves. Distal inner-shelf sediments resulted from storm-wave reworking below fair-weather wave base. Sedimentation in the outer shelf setting was dominated by geostrophic flows and suspension settling of muds under fair-weather conditions.

Progradational packages developed under storm- and fair-weather wave conditions. Coarsening- and thickening-upward sequences on westerly thrust sheets were generated during progradation of shoreface, inner-shelf and outer-shelf

environments. Outer-shelf facies predominate on easterly thrust sheets. Intertidal-flat deposits on the most westerly thrust sheet erosively overlie progradational shoreface sediments and developed during transgression in an embayment in which the tidal wave was amplified. More distal transgressive deposits consist of fining- and thinning-upward sequences with glauconitic horizons, and condensed sections in mudstones.

INTRODUCTION

The upper Precambrian to lower Cambrian Chilhowee Group in southwestern and central Virginia consists of the basal Unicoi Formation overlain by the Hampton and Erwin Formations. On the basis of textural and compositional maturity, paleocurrent patterns and presence of trace fossils, arenites in the Hampton and Erwin Formations and equivalents were interpreted as shallow-marine deposits (Schwab, 1970; 1971; 1972; Mack, 1980). However, specific depositional processes and subenvironments are not well understood.

Recent investigations show that tidal, storm, wave and eolian processes generate unique suites of sedimentary structures, which can be used to discriminate depositional environments (*e.g.* Hunter, 1977; Hamblin and Walker, 1979; Visser, 1980; Boersma and Terwindt, 1981; Kocureck and Dott, 1981; Dott and Bourgeois, 1982; Kreisa, 1981; de Mowbray and Visser, 1984; Dott *et al.*, 1986; Kreisa and

Moiola, 1986). A variety of sedimentary features thought to be restricted to tidal environments, for example, herringbone cross bedding, reactivation surfaces and bimodal-bipolar paleocurrent trends (Klein, 1977), are now recognized from diverse depositional environments (Collinson, 1970; Allen, 1973; McCabe and Jones, 1977; Alam *et al.*, 1985). Neap/spring cyclicity is a criterion that unequivocably proves tidal overprinting within a subtidal regime. Rhythmic, mudstone-draped bundles of foresets in subtidal sandwaves consisting of fine-grained sandstones exhibit neap/spring cyclicity of a synodic month (Visser, 1980; J. R. L. Allen, 1981; Boersma and Terwindt, 1981; Nio *et al.*, 1983; de Mowbray and Visser, 1984; Yang and Nio, 1985; Kreisa and Moiola, 1986); rhythmic, reactivation surfaces defining foreset bundles in coarse-grained tidal deposits also exhibit neap/spring periodicity (Allen and Homewood, 1984; Harris and Eriksson, in prep). Wave-generated sedimentary structures and hummocky cross stratification provide unambiguous evidence for storm and wave activity (de Raaf, *et al.*, 1977; Hamblin and Walker, 1981; Harms, *et al.*, 1982; Dott and Bourgeois, 1982; Hunter and Clifton, 1982; Swift *et al.*, 1983; Walker *et al.*, 1983). Microstructures generated in eolian environments, such as inversely graded, subcritically climbing translatent stratification (Hunter, 1977; Kocureck and Dott, 1981), adhesion structures (Kocureck and Fielder, 1982) and corrugated set boundaries (Simpson and Loope, 1985), facilitate discrimination of eolian processes on a microscopic and mesoscopic scale.

In light of the above studies, it is now possible to better constrain depositional systems represented within the Hampton and Erwin Formations where exposed in the Blue Ridge Province (Fig. 19). The occurrence of the Hampton and Erwin Formations within a number of thrust sheets subparallel to depositional strike presents

Figure 19. Geologic map of portion of the Blue Ridge Province (modified from Wehr and Glover, 1985). Inset shows locations of study area in relation to surrounding states. Localities of measured sections are: 1) Damascus; 2) Laurel Creek (Virginia Creeper Trail section); 3) Short Mountain; 4) Elk Creek; 5) Poplar Camp Quarry; 6) Poplar Camp; 7) Buchanan; 8) Arcadia; 9) Natural Bridge Quarry; 10) James River sections including Balcony Falls section; 11) Buena Vista; and 12) Vesuvius.

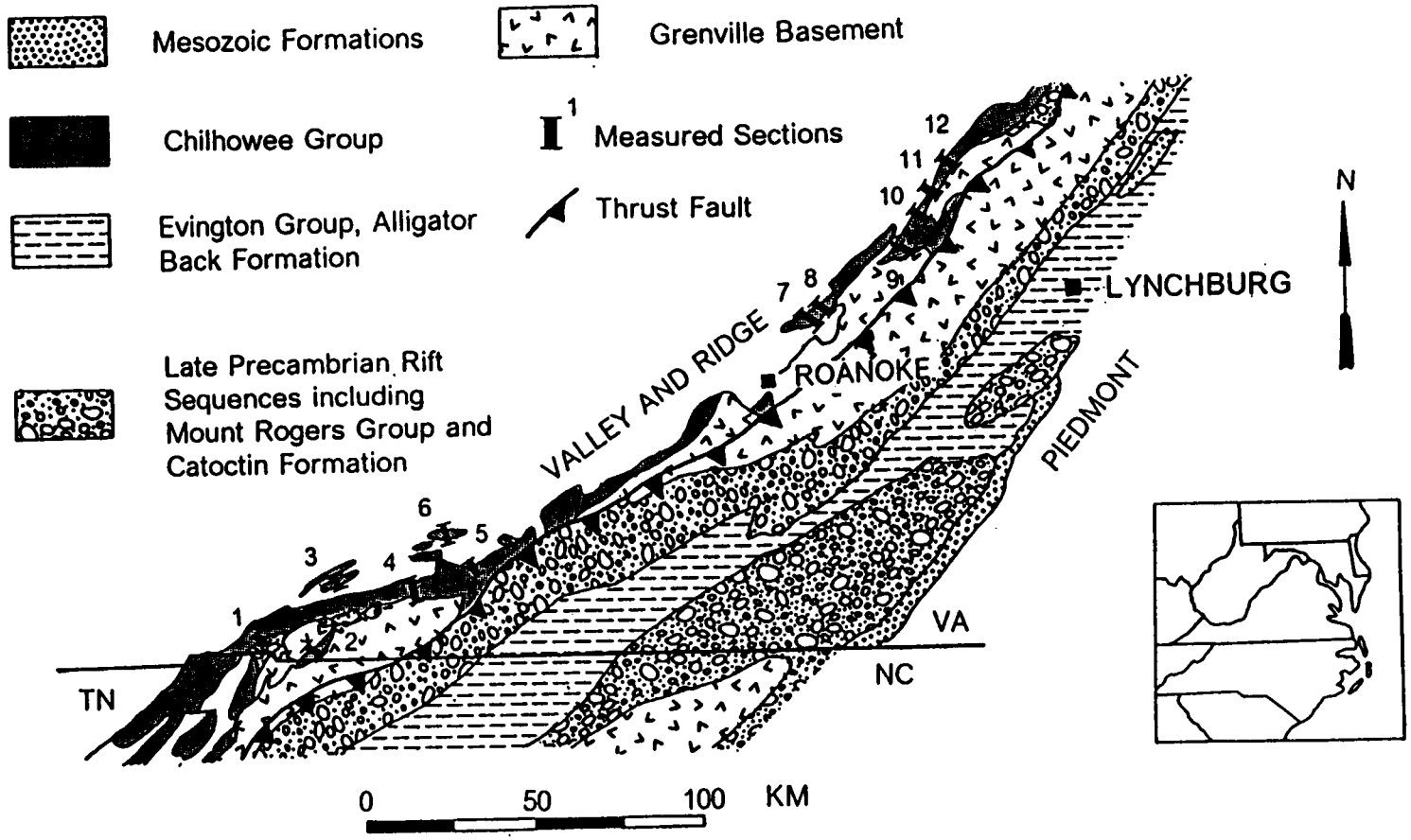
Mesozoic Formations
Grenville Basement
Chilhowee Group
Measured Sections
Thrust Fault
Evington Group, Alligator Back Formation
Late Precambrian Rift Sequences including Mount Rogers Group and Catoctin Formation
VALLEY AND RIDGE
PIEDMONT
ROANOKE
LYNCHBURG
TN
VA
NC
N
1
2
3
4
5
6
7
8
9
10
11
12
0
50
100
KM

an unique opportunity to reconstruct proximal-to-distal facies transitions across the paleoslope. In this way it is possible to characterize depositional processes and environments which existed along the Cambrian Iapetus passive margin, and provide a framework within which to understand changes in depositional processes in both space and time. This study thus has an advantage over previous detailed facies analyses of the Chilhowee Group which were confined to a single thrust sheet (*cf.* Cudzil and Driese, in press).

STRATIGRAPHY

In central and southwestern Virginia and northeastern Tennessee, the Chilhowee Group consists of three formations from oldest to youngest: 1) Unicoi; 2) Hampton; and 3) Erwin Formations (Fig. 20). In northern Virginia and Maryland correlative formations are the Weaverton, Harpers and Antietam Formations (Fig. 20); for simplicity Unicoi, Hampton and Erwin are substituted for these northern equivalents. The Unicoi Formation overlies Catoctin Formation greenstones in northern Virginia, Grenville basement in central Virginia, and Grenville basement and Mount Rogers Group in southwestern Virginia (Fig. 19). Alluvial, feldspathic sandstones and conglomerates, and subordinate basalts constitute the lower Unicoi Formation. The upper Unicoi Formation consists of tide- and wave-influenced, shallow-marine shelf sandstones (Simpson and Eriksson, submitted). Five, shallow-marine, progradational sequences are superimposed on a regressive package that constitutes the overlying Hampton and Erwin Formations. Distal-shelf, slope and rise deposits of the Evington Group outcrop on the eastern limb of the Blue Ridge Anticlinorium and are considered to be temporal equivalents of the Chilhowee Group (Fig. 19; Wehr and Glover, 1985;

Figure 20. Stratigraphic correlation chart for the Chilhowee Group from northeastern Tennessee to northern Virginia.

	EASTERN TENNESSEE	NORTHEASTERN TENNESSEE SOUTHWESTERN AND CENTRAL VIRGINIA	NORTHERN VIRGINIA AND MARYLAND
	SHADY DOLOMITE	SHADY DOLOMITE	TOMSTOWN DOLOMITE
CHILHOWEE GROUP	HESSE QUARTZITE MURRAY SHALE NEBO QUARTZITE	ERWIN FORMATION	ANTIETAM FORMATION
	NICHOLS FORMATION	HAMPTON FORMATION	HARPERS FORMATION
	COCHRAN FORMATION	UNICOI FORMATION	WEAVERTON FORMATION
	OCOEE GROUP	MOUNT ROGERS FORMATION OR BASEMENT	CATOCTIN FORMATION

Schwab, 1986; Patterson; 1987). Previous studies of the Chilhowee Group and related strata have established a general northeast to southwest orientation for depositional strike (Brown, 1970; Schwab, 1970; 1971; 1972; Wehr and Glover, 1985).

Biostratigraphic resolution within the Chilhowee Group is limited. Cambrian body fossils are known from the Erwin Formation and its equivalents (Walcott, 1891; Stose and Stose, 1957; Laurence and Palmer, 1963; Wood and Clendening, 1982). A fragment of a hyolithid in the lower Hampton Formation and *Rusophycus* in the Unicoi Formation, establish the age of the Chilhowee Group as mostly Early Cambrian (Simpson and Sundberg, 1987).

TECTONIC SETTING

The Unicoi Formation records the waning stages of rifting through the initial development of a passive margin bordering the Iapetus Ocean (Simpson and Eriksson, submitted). The Hampton and Erwin Formations and overlying Shady Dolomite record the evolution of the passive margin from a prograding siliciclastic shelf to a carbonate ramp followed by a rimmed shelf (Barnaby and Simpson, 1987). Passive-margin strata extend from Georgia to Newfoundland (Mack, 1980; Hiscott, 1983; Bond *et al.*, 1984; Fichter and Diecchio, 1986; Simpson and Sundberg, 1987). In response to plate collision during the Taconic orogeny (Middle to Late Ordovician), rift and passive-margin strata were incorporated into the foreland fold-and-thrust belt (Wehr and Glover, 1985).

METHODOLOGY

On different thrust sheets, stratigraphic sections were measured on a cm-by-cm scale recording grain size, mineralogy, sedimentary structures, and bedding morphology. Samples were collected for slabbing and thin-sections. Based on detailed facies analysis, processes are reconstructed at the facies level. Facies are grouped into five associations at which level shelf subenvironments are interpreted within different thrust sheets.

FACIES ASSOCIATION A: INTERTIDAL FLAT

Description

Thin- to medium-bedded, upper medium- to lower coarse-grained, quartz sandstone and subordinate mudstone characterize this association which is present only in the Natural Bridge Quarry (Fig. 19). This facies association attains a maximum thickness of 1.65 m (Figure 21). Erosional contacts separate facies association A from underlying and overlying sediments of facies association B (Fig. 21).

The basal erosional surface displays a diverse suite of exhumed bedforms including current ripples, megaripples, and isolated, random, scoop-shaped depressions, and topographic highs. Current ripples are developed extensively on this surface in medium-grained sandstone; crests are straight to slightly sinuous and wavelengths average 20 cm. Ripples yield a dominant southwest and a subordinate

Figure 21. Stratigraphic section of facies association A at Natural Bridge Quarry. Facies association A is in erosional contact with sediments below and above. Stratigraphic sequence consists of interlayered mudstone and thin- and medium-bedded sandstone. Medium-bedded sandstones labelled A through D. A) Sigmoidal, sand-filled trough of type II megaripple. Fill is capped by wave-generated cross laminations. Sandstone bed is underlain and overlain and underlain by interbedded mudstone and fine-grained, wave-rippled sandstone. Vertical lines are *Skolithos* burrows. B) Unidirectional and wave-produced cross laminations in thin-bedded, fine-grained sandstone.

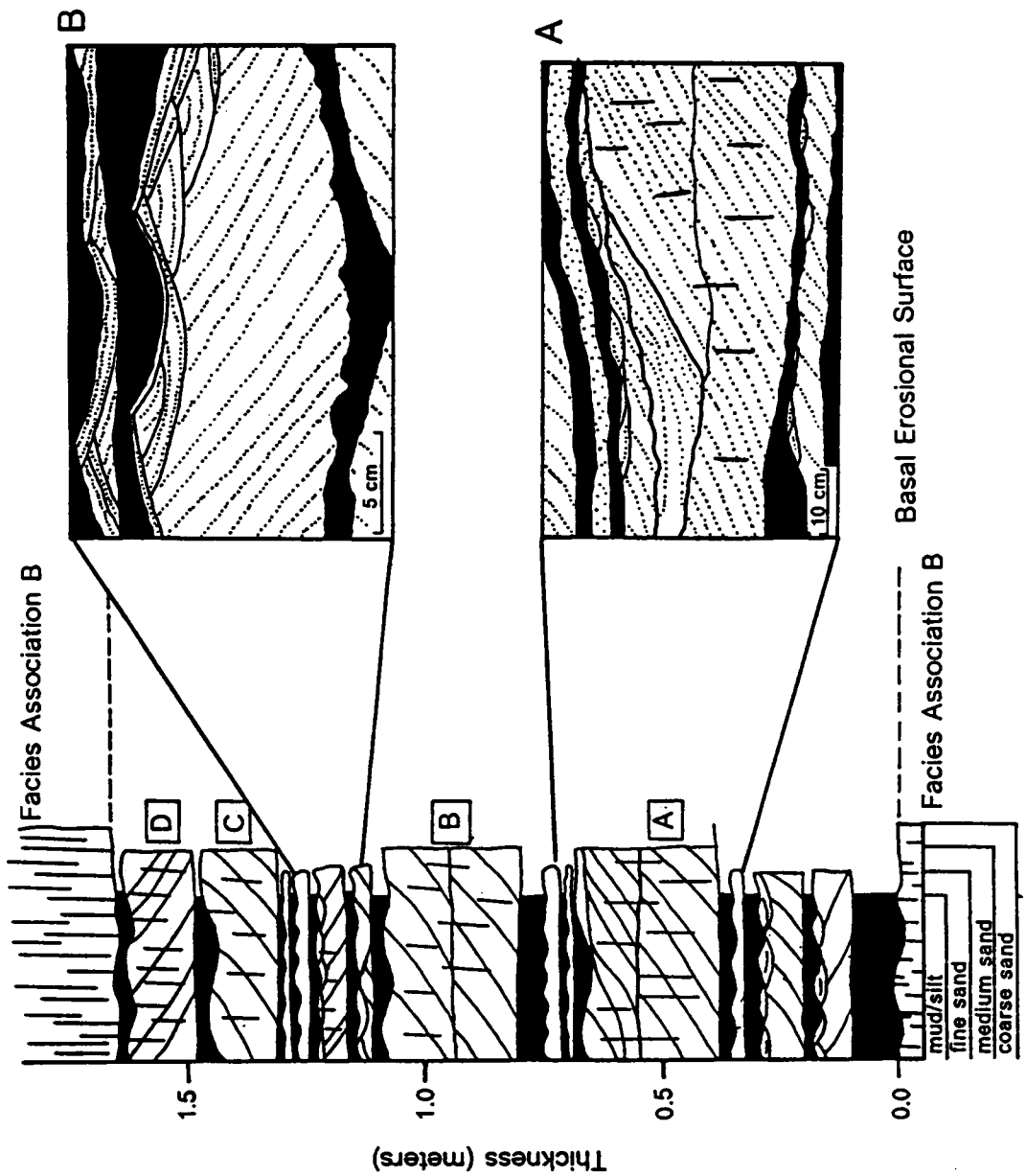
B
A
5 cm
10 cm
Facies Association B
D
C
B
A
Basal Erosional Surface
Facies Association B
mud/silt
fine sand
medium sand
coarse sand
1.5
1.0
0.5
0.0
Thickness (meters)

northeast paleocurrent mode (Figure 22A). Intact, vertical *Skolithos linearis* tubes blanket the entire surface. Also present are recumbent-to-inclined, mud-lined tubes and subordinate inclined *Skolithos linearis* tubes; the tubes are aligned and inclined parallel to the local paleocurrent direction.

Type I and type II megaripples similar to those described by Dalrymple *et al.*, (1977) occur within a restricted zone on the erosional surface in upper medium- to lower coarse-grained sandstone. Type I megaripples are sinuous, whereas type II megaripples are lunate-shaped with prominent scour pits; adjacent lunate megaripples define a crude crestline trend. Bedform parameters include: 1) wavelengths that vary from 3.20 to 6.00 m; 2) amplitudes that vary from 0.18 to 0.37 m; 3) ripple indices (wavelength / amplitude) that vary from 8.8 to 18.8; and 4) ripple asymmetry indices (crest to trough length / wavelength) that range from 0.04 to 0.26. Megaripples yield a westnorthwest paleocurrent mode (Figure 22B). Stoss-sides of megaripples are covered by westnorthwest-directed current ripples (Fig 22C). Lee-sides of some megaripples are oversteepened to approximately 40 degrees versus unmodified inclinations of 20 degrees (Fig. 23A). Megaripples with associated oversteepened slipfaces contain south-directed current ripples in their troughs (Fig. 22C and 23A). On crests of megaripples, broken *Skolithos linearis* tubes are oriented randomly or perpendicular to the paleocurrent trend.

Isolated depressions are randomly distributed across the erosional surface; these attain a maximum depth of 15 to 20 cm. Depressions are crescent shaped and in cross-section possess a steep northern side which tapers towards the south to merge with the erosion surface. Mudstone drapes the depression and is overlain by sigmoidal foresets. Both the base of the depressions and the top of the sandstone infill

Figure 22. Paleocurrent data from facies association A. N = number of observations. Vm = vector mean. Sd = standard deviation.

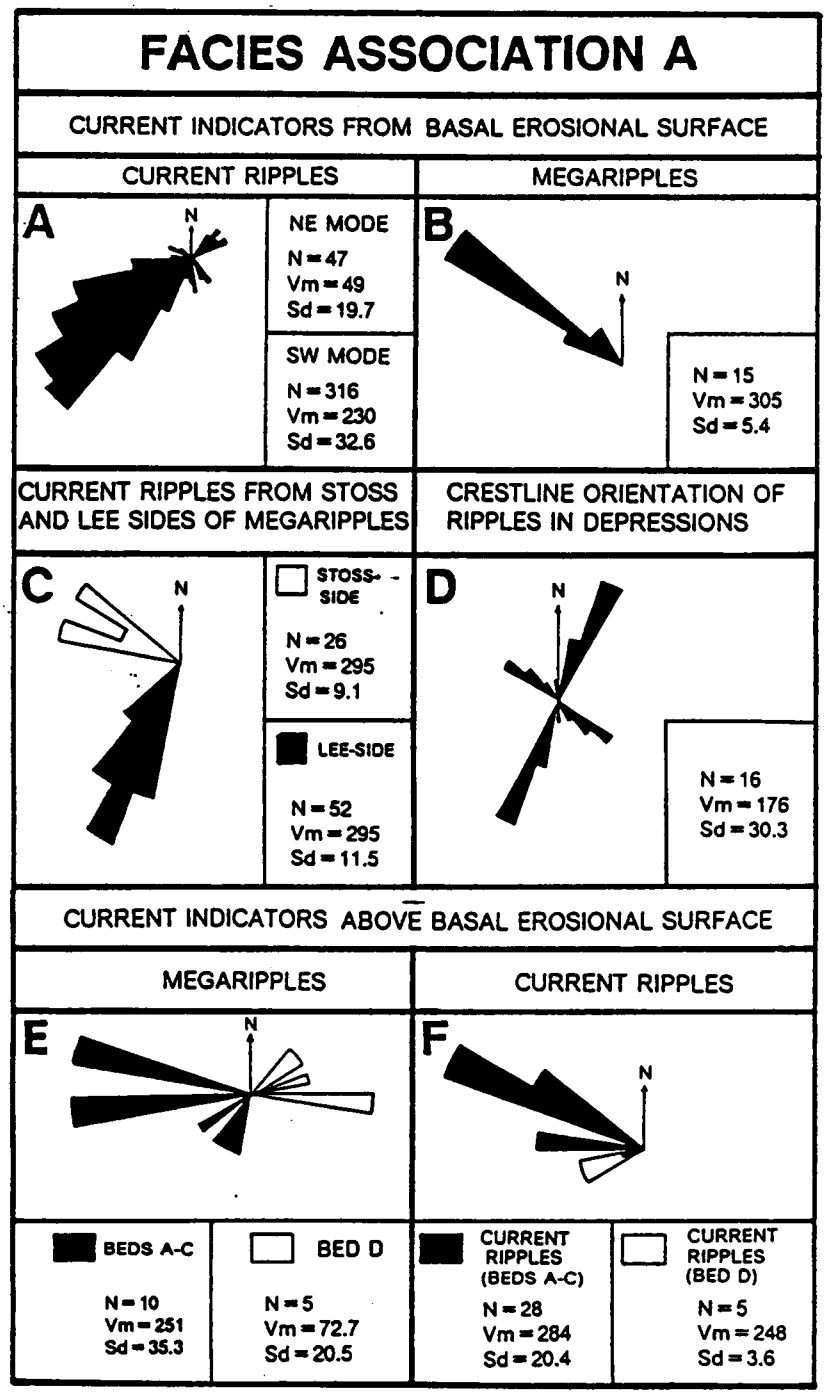
FACIES ASSOCIATION A
CURRENT INDICATORS FROM BASAL EROSIONAL SURFACE
CURRENT RIPPLES
MEGARIPPLES
A
N
NE MODE
N = 47
Vm = 49
Sd = 19.7
SW MODE
N = 316
Vm = 230
Sd = 32.6
B
N
N = 15
Vm = 305
Sd = 5.4
CURRENT RIPPLES FROM STOSS AND LEE SIDES OF MEGARIPPLES
CRESTLINE ORIENTATION OF RIPPLES IN DEPRESSIONS
C
N
STOSS-SIDE
N = 26
Vm = 295
Sd = 9.1
LEE-SIDE
N = 52
Vm = 295
Sd = 11.5
D
N
N = 16
Vm = 176
Sd = 30.3
CURRENT INDICATORS ABOVE BASAL EROSIONAL SURFACE
MEGARIPPLES
CURRENT RIPPLES
E
N
F
N
BEDS A-C
N = 10
Vm = 251
Sd = 35.3
BED D
N = 5
Vm = 72.7
Sd = 20.5
CURRENT RIPPLES (BEDS A-C)
N = 28
Vm = 284
Sd = 20.4
CURRENT RIPPLES (BED D)
N = 5
Vm = 248
Sd = 3.6

Figure 23. Photographs of facies association A: A) Oversteepened Type I megaripple with superimposed current ripples in trough. B) Microdelta created by low-stage runoff. Current ripples with oversteepened troughs and cuspate cross-sectional geometries are located on the center left.

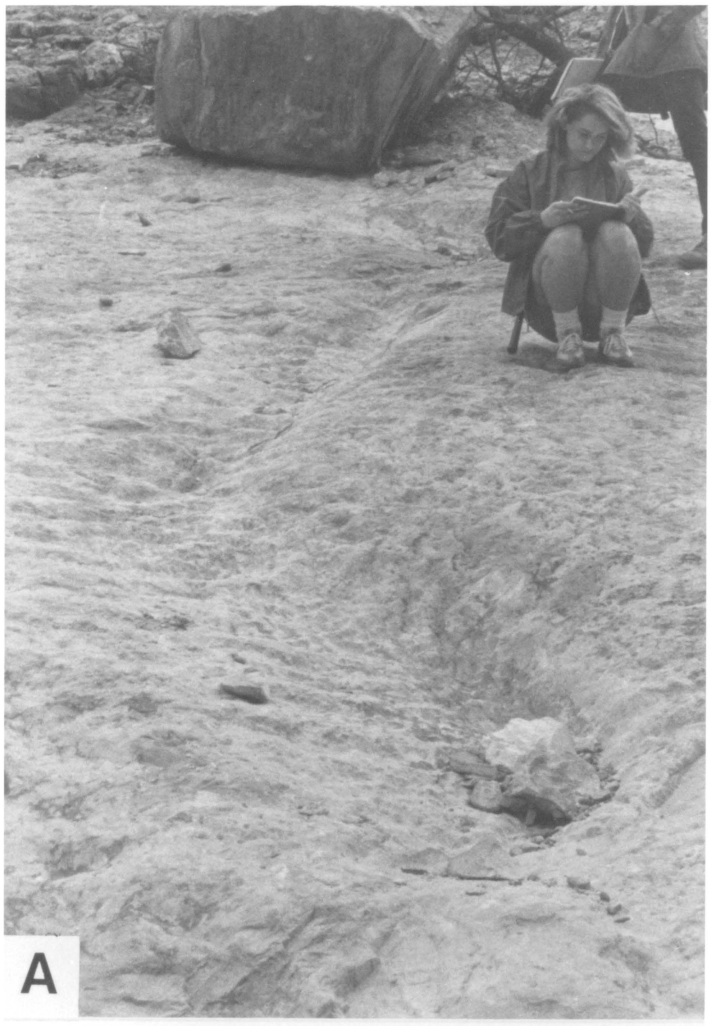
A

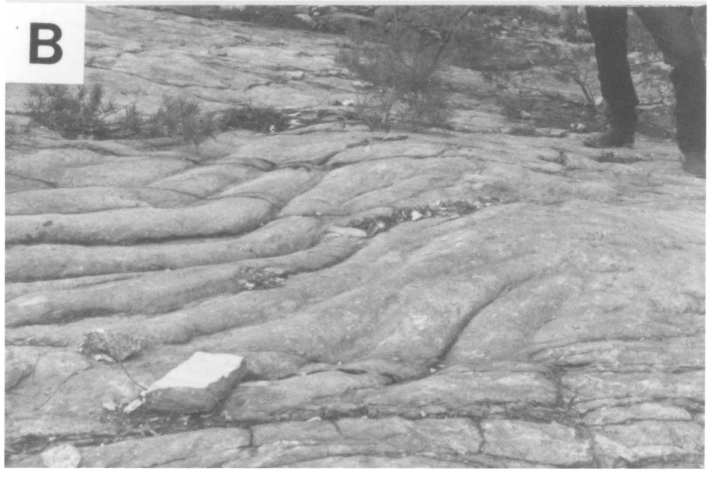
B

are covered by ripples with a cuspate profile and north-south oriented crests (Fig. 22 D).

A mudstone bed drapes the entire erosion surface followed by interlayered tabular mudstone and sandstone beds (Fig. 21). Mudstone horizons are up to 3 cm thick; sedimentary structures include: 1) massive beds; 2) unidentified, sinuous, horizontal burrows that commonly overlap; and 3) massive sandstone dikelets that penetrate the mudstone from the overlying sandstone bed. On bedding planes, dikelets are orthogonal and regular but discontinuous. Intermixing of dikelets and burrows occurs, but these can be distinguished on the basis of their angular relationships and overlapping nature. Mudstone is also present as discontinuous drapes on reactivation surfaces.

Sandstones are either thin or medium bedded. Four medium-bedded sandstone beds are present (A-D, Fig. 21). Grain size varies from lower medium- to lower coarse-grained sandstone and bed thickness ranges 23.0 cm to 35.0 cm. Beds pinch and swell due to preservation of bedforms on upper bedding planes. Internal sedimentary structures include trough cross beds and tabular-planar, cross-bed sets with reactivation surfaces that are concordant with preserved bedforms. Symmetrical ripples may cap cross-bed cosets. Bedforms preserved on tops of beds consist of sinuous-crested type I and type II megaripples. Paleocurrents from the megaripples yield a bimodal distribution with vector means to the west southwest and east northeast (Figure 22E). The three lower beds possess the generally west-directed megaripples whereas the uppermost bed contains the generally east-directed megaripples. Generally west-directed current ripples also are developed on tops of beds (Fig. 22F). The west northwest mode (Fig. 22F) is from obliquely oriented current ripples on

stoss sides of west-directed megaripples. The preservation of bedform morphology is enhanced by either mudstone drapes on troughs and crests of bedforms, or sigmoidal-shaped foresets infilling troughs (Fig. 21A).

Westnorthwest-directed current ripples on stoss sides of megaripples on the top of bed C (Fig. 21), are oversteepened to give trough-to-trough cross sections with a cuspate profile (Fig. 23B); when troughs are traced southward, they terminate in massive lobate-shaped sandstone bodies. Approaching the sandstone mass, ripple troughs become shallower and narrower and eventually merge with the mass. These sandstone masses are approximately 1.5 m in diameter and possess a superimposed rivulet pattern on their upper surface (Figure 23B).

Thin-bedded sandstones are fine to medium grained and range in thickness from 3.0 to 15.0 cm (Fig. 21). These beds are restricted to the lower portions of the facies association. Sedimentary structures include: 1) massive beds; 2) unidirectional ripple laminations; 3) chevron-bundled, ripple laminations; 4) unidirectional rippled base overlain by chevron-bundled rippled tops (Figure 21B); and 5) bidirectional foresets capped by unidirectional ripples. Bedding planes possess straight-crested ripples which are slightly asymmetric, and complex, equant, three-dimensional ripples with foresets that exhibit random orientations (*cf.* Sleath, 1984).

Trace fossil diversity is low within the thin- and medium-bedded sandstones. The tops of bedding planes possess circular burrows of two sizes. Large burrows possess a vertical central tube and in cross-section contain funnel-shaped laminations diagnostic of the ichnogenus *Monocraterion sp.* Smaller burrows possess vertical parallel sides characteristic of *Skolithos linearis*. Both ichnogenera penetrate the complete thickness of the beds. *Monocraterion sp.* is restricted to the uppermost bed,

whereas *Skolithos linearis* is found throughout all beds (Fig. 21). Horizontal to sub-horizontal burrows disrupt the upper 5.0 to 8.0 cm of some beds.

Interpretation

Exhumed bedforms in facies association A have counterparts on Holocene tidal flats, such as the Wash (Evans, 1965; 1975), Bay of Fundy (Dalrymple, 1984a; 1984b), and the coast of South Wales (Hawley, 1982). By comparison with flow patterns on Holocene tidal flats, and through hydrodynamic interpretation of bedforms and associated sedimentary structures, a process-response model for the ebb through flood cycle can be reconstructed.

Bedforms and related structures on the basal erosional surface which are considered to have resulted from flood and ebb flow, are illustrated on Figure 24. The type I and type II megaripples with a northwest or onshore-directed vector mean (Fig. 22B), are interpreted as flood-produced bedforms. Measured megaripple parameters such as wavelength, height, grainsize and morphology are consistent with values described by Dalrymple *et al.*. (1977) from the Bay of Fundy. Their study demonstrates that the transition from type I and type II megaripples occurs at velocities greater than 0.7 to 0.8 m/sec depending on flow depth. Synthesizing both flume and field studies, Harms *et al.*. (1982) conclude that the transformation from type I to type II megaripples takes place at a velocity of approximately 0.5 m/sec with current ripples stable at velocities less than 0.4 m/sec. These studies constrain the velocity that produced the type I and type II megaripples in facies association A to be between 0.5 and 0.8 m/sec. Current ripples present on the stoss-sides of the megaripples, and with

Figure 24. Interpreted flood- and ebb-produced bedforms and related structures on the basal erosional surfaceof facies association A. A) Megaripple field consisting of type I and type II megaripples. B) Northwest-oriented current ripples on stoss-sides of megaripples. C) Southwest-oriented current ripples. D) South-directed current ripples in megaripple troughs. E) Scour depressions oriented in ebb direction. F) Sand-filled scour depression with a modified current-ripple cap.

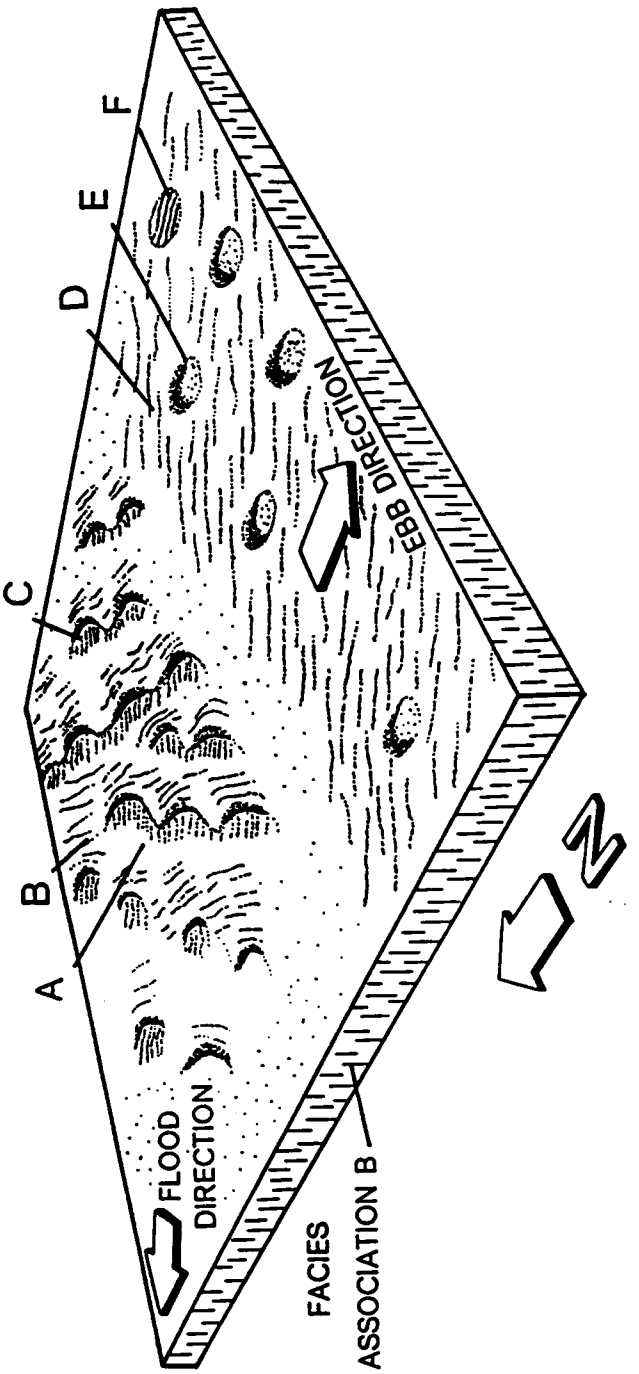
A
B
C
D
E
F
EBB DIRECTION
FLOOD DIRECTION
FACIES ASSOCIATION B
N

crests parallel to those of the megaripples (Fig. 24C), are considered to have developed as flood velocities decreased. In the Wash, flood-produced bedforms may be modified by offshore ebb flow but most ebb-generated bedforms and associated structures are related to late-stage runoff parallel to the crests of flood-produced bedforms. By analogy, the ubiquitous current ripples on the basal erosional surface with southwesterly vector mean (Fig. 22A) are interpreted as ebb-generated bedforms. During late-stage ebb runoff, water was funneled into megaripple troughs and attained sufficient velocities to undercut and oversteepen lee facies of megaripples. South-directed current ripples developed in the megaripple troughs as ebb velocities decreased (Fig 22C, 23A). Isolated depressions on the basal erosional surface are analogous to scours described from the intertidal zone along the south coast of Wales and which taper in a seaward direction (Hawley, 1982). Genesis of these structures is problematic. The depressions in facies association A merge with the basal erosional surface towards the south suggesting that they were generated by ebb runoff. Following their formation, some depressions were draped with mud; these drapes accumulated either in ebb-lowstand pools or during the transition from the flood to ebb cycle when current velocities were minimal. Sigmoidal infilling of scour pits took place during a subsequent ebb cycle. During a later flood cycle or at a stillstand, currents or waves reworked the sandfill into generally north-south trending ripples (Fig. 22D). These ripples were modified into a cuspate profile during ebb runoff. The mudstone drape on the basal erosional surface accumulated during one or more high tide, slack-water periods.

Cross beds in the medium-bedded sandstones above the basal erosional surface resulted from migrations of type I and type II megaripples similar to those preserved

on the tops of the beds. West-directed megaripples (Fig. 22E) were generated during peak flood flow whereas current ripples with a similar orientation (Fig. 22F) resulted from weaker flood currents. East-directed megaripples on the top of bed D (Fig. 22F) provide the only evidence in facies association A of peak ebb flow. During late-stage ebb runoff, flood-oriented current ripples on stoss sides of megaripples were modified into cuspate shapes. The lobate-shaped sandstone bodies at the southerly termination of the modified ripples are comparable to runoff microdeltas described by Dalrymple (1984b) and indicate that, as on the basal erosional surface, ebb runoff was to the south. Reactivation surfaces developed within the medium-bedded sandstones may have been generated by migration of superimposed bedforms (McCabe and Jones, 1977) or subordinate strength flood or ebb flow (Klein, 1971). The presence of current ripples on stoss sides of megaripples on beds A, B, and C, and currents ripples oriented at 180 degrees to megaripples on bed D (Figs. 22E and F), suggests that both processes were operative.

The different types of cross laminae present in the thin-bedded sandstones indicate a combination of unidirectional, combined and oscillatory flow (*cf.* Fig. 21B). It is not possible to assign the unidirectional cross laminae to either flood or ebb flow although it is probable that the combined- and oscillatory-flow ripples developed during tidal highstand. Mudstone intercalated within both the thin- and medium-bedded sandstones and present on forests (Fig. 21A) and along reactivation surfaces, accumulated during high-tide, slack-water periods.

Sandstone dikelets developed at the base of fine-grained sandstones may have been generated by desiccation or synaeresis. Discontinuous dikelets are considered to be characteristic of synaeresis cracks which are of no paleoenvironmental value

(Donovan and Foster, 1972; Anderton, 1976; Soegaard and Eriksson, 1985). Alternatively, the discontinuity of the dikelets could be due to limited exposure in the tidal cycle which prevented muds from completely drying (*cf.* Allen, 1983).

Ichnofauna preserved within facies association A belong to the *Skolithos* ichnofacies (Seilacher, 1969; Frey and Seilacher, 1980) which characterizes shifting substrates and extends from intertidal to subtidal settings. The mud-lined tubes on the basal erosional surface probably were produced by a polychaete with a similar habitat to the Holocene *Lanice conchilega* (Carey, 1987). Semi-rigid tubes were tilted and aligned with ebb currents during waning ebb flow. Walls of *Skolithos linearis* tubes were supported by organic secretions giving them strength by cementing sand grains. Degradation on the basal erosional surface exhumed the *Skolithos* tubes from underlying sediments; these were broken and incorporated as clasts into megaripple bedforms. *Skolithos* and *Monocraterion* burrows developed in medium-bedded sandstones are consistent with a high energy-interpretation of the bedforms. Horizontal traces within mudstones and in tops of the medium-bedded sandstones are feeding traces and are not diagnostic of a particular ichnofacies.

Many Holocene tidal flats consist of lower sand flats which grade into upper mud flats (Reineck, 1963; Evans, 1965; 1975; Semeniuk, 1981; Yeo and Risk, 1981). Structures within facies association A are similar to megaripple and current ripple bedforms and exposure indicators from the Holocene sand flats.. Sand flats in the Wash are exposed only during low-water Spring tide (Evans, 1975); exposure features in facies association A thus may not reflect daily exposure of the intertidal zone. Comparable deposits to those present on Holocene mid to upper flats are not present in facies association A. Deposits from higher portions of tidal flats have lower

preservation potential than those from subtidal or lower intertidal environments (Nio *et al.*, 1980). Higher tidal-flat deposits may have been eliminated during development of the erosional surface which caps facies association A.

FACIES ASSOCIATION B: UPPER SHOREFACE

Description

Facies association B consists of very thick-bedded, upper coarse- to upper very coarse-grained quartz sandstone. This facies association is present in measured sections at 1) Balcony Falls (Hampton and Erwin Formations); 2) Buena Vista (Erwin Formation); 3) Steeles Tavern (Erwin Formation); and 4) Buchanan (Hampton Formation) (Fig. 19).

Massive beds and trough and tabular-tangential cross bedding dominate facies association B. Bedding planes are defined by mudstone partings or pressure-solved contacts. Reactivation surfaces are very rare. *Skolithos linearis* is the only ichnofossil present (Fig. 25) and density ranges from a minimum of 832 tubes/m^2 to a maximum of 4592 tubes/m^2 within the Erwin Formation. Tubes can be traced vertically for up to 1.2 m. *Skolithos linearis* tubes are less abundant within the Hampton Formation. Where *Skolithos linearis* density is high, as in much of this facies association, primary sedimentary structures are obscured (Fig 26A). However, as concentration of tubes decreases, boundaries of sets are apparent; sets range from a few centimeters to maximum of 25 cm in thickness (Fig. 26B). Where *Skolithos*

Figure 25. Photograph of facies association B: Showing dense *Skolithos linearis* ichnofossils.


Nikon

Figure 26. Measured section through facies association B at Natural Bridge Quarry (locality number 9) showing sandstone interval with *Skolithos* burrows. A) Dense ***Skolithos linearis*** ichnofossils and absence of primary sedimentary structures. B) Reduction in density of ***Skolithos linearis*** ichnofossils and appearance of diffuse bedding. C) Limited number of ***Skolithos linearis*** ichnofossils and preservation of tabular-tangential cross bedding.

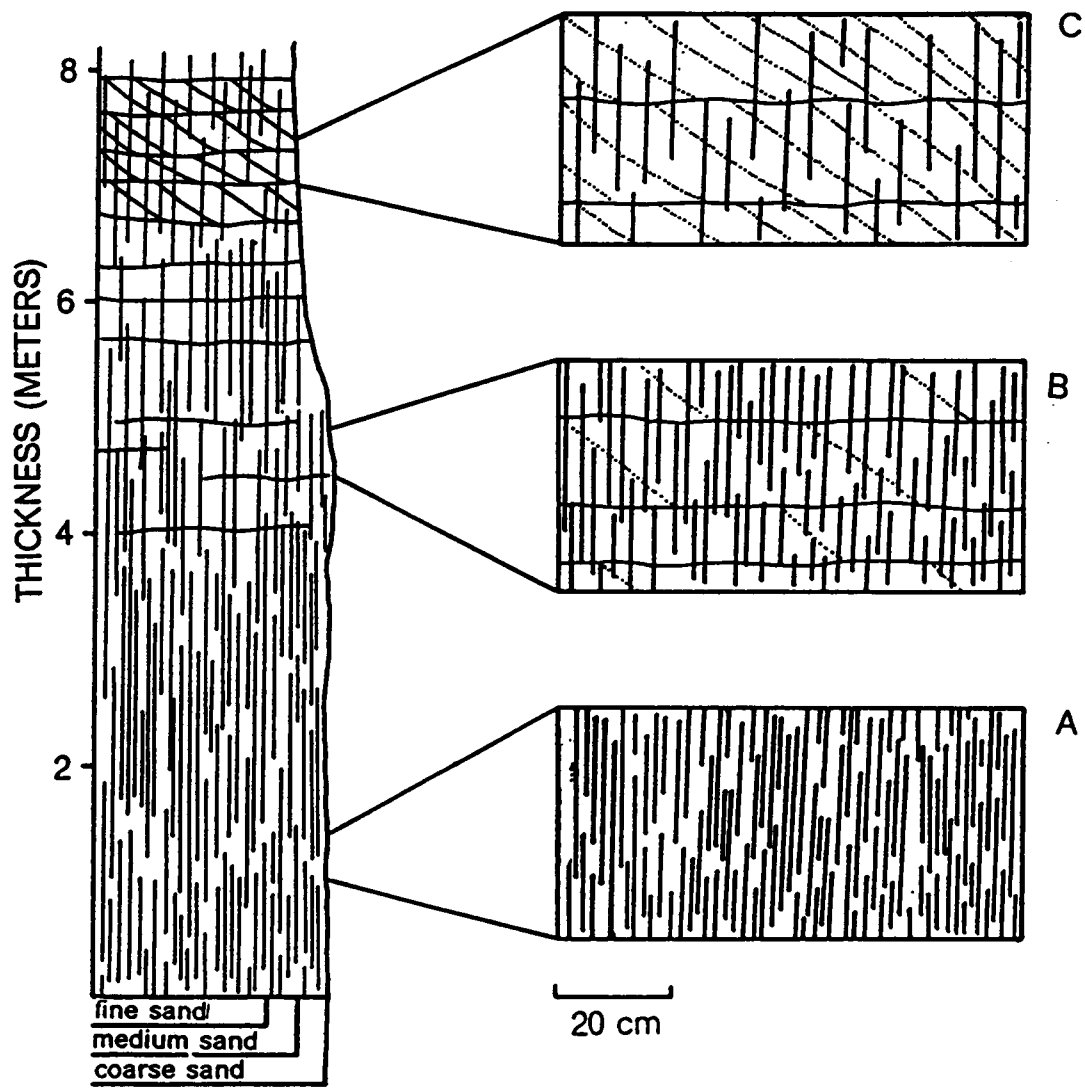
THICKNESS (METERS)
8
6
4
2
C
B
A
fine sand
medium sand
coarse sand
20 cm

linearis density is low or absent, medium-scale, tabular-tangential and trough cross bedding are preserved (Fig. 26C). Foresets exhibit normal grading from coarse- to upper medium-grained sandstone. Density of *Skolithos linearis* tubes displays a direct relationship to sediment grain size (Fig. 26). Paleocurrent data are sparse from facies association B but rare exposures of trough axes give northeast and southwest and a subordinate southeast mode (Fig. 27A).

Interpretation

Obliteration of primary sedimentary structures by bioturbation permits only a generalized paleoenvironmental interpretation for this facies association. The ubiquitous *Skolithos linearis* ichnofossils indicate a marine environment of deposition.

Trough and tabular-tangential cross bedding in coarse-grained sandstone indicate current velocities of greater than 40 to 50 cm/sec. Migration of type I and type II megaripples at low angles of climb produced the decimeter-thick, cross-bed sets. The northeast and southwest paleocurrent directions parallel the ancient strandline, whereas the southeast-mode is offshore (Fig. 27A). Shore-parallel flow may be initiated by either oblique shoaling waves which generate longshore currents (Komar and Inman, 1970), or tidally induced longshore flow (Seymour, 1980; Wright, 1981). Longshore flow related to oblique shoaling waves is restricted generally to the breaker and swash zones (Komar and Inman, 1970). The width of the zone of longshore transport depends upon the wave regime, being wider during storm than fair-weather conditions (Elliott, 1986). Bimodal-bipolar paleocurrent directions may be produced

Figure 27. Paleocurrent summary for facies associations B, C, D and E. N = number of observations. Vm = vector mean. Sd = standard deviation.

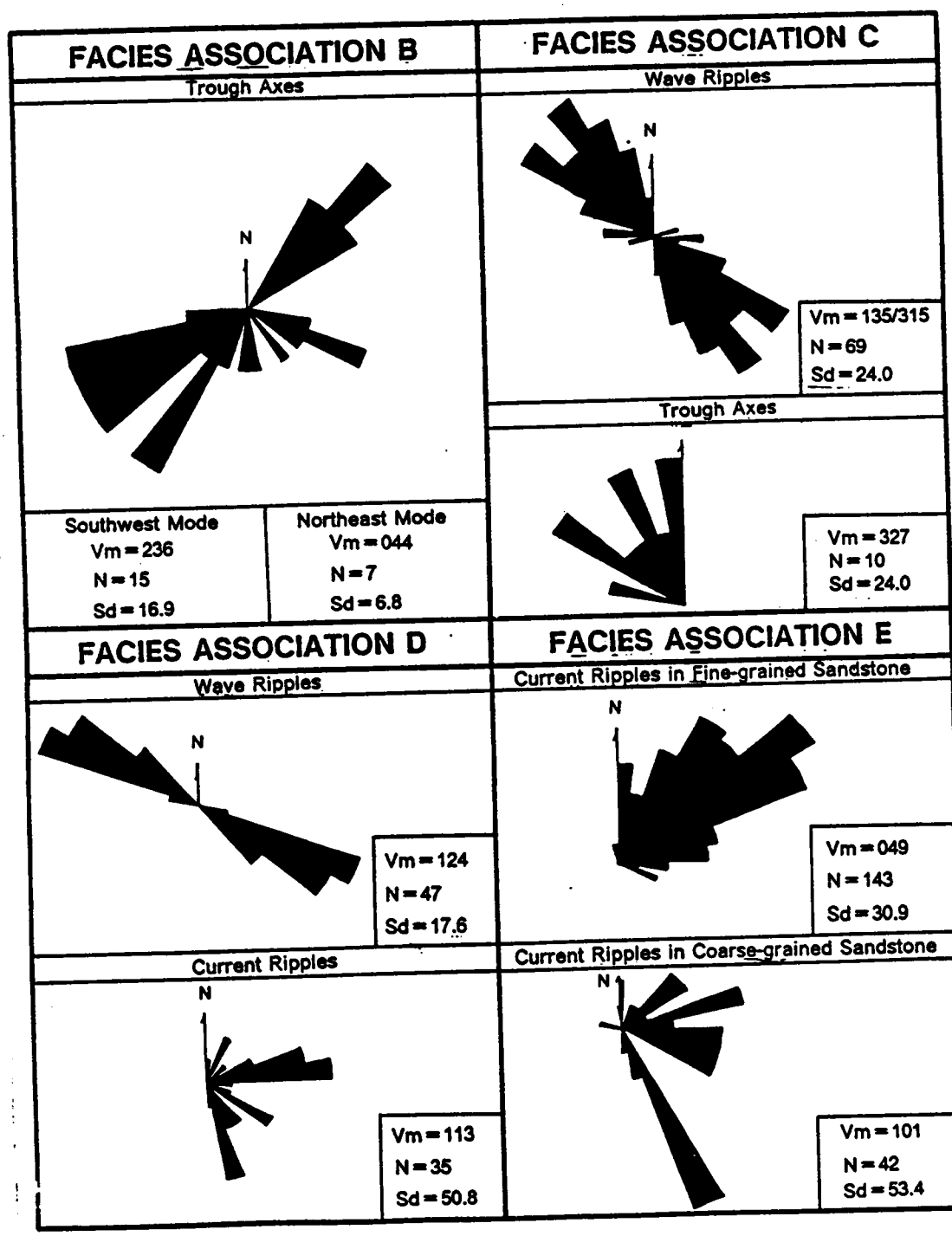
FACIES ASSOCIATION B
Trough Axes
N
Southwest Mode
Vm = 236
N = 15
Sd = 16.9
Northeast Mode
Vm = 044
N = 7
Sd = 6.8
FACIES ASSOCIATION C
Wave Ripples
N
Vm = 135/315
N = 69
Sd = 24.0
Trough Axes
Vm = 327
N = 10
Sd = 24.0
FACIES ASSOCIATION D
Wave Ripples
N
Vm = 124
N = 47
Sd = 17.6
Current Ripples
N
Vm = 113
N = 35
Sd = 50.8
FACIES ASSOCIATION E
Current Ripples in Fine-grained Sandstone
N
Vm = 049
N = 143
Sd = 30.9
Current Ripples in Coarse-grained Sandstone
N
Vm = 101
N = 42
Sd = 53.4

by shifts in the direction of oblique wave approach which would cause opposed directions of longshore flow. In the Gallop sandstone (Upper Cretaceous) bimodal-bipolar paleocurrent patterns are attributed to variations in wave approach (McCubin, 1972; 1982). Few studies have examined the effects of nearshore tide-generated currents which could transport sand seaward of the breaker zone (Seymour, 1980; Wright, 1981). Bimodal-bipolar paleocurrent trends develop when ebb and flood currents are of equal magnitude or when a temporal switch in the dominant flow direction takes place. More commonly tidal currents display a time-velocity asymmetry (Seymour, 1980; Wright, 1981). Sand is transported during the dominant flow, whereas the subordinate flow moves only suspended material (Wright, 1981). On the basis of paleocurrent data alone it is not possible to distinguish tidal processes from shoaling waves but the harmonic nature of tidal currents may permit separation. Periodic bundled foresets may be produced within tidal environments in response to variable strength tidal flow related to neap/spring cyclicity (Visser, 1980; Boersma and Terwindt, 1980; J. R. L. Allen, 1981; Nio *et al.*, 1983, de Mowbray and Visser, 1983; Yang and Nio, 1985; Kreisa and Moiola, 1986). Bundled foresets have been described from estuarine settings but not from shoreface environments. The trough and tabular-tangential cross beds within facies association B do not display any cyclicity of foresets thicknesses. This facies association thus is considered to be the result of longshore transport related to oblique wave approach.

The subordinate southeast paleocurrent mode may have been generated by either rip currents or offshore transport of sand during storms. Rip currents are narrow zones of high velocity currents oriented perpendicular to the shoreline. They are

initiated by variations in water height within the longshore current regime (Shepard and Inman, 1950; Komar and Inman, 1970). Storm-surge ebb currents may also move material perpendicular to the shoreline (Walker, 1984).

Skolithos is diagnostic of the *Skolithos* ichnofacies, which is developed commonly in shallow-marine subtidal to intertidal areas on mobile substrates (Seilacher, 1969). The *Skolithos* -producing organism is not known, but probably possessed a suspension-feeding habit (Sundberg, 1983). Suspension feeders are common in areas of strong currents; steady currents are required to deliver nutrients to the organism (Dodd and Stanton, 1981). The vertical change in abundance of *Skolithos* tubes coupled with a reduction in grain size probably was caused by a decrease in current strength related to increasing water depth. Longshore currents are steady and display decreasing strength with depth (Komar and Inman, 1970).

Sedimentary structures in facies association B thus were produced mainly by longshore currents. This association accumulated landward of the breaker zone in an upper shoreface environment. Recognizable storm or rip-current processes are compatible with this interpretation.

FACIES ASSOCIATION C: LOWER SHOREFACE TO PROXIMAL INNER SHELF

Description

Facies association C consists of medium- to thick-bedded, fine- to coarse-grained

quartz sandstone and subordinate siltstone and mudstone. Thicknesses of sandstone beds range from 0.5 to 9.5 m (Fig. 28). This facies association is present in the Buchanan, Balcony Falls, Buena Vista, Elk Creek, Natural Bridge Quarry and Poplar Camp sections with in the Erwin Formation and in the Hampton Formation at Buchanan, Balcony Falls and Damascus (Fig. 19).

Massive, thick-bedded, medium-grained sandstones predominate in this facies association; these beds display crude grading in some instances and rare horizontal stratification. Beds have sharp basal contacts and are capped by straight-crested or hummocky megaripples (Fig. 28A, 28B, and 29A). Megaripples are draped by laminated, very fine-grained sandstone and siltstone. The vertical transition into hummocky megaripples is gradational, whereas the passage into straight-crested ripples is sharp and delimited by an increase in grain size (Fig. 28A). Straight-crested megaripples are developed in coarse-grained and hummocky megaripples in fine- to medium-grained sandstone. In cross-section, straight-crested ripples are rounded and have slightly flattened crests (Fig. 28A). Megaripple wavelengths vary from 42 to 87 cm. Megaripple heights range from 3.5 to 9.0 cm. Megaripple indices vary from 8.8 to 19.6, and ripple asymmetry indices are 0.47 to 0.54. Preserved megaripples are form-discordant to internal stratification. Rarely, glaconite grains are present within megaripples. In one case, straight-crested megaripples occur as four superimposed sets separated by discontinuous mudstone drapes (Figure 28A). Paleocurrents from straight-crested megaripples reveal northwest-southeast oscillatory flow (Fig. 28B). In some megaripples, unidirectional foresets are oriented to the northwest. Thinner beds (0.50 to 1.10 m) within this facies association possess a sharp base overlain by hummocky cross-stratified, lower medium- to lower fine-grained sandstone which

Figure 28. Partial measured section through facies association C at Buchanan (locality number 7) showing interbedded massive sandstones and fine-grained sandstone and mudstones. A) Four sets of coarse-grained, straight-crested megaripples. B) Block diagram of hummocky cross stratification. Arrows point to beds capped by hummocky megaripples.

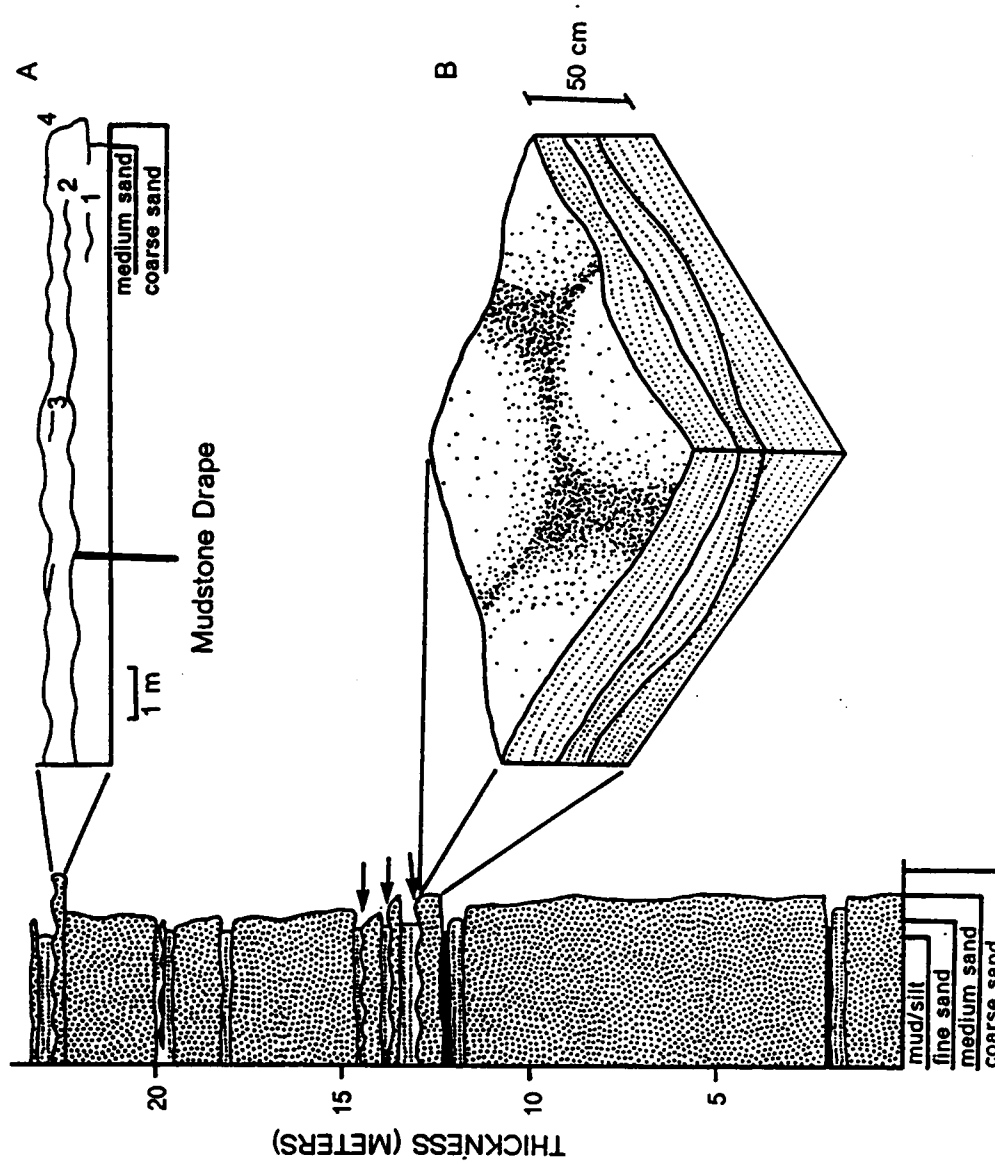
A
B
4
2
1
3
medium sand
coarse sand
Mudstone Drape
1 m
50 cm
THICKNESS (METERS)
20
15
10
5
mud/silt
fine sand
medium sand
coarse sand

Figure 29. Photographs of facies association C: A) Bedding-plane view of straight-crested wave ripples. B) Slab of hummocky cross stratification with megarippled top.


A
0 1 2 3CM
B

may be capped by hummocky megaripples (Fig. 29B). Rare vertical burrows (*Skolithos?*) are present within sandstones of this facies association.

Subordinate cross-stratified, medium-grained sandstones are associated with the structures described above and are included in this facies association. This facies is best developed in the Natural Bridge Quarry (Fig. 19). Trough cross bedding predominates with subordinate tabular-planar(?) sets. Paleocurrent data from trough axes yield a north to northwest mode (Fig. 27C). This facies is different from the trough cross-beds facies association B in that sandstones are medium-grained, *Skolithos* tubes are lacking, and a different paleocurrent mode exists.

Interpretation

The thick massive sandstone beds which typify this facies association may be the result of: 1) pressure solution of grains with destruction of primary stratification; 2) good sorting to preclude recognition of primary stratification; 3) bioturbation with elimination of preexisting primary structures; 4) dewatering with elimination of primary stratification; or 5) rapid sedimentation from suspension with destruction of primary structures by shearing (*cf.* Middleton, 1967). Thin-sections and slabs of the massive beds show well-preserved primary grain textures, and little pressure solution. Sorting is moderate with sufficient grain-size variation to permit recognition of any primary structures. In other facies associations, homogenization by biological activity is manifested by destruction and modification of bedding planes; intense bioturbation disrupts bedding planes. Bedding planes in facies association C lack trace fossils and intervening beds show few traces. Furthermore evidence of dewatering is lacking within beds and on bedding planes. The massive character of many beds in this facies

association thus is considered to be primary.

Massive-to-graded and horizontally stratified beds comparable to those in facies association C have been described from Miocene to Holocene lower shoreface to inner-shelf deposits (Kumar and Sanders, 1976). Beds range up to a maximum thickness of 4.2 m; they are attributed to storm events and are believed to be produced by the interaction of rapid suspension fallout and tractional processes. Maximum bed thicknesses from Holocene settings are comparable to those in this facies association C. Thick beds within this facies association may be amalgamated thinner beds; their massive character may not permit discrimination of thinner beds.

The straight-crested wave ripples which cap some of the massive beds are vortex ripples which can be employed to reconstruct wave parameters, which were reconstructed using the techniques of Diem (1985). The methods of Allen (1984) and Clifton and Dingler (1984) were applied to these megaripples and yielded similar results. Bottom wave orbital diameters ranged from 64.6 to 133.5 cm. Lower threshold velocities varied from a minimum of 27.2 to a maximum of 32.0 cm/sec; upper threshold velocities at which wave ripples change to upper plane beds varied from 84.2 to 121.0 cm/sec. Reconstructed wave periods ranged from a minimum of 2.4 to 3.5 seconds to a maximum to 7.5 to 13.1 seconds. Equations yield a maximum deep-water wavelength of an open ocean wave of 86.8 to 267.9 m and wave heights between 12.3 to 38.0 m. Maximum water depths varied from 50.2 to 66.5 m.

Wave ripples with similar morphology and grainsize have been reported from Southern Monterey Bay by Dingler *et al.*. (1985); measured water depths and wave parameters compare well with reconstructed parameters from facies association C. Coarse-grained ripples in Monterey Bay occur as thin, coarse-grained veneers on top

of fine-grained sand. These sand patches migrate landward and change morphology intermittently under the possible influence of long-period waves. Superimposed sets of wave ripples in facies association C similarly are considered to have resulted from shifting sand patches. Northwest-dipping internal stratification in some megaripples was generated as the sand patches migrated shoreward.

The beds in this facies association with hummocky cross-stratification and wave-rippled tops are comparable to hummocky sequences described by Dott and Bourgeois (1982) and other workers. The origin of hummocky cross stratification is problematic; it is believed to be generated by either pure oscillatory flow or a combination of oscillatory flow and unidirectional flow (Dott and Bourgeois, 1982; Swift et al., 1983; Allen, 1985; Kreisa, 1981; 1985; Duke, 1987; Nottvedt and Kreisa, 1987; Swift and Nummedal, 1987). Hummocky cross stratification may also be a a product of migrating equilibrium bedforms which are related genetically to trough cross stratification (Nottvedt and Kreisa, 1987). The basal portions of hummocky beds in this facies association are interpreted as aggradational, upper flow regime deposits. Hummocky megarippled tops on both massive and hummocky cross-stratified beds were generated upon return to fair-weather conditions.

The rare trough and tabular-tangential cross-bedded sandstones with northwest-directed paleocurrents (Fig. 27C) were produced by onshore-directed currents of relatively high velocity (Fig. 26C). Onshore-directed flow may take place during the initial coastal setup preceding a storm or upon return to fair-weather conditions (Niedoroda *et al.*, 1984).

Based on the preceding discussion, facies association C is interpreted to have been deposited in a lower shoreface to proximal inner-shelf setting under the influence of

both storm and fair-weather waves. Calculated water depths are compatible with the straight-crested megaripples having developed in an inner-shelf zone defined by Harms *et al.* (1982) as extending from 20 to 200 m. Sediment as well as the fauna which produced the ichnofossils were supplied from the upper shoreface during storms (*cf.* Frey and Pemberton, 1984; Howard and Frey, 1984). The *Skolithos* trace fossils in this facies association are thus independent of water depth but are energy-level dependent.

FACIES ASSOCIATION D: DISTAL INNER SHELF

Description

Lower medium- to upper fine-grained sandstones, siltstones and mudstones typify this facies association which is present in both the Erwin and Hampton Formations at the Damascus, Elk Creek, Poplar Camp, Poplar Camp Quarry and Buchanan sections (Fig. 19). Bedding thicknesses range from 1 to 31 cm (Fig. 30). Beds typically display a pinch-and-swell geometry related to bedform preservation. Facies association D is composed mostly of quartz sandstones with minor proportions of subfeldspathic and sublithic sandstones. In three beds glauconite makes up to 40 percent of the framework grains. In other beds, glauconite occurs in trace amounts up to 1-2 percent.

Sandstone beds contain abundant sedimentary structures. Basal contacts are typically sharp and exhibit rare irregularities, including narrow, sand-filled channels similar to Type A gutter casts of Goldring and Aigner (1982), and load structures.

Figure 30. Partial measured section through facies association D at Buchanan (locality number 7) showing interbedded, fine-grained sandstones and mudstones. A) Block diagram of parallel-laminated sandstone capped by symmetrical, ripples. B) Block diagram of micro-hummocky cross stratification.

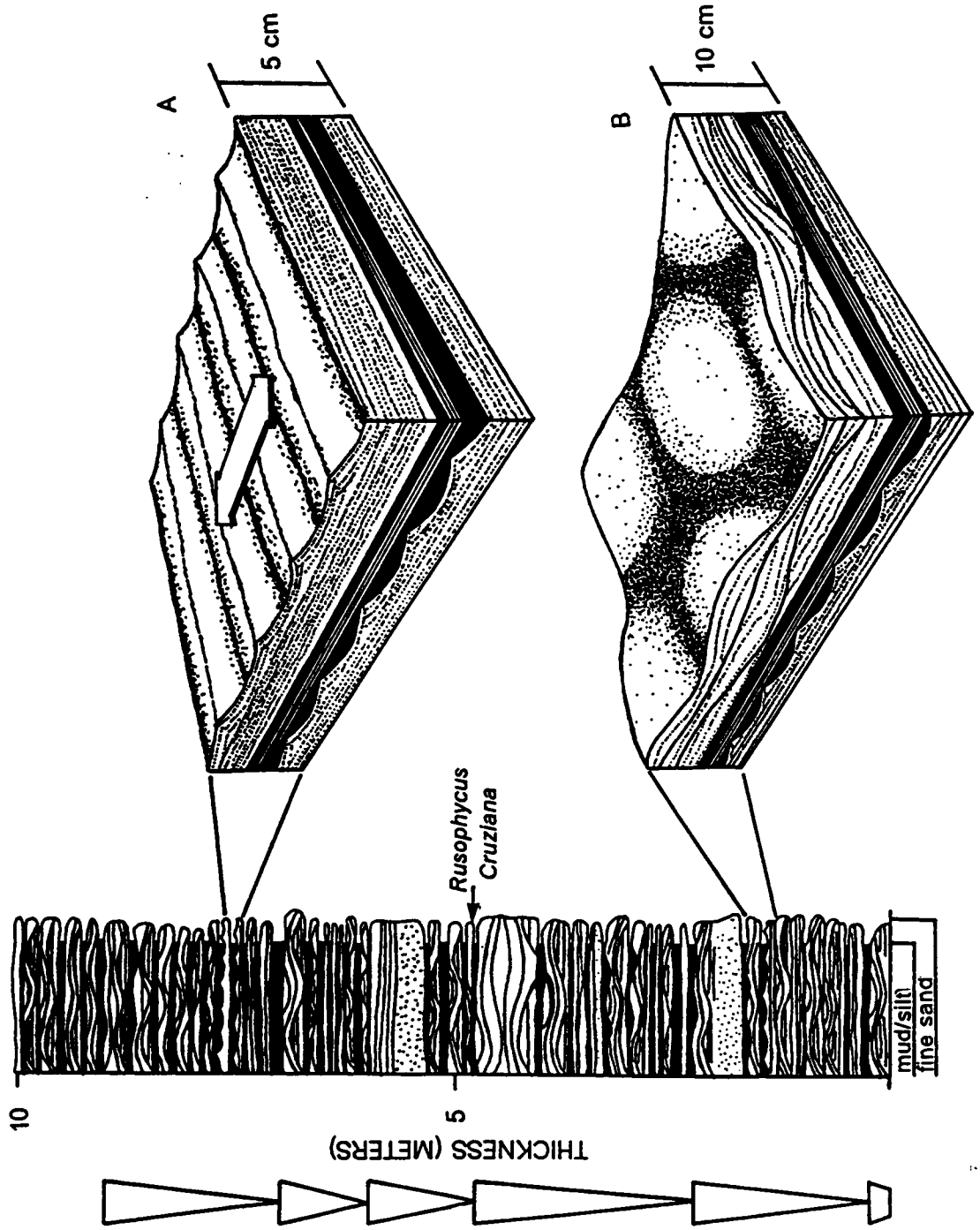
A
5 cm
B
10 cm
Rusophycus
Cruziana
mud/silt
fine sand
10
5
THICKNESS (METERS)

The most common sequence of sedimentary structures within a bed is (from bottom to top): 1) horizontally stratified sandstone, which grades from lower medium- to upper fine-grained sandstone; 2) bidirectional or chevron-bundled cross laminations capped by symmetrical ripples; 3) bioturbated, parallel-laminated, fine-grained sandstone and siltstone couplets; and 4) bioturbated mudstone (Fig. 30A). Subordinate beds are: 1) horizontally stratified, fine-grained sandstone overlain by alternating bioturbated, parallel-laminated siltstone and mudstone couplets (top Fig. 31A). 2) massive, medium-grained sandstone and horizontally stratified, fine-grained sandstone overlain by parallel-laminated, very fine-grained sandstone and siltstone couplets; 3) micro-hummocky, fine-grained sandstone overlain by laminated siltstone and mudstone couplets (Figs. 30B and 31B); 4) form-discordant ripples overlain by bioturbated siltstone and mudstone (bottom Fig. 31A); 5) current-rippled base with form-discordant rippled top; 6) Climbing wave-ripple laminations (Figure 31C); and 7) lenses consisting of horizontally stratified, fine-grained sandstone overlain by form-discordant, parallel-laminated siltstone and mudstone. Some parallel-laminated sandstones contain mudstone clasts. In rare bedding-plane views, lunate ripples in siltstone cap parallel-laminated, fine-grained sandstone and mudstone. Wave ripples indicate northwest/southeast oscillatory flow (Fig. 27D), whereas current ripples yield paleocurrent modes to the east and south (Fig. 27E).

Beds are arranged commonly into 0.7 to 3.0 m thickening- and coarsening-upward packages which are superimposed on 60 to 82 m-thick, thickening- and coarsening-upward sequences (Fig. 30). Thinning- and fining-upward sequences which vary from 1.0 to 8.5 m in thickness are developed at the base of the facies association. Glauconite is confined to these sequences.

Figure 31. Photographs of facies association D: A) Beds of horizontally stratified, fine-grained sandstone overlain by bioturbated siltstone and mudstone (top), and form-discordant ripples overlain by bioturbated siltstone and mudstone (bottom). Note mud-lined burrow cross-cutting wave-rippled sandstone. B) Micro-hummocky cross stratification (scale is 19 mm in diameter). C) Climbing wave-ripple laminations.

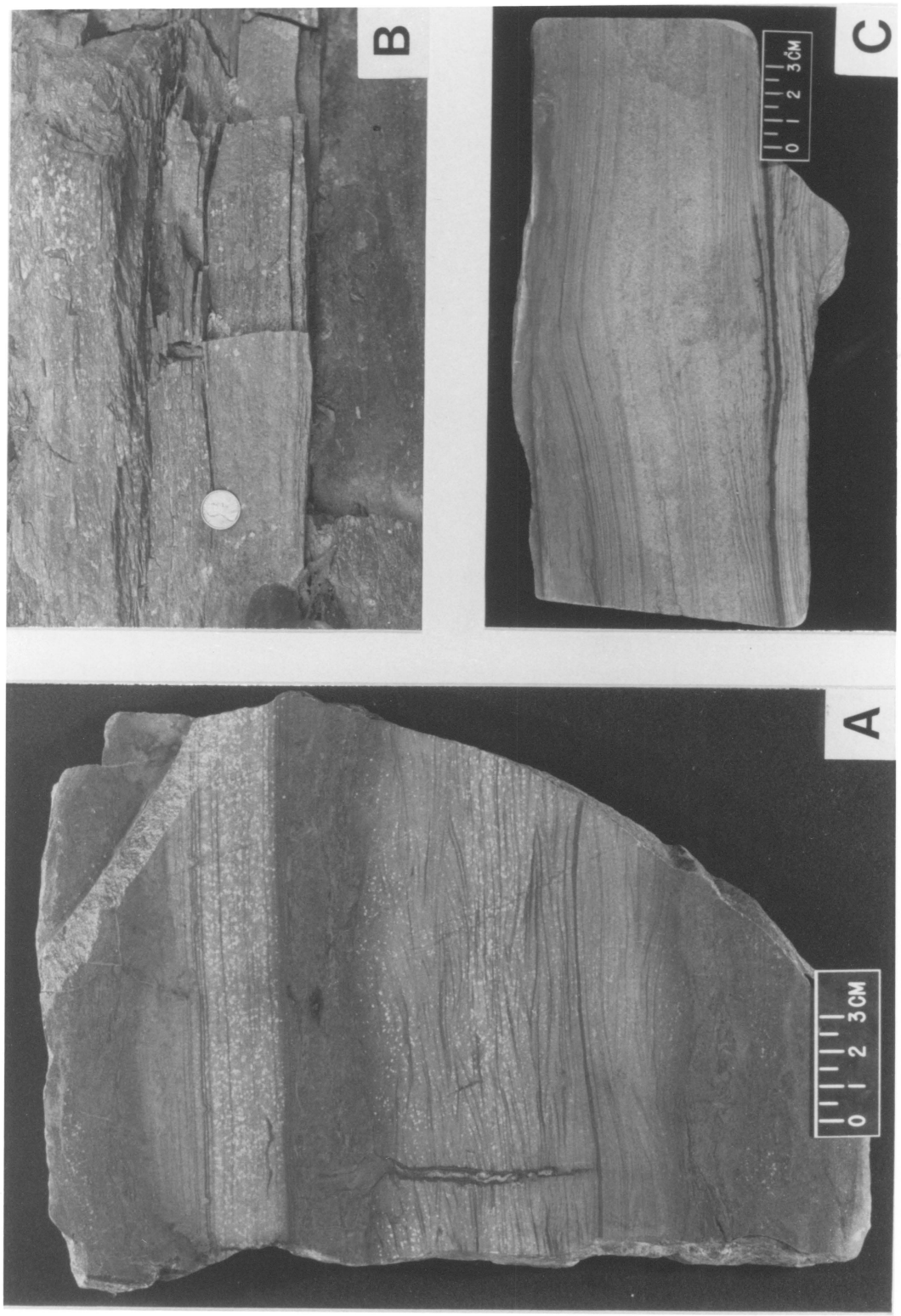
A
0 1 2 3CM
B
C
0 1 2 3CM

Trace fossils in this facies association include: *Diplichnites sp., Rusophycus sp., Cruziana sp., Planolites beverliensis, Teichichnus sp., and ?Phycodes pedum* Seilacher (F. Sundberg, pers. comm. 1986). Commonly, bioturbation completely disrupts primary stratification within siltstone and mudstone (Fig. 31A). Tops of sandstone beds are modified into a scalloped appearance by burrowing. Mud-lined burrows are prevalent within bioturbated siltstone and mudstone, and also cross-cut underlying wave-rippled intervals (Fig. 31A).

Interpretation

Beds of horizontally stratified sandstone with wave-rippled tops overlain by bioturbated siltstone and mudstone (Fig. 30A) which predominate in facies association D are analogous to beds described elsewhere and interpreted as storm-produced sequences (Kreisa, 1981; Aigner, 1985; Soegaard and Eriksson, 1985). Depositional processes which produce horizontal stratification are equivocal; it can be generated by: 1) lower regime unidirectional flow, 2) upper regime unidirectional flow, or 3) upper-regime oscillatory flow; (Clifton, 1976; Harms *et al.*, 1982). Grain-size within the horizontally stratified sandstones is too fine to have lower plane beds as equilibrium bedform (Harms *et al.*, 1982). Plane beds produced by oscillatory flow typically contain bimodal-bipolar oriented sole markings (Aigner, 1985) and are capped by wave ripples generated during waning oscillatory flow (Clifton, 1976; Harms *et al.*, 1983). In the absence of sole markings and the lack of wave ripples at the tops of many beds in facies association D, an oscillatory origin for most of the horizontal stratification is considered unlikely. The most plausible explanation for the ubiquitous horizontal stratification is deposition from upper regime unidirectional

currents generated by storm-surge ebb flow. Offshore-directed current ripples in associated beds support this contention. The abundant wave-rippled tops to beds (Fig. 31A) are visualized as a product of subsequent oscillatory wave reworking of the horizontally stratified sand. As wave base rises, current velocities are reduced to ambient fair-weather conditions permitting suspension settling of silt and mud which caps most sandstone beds in facies association D.

Beds of graded, massive to horizontally stratified sandstone overlain by parallel-laminated sandstone and siltstone are interpreted as the product of fallout from a turbulent suspension current followed by upper regime tractional deposition and return to fair-weather conditions. Beds of this type have been related to weak turbidity flows (Hayes, 1967; Soegaard and Eriksson, 1985).

In addition to the wave ripples capping many sandstone beds, others structures in this facies association which indicate oscillatory and combined-flow currents generated by wave and storm processes are: 1) micro-hummocky cross stratification (*cf.* Dott and Bourgeois, 1982; Fig. 30B and 31B); 2) form-discordant ripples (*cf.* P. A. Allen, 1981); 3) lenses of horizontally stratified sandstone overlain by form-discordant, parallel-laminated siltstone and mudstone (*cf.* Soegaard and Eriksson, 1985) and 4) climbing wave-ripple laminations (Fig. 31C; *.cf* Aigner, 1985).

Offshore transport of sand in both ancient and modern settings has been attributed to shore-perpendicular, storm-surge ebb currents (Aigner and Reineck, 1982; Nelson, 1982a; 1982b; Soegaard and Eriksson, 1985), but there is disagreement regarding the distances that such currents can transport sediment offshore (Walker, 1984). Paleocurrent data from current ripples in this facies association range from shore-perpendicular to shore-parallel; similar data have been interpreted as the product

of storm-surge ebb evolving into geostrophic currents (Morton, 1981; Swift *et al.*, 1983; Walker, 1984; Snedden and Nummedal, 1986). As storm-induced return flows move offshore, the Coriolis force deflects the flow which eventually assumes a shore-parallel orientation (Walker, 1984; Swift and Nummedal, 1987). The distance from the shoreline that the flow becomes isobath-parallel is controlled by the initial velocity of the return flow and the bottom frictional forces that retard the flow velocity; weak storm-surge ebb currents rapidly become shoreline parallel whereas strong flows may retain a shoreline-perpendicular orientation for greater distances.

The trilobite resting, furrowing and walking traces (*Rusophycus sp., Cruziana sp., and Diplichnites sp.,*) are diagnostic forms of the *Cruziana* ichnofacies (Seilacher, 1969; Crimes, 1969). The *Cruziana* ichnofacies develops in subtidal environments below fair-weather wave base but above storm-wave base in low-energy conditions (Frey and Seilacher, 1980). *Planolites* and mud-lined, feeding burrows in the tops of the beds developed during low-energy, fair-weather conditions after storm events.

Process interpretation of facies association D reveals that sedimentation was influenced by unidirectional, oscillatory, and combined-flow currents. These currents were generated by a combination storm-surge ebb flows which evolved into geostrophic flows, and waning storm waves. The ichnofacies, together with the abundance of mudstone indicate that facies association accumulated above storm-wave base but below fair-weather wave base. Wave-generated structures are considered to have been produced exclusively by storm waves. A distal inner shelf is the preferred environment of deposition and is distinguished from the proximal inner shelf on the basis of different bed types and lesser bed thickness.

FACIES ASSOCIATION E: OUTER SHELF

Description

This facies association consists of fine-grained sandstones, siltstones, and mudstones, with subordinate coarse-grained sandstone. Maximum thicknesses are unknown due to structural complication, but measured sections are up to 250 m thick. This facies association composes the majority of the Hampton Formation at all localities and the Erwin Formation at Poplar Camp and Poplar Camp Quarry (Fig 19). The sandstones are quartzose with minor proportions of feldspathic and lithic components. Glauconite may be present in trace amounts.

Mudstones and slates predominate in the lower portion of the Hampton Formation (Fig. 32); these are typically black and contain fine- to medium-grained sandstone and siltstone stringers that vary in thickness from one grain diameter up to 0.5 cm. The thicker laminations are typically graded and rarely contain microload, flame, dewatering structures, and scours at their bases. Bioturbation is rare in the mudstones.

Thin- to medium-bedded, fine-grained sandstones, siltstones and mudstones dominate the upper two thirds of this facies association and vary in thickness 1 to 25 cm (Fig. 32). The most common bed type consists of 1) a sharp base overlain by horizontally stratified, fine-grained sandstone, 2) parallel-laminated, alternating fine-grained sandstone and siltstone; and 3) mudstone (Fig. 32A inset). Less common variations include: 1) alternating, parallel-laminated, fine-grained sandstone and siltstone overlain by mudstone; 2) upward-thinning laminations of horizontally stratified, medium- to fine-grained sandstone capped by mudstone (Fig. 33A); 3)

Figure 32. Partial stratigraphic section of a coarsening- and thickening-upward sequence through facies association E at Damascus (locality number 2): A) Interbedded sandstone, siltstone and mudstone. Inset illustrates beds consisting of horizontally stratified, fine-grained sandstone overlain by parallel-laminated sandstone and siltstone and capped by mudstone. B) Thickening-upward sequence consisting of thin- to medium-bedded sandstone and mudstone. Inset shows beds consisting of horizontally stratified, fine-grained sandstone overlain by current-rippled sandstone and capped by mudstone. C) Bioturbated sandstone and subordinate mudstone.

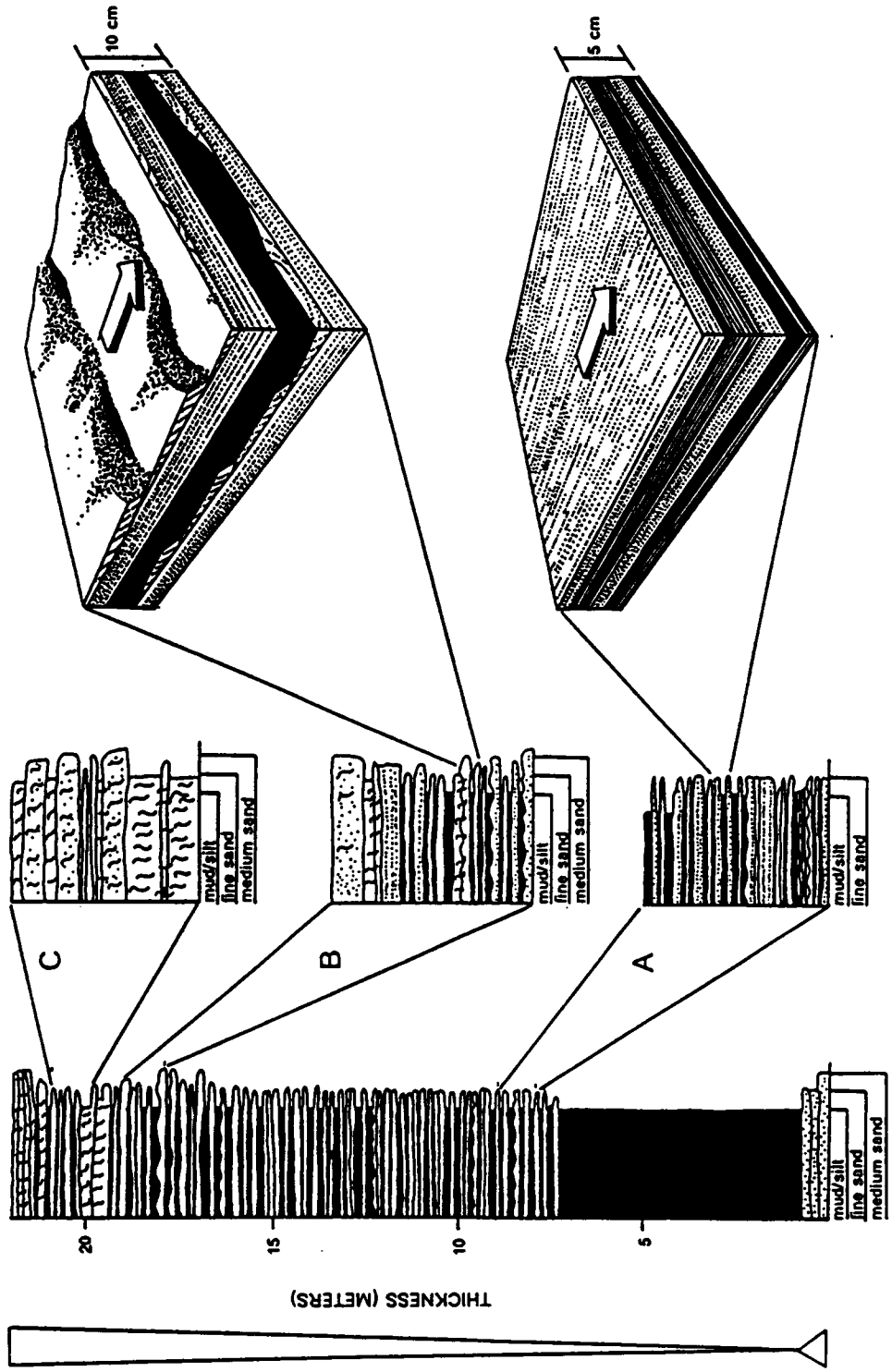
10 cm
5 cm
mud/silt
fine sand
medium sand
C
B
A
20
15
10
5
THICKNESS (METERS)

Figure 33. Photographs of facies association E: A) Bed consisting of upward-thinning, horizontally stratified, laminations of medium- to fine-grained sandstone capped by mudstone; B) Horizontally stratified, fine-grained sandstone overlain by current-rippled sandstone and capped by mudstone; C) Bioturbated, fine-grained sandstone, siltstone and mudstone.

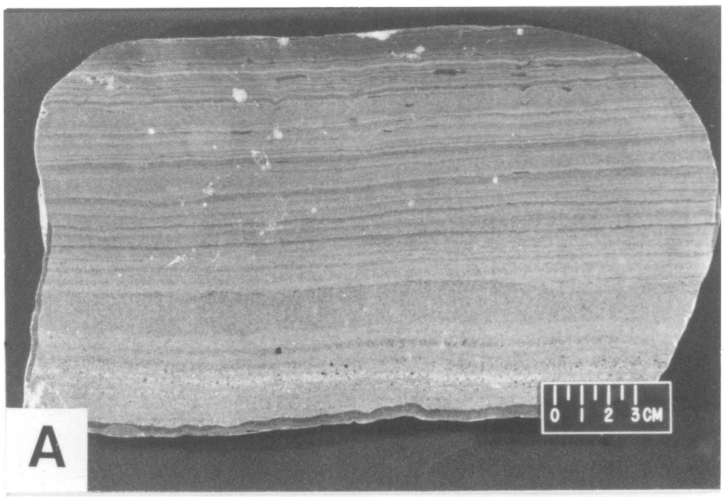

A

B

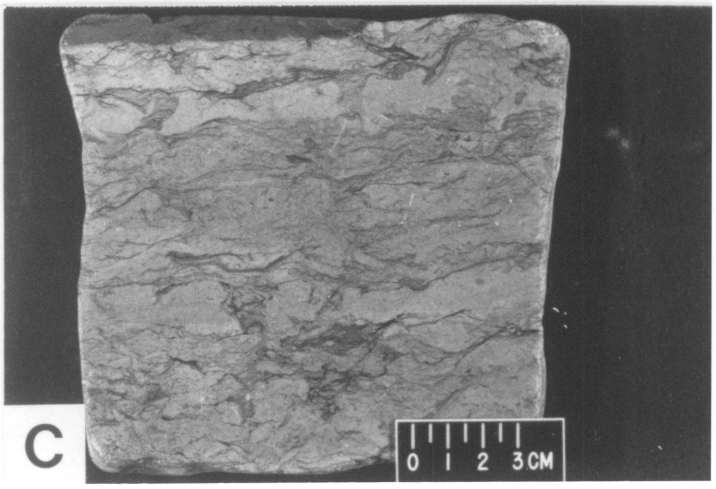

C

scoured, irregular base overlain by massive, graded, medium- to fine-grained sandstone passing upward into horizontally stratified, fine-grained sandstone and capped by mudstone; and 4) siltstone-shale couplets. Subordinate bedding styles include: 1) massive, normally graded, pebble/granule conglomerate to fine-grained sandstone beds; these beds contain discoid mudstone clasts or ferruginous medium-grained sandstone clasts; 2) isolated current ripples encased within mudstone; 3) 1.0 to 5.0 cm-thick beds of climbing current ripples; and 4) horizontally stratified, fine-grained sandstones capped by current-ripple cross laminations (Figs. 32B inset and 33B). Ripple foresets are normally graded from upper fine-grained sandstone to siltstone. In rare bedding-plane views, ripples are lunate-shaped. The predominant paleocurrent direction from current ripples and current-ripples cross laminations is to the northeast (Figure 27F). Gutter casts may occur at the base of beds; these are filled with parallel-laminated, medium-grained sandstone with occasional mudstone clasts.

Distributed throughout this facies association are coarse-grained sandstones beds which range in thickness from 10 to 45 cm. Most beds possess angle-of-repose foresets that grade from coarse- to fine-grained sand. Trough cross bedding predominates and current ripples and megaripples are often preserved on tops of beds. Paleocurrents are highly variable; flow directions range from north to south with a dominant mode towards the southeast (Figure 27G).

Within this facies association bioturbation ranges from 1 to 5 (Droser and Bottjer, 1986). In the 1 to 3 range, burrows are concentrated in siltstone and mudstone; and may extend downward into the sandstone component of any of the beds described above (Fig. 32C). Homogenization of siltstone and mudstone and disruption of sandstone beds occurs most commonly in classes 4 to 5 (Fig. 33C). Some burrows

are mud-lined. In class 5, bedding is preserved as vague color alterations and grainsize changes. Within some stratigraphic intervals, zones of intense bioturbation, alternate with zones displaying weak or no bioturbation; the scale of alternation varies from 10 to 20 m. The only identifiable trace in this facies association is *Planolites sp.* which occurs rarely on bedding planes.

The various bed types in this facies association are arranged in 0.75 to 8.0 m-thick, fining- and thinning-upward and 10 to 150 m-thick, coarsening- and thickening-upward sequences. Examples of these sequences are illustrated in Figure 33. Upwards in the coarsening- and thickening-upward sequences, grain size of sandstones increases from fine-grained to upper medium- to coarse-grained and sandstone beds increase in thickness from 1 to 45 cm. Primary structures within beds also change upwards (see Fig. 32) and bioturbation increases in general from 1 at the base to 4 or 5 near the top. Within the 10 to 150 m-thick sequences are thinner 0.5 to 1.5 m-thick increments which display an upward thickening of beds.

Interpretation

Comparable beds to those present in facies association E have been documented from Holocene shelves and ancient shelf sequences and attributed to turbidity currents (Hayes, 1967; Hamblin and Walker, 1979; Nelson, 1982a; 1982b; Hobday and Morton, 1984; Soegaard and Eriksson, 1985; Snedden and Nummedal, 1986). Stringers of fine- to medium-grained sandstone and siltstone in the lower part of the

sequences were deposited from dilute turbidity currents in an environment dominated by suspension sedimentation. The presence of soft-sediment deformation structures indicates that the muds were saturated. Sandstone beds in the upper two thirds of the facies association resemble Tae, Tabe, Tbde, Tbe, Tbcde and Tcde Bouma sequences. The most common beds which commence with horizontally stratified sandstone typically have been related to weaker turbidity currents than those which commence with a graded interval (Soegaard and Eriksson, 1985).

Paleocurrent data from current ripples in fine-grained sandstone beds are shoreline parallel (Fig. 27F) and can be related to geostrophic flow. Current ripples in coarse-grained sandstone give paleocurrent data which vary from shoreline perpendicular to shoreline parallel (Fig. 27G), indicating both offshore-directed and geostrophic components of flow. These divergent data can be attributed to different flow strengths; weaker turbidity currents evolve into geostrophic flows closer to the shoreline than stronger currents.

Intensity of bioturbation has been related to: 1) sedimentation rates in which the slower the rate of sedimentation the more intense is the bioturbation and 2) the oxygen content at the sediment-water interface (Dodd and Stanton; 1981; Savrda *et al.*. 1984). The first hypothesis can be discounted for this facies association in favor of the second. The lower, shale-dominated part of the sequence reflects slow sedimentation rates but displays a low intensity of bioturbation because of the prevailing anoxygenic conditions implied by the black color of the sediment. The converse of this argument applies to the upper, sand-dominated interval. Changes in the percentage of dissolved oxygen within the water column may be a viable mechanism for explaining the differing intensities of bioturbation within 10 to 15 m-thick intervals. Variation in

intensity of bioturbation within the anoxic-silled basins of California borderlands is a function of fluctuations in the percentage of dissolved oxygen in the water column (Savrda *et al.*, 1984).

The lack of wave-produced sedimentary structures in this facies association indicate that sedimentation took place exclusively below storm-wave base. Facies association E thus is assigned to an outer-shelf depositional setting according to the shelf classification of Harms *et al.* (1982).

SEQUENCE ANALYSIS

Facies associations in the Hampton and Erwin Formations are dominated by stacked 65 to 185 m-thick progradational sequences which vary from westerly to easterly thrust sheets (Fig. 34). Western thrust sheets contain more complete sequences, including the most proximal facies associations, than eastern thrust sheets which are characterized by less well-developed sequences dominated by distal facies associations. Progradational sequences are upward coarsening and upward thickening; these grain-size and bed-thickness trends are best developed in gradational outer- to inner-shelf facies association (Fig. 34). The progradational sequences are capped by 1.0 to 8.5 m-thick upward fining and upward thinning transgressive intervals.

The Hampton Formation in western thrust sheets consists of progradational outer-shelf to inner-shelf to shoreface sequences whereas in eastern thrust sheets the formation is composed of stacked outer-shelf facies associations (Fig. 34). Upper contacts of progradational sequences are demarcated by a interval of massive

Figure 34. Cross-section from west to east across the Hampton and Erwin shelf using base of Shady Dolomite as a datum. Thin intertidal-flat deposits are restricted to the Natural Bridge section. Bottom axis is approximately equivalent to grainsize.

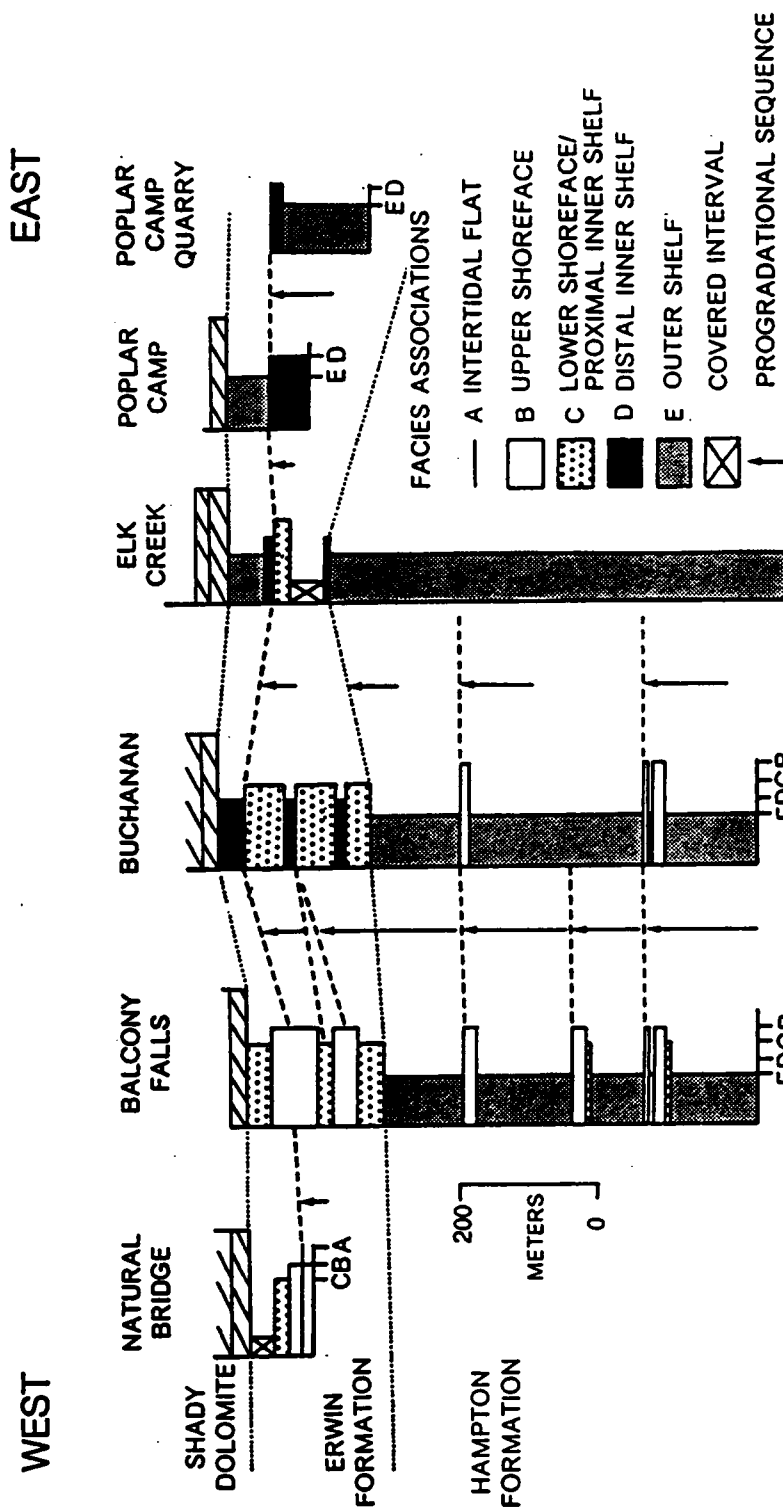
WEST
EAST
NATURAL BRIDGE
BALCONY FALLS
BUCHANAN
ELK CREEK
POPLAR CAMP
POPLAR CAMP QUARRY
SHADY DOLOMITE
ERWIN FORMATION
HAMPTON FORMATION
CBA
EDCB
EDCB
EDC
ED
ED
200
METERS
0
FACIES ASSOCIATIONS
A INTERTIDAL FLAT
B UPPER SHOREFACE
C LOWER SHOREFACE/ PROXIMAL INNER SHELF
D DISTAL INNER SHELF
E OUTER SHELF
COVERED INTERVAL
PROGRADATIONAL SEQUENCE

sandstone with broken *Skolithos* tubes and mudstone clasts, overlain by outer-shelf deposits.

Within western thrust sheets, the Erwin Formation consists of progradational proximal inner-shelf to shoreface sequences (Fig. 34). The transition into overlying proximal inner-shelf deposits is gradational. Intertidal-flat deposits are confined to the westernmost thrust sheet (Fig. 34) and are separated from underlying and overlying shoreface deposits by erosional contacts. Progradational sequences in medial thrust sheets consist of distal inner-shelf overlain by proximal inner-shelf to lower shoreface facies associations (Fig. 34). Within eastern thrust sheets, the Erwin Formation consists of progradational outer-shelf to distal inner-shelf sequences (Fig. 34).

DEPOSITIONAL MODELS

The vertical arrangement of facies associations in the Hampton and Erwin Formations reflect progradational outbuilding of the facies belts interrupted periodically by transgression. Progradation results from the interaction of four parameters: sediment supply, subsidence, rate of sea level change and fluid power expenditure (Neidoroda *et al.*, 1984). If sediment supply exceeds subsidence progradation will commence following the maximum rate of sea level rise, assuming a constant thermal subsidence (Bond *et al.*, 1983). Reduction in the rate of rise lessens the rate of drowning and permits outbuilding of the facies belts (Pittman, 1978). Progradation continues through the maximum regression with possible subaerial exposure of shallow-marine deposits. By moving material back onto the shoreface, fluid power expenditure also can enhance the rate of progradation. Transgression of

Figure 35. Depositional models for Chilhowee shelf. A) Distribution of processes during storm conditions across an idealized progradational shelf. B) Distribution of processes during storm condition across an idealized progradational shelf.

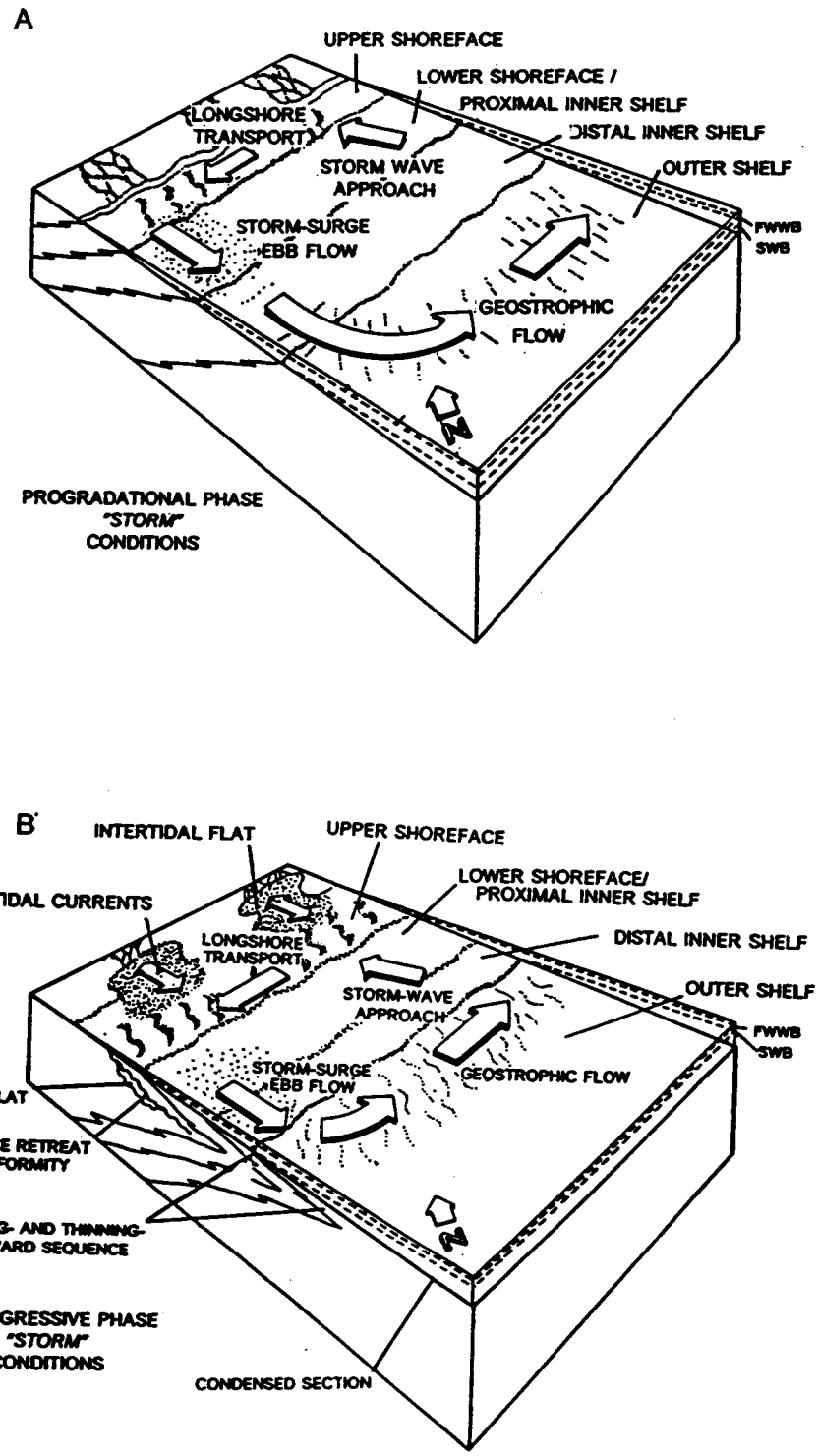
A
UPPER SHOREFACE
LOWER SHOREFACE /
PROXIMAL INNER SHELF
DISTAL INNER SHELF
OUTER SHELF
LONGSHORE TRANSPORT
STORM WAVE APPROACH
STORM-SURGE EBB FLOW
GEOSTROPHIC FLOW
FWWB
SWB
PROGRADATIONAL PHASE
"STORM" CONDITIONS
B
INTERTIDAL FLAT
UPPER SHOREFACE
LOWER SHOREFACE/
PROXIMAL INNER SHELF
TIDAL CURRENTS
LONGSHORE TRANSPORT
DISTAL INNER SHELF
OUTER SHELF
STORM-WAVE APPROACH
FWWB
SWB
STORM-SURGE EBB FLOW
GEOSTROPHIC FLOW
INTERTIDAL FLAT
SHOREFACE RETREAT UNCONFORMITY
FINING- AND THINNING-UPWARD SEQUENCE
TRANSGRESSIVE PHASE
"STORM" CONDITIONS
CONDENSED SECTION

the progradational package occurs when the rate of sea level rise is greater than the progradational rate. Transgression continues until the rate of sea level rise equals the rate of sediment influx at which time maximum transgression has occurred and progradation begins. Tectonic subsidence also may initiate transgression.

Prograding clastic shorelines have a higher preservation potential than transgressive coastal sequences (Davis and Clifton, 1984) and, as a result, wave- and storm-dominated, progradational shelf sequences dominate the stratigraphic record (Duke, 1985; Johnson and Baldwin, 1986). The five coarsening- and thickening-upward sequences in the Hampton and Erwin Formations developed during progradation (Fig. 35A). During these times shorelines were long, linear belts with few tidal inlets. Shoaling fair-weather and storm waves initiated longshore currents that transported sand parallel to the shoreline in the upper shoreface. Sediment was entrained by storm-surge ebb currents and transported offshore. When the storm currents lost their competence in the lower shoreface to proximal inner-shelf, thick massive beds formed by rapid suspension fallout. Sand deposited farther offshore was molded into hummocky cross stratification, or wave-produced sedimentary structures by combined and oscillatory flows. The storm-surge ebb currents evolved into unidirectional geostrophic flows below storm-wave base. The distance offshore that the flows evolved into geostrophic flows was determined by the initial velocity and bedform frictional forces (Walker, 1984; Swift and Nummendal, 1987). Beds display a proximality trend of increasing thickness towards the shoreline with a corresponding transition from *Skolithos* to *Cruziana* ichnofacies. Sediment that moved onto the shelf slowly infilled depositional space created during rising sea level. Deposits shoaled to storm-wave base and finally fair-weather wave base.

Infilling resulted in the development of coarsening- and thickening-upward progradational sequences and a vertical hierarchical change in processes. A constructional graded-equilibrium shelf (Johnson and Baldwin, 1986) or a storm-dominated allochthonous shelf (Swift, 1974) thus existed during the progradational phases (Fig. 35A).

Studies on Holocene shelves have demonstrated that material may not be lost to the inner shelf but can be reworked back into the shoreface by asymmetrical orbital currents at shallower depths, and wave-current interactions at greater depths (Neidoroda, 1980; Neidoroda and Swift, 1981; Vincent *et al.*, 1983; Neidoroda *et al.*, 1984). In the lower shoreface to proximal inner-shelf intermittent landward reworking of detritus by fair-weather or long period waves left lags of coarse sand which were molded into patches of two-dimensional wave ripples. Distal inner and outer shelf sites acted as permanent sediment sinks from which material was not transported landward.

Transgressive shorelines have less preservation potential because shoreline retreat eliminates uppermost shoreface and stratigraphically higher sediments (Davis and Clifton, 1984). Some shelves exhibit a change from storm-dominated sedimentation during the regressive (progradational) phase to more tide-influenced sedimentation during transgression (Nio *et al.*, 1976, Nummedal and Singh, 1986; Wright, 1986; Harris and Eriksson, in prep.). A few shelf sequences contain storm-dominated deposits in the transgressive phase (*cf.* Bourgeois, 1980).

The nature of transgressive deposits in the Hampton and Erwin Formations vary according to the position on the shelf (Fig. 35B). During the final progradational phase, shoreface deposits were exposed to erosion with the development of an

unconformity. The intertidal-flat sediments accumulated on this surface in what probably was an embayment which promoted amplification of the tidal wave. As transgression proceeded, shoreface retreat eliminated upper tidal-flat deposits. In most cases, shoreface erosion removed all record of environmentally more proximal facies with amalgamation of upper shoreface deposits. During transgression detritus may have been transported out of tidal embayments and redistributed offshore by storms or transported shore-parallel by longshore currents (Figure 35B). Generally, very little new material was added to the system during transgression; instead progradational sequences were reworked to develop the thin, fining- and thinning-upward transgressive sequences containing glauconite. These sequences are confined to proximal to medial portions of the shelf. In more distal settings, the transgression is reflected by condensed sections which consist of thick mudstones (Fig. 35B). Hiatuses between progradational intervals may have been on the order of 10^3-10^6 years, the time proposed for the generation of glaconitic smectite to illite (Odin and Matter, 1981).

Hierarchical superposition of different magnitudes of sea level changes has been recognized, first order representing the maximum and fourth or fifth order cycles the minimum (Vail *et al.*, 1977). Inferred time durations range from 200-400 Ma for first-order cycles to 0.2-0.5 Ma for the fourth-order cycles. The basal Hampton Formation consists of a condensed section related to transgression commencing in the upper Unicoi Formation (Simpson and Eriksson, submitted). The initial transgression reflects the first-order Precambrian to Early Triassic cycle of Vail *et al.* (1977), whereas the Hampton and Erwin Formations reflect outbuilding of the Chilhowee passive margin related to a second-order cycle superimposed on a first order cycle.

Based on maximum ages from possible faunal zones, the Hampton and Erwin Formations may span a maximum 30 Ma and probably less (Simpson and Sundberg, 1987). The five progradation packages in the Erwin and Hampton Formations thus span approximately 6 Ma each and are comparable to third-order cycles.

CONCLUSIONS

1) The occcurrence of Hampton and Erwin Formations on different thrust sheets has permitted a reconstruction of Early Cambrain Chilhowee shelf in space and time.

2) The Hampton and Erwin Formations represent an overall regressive sequence punctuated by five progradational packages.

3) Progradational packagees developed under strom- and fair-weather wave conditions. On westerly thrust sheets the packages are upward coarsening and thickneing and consist of outer- to inner-shelf to shoreface facies. Outer-shelf facies predominate on easterly thrust sheets.

4) Transgressive deposits separate the progradational packages and on the most westerly thrust sheet consist of intertidal-flat deposits; thee erosively overlie shoreface sedimetns and developed on an embayment in which the tidal wave was amplified. More distal transgressive deposits consist of thin, fining-and-thinning upward sequences with glauconitic horizons, and condensed sections in mudstones.

5) The five progradational packages each developed during approximately 6 Ma and thus correspond to third-order, sea-level cycles.

REFERENCES

Aigner, T., 1985, Storm depositional systems: dynamic stratigraphy in modern and ancient shallow-marine sequences: Lecture Notes in Earth Sciences 3, Springer-Verlag, New York, pp. 173.

Aigner, T., and Reineck, H. E., 1982, Proximality trends in modern storm sands from the Helgoland Bight (North Sea) and their implications for basin analysis: Senckenbergiana Maritima, v. 14, p. 183-215.

Alam, M. M., Crook, K. A. W., and Taylor, G., 1985, Fluvial herring-bone cross-stratification in a modern tributary mouth bar, Coonamble, New South Wales, Australia: Sedimentology, v. 32, p. 235-244.

Allen, J. R. L., 1973, Features of cross-stratified units due to random and other changes in bedforms: Sedimentology, v. 20, p. 189-202.

Allen, J. R. L., 1980, Sand waves: a model of origin and internal structure, Marine Geology, v. v. 26, p. 281-328.

Allen, J. R. L., 1981, Lower Cretaceous tides revealed by cross-bedding with mud drapes: Nature, v. 289, p. 579-581.

Allen, J. R. L., 1983, Sedimentary Structures: their character and physical basis: Developments in Sedimentology no 30, 663 p.

Allen, P. A., 1981, Wave-generated structures in the Devonian lacustrine sediments of southeast Shetland and ancient wave conditions: Sedimentology, v. 28, p. 369-379.

Allen, P. A., 1984, Reconstruction of ancient sea conditions with an example from the Swiss molasse: Marine Geology, v. 60, p. 455-473.

Allen, P. A., 1985, Hummocky cross-stratification is not produced purely under progressive gravity waves: Nature, v. 313, p. 562-564.

Allen, P. A., and Homewood, P., 1984, Evolution and mechanics of a Miocene tidal sandwave: Sedimentology, v. 31, p. 63-81.

Alpert, S. P., 1977, Traces fossils and the basal Cambrian boundary, *in* Crimes, T. P., and Harper, J. C., eds., *Trace Fossils 2*: Geological Journal Special Issue No. 9, p. 1-8.

Anderton, R., 1976, Tidal-shelf sedimentation: an example from the Scottish Dalradian: Sedimentology, v. 23, p. 429-458.

Barnaby, R. J., and Simpson, E. L., 1987, Evolution of Early Cambrian passive margin, southwest Virginia: Geological Society of America Abstracts with Programs, v. 19, p. 76.

Belderson, R. H., Johnson, M. A., and Kenyon, W. H., 1982, Bedforms, *in* Stride, A. H., ed., *Offshore Tidal Sands, Processes and Deposits*: Chapman and Hall, London, p. 22 -57.

Bergstrom, J., 1981, Lower Cambrian shelly faunas and biostratigraphy in Scandinavia, *in* Taylor, M. E., ed., *Short papers for the Second International Symposium on the Cambrian System*: U. S. Geological Survey Open-file Report 81-743.

Beverage, J. P., and Culbertson. J.K., 1964, Hyperconcentration of suspended sediment: Journal of the Hydraulics Division, Proceedings of Society of American Civil Engineers, p. 117-128.

Blondeau, K. M., and Lowe, D. R., 1972, Upper Precambrian glacial deposits of the Mount Rogers Formation, central Appalachians, U.S.A.: International Geological Congress., 24th, Montreal 1972, Proceeding Series 1, P. 325-332.

Boersma, J. R., and Terwindt, J. H. J., 1981, Neap-spring tidal sequences of intertidal shoal deposits in a mesotidal estuary: Sedimentology, v. 28, p. 151-170.

Bond, G. C., Nickeson, P. A., and Kominz, M. A., 1984, Breakup of a supercontinent between 625 Ma and 555 Ma: New evidence and implications for continental histories: Earth and Planetary Science Letters, v. 70, p. 325-345.

Boothroyd, J. C., and Ashley, 1975, Process, bar morphology and sedimentary structures on braided outwash fans, North-eastern Gulf of Alaska, *in* Jopling, A. V., McDonald, B. C., eds., *Glaciofluvial and glaciolacustrine Sedimentation:* Society of Economic Paleontologists and Mineralogists Special Publication No. 23, p. 193-222.

Bott, M. H. P., 1979, Subsidence mechanisms at passive continental margins, *in* Watkins, J. S., Montadert, L., and Dickerson, P. G., eds., *Geological and Geophysical Investigations of Continental Margins*: American Association of Petroleum Geologists Memoir 7, p. 3-9.

Bourgeois, J., 1980, A transgressive shelf sequence exhibiting hummocky stratification: the Cape Sebastian Sandstone (Upper Cretaceous), southwestern Oregon: Journal of Sedimentary Petrology, v. 50, p. 681-702.

Boyer, S. E., and Elliott, D., 1982, Thrust systems: American Association of Petroleum Geologists Bulletin, v. 66, p. 1196-1230.

Bradley, W. C., Fahnestock, R. K., and Rowekamp, E. T., 11972, Coarse sediment transport by flood flows in Knik River, Alaska: Geological Society of America Bulletin, v. 83, p. 1261-1284.

Brasier. M. D., 1984, Microfossils and small shelly fossils from the Lower Cambrian *Hyolithus* Limestone at Nuneaton, English Midlands: Geological Magazine, v.

121, p. 229-253.

Brasier, M. D., Hewitt, R. A., and Brasier, J., 1978, On the Late PreCambrian-Early Cambrian Hartshill Formation of Warwickshire: Geological Magazine, v. 115, p. 21-36.

Brown, W. R., 1970, Investigations of the sedimentary record in the Piedmont and Blue Ridge on Virginia, *in* Fisher, G. W., Pettijohn, F. J., Reed, J.C., and Weaver, K. N., eds., *Studies of Appalachian Geology: central and southern:* New York, Interscience, p. 335-349.

Bruun, P., 1962, Sea level rise as a cause of shoreface erosion: Proceedings of American Society of Civil Engineers, Journal Waterways and Harbors Division, v. 88, p. 117-130.

Bull, W. B., 1972, Recognition of alluvial-fan deposits in the stratigraphic record, *in* Hamblin, W. K.,and Rigby, J. K., eds., *Recognition of ancient sedimentary environments*: Society of Economic Paleontologist and Mineralogists, Special Publication 16, p. 63-83.

Burke, K., and Kidd, W. S. F., 1980, Volcanism on earth through time, *in* Strangeway, D. W., ed., *The continental crust and its mineral deposits*: Geological Association of Canada Special Paper 20, p. 503-522.

Carey, D.A., 1987, Sedimentological effects and palaeoecological implications of the tube-building polychaete *Lanice conchilega* Pallas: Sedimentology, v. 34, p. 49-66.

Cas, R., 1979, Mass-flow arenites from Paleozoic interarc basin, New South Wales, Australia: mode and environment of emplacement: Journal of Sedimentary Petrology: v. 49, p. 29-44.

Clifton, H. E., 1976, Wave-formed sedimentary structures - a conceptual model, in R. A. Davis and R. L. Ethington, eds., *Beach and Nearshore Sedimentation*:: Society of Economic Paleontologists and Mineralogists Special Publication 24, p. 126-148.

Clifton, H. E., and Dingler, J. R., 1984, Wave-formed structures and palaeoenvironmental reconstruction: Marine Geology, v. 60, p. 165-198.

Clifton, H.E., Hunter, R.E., and Phillips, R.C., 1971, Depositional structures and processes in the non-barred, high energy nearshore: Journal Sedimentary Petrology, v. 41, p. 651-670.

Cloud, P., Wright, J., and Glover, L., III, 1976, Traces of animal life from 620-million-year-old rocks in North Carolina: American Scientist, v. 64, p. 396-406.

Coleman, J. M., 1969, Brahmaputra River, channel processes and sedimentation: Sedimentary Geology, v. 3, p. 129-239.

Collinson, J. D., 1970, Bedforms of the Tana River, Norway: Geografiska Annaler, v. 52A, p. 31-56.

Crittenden, Jr., M. D., Christie-Blick, N. and Link, P. K., 1983, Evidence for two pulses of glaciation during the late Proterozoic in northern Utah and southeastern Idaho: Geological Society of America Bulletin, v. 94, p. 437-450.

Crossley, R., 1979, Structure and volcanism in the South Kenya rift system, Academia Nazionale die Lincei, Roma, p. 89-98.

Cudzil, M. R., 1985, Fluvial, tidal and storm sedimentation in the Chilhowee Group (Lower Cambrian, northeastern Tennessee {M.S. thesis}: Knoxville, Tennessee, 164 p.

Cudzil, M. R., and Driese, S. G., in press, Fluvial, tidal and storm sedimentation in the Chilhowee Group (Lower Cambrian), northeastern Tennessee, U.S.A.: Sedimentology.

Dalrymple, R.W., 1984a, Morphology and internal structure of sandwaves in the Bay of Fundy: Sedimentology, v. 31, p. 365 - 382.

Dalrymple, R. W., 1984b, Runoff microdeltas: a potential emergence indicator in cross-bedded sandstones: Journal of Sedimentary Petrology, v. 54, p. 825-830.

Dalrymple, R. W., Knight, R. J., and Lambiase, J. J., 1977, Bedforms and their hydraulic stability relationships in a tidal environment, Bay of Fundy, Canada: Nature, v. 275, p. 100 - 104.

Davis, G. L., Tilton, G. R., and Wetherill, G. W., 1962, Mineral ages from the Appalachian province in North Carolina and Tennessee: Journal of Geophysical Research, v. 67, p. 1987-1996.

Davis, R. A., Jr., and Clifton, H. E., 1984, Sea-level changes and preservation potential of wave-dominated and tide-dominated coastal sequences: Society of Economic Paleontologists and Mineralogists Annual Midyear Meeting Abstracts, v. 1, p. 23.

de Mowbray, T., and Visser, M. J., 1984, Reactivation surfaces in subtidal channel deposits, Oosterschelde, southwest Netherlands: Journal of Sedimentary Petrology, v. 54, p. 811-824.

de Raaf, J. M. F., Boersma, J. R., and van Gelder, A., 1977, Wave-generated structures and sequences from a shallow marine succession, Lower Carboniferous, county Cork, Ireland: Sedimentology, v. 24, p. 451-483.

Deslages, T. A., and Church, M., 1987, Channel and floodplain facies in a wandering gravel bed river *in* Ethridge, F. G., Flores R. M., and Harvey, M.D., eds., *Recent Developments in Fluvial Sedimentology: Contributions from the Third International Fluvial Sedimentology Conference*: Society of Economic

Paleontologists and Mineralogists Special Publication No. 39, p. 99-109.

Diem, B., 1985, Analytical method for estimating paleowave climate and water depth from wave ripple marks: Sedimentology, v. 32, p. 705-720.

Dingler, J. R., Hunter, R. E., and Richmond, B. M., 1985, Coarse-sediment bands in the nearshore of southern Monterey Bay, California: Society of Economic Paleontologists and Mineralogists Annual Midyear Meeting Abstracts, V. 2, p. 25.

Dodd, J.R., and Stanton, R.J. Jr., 1981, Paleoecology, concepts and applications: John Wiley and Sons, New York, 559 p.

Donovan, D. T., and Jones, E J. W., 1979, Causes of world-wide changes in sea level: Journal of the Geological Society of London, v. 136, p. 187-192.

Donovan, R. N., and Foster, R. J., 1972, Subaqueous shrinkage cracks from the Caithness Flagstone Series (Middle Devonian) of north Scotland: Journal of Sedimentary Petrology, v. 42, p. 309-317.

Dott, R. H. Jr., and Bourgeois, J., 1982, Hummocky stratification: significance of its variable bedding sequence: Bulletin of the Geological Society of America, v. 93, p. 663-680.

Dott, R. H., Jr., Byers, C. W., Fielder, G. W., Stenzel, S. R., and Winfree, K. E., 1986, Aeolian to marine transition in Cambro-Ordovician cratonic sheet sandstones on the northern Mississippi valley, U.S.A.: Sedimentology, v. 33, p. 345-368.

Droser, M. L., and Bottjer, 1986, A semiquantitative field classification of Ichnofacies: Journal of Sedimentary Petrology, v. 56, p. 558-559.

Duke, W. L., 1985, Hummocky cross-stratification, tropical hurricanes, and intense winter storms: Sedimentology, v. 32, p. 167-194.

Duke, W. L., 1987, Reply: Hummocky cross-stratification, tropical hurricanes, and intense winter storms: Sedimentology, v. 34, p. 344-357.

Elliot, T., 1986, Siliciclastic shorelines, in Reading, H. G., ed., *Sedimentary Environments and Facies*: Blackwell Scientific Publications, Boston, Massachusetts, p. 155-188.

Evans, G., 1965, Intertidal flat sediments and their environments of deposition in the Wash: Quarterly Journal of the Geological Society of London, v. 121, p. 209-245.

Evans, G., 1975, Intertidal flat deposits of the Wash, western margin of the North Sea: in Ginsberg, R. N., ed., *Tidal deposits: a casebook of recent examples and fossil counterparts:* Springer Verlag, Berlin, p. 13-20.

Fedonkin, M. A., 1981, Paleoichnology of the PreCambrian-Cambrian Transition, *in* Taylor, M. E., ed., *Short papers from the Second International Symposium on the Cambrian System*: U. S. Geological Survey Open-file Report 81-743, p. 89-90.

Fichter, L. S., and Diecchio, R. J., 1986, Stratigraphic model for timing the opening of the Proto-Atlantic Ocean in northern Virginia: Geology, v. 14, p. 307-309.

Fritz, W. H., 1972, Lower Cambrian trilobites from the Sekwi Formation type section, Mackenzie Mountains, north-western Canada: Geological Survey of Canada Bulletin, v. 212, p. 1-58.

Fritz, W. H., And Crimes, T. P., 1985, Lithology, trace fossils and correlation of the Precambrian-Cambrian Boundary beds, Cassiar Mountains, north-central British Columbia: Geological Survey of Canada Paper 83-13, 24 p.

Frey, R.W., and Seilacher, A., Uniformity in marine invertebrate ichnology: Lethaia, v. 13, p. 183-207.

Frey, R. W., and Pemberton, S. G., 1984, Trace fossils facies models in Walker, R.G., ed., *Facies Models*: Geoscience Reprint Series 1, p. 189-207.

Germs, G. J. B., 1972, New shelly fossil from Nama Group, southwest Africa: American Journal of Science, v. 272, p. 752-761.

Glaessner, M. F., 1984, The dawn of animal life, a biohistorical study: Cambridge, England, Cambridge University Press, 244 p.

Goldring, R., and Aigner, T., 1982, Scour and fill: the significance of event separation, *in*, Einsele, G., and Seilacher, A., eds., *Cyclic and Event Stratification*, Springer-Verlag, New York, New York, pp. 354-362.

Hamblin, A. P., and Walker, R. G., 1979, Storm dominated shallow marine deposits: the Fernie-Kootenay (Jurassic) transition, southern Rocky Mountains: Canadian Journal of Earth Sciences, v. 16, p. 1673-1690.

Hampton, M. A., 1975, Competence of fine-grained debris flows: Journal of Sedimentary Petrology, v. 45, p. 834-844.

Hantzchel, W., 1975, Trace fossils and problematica, *in* Teichert, c., ed., Treatise in invertebrate paleontology, Part W. Miscellanea: Lawrence, Kansas, Geological Society of America and University of Kansas, 269 p.

Harland, W. B., 1983, The Proterozoic glacial record, *in* Medaris, L. G., Jr., Byers, C. W., Michelson, D. M., and Shanks, W. C., eds., *Proterozoic Geology*, Geological Society of America Memior 161, p. 279-288.

Harms, J. C., Southard, J. B., and Walker, R. G., 1982, Structures and sequences in clastic rocks: Society of Economic Paleontologists and Mineralogists short course 9, Calgary. 251 p.

Harris, C. W., and Eriksson, K. A., in prep, Progradational sequences in the Early Proterozoic Uncompahgre Group, southwest Colorado: cyclic controls on shallow-marine sedimentation in a storm- to tide-dominated shelf.

Hawley, N., 1982, Intertidal sedimentary structures on macrotidal beaches: Journal of Sedimentary Petrology, v. 52, p. 785-795.

Hayes, M. O., 1967, Hurricanes as geologic agents, south Texas coast: American Association of Petroleum Geologists Bulletin, v. 51, p. 937-942.

Hayes, M. O., 1980, General morphology and sediment patterns in tidal inlets: Sedimentary Geology, v. 26, p. 139-156.

Hein, F. J., and Walker, R. G., 1977, Bar evolution and development of stratification in the gravelly, braided Kicking Horse River, B. C.: Canadian Journal of Earth Sciences, v. 14, p. 562-570.

Heward, A. P., 1978, Alluvial fan sequences and megasequence models: with examples from Westphalian D - Stephanian B coal-fields, Northern Spain, *in* A. D. Miall, ed., *Fluvial Sedimentology*: Canadian Society of Petroleum Geologists, Memoir 5, p. 669-702.

Hobday, D. K., and Morton, R.A., 1984, Lower Cretaceous shelf storm deposits, northeast Texas, in Tillman R.W., and Siemers, C.T., eds., *Siliciclastic Shelf Sandstones*: Society of Economic Paleontologist sand Mineralogists Special Publication 34, p. 205-213.

Howard, J. D., and Frey, R. W., 1984, Characteristic trace fossils in nearshore to offshore sequences, upper Cretaceous of east-central Utah: Canadian Journal of Earth Science, v. 21, p. 200-219.

Hiscott, R. N., 1983, Tidal deposits of the Lower Cambrian Random Formation, eastern Newfoundland: facies and paleoenvironments: Canadian Journal of Earth Sciences, v. 19, p. 2028-2042.

Houbolt, J. J. H. C., 1968, Recent sediments in the southern bight of the North Sea: Geologie en Mijnbouw, v. 49, p. 254-273.

Hubert, J F., and Hyde, M. G., 1983, Sheet flow deposits of graded beds and mudstones on an alluvial sandsflat-playa system: Upper Triassic Blomidon redbeds, St. Mary's Bay, Nova Scotia: Sedimentology, v. 29, p. 457-474.

Hunter, R. E., 1977, Basic types of stratification in small eolian dunes: Sedimentology, v. 24, p. 361-387.

Hunter, R. E., and Clifton, H. E., 1982, Cyclic deposits and hummocky cross-stratification of probable storm origin in upper Cretaceous rocks of the Cape Sebastian area, southwestern Oregon: Journal of Sedimentary Petrology, v. 52, p. 127-143.

Hunter, R. E., Clifton, H.E., and Phillips, R.L., 1979, Depositional processes, sedimentary structures and predicted vertical sequence in barred nearshore systems, south Oregon coast: Journal Sedimentary Petrology, v. 46, p. 711-726.

Jaing Zhiwen, 1981, Shelly fossil assemblages and the trace-fossil sequence in the Meishucun Stage, China, *in* Taylor, M. E., ed., *Short papers for the Second International Symposium on the Cambrian System*: U. S. Geological Survey Open-File Report 81-743, p. 98-99.

Johnson, H. D., and Baldwin, C. T., 1986, Shallow siliciclastic seas, in H. G. Reading, ed., *Sedimentary Environments and Facies*, Blackwell Scientific Publications, Boston, Massachusetts, p. 229-282.

Karner, G. D., 1986, Effects of lithospheric in-plane stress on sedimentary stratigraphy: Tectonics, v. 5, p. 573-588.

Kenyon, N. H., Belderson, R.H., Stride, A.H., and Johnson, M.A., 1981, Offshore tidal sand banks as indicators of net sand transport and as a potential deposits, *in* Nio, Si-Di, Shuttenheln R.T.E., and vanVeering, T.C.E., ed., *Holocene Sedimentation in the North Sea Basin*: Special Publication International Association Sedimentologists. No. 5, p. 257-268.

King, P. B., 1949, The base of the Cambrian in the southern Appalachians: American Journal of Science, v. 247, p. 513-530, 622-645.

King. P. B., and Ferguson, H. W., 1960, Geology of northeasternmost Tennessee: U. S. Geological Survey Professional Paper 311, 136 p.

Kinsman, D. J. J., 1975, Rift valley basins and sedimentary history of trailing continental margins, *in* Fischer, A. G., and Judson, S., eds., *Petroleum and global tectonics*: Princeton, New Jersey, Princeton University Press. p. 83-126.

Klein, G., de V., 1971, A sedimentary model for determining paleotidal range: Geological Society of America Bulletin, v. 89, p. 2585-2592.

Klein, G., de V., 1977, Clastic tidal facies: Continuing Education Publication Company, Champaign, Illinois, 149 p.

Knoll, A. H., And Keller, F. B., 1979, Late Precambrian microfossils from the Walden Creek Group, Ocoee Supergroup, Tennessee: Geological Society of America Abstracts with Programs, v. 11, p. 185,

Kocurek, G., and Dott, R. H. Jr., 1981, Distinctions and uses of stratification types in the interpretation of eolian sand: Journal of Sedimentary Petrology, V. 51, p. 579-595.

Kocurek, G., and Fielder, G., 1982, Adhesion structures: Journal of Sedimentary Petrology, v. 51, p. 1229-1241.

Komar, P. D., and Inman, D. L., 1970, Longshore sand transport on beaches: Journal of Geophysical Research, v. 75, p. 5914-5927.

Kreisa, R. D., 1981, Storm-generated sedimentary structures in subtidal marine facies with examples from the middle Ordovician of southwestern Virginia: Journal of Sedimentary Petrology, v. 51, p. 823-848.

Kreisa, R. D., 1985, On hummocks and swales: Storm stratification as a function of storm-processes and grainsize: Society of Economic Paleontologists and Mineralogists Annual Midyear meeting Abstracts, v. 2, p. 52.

Kreisa, R. D., and Moiola, R.J., 1986, Sigmoidal tidal bundles and other tide-generated sedimentary structures of the Curtis Formation, Utah: Geological Society of America Bulletin, V. 97, p. 381-387.

Kumar, G., Raina, B. K., Bhargava, O. N., Maithy, P. K., and Babu, R., 1984, The Precambrian-Cambrian boundary problem and its prospects in northwest Himalaya, India: Geological Magazine, v. 121, p. 211-219.

Kumar, N., and Sanders, J. E., 1974, Inlet sequence: a vertical succession of sedimentary structures and textures created by the lateral migration of tidal inlets: Sedimentology, v. 21, p. 491-532.

Kumar, N., and Sanders, J. E., 1976, Characteristics of shoreface deposits:modern and ancient examples: Journal of Sedimentary Petrology, v. 46, p. 145-162.

Land, C. B., Jr., 1972, Stratigraphy of Fox Hills Sandstone and associated formations, Rock Springs uplift and Wamsutter arch area, Sweetwater County Wyoming: a shoreline-estuary sandstone model for the Late Cretaceous: Quarterly Journal of Colorado School of Mines, v. 67, no. 2, 69 pp.

Laurence, R. A., and Palmer, A. R., 1963, Age of the Murray Shale and Hesse Quartzite on Chilhowee Mountain, Blount County Tennessee: United States Geological Survey Professional Paper 475-C, p. c53-c54.

Lawson, D. E., 1981,Mobilization, movement and deposition of active subaerial flows: Journal of Geology, v. 90, p. 279-300 p. 8.

Lowe, D. R., 1976, Subaqueous liquefied and fluidized sediment flows and their deposits: Sedimentology, v. 23, p. 285-308.

Mack, G. H., 1980, Stratigraphy and depositional environments of the Chilhowee Group (Cambrian) in Georgia and Alabama: American Journal of Science, v. 280, p. 497-517.

McCabe, P. J., and Jones, C. M., 1977, Formation of reactivation surfaces within superimposed deltas and bedforms: Journal of Sedimentary Petrology, v. 47, p. 707-715.

McCubbin, D. G., 1972, Facies and paleocurrents of the Gallup sandstones, a model

for alternating deltaic and strand-plain progradation: American Association of Petroleum Geologists Bulletin, v. 56, p. 638.

McCubbin, D. G., 1982, Barrier island and strand plain facies, *in* Scholle, P.A., ed., *Sandstone Depositional Environments*: American Association of Petroleum Geologists Memoir 31, p. 247-279.

McGowen, J. H., 1970, Gum Hollow fan delta, Neuces Bay, Texas: The University of Texas at Austin, Bureau of Economic Geology Report of Investigations 69, 91 p.

McKee, E. D., Crosby, E. J., Berryhill, H. L., Jr., 1967, Flood deposits, Bijou Creek, Colorado, June 1965: Journal of Sedimentary Petrology, v. 37, p. 829-851.

McPherson, J. G., Shanmugam, G., Moiola, R. J., 1986, Fan deltas and braid deltas: conceptual problems: American Association of Petroleum Geologists Bulletin, v. 70 p. 619.

Miall, A.D., 1977, A review of the braided-river depositional environment: Earth-science Review, v. 13, p. 1-62.

Miall, A. D., 1981, Analysis of fluvial depositional systems: American Association of Petroleum Geologists, Education Short Course Notes Series, No. 20, 75 pp.

Miall, A. D., 1985, Architectural-element analysis: a new method of facies analysis applied to fluvial deposits: Earth-Science Reviews, v. 22, p. 261-308.

Middleton, G. V., 1970, Experimental studies related to problems of flysch sedimentation, *in* Lajoie, J., ed., *Flysch Sedimentology in North America*, Geological Association of Canada Special Paper No. 7, p. 253-272.

Middleton, G. V.1967, Experiments on density and turbidity currents III. deposition of sediment: Canadian Journal of Earth Science, v. 4. P. 475-505.

Middleton, G. V., and Hampton, M. A., 1976, Subaqueous sediment transport and deposition by sediment gravity flows, *in* Stanley, D. J., Swift, D. J. P., eds., *Marine Sediment Transport and Environmental Management*, Wiley, New York, p. 197-218.

Miller, J. M. G., 1986, Upper Proterozoic glaciogenic rift-valley sedimentation: upper Mount Rogers Formation, southwestern Virginia: American Association of Petroleum Geologist Bulletin: v. 70, p. 621.

Miller, J. M. G., 1987, Paleotectonic and stratigraphic implications of the Kingston Peak-Noonday Contact in the Panamint Range, eastern California: Journal of Geology, v. 95, p. 75-86.

Morton, R. A., 1981, Formation of storm deposits by wind-forced currents in the Gulf of Mexico and the North Sea, *in* Nio, Si-D, Shuttenhelm, R. T. E., and van

Wering, J. C. E., eds., *Holocene Marine Sedimentation in the North Sea Basin*, Special Publication of the International Association of Sedimentologists 5, p. 385-396.

Mose, D. G., and Nagel, S., 1984, Rb-Sr age from the Robertson River pluton in Virginia and its implication on the age of the Catoctin Formation: Geological Society of America Special Publication 194, p. 167-173.

Moslow, T. F., 1984, Depositional models of shelf and shoreline sandstones: American Association of Petroleum Geologists, Continuing Education Course Notes series 27, 102 pp.

Neidoroda, A. W., 1980, Shoreface-surf zone sediment exchange processes and shoreface dynamics: National Oceananic and Atmospheric Administration Technical Memo OMPA-1, 89 pp.

Neidoroda, A. W., and Swift, D. J. P., 1981, Maintence of shoreface by wave orbital currents and mean flow: observations from Long Island coast: Geophysical Research Letters, v. 8, p. 337-340.

Neidoroda, A. W., Swift, D. J. P., Hopkins., T. S., Chen-Mean, M. 1984, Shoreface morphodynamics on wave-dominated coasts: Marine Geology, v. 60, p. 331-354.

Nelson, C. H., 1982a, Modern shallow-water graded sand layers from storm surges, Bering shelf: a mimic of bouma sequences and turbidite systems: Journal of Sedimentary Petrology, v. 52, p. 537-545.

Nelson, C. H., 1982b, Late Pleistocene-Holocene transgressive sedimentation in deltaic and non-deltaic areas of the north-eastern Bering epicontinental shelf, *in* Nelson, C.H., and Nio, S.D., eds., The northeastern Bering shelf: new perspectives of epicontinental shelf processes and depositional products: Geologie Mijnbouw, v. 61, p. 37-48.

Nemec, W., and Muszynski, A. 1982, Volcaniclastic alluvial aprons in the Tertiary of Sofia District (Bulgaria): Annales Societatis Geologorum Poloniaz, v. 52, p. 239-303.

Nio, S-D, 1976, Marine transgressions as a factor in the formation of sandwave complexes: Geologie en Mijnbouw, v. 55, p. 18-40.

Nio, S-D., van den Berg, J. H., Goesten, M., and Smulders, F., 1980, Dynamics and sequential analysis of a mesotidal shoal and intershoal channel complex in the eastern Scheldt (southwestern Netherlands): Sedimentary Geology, v. 26, p. 263-279.

Nio, S-D., Siegenthaler, C., and Yang, C. S., 1983, Megaripple cross-bedding as a tool for the reconstruction of the palaeo-hydraulics in a Holocene subtidal environment, S.W. Netherlands: Geologie en Mijnbouw, v. 62, p. 499-510.

Nottvedt, A., and Kreisa, R. D., 1987, Model for combined flow origin of hummocky cross-stratification: Geology, v. 15, p. 357-361.

Nowlen, G. S., Narbonne, G. M., and Fritz, W. H., 1985, Small shelly fossils and trace fossils near the Precambrian-Cambrian boundary in the Yukon Territory, Canada: Lethaia, v. 18, p. 232-256.

Nummedal, D., 1986, Storm- verses tide-dominated structures in the Tocito Sandstone, Coniacian of San Juan Basin, New Mexico: Geological Society of America Abstracts with Programs, v. 18, p. 709.

Nunan, W. E., 1980, Stratigraphy of the Weaverton Formation, northern Blue Ridge anticlinorium: The University of North Carolina at Chapel Hill Unpublished Ph. D. Dissertation, 215 p.

Odin, G. S., and Matter, A., 1981, De glauconiarum origine: Sedimentology, v. 28, p. 611-641.

Odom, 1971, A Rb-Sr isotopic study: implications regarding the age, origin, and evolution of a portion of the southern Appalachians, western North Carolina, southwestern Virginia, northwestern Tennessee: Ph. D. dissertation, University of North Carolina, Chapel Hill, 92 p.

Odom, A.L., and Fullagar, P. D., 1971, A major discordancy between U-Pb zircon ages and Rb-Sr whole-rock ages of Late Precambrian granites in the Blue Ridge Provinance: Geological Society of America Abstracts with Programs, v. 3, p. 663.

Odom, A. L., and Fullagar, P. D., 1984, Rb-Sr and inherited zircon ages of the plutonic suite of Crossnore Complex, southern Appalachians, and their implications regarding the time of the opening of the Iapetus Ocean: Geological Society of America Special Paper,194, p. 255-261.

Palmer, A. R., 1981, Subdivision of the Suak Sequence, *in* Taylor, M. E., ed., *Short papers for the Second International Symposium on the Cambrian System*: U. S. Geological Survey Open-file Report 81-743, p. 160-161.

Palmer, A. R., 1983, The Decade of North American Geology 1983 geological time scale: Geology, v. 1, p. 503-504.

Patterson, J. G., 1987, Evolution of the late Proterozic (?) to early Paleozoic distal passive margin to ancestral North America, in the central Appalachians: Geological Society of America Abstracts with Programs, v. 19, p. 123.

Pittman, W. C., III, 1978, Relationship between eustacy and stratigraphic sequences of passive margins: Geological Society of American Bulletin, v. 89, p. 1389-1403.

Rankin, D. W., 1967, Guide to the geology of the Mount Rogers area, Virginia, North Carolina and Tennessee: Carolina Geological Society Field Trip Guide

Book, 48 p.

Rankin, D. W., 1970, Stratigraphy and structure of Precambrian rocks in north-western North Carolina, *in* Fisher, G. W., and others, eds., *Studies of Appalachian geology: Central and Southern*: New York, Interscience Publishers. p. 227-245.

Rankin, D. W., 1975, The continental margin of eastern North America in the southern Appalachians: the opening and closing of the proto-Atlantic Ocean: American Journal of Science: v. 275-A, p. 298-336.

Rankin, D. W., 1976, Appalachian salients and recesses Late Precambrian continental breakup and the opening of the Iapetus Ocean: Journal of Geophysical Research: v. 81, p. 5605-5619

Rankin, D. W., Stern, T. W., Reed, J. C., Jr., and Newell, M. F., 1969, Zircon ages of felsic volcanic rocks in the upper Precambrian of the Blue Ridge central and southern Appalachian Mountains: Science, v. 166, p. 741-744.

Rast, N., and Kohles, K. M., 1986, The origin of the Ocoee Supergroup: American Journal of Science, v. 286, p. 593-616.

Read, J. F., in press, Evolution of Cambro-Ordovician passive margins, U. S. Appalachians: Decade of North America Geology Synthesis Vol. Appalachian-Ouachita.

Reineck, H. E., 1963, Sedimentgefuge im Bereich der Sudliche Nordsee: Abhandl. senckenbergiana naturforsch Gesell: 505, 138 p.

Reineck, H. E., and Wunderlich, F., 1972, Genesis of laminated sands and graded rhythmites in storm-sand layers of shelf mud: Sedimentology, v. 18, p. 123-128.

Rhoads, D.C., 1975, The paleoecological and environmental significance of trace fossils: *in* Frey, R.W., *The Study of Trace Fossils:* Springer Verlag, New York, p. 147-160.

Rogers, J., 1972, Latest Precambrian (post-Grenville) rocks of the Appalachian region: American Journal of Science, v. 272, p. 507-520.

Rubin, D. M., and Hunter, R. E., 1982, Bedform climbing and theory and nature, Sedimentology, v. 29, p. 121-138.

Savrda, C. E., Bottjer, D. J., and Gorsline, D. S., 1984, Development of a comprehensive oxygen-deficent marine biofacies model: evidence from Santa Monica, San Pedro, and Santa Barbara Basins, California continental borderland: American Association of Petroleum Geologists Bulletin, v. 68, p. 1179-1192.

Schumm, S. A., 1968, Speculations concerning paleohydrological controls of terrestrial sedimentation: Geological Society of America Bulletin, v. 79, p.

1573-1588.

Schwab, F. L., 1970, Origin of the Antietam Formation (Late Precambrian?-Lower Cambrian), central Virginia: Journal of Sedimentary Petrology, v. 40, p. 354-366.

Schwab, F. L., 1971, Harpers Formation, Central Virginia: a sedimentary model: Journal of Sedimentary Petrology, v. 41, p. 139-149.

Schwab, F. L., 1972, The Chilhowee Group and late Precambrian, early Paleozoic sedimentary framework in the central and southern Appalachians, in Lessing, P., Hayhurst, R. I., Barlow, J. A., and Woodfork, L. D., eds., *Appalachian structures: Origin, Evolution and Possible Potential for Exploration Frontiers, a Seminar:* West Virginia University and West Virginia Geological and Economic Survey, p. 59-101.

Schwab, F. L., 1976, Depositional environments, provenance, and tectonic framework: Upper part of the late Precambrian Mount Rogers Formation, Blue Ridge Province, southwestern Virginia: Journal of Sedimentary Petrology, v. 46, p. 3 -13.

Schwab, F. L., 1981, Late Precambrian tillites of the Appalachians, *in* Hambrey, M. J., and Harland, W. B., eds., *Earth's PrePleistocene Glacial Record*: Cambridge University Press, Cambridge, p. 751-755.

Schwab, F. L., 1986, Upper Precambrian-lower Paleozoic clastic sequences, Blue Ridge and adjacent areas, Virginia and North Carolina: initial rifting and continental margin development, Appalachian orogen: D. A. Textoris. ed., Society of Economic Paleontologists and Mineralogists field guidebooks, southeastern United States Third Annual Meeting: Raleigh, North Carolina, p 1-42.

Seilacher, A., 1969, Bathymetry of trace fossils: Marine Geology, v. 5, p. 413-428.

Semeniuk, V., Sedimentology and stratigraphic sequence of a tropical tidal flat, NW Australia: Sedimentary Geology, v. 29, p. 195-221.

Sepkoski, J. J., Jr., and Knoll, A. H., 1983, PreCambrian-Cambrian boundary: The spike is driven and the monolith crumbles: Paleobiology, v. 9, p. 199-206.

Sneh, A., 1983, Desert stream sequences in the Sinai Peninsula: Journal of Sedimentary Petrology: v. 53, p. 1271-1281.

Seymour, R. J., 1980, Longshore sediment transport by tidal currents: Journal of Geophysical Research, v. 85, p. 1899-1904.

Shepard, F. P., and Inman, D. L., 1950, Nearshore water circulation related to bottom topography and wave refraction: Transactions of the American Geophysical Union, v. 31, p. 196-212.

Simpson, E. L., and Loope, D. B., 1985, Amalgamated interdune deposits,White Sands, New Mexico: Journal of Sedimentary Petrology, v. 55, p. 361-365.

Simpson, E L., and Sundberg, F. A., 1987, Early Cambrian Age from synrift deposits of the Chilhowee Group of southwestern Virginia: Geology, v. 12, p.123-126.

Simpson, E. L., and Eriksson, K. A., 1986, Wave- and storm-dominated sedimentation in the Lower Cambrian Hampton and Erwin Formations of the Chilhowee Group in central and southern Virginia: American Association of Petroleum Geologists Bulletin, v. 70, p. 648.

Sleath, J .F. A., 1984, Sea bed mechanics, John Wiley and Sons, New York, New York, 335 p.

Smith, D. G., 1973, Aggradation of the Alexandria-South Saskatchewan River, baniff Park, Alberta, *in* Morisawa, M., ed., *Fluvial Geomorphology,* Proceedings fourth annual Geomorphology Symposium, Publication in Geomorphology, SUNY Binghamton, New York , New York, p. 201-219.

Snedden, J., and Nummedal, D., 1986, Storm-deposited sand beds in modern sediments of the Texas continental shelf: Society of Economic Paleontologists and Mineralogists Annual Midyear Meeting Abstracts, v. 3, p. 104.

Soegaard, K., and Eriksson, K. A., 1985, Evidence of tide, storm, and wave interaction on a Precambrian siliciclastic shelf: the 1,700 M.Y. Ortega Group, New Mexico: Journal of Sedimentary Petrology, v. 85, p. 672-684.

Stose, A. J., and Stose, G. W., 1957, Geology and mineral resources of the Gossan lead district and adjacent areas: Virginia Division of Mineral Resources Bulletin 72, 233 p.

Stow, D. A. V., 1985, Deep-sea clastics: where are we an where are we going?*in* Brenchley, P. J.,, and Williams, B. J. P., eds., *Sedimentology: Recent Developments and Applied Aspects:* Special Publication Geological Society of London, p. 67-93.

Sundberg, F. A., 1983, *Skolithos linearis* Haldeman from the Carrara Formation (Cambrian) of California: Journal of Paleontology, v. 57, p. 145-149.

Swift, D. J. P., 1970, Quaternary shelves and return to grade: Marine Geology, v. 8, p. 15-30.

Swift, D. J. P., 1974, Continental shelf sedimentation, in C. A. Burk and C. L., Drake, eds., The Geology of Continental Margins: Springer-Verlag, New York, New York, p. 117-135.

Swift, D. J. P., and Nummedal, D., 1987, Discussion: Hummocky cross-stratification, tropical hurricanes and intense winter storms: Sedimentology, v. 34, p. 338-344.

Swift, D. J. P., Figueiredo, A. G., Freeland, G. L., and Oertel, G. F., 1983, Hummocky cross stratification and megaripples: a geologic double standard: Journal of Sedimentary Petrology, v. 53, p. 1295-1317.

Vail, P. R., Mitchum, Jr., and Thompson, S., III, 1977, Seismic stratigraphy and global changes of sea level, Part 4: Global cycles of relative changes of sea level, in Payton, C. E., ed., *Seismic Stratigraphy-application to hydrocarbon exploration:* American Association of Petroleum Geologists Memoir 26, p. 83-98.

van Beek, J. L., and Koster, E. A., 1972, Fluvial and estuarine sediments exposed along the Oude Maas (The Netherlands): Sedimentology, v. 19, p. 237-256.

Vincent, C. E., Young, R. A., and Swift, D. J. P., 1983, Sediment transport in the Long Island shoreface, north Atlantic shelf: Role of waves and currents in shoreface maintenance: Continental Shelf Research, v. 2, p. 163-181.

Visser, M. J., 1980, Neap/Spring cycles reflected in Holocene subtidal large-scale bedforms deposits, a preliminary note: Geology, v. 8, p. 543-546.

Walcott, C. D., 1891, Correlation papers, Cambrian: United States Geological Survey Bulletin, v. 81, 447 p.

Walker, R. G., 1978, Deep water sandstone facies and ancient submarine fans: models for exploration for stratigraphic traps: American Association of Petroleum Geologists Bulletin, v. 62, p. 932-966.

Walker, R. G., 1984, Shelf and shallow marine sands, in R. G. Walker, ed., Facies Models: Geoscience Canada Reprint Series 1, Toronto, Canada, p. 141-170

Walker, R. G., Duke, W. L., and Leckie, D. A., 1983, Hummocky stratification: significance of its variable bedding sequences: discussion: Geological Society of America Bulletin: v. 94, p. 1245-1249.

Wasson, R. J., 1977, Last-glacial alluvial fan sedimentation in the Lower Derwnt Valley, Tasmania: Sedimentology, v. 24, p. 781-799.

Wasson, R. J., 1979, Sedimentation history of the Mundi Mundi alluvial fans, western New South Wales: Sedimentary Geology, v. 22, p. 21-51.

Wehr, F., 1985, Stratigraphy of the Lynchburg Group and Swift Run Formation, Late Proterozoic (730-570 Ma), central Virginia, Southeast Geology, v. 25, p. 225-239.

Wehr, F., 1986, A proglacial origin for the Upper Proterozoic Rockfish Conglomerate, central Virginia, U.S.A., Precambrian Research, v. 34, p. 157-174.

Wehr, F., and Glover, L., III, 1985, Stratigraphy and tectonics of the Virginia-North

Carolina Blue Ridge: Evolution of a late Precambrian-early Paleozoic hinge zone: Geological Society of America Bulletin, v. 96, p. 285-295.

Wells. N. A., 1984, Sheet debris flow and sheetflood conglomerates in Cretaceous cool-maritime alluvial fans, South Orkney Islands, Antarctica, *in* Koster, E. H., and Steel, E. J., eds., *Sedimentology of Gravels and Conglomerates:* Canadian Society of Petroleum Geologiasts Memior 10, p. 133-145.

Whisonant, R. C., 1974, Petrology of the Chilhowee Group (Cambrian and Cambrian (?)) in central-eastern and southern Tennessee: Journal of Sedimentary Petrology, v. 44, p. 228-241.

Whisonant, R. C., 1970, Paleocurrents in basal Cambrian rocks on eastern Tennessee: Geological Society of America Bulletin, v. 81, p. 2781-2786.

Williams, G. E., 1971, Flood deposits on the sand-bed ephemeral streams of central Australia: Sedimentology, v. 17, p. 1-40.

Williams, H., Gillespie, R. T., and Van Breemen, O., 1985, A late Precambrian rift-related igneous suite in western Newfoundland: Canadian Journal of Earth Sciences, v. 22, p. 1727-1735.

Williams, P. F., and Rust, B. R., 1969, The sedimentology of a braided river: Journal of Sedimentary Petrology, v. 39, p. 649-679.

Wood, G. D., and Clendening, J. A., 1982, Acritarchs from the Lower Cambrian Murray Shale, Chilhowee Group, of Tennessee, U.S.A.: Palynology, v. 6, p. 255-265.

Wright, L. D., 1981, Nearshore tidal currents and sand transport in a macrotidal environment: Geo-Marine Letters, v. 1, p. 173-179.

Wright, R., 1986, Cycle stratigraphy as a paleographic tool: Point Lookout Sandstone, Southeastern San Jaun Basin, New Mexico: Geological Society of America Bulletin, v. 97, p. 661-673.

Xing Yusheng and Luo Huilin, 1984, Precambrian-Cambrian boundary candidate, Meishucun, Jinning, Yunnan, China: Geological Magazine, v. 121, p. 143-154.

Yang, C. S., and Nio, S., 1985, The estimation of paleohydrodynamic processes from subtidal deposits using time series analysis methods: Sedimentology , v. 32, p. 41-57.

Yeo, R. K., and Risk, J. R., 1981, The sedimentology, stratigraphy, and preservation of intertidal deposits in the Minas Basin System, Bay of Fundy: Journal Sedimentary Petrology, v. 51, p. 245-260.

APPENDIX I: WAVE EQUATIONS FROM DIEM (1985)

APPENDIX I

Bottom Orbital Diameter

d_0 $d_0 = lamda/0.65$ provided $lamda<0.0028*D^{1.68}$

Threshold Velocity

Ut

$Ut^2 = 0.21(d_0/D)^{1/2}(ps-p)gD/p$ where $D< 0.5mm$

$Ut^2 = 0.46\pi(d_0/D)^{1/4}(ps-p)gD/p$ where $D\geq 0.5mm$

Bottom Orbital Velocity (Maximum)

Um

$Ut < Um \leq \sqrt{0.112gd_0}$

Wave Period

T $\pi\sqrt{8.9d_0/g} \leq T < \pi d_0/Ut$

Maximum Possible Deep Water Wavelength

$L_{t\infty}$ $L_{t\infty} = (\pi g d_0^2)/(2Ut^2)$

Wavelength

L $L_{max} = (L_{t\infty}/\sqrt{2})\sqrt{(1+\sqrt{(1-80.4*Ut/(g^2d_0^2)})}$

$L_{min} = (L_{t\infty}/\sqrt{2})\sqrt{(1-\sqrt{(1-80.4*Ut/(g^2d_0^2)})}$

Water Depth Range At A Given Wavelength

h $(L/2\pi)\text{artanh}(L/L_{t\infty}) < h \leq (L/2\pi)\text{arcosh}\,(0.142\,L_{max}d_0)$

Water Depth

h $h < (L_{max}/2\pi)\text{arcosh}(0.142L_{max}/d_0)$

Wave Height

H $H < d_0 \sinh(2\pi h_{max}/L_{max})$

APPENDIX II: WAVE CALCULATION SUMMARY TABLE.

APPENDIX II: Wave Calculation Summary Table

167m Buchanan Section

Ripple number	Wavelength (cm)	Orbital Diameter (cm) D_o	Threshold velocity (cm/sec) U_t	Bottom orbital velocity (minimum) (cm/sec) U_t	Bottom orbital velocity (maximum) (cm/sec)
A1	42.0	64.6	27.2	27.2	84.2
A2	48.0	73.9	29.8	29.8	90.1
B2	67.5	103.9	30.1	30.1	106.8
B3	51.0	78.5	29.0	29.0	92.8
C1	47.0	72.3	28.7	28.7	89.1
D1	76.0	116.9	31.4	31.4	113.3
D2	87.0	133.5	32.0	32.0	121.0
1	47.0	72.3	28.7	28.7	89.1
2	60.0	92.3	29.6	29.6	100.6
3	60.0	92.3	29.6	29.6	100.6

Ripple Number	Maximum Wavelength (M)	Maximum Water Depth (M)	Maximum Wave Height (M)
A1	86.7	50.2	12.3
A2	94.6	54.1	13.4
B2	183.3	114.2	26.0
B3	112.7	66.5	16.0
C1	97.6	56.6	13.8
D1	213.6	134.2	30.3
D2	267.7	172.2	38.0
1	97.6	56.6	13.8
2	149.6	91.2	21.3
3	149.6	91.2	21.3

Ripple Number	Wave Period (Minimum) (seconds)	Wave Period (Maximum) (seconds)	Maximum Deep Water Wavelength (M)	Minimum Wavelength (M)
A1	2.4	7.5	86.8	4.6
A2	2.4	7.7	94.7	5.2
B2	3.1	10.8	183.4	7.3
B3	2.8	8.5	112.8	5.5
C1	2.6	7.9	97.7	5.1
D1	3.2	11.7	213.8	8.3
D2	3.5	13.1	267.9	9.4
1	2.5	7.9	97.7	5.1
2	2.9	9.8	149.7	6.5
3	2.9	9.8	149.7	6.5

APPENDIX III: STRATIGRAPHIC SECTIONS.

Geologic map of portion of the Blue Ridge Province (modified from Wehr and Glover, 1985). Inset shows locations of study area in relation to surrounding states. Localities of measured sections are 1) Damascus; 2) Laurel Creek (Virginia Creeper Trail section); 3) Short Mountain; 4) Elk Creek; 5) Poplar Camp Quarry; 6) Poplar Camp; 7) Buchanan; 8) Arcadia; 9) Natural Bridge; 10) James River sections including Balcony Falls section; 11) Buena Vista; and 12) Vesuvius.

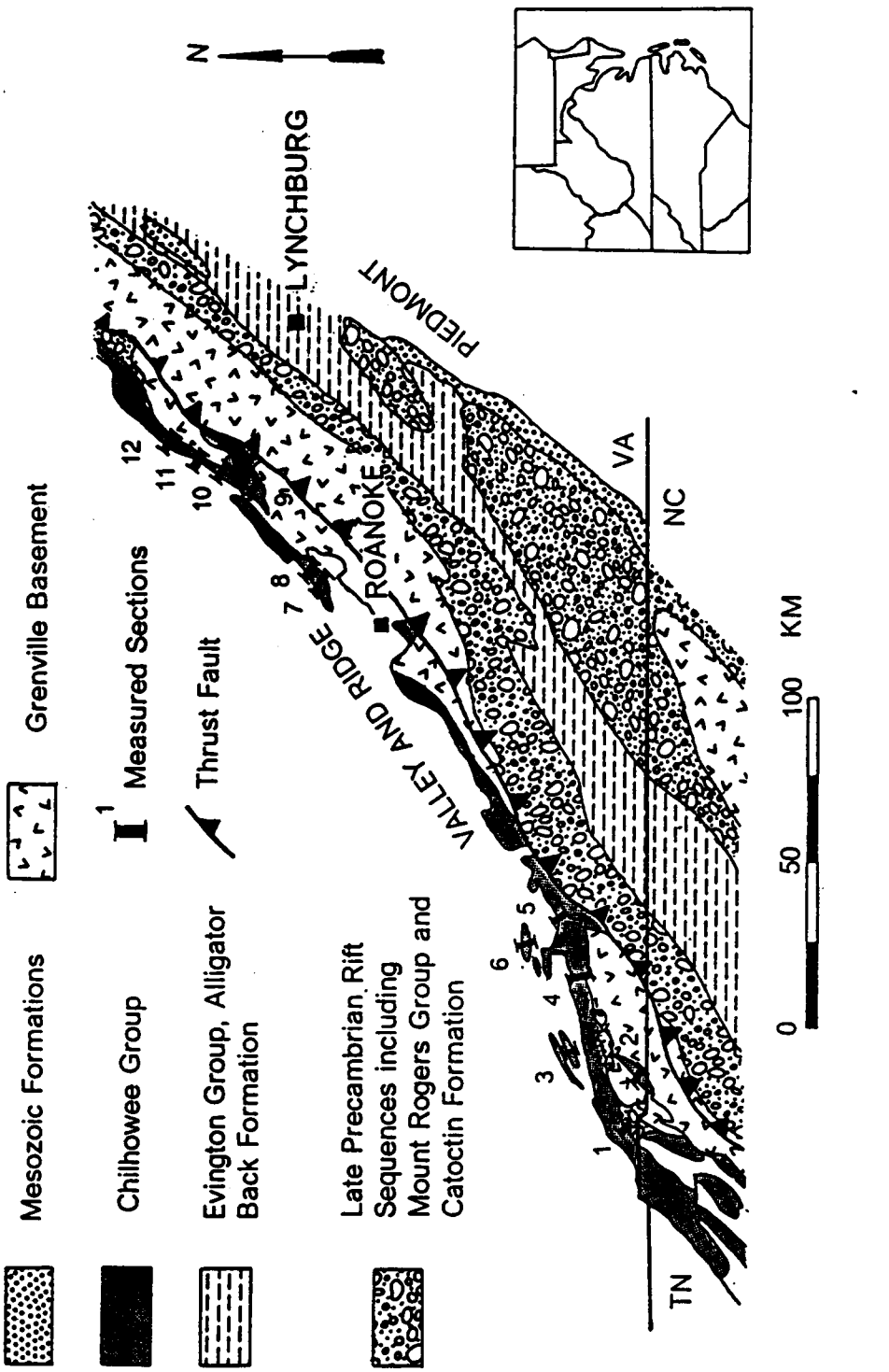
Mesozoic Formations
Chilhowee Group
Evington Group, Alligator Back Formation
Late Precambrian Rift Sequences including Mount Rogers Group and Catoctin Formation
Grenville Basement
Measured Sections
Thrust Fault
N
LYNCHBURG
ROANOKE
PIEDMONT
VALLEY AND RIDGE
VA
NC
TN
0
50
100
KM

KEY

VERTICAL AXIS (THICKNESS IN METERS)

HORIZONTAL AXIS (GRAIN SIZE)

C	CONGLOMERATE
S	SANDSTONE
M	MUDSTONE
HCS	HUMMOCKY CROSS STRATIFICATION
MHCS	MICROHUMMOCKY CROSS STRATIFICATION
RUS	*RUSOPHYCUS*
MR TOP	MEGARIPPLED TOP
G	GLAUCONITE
	SCOURS
	GRADED BEDS: SILTSTONE TO MUDSTONE
	COVERED INTERVAL
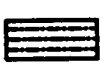	INTERBEDDED SANDSTONE AND MUDSTONE
	MASSIVE SANDSTONE WITH *SKOLITHOS*


MUDSTONES


MASSIVE SANDSTONE


MASSIVE CONGLOMERATE


CROSS-STRATIFIED CONGLOMERATE


TROUGH CROSS-STRATIFIED CONGLOMERATE


HORIZONTALLY STRATIFIED SANDSTONE

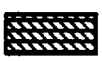
COMPOUND AND SIMPLE, TABULAR PLANAR, CROSS-STRATIFIED SANDSTONE


DIAMICTITE

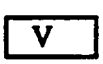
BASALTIC VOLCANICS


SKOLITHOS BURROWED SANDSTONE


CURRENT- RIPPLED BEDS


BIOTURBATED MUDSTONE

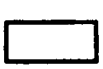
PEBBLE CONGLOMERATE WITH MUDSTONE CLASTS


WEDGE PLANAR CROSS-STRATIFICATION


FINE PEBBLE CONGLOMERATE

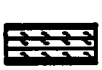
BIOTURBATED THIN-BEDDED SAND


BIOTURBATED INTERBEDDED SANDSTONE ANSD SHALE

DAMASCUS SECTION (LOCALITY 1)

KONNAROCK QUADRANGLE

PARTIAL SECTION IN THE HAMPTON FORMATION

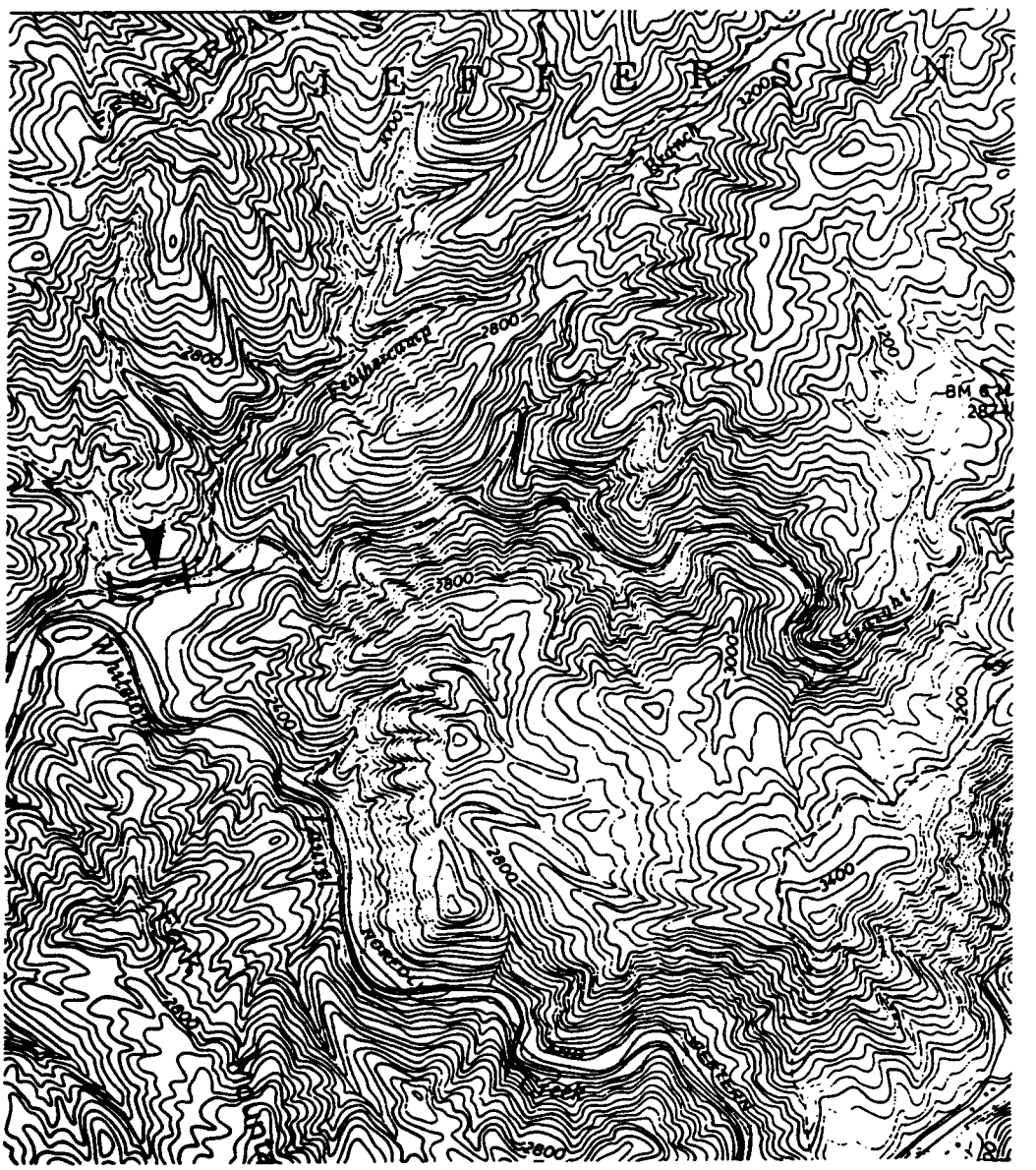

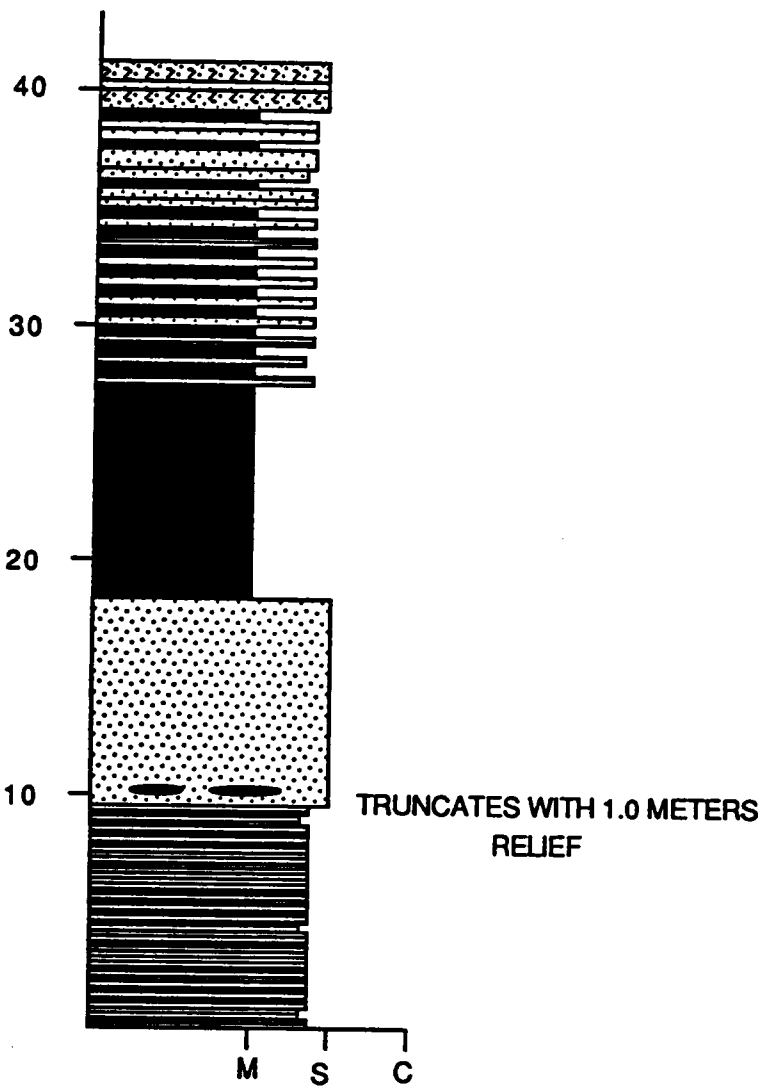
40
30
20
10
TRUNCATES WITH 1.0 METERS
RELIEF
M
S
C

VIRGINIA CREEPER TRAIL SECTION (LOCALITY 2)

KONNAROCK QUADRANGLE

MOUNT ROGERS FORMATION UPPER SEDIMENTARY MEMBER/UNICOI FORMATION CONTACT LOCATED AT 89 METERS.

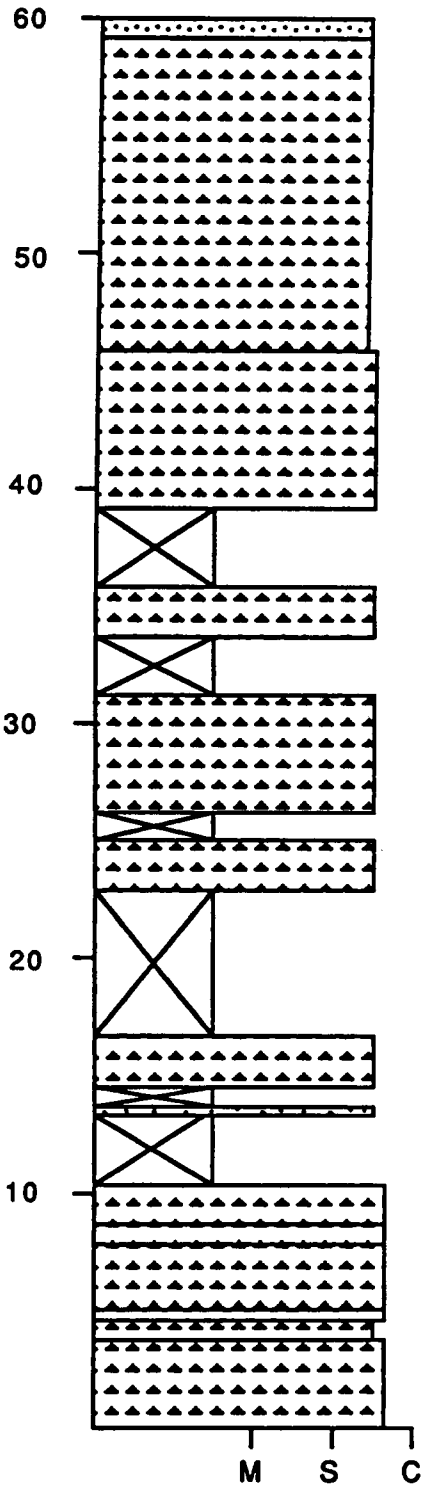
60
50
40
30
20
10
M
S
C

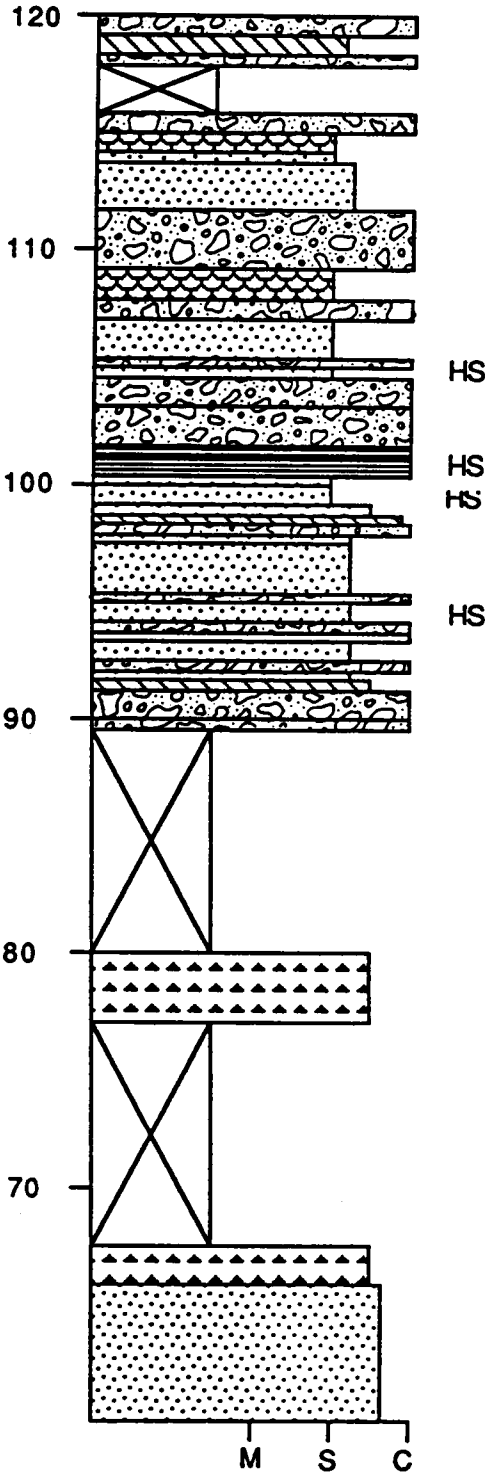
120
110
100
90
80
70
HS
HS
HS
HS
M
S
C

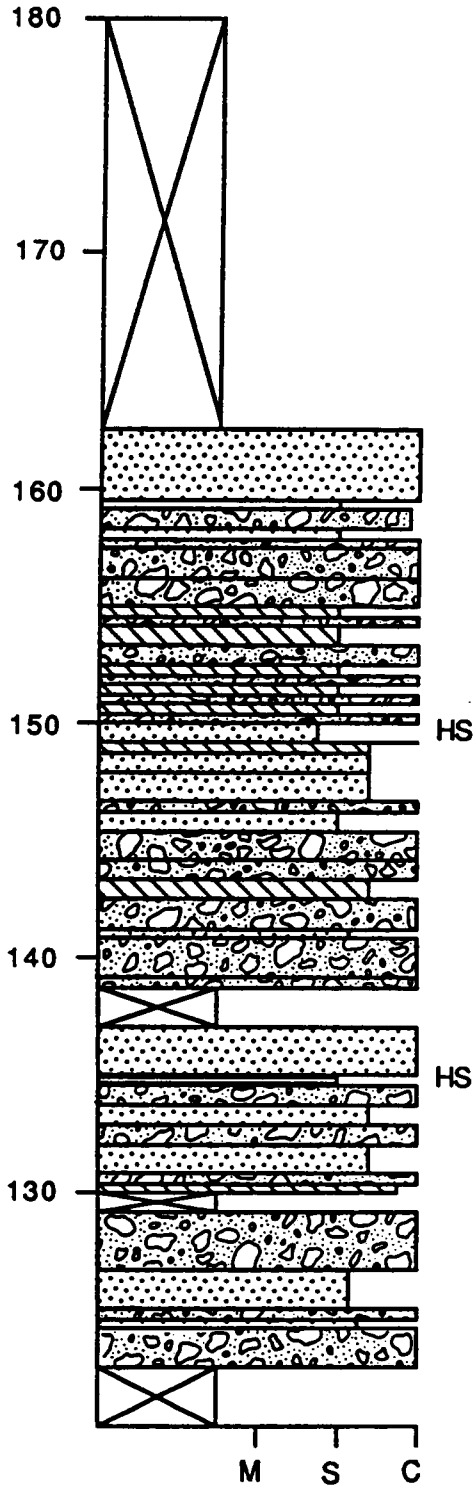
180
170
160
150
140
130
HS
HS
M
S
C

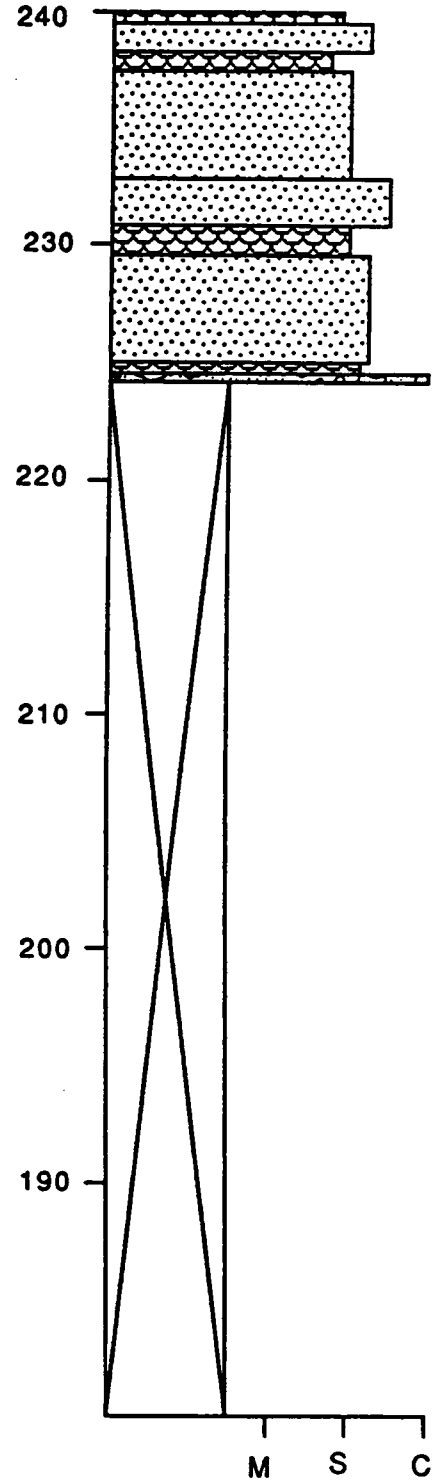
240
230
220
210
200
190
M
S
C

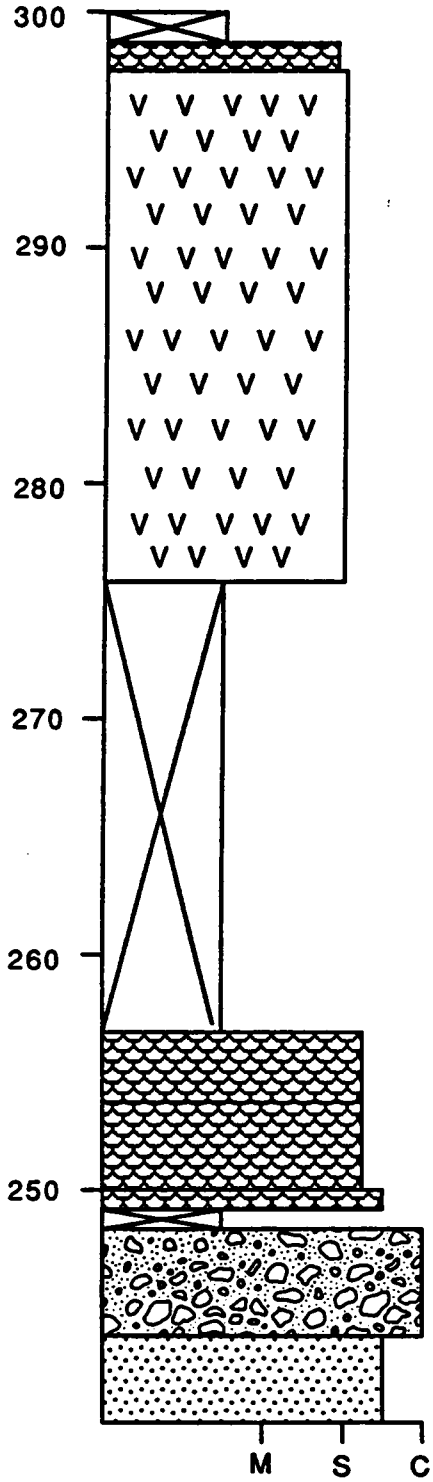
300
290
280
270
260
250
M
S
C

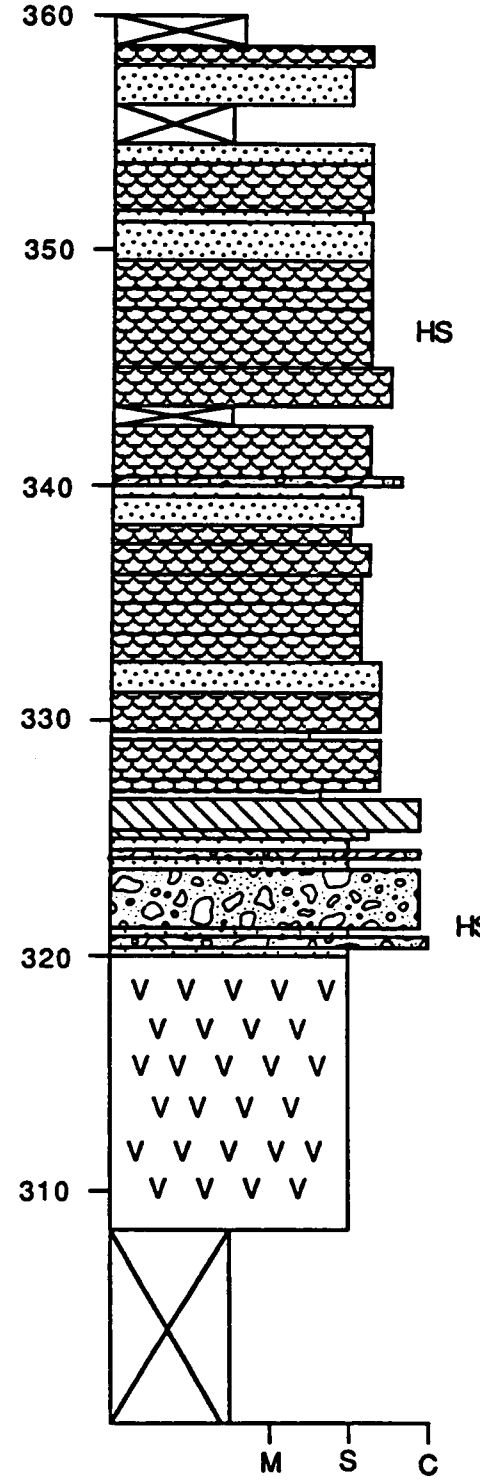
360
350
340
330
320
310
HS
HS
M
S
C

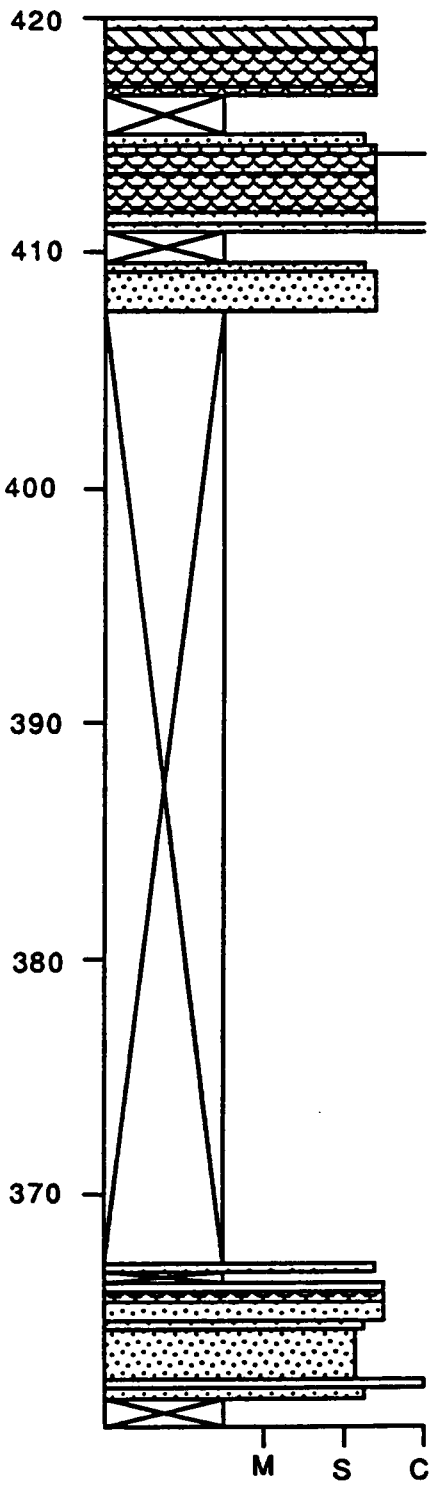
420
410
400
390
380
370
M
S
C

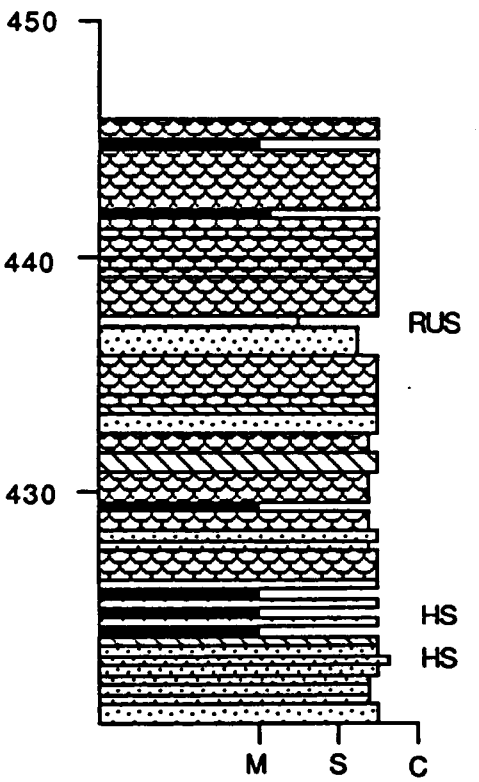
450
440
430
RUS
HS
HS
M
S
C

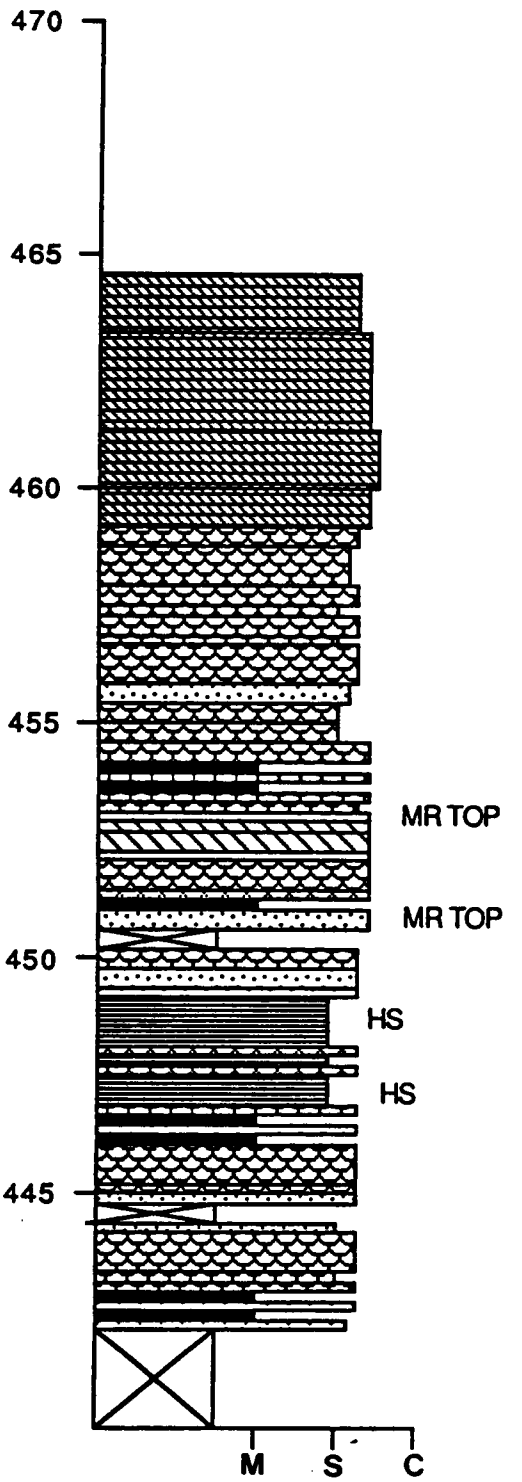
470
465
460
455
450
445
MR TOP
MR TOP
HS
HS
M
S
C

SHORT MOUNTAIN SECTION (LOCALITY 3)

MARION QUADRANGLE

UPPER ERWIN FORMATION OVERLAIN BY SHADY DOLOMITE.

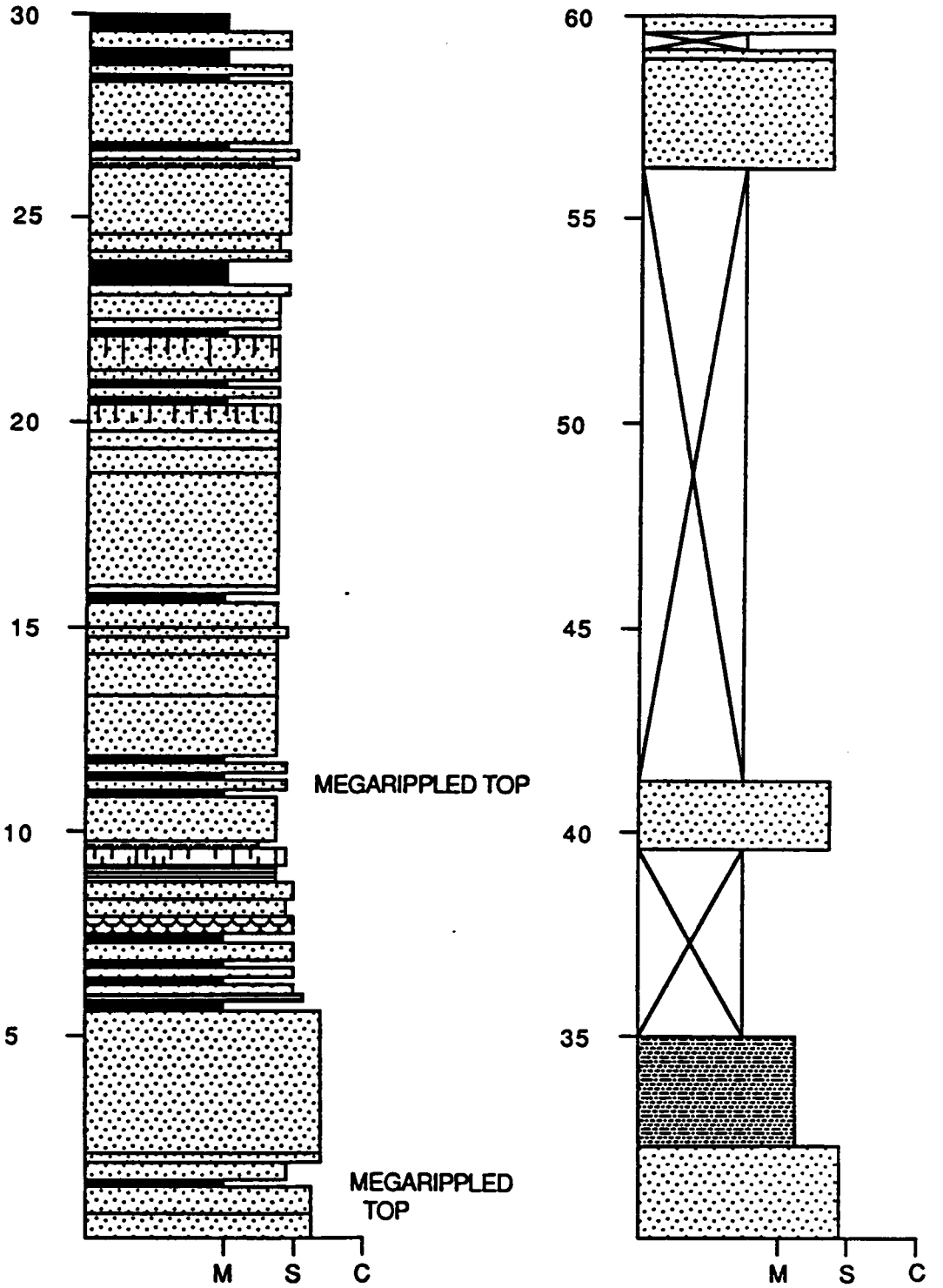
30
25
20
15
10
5
MEGARIPPLED TOP
MEGARIPPLED TOP
M
S
C
60
55
50
45
40
35
M
S
C

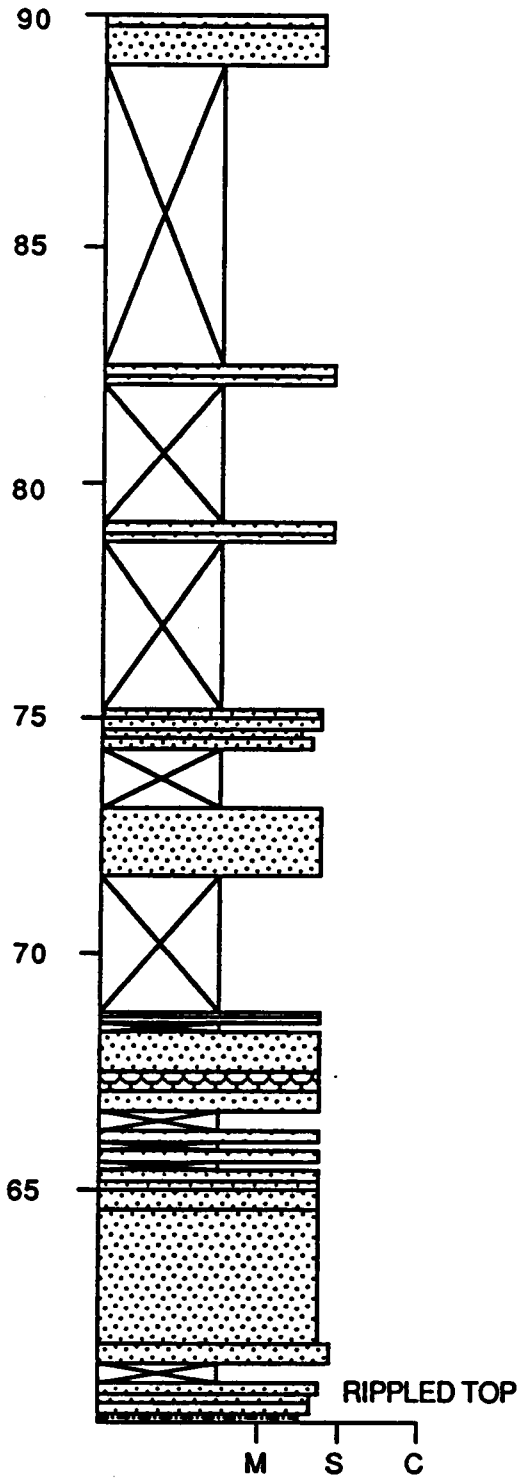
90
85
80
75
70
65
RIPPLED TOP
M
S
C

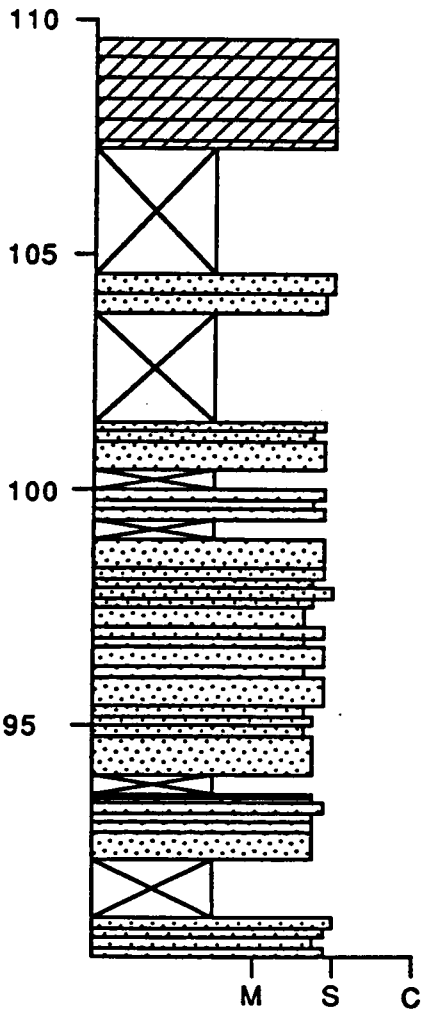
110
105
100
95
M
S
C

ELK CREEK SECTION (LOCALITY 4)

SPEEDWELL QUADRANGLE

GRENVILLE BASEMENT OVERLAIN BY UNICOI FORMATION. TOP OF STRATIGRAPHIC SECTION EXTENDS INTO THE BASE OF THE HAMPTON FORMATION.

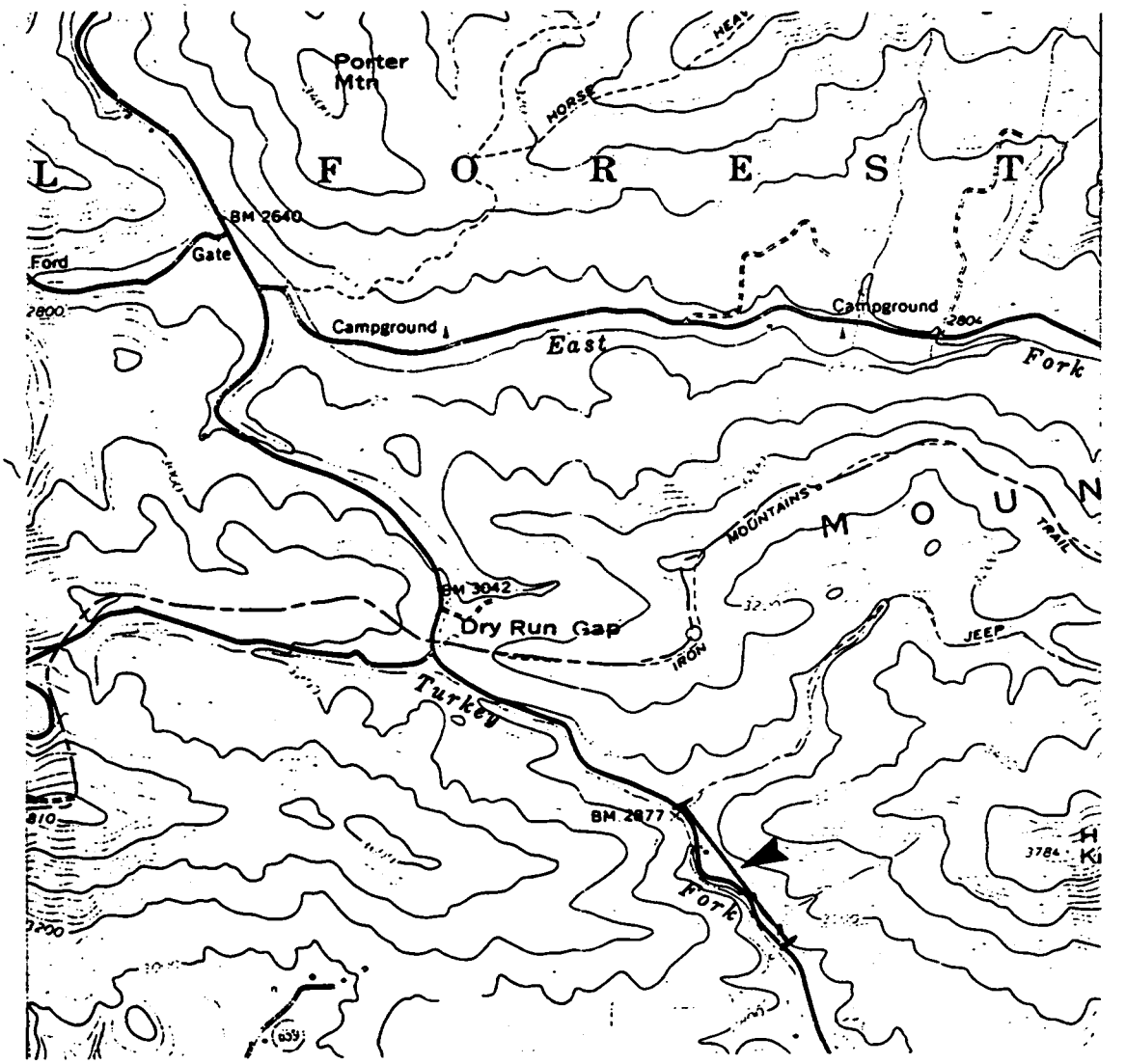

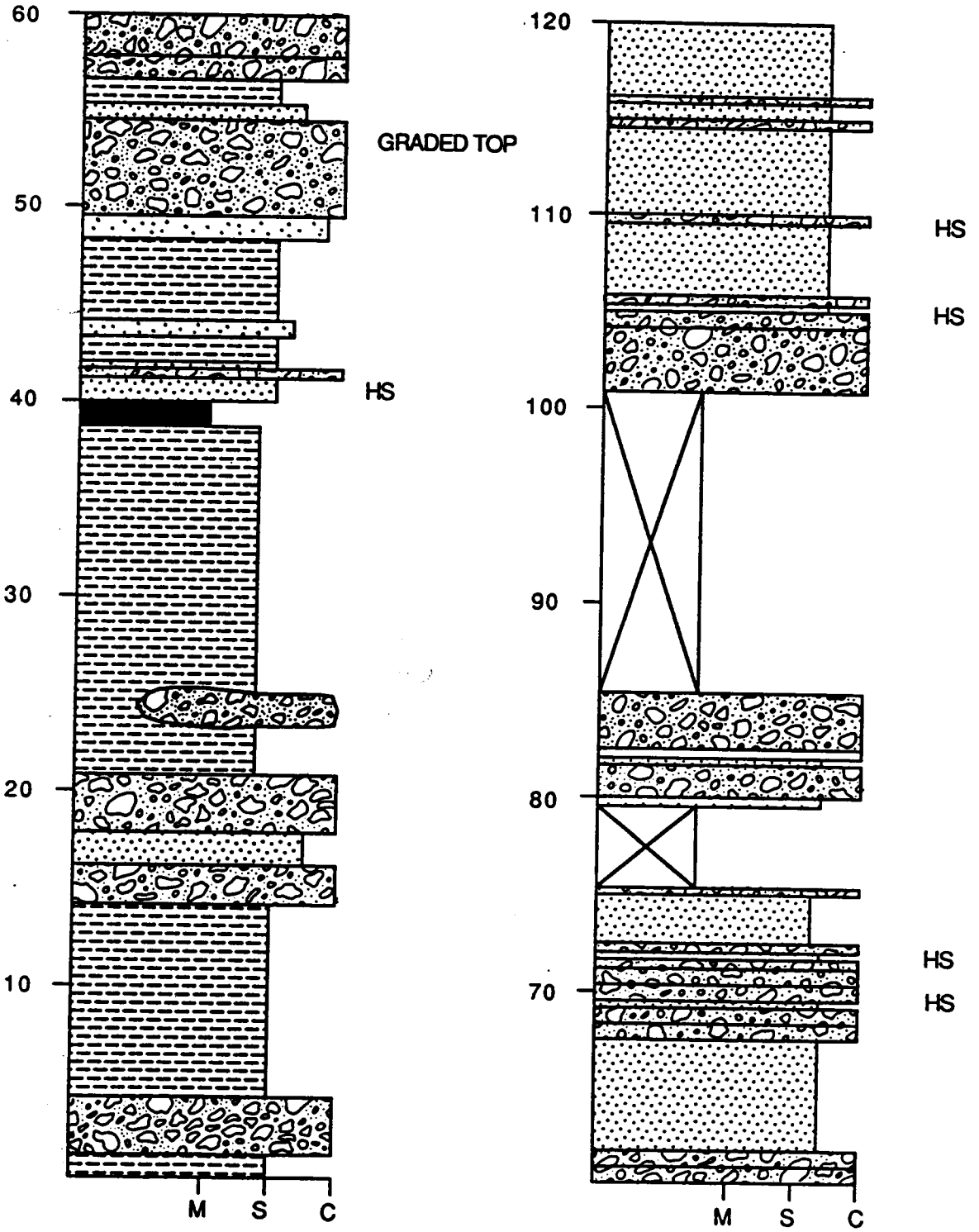
60
50
40
30
20
10
GRADED TOP
HS
M
S
C
120
110
100
90
80
70
HS
HS
HS
HS
M
S
C

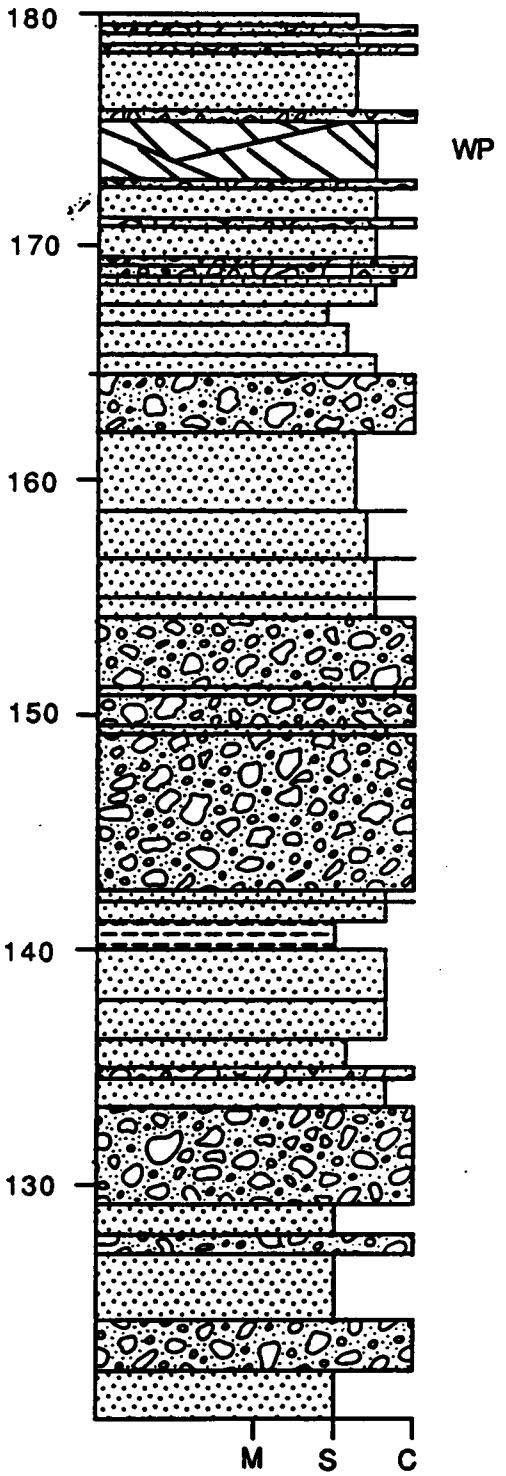
180
170
160
150
140
130
WP
M
S
C

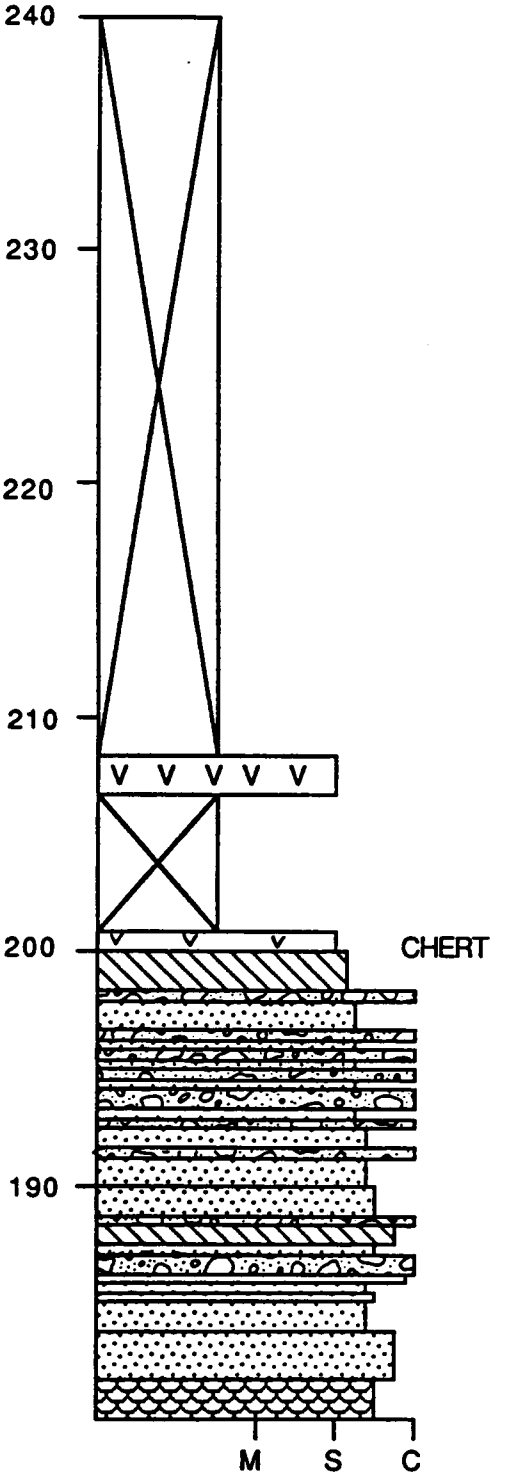
240
230
220
210
200
190
CHERT
M
S
C

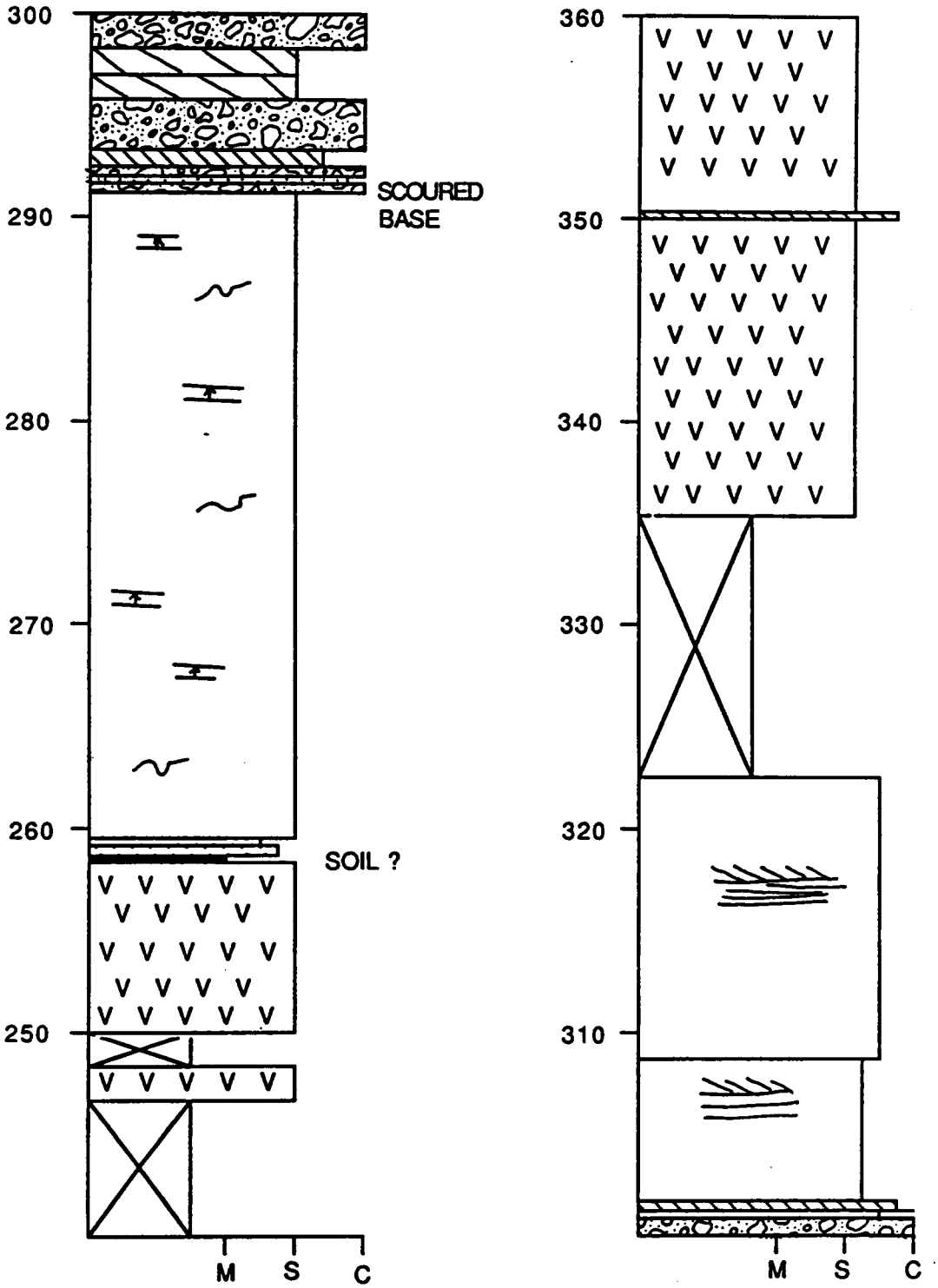
300
290
280
270
260
250
SCOURED
BASE
SOIL ?
M
S
C
360
350
340
330
320
310
M
S
C

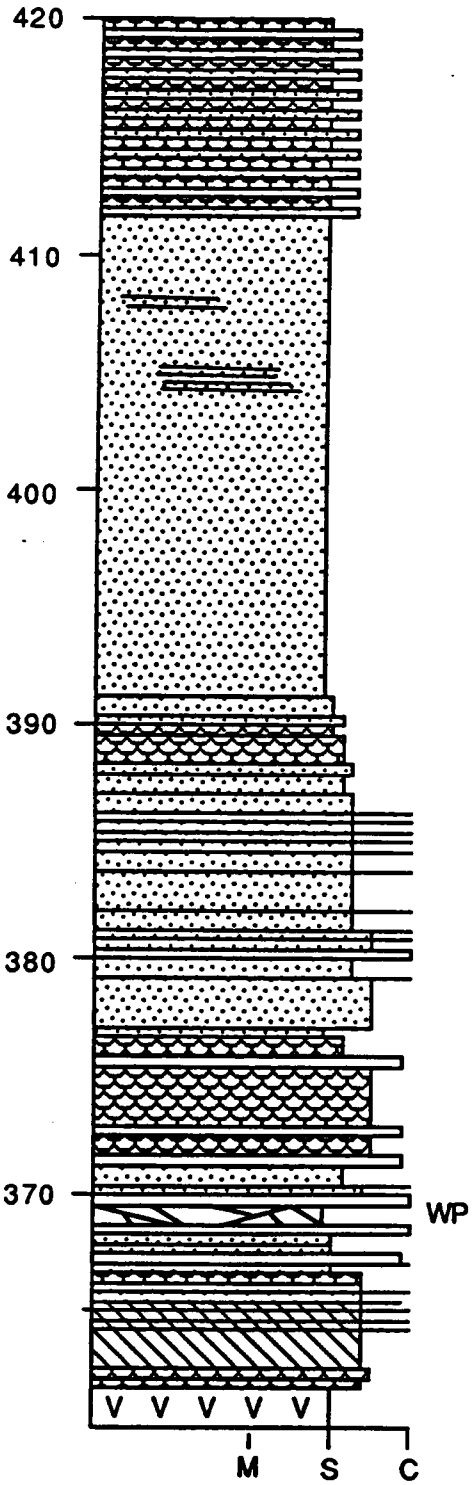
420
410
400
390
380
370
WP
V V V V V
M
S
C

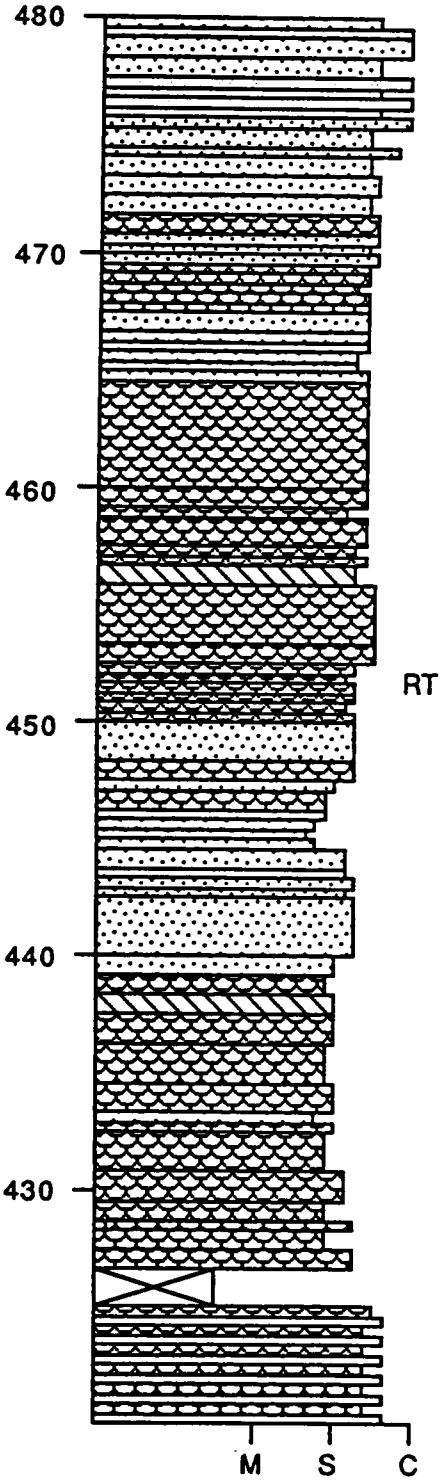
480
470
460
RT
450
440
430
M
S
C

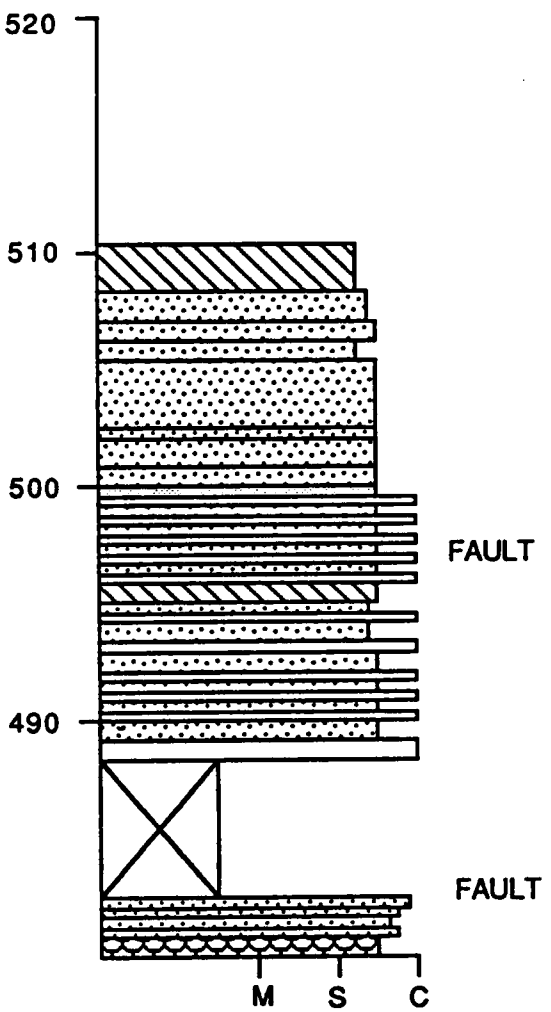
520
510
500
490
FAULT
FAULT
M
S
C

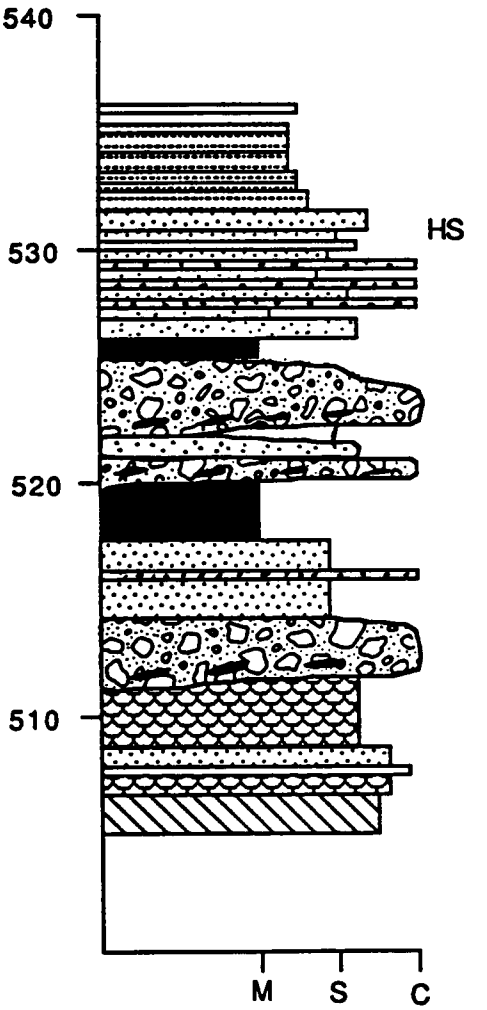
540
530
520
510
HS
M
S
C

ELK CREEK SECTION2 (LOCALITY 4)

SPEEDWELL QUADRANGLE

ERWIN FORMATION OVERLAIN BY SHADY DOLOMITE.

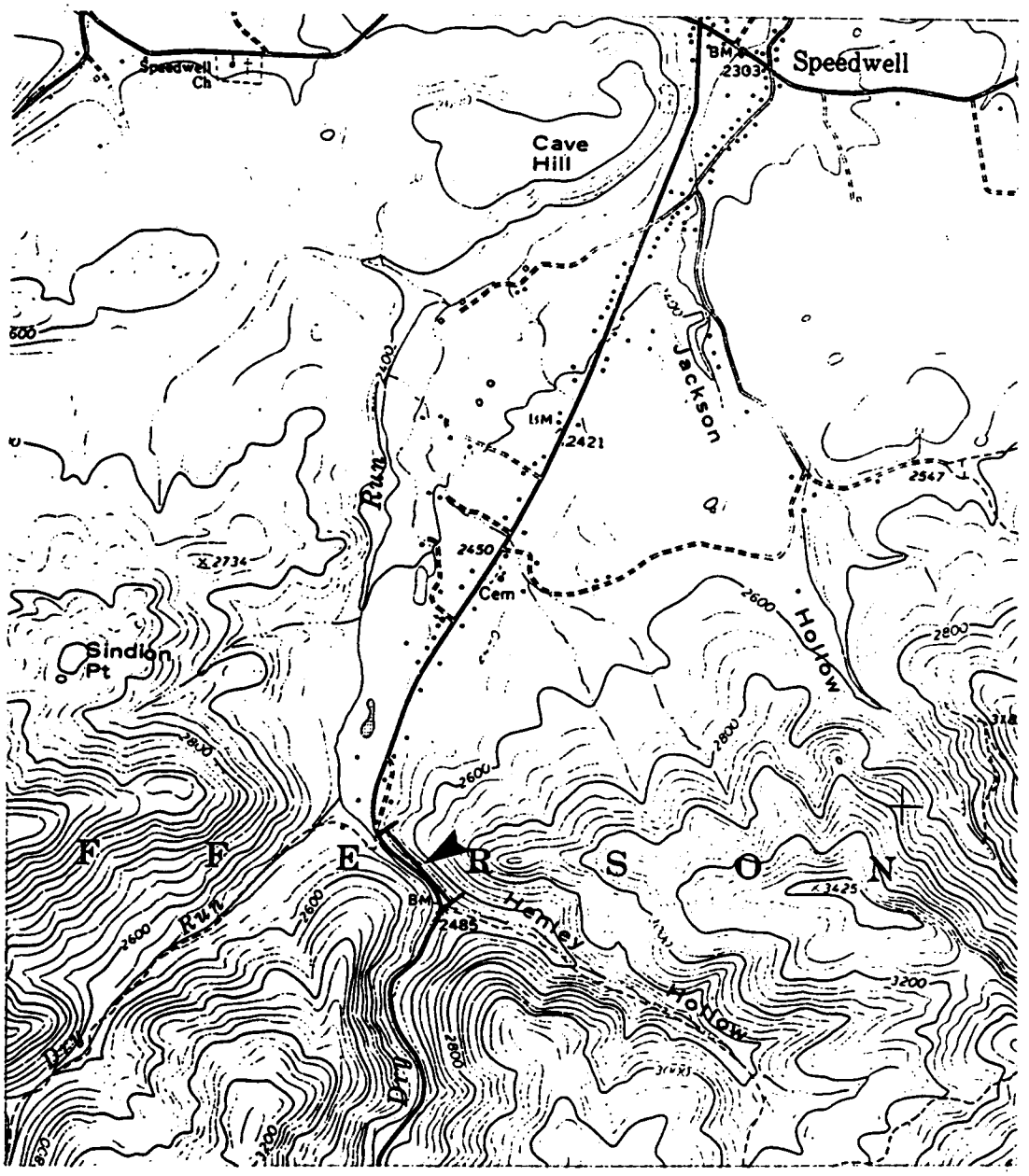

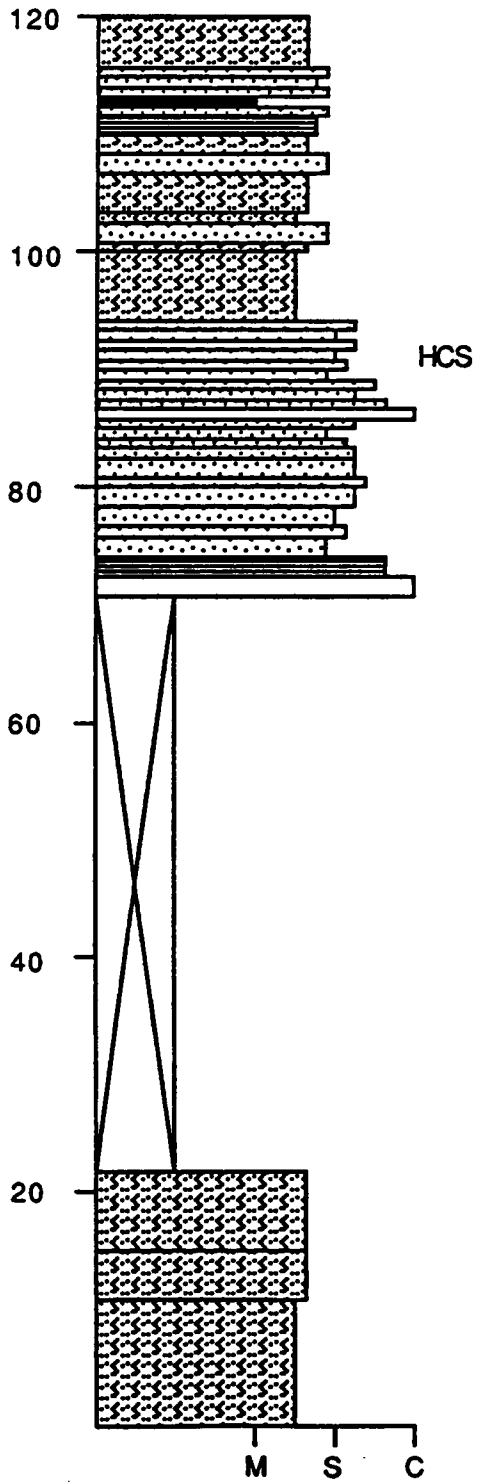
120
100
80
60
40
20
HCS
M
S
C

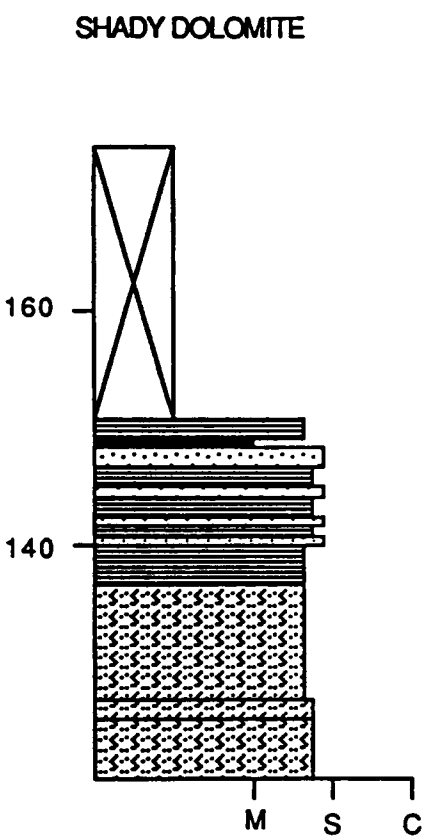
SHADY DOLOMITE
160
140
M
S
C

POPLAR CAMP QUARRY SECTION (LOCALITY 5)

SYLVATUS QUADRANGLE

ERWIN FORMATION.

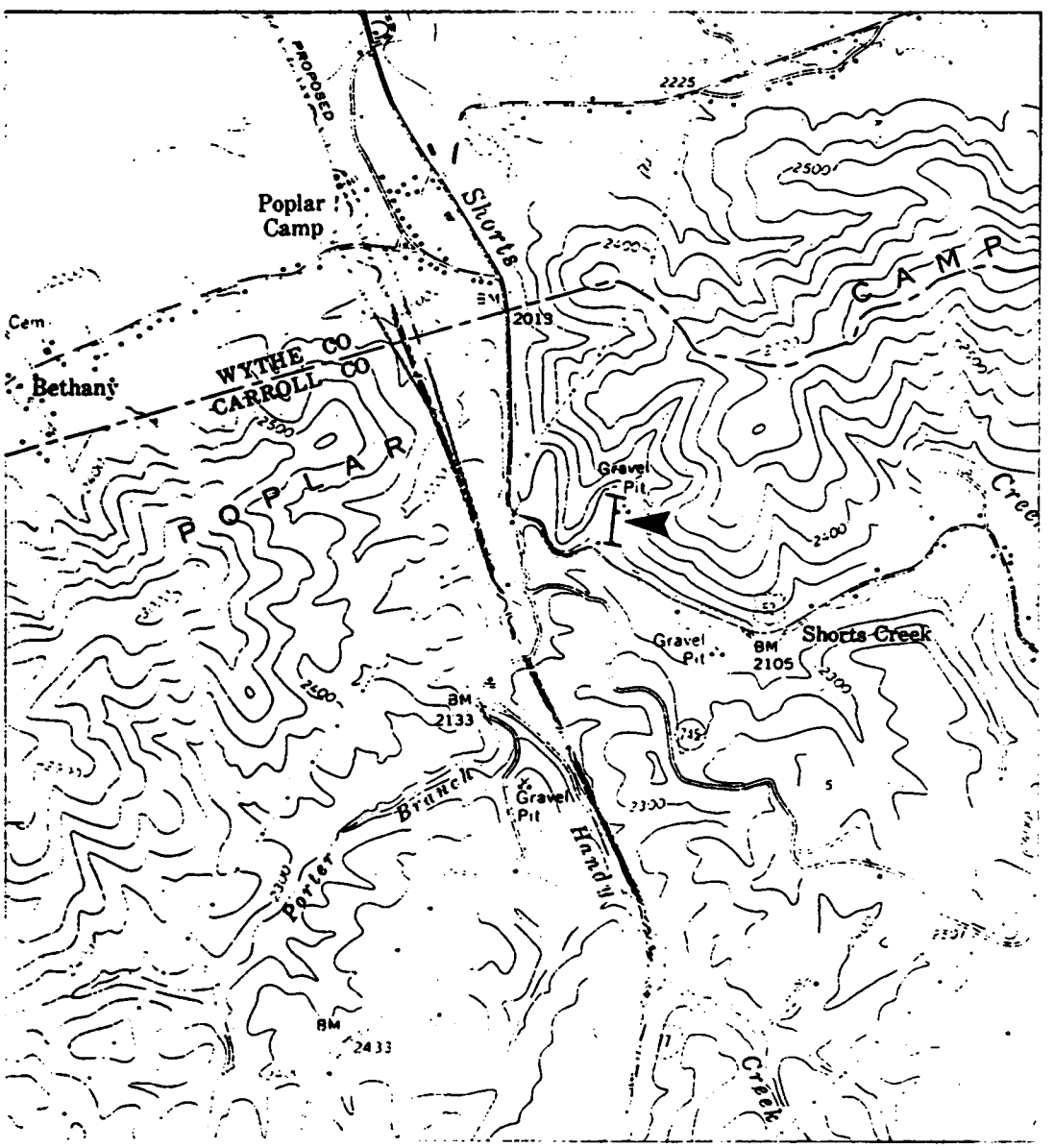

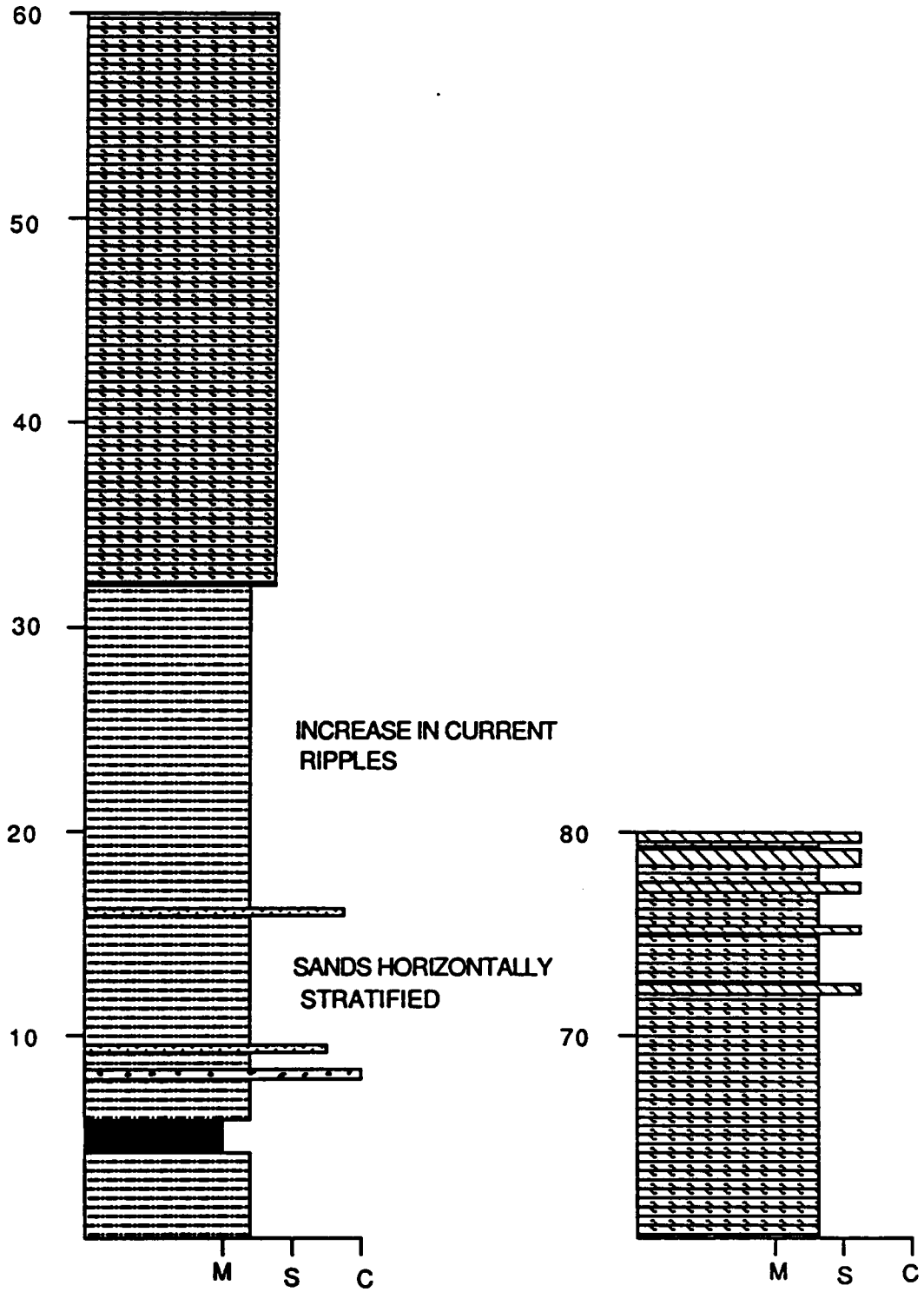
60
50
40
30
20
10
INCREASE IN CURRENT RIPPLES
SANDS HORIZONTALLY STRATIFIED
M
S
C
80
70
M
S
C

POPULAR CAMP SECTION (LOCALITY 6)

FOSTER FALLS QUADRANGLE

ERWIN FORMATION OVERLAIN BY SHADY DOLOMITE.

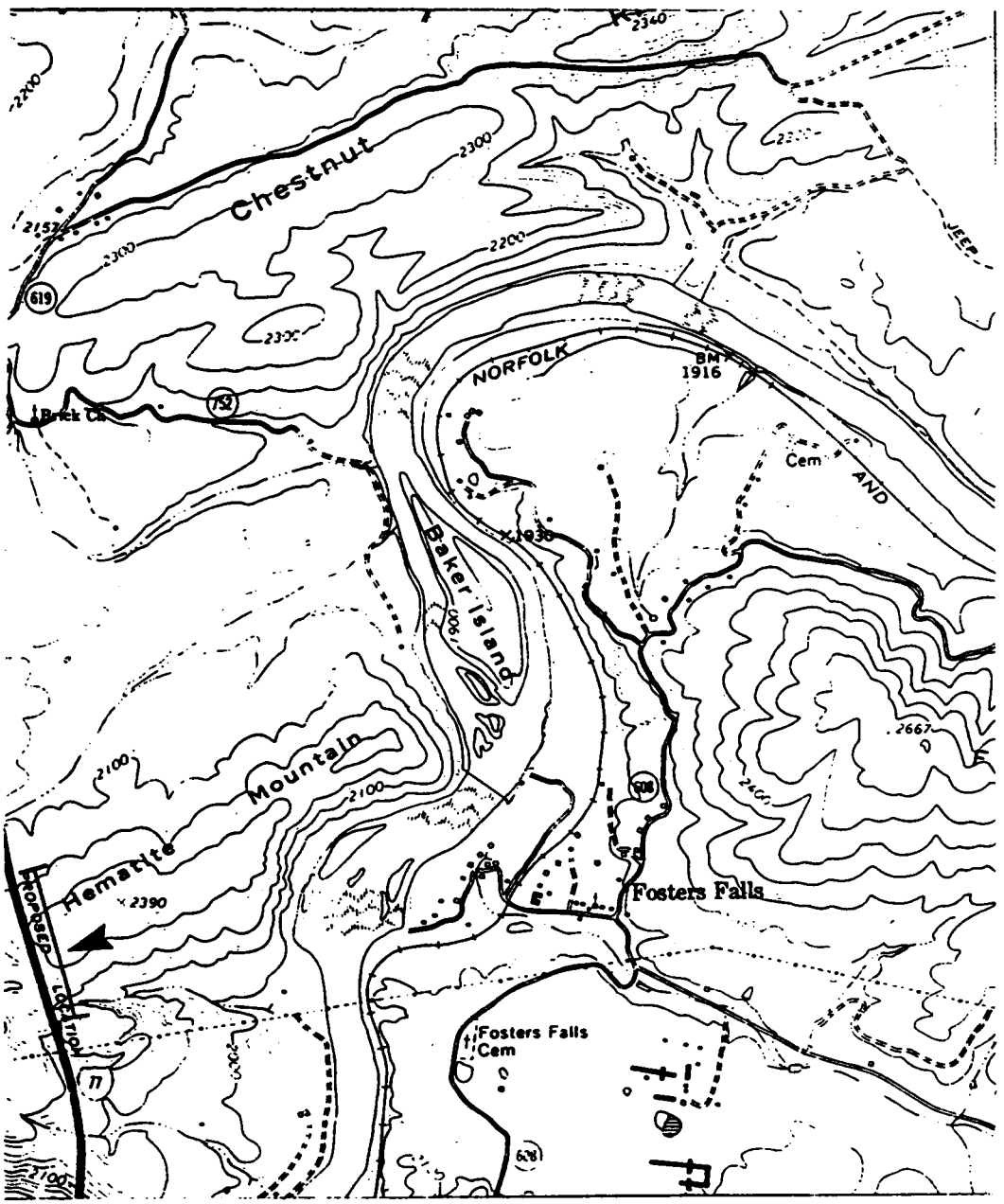

POPLAR CAMP SECTION 1

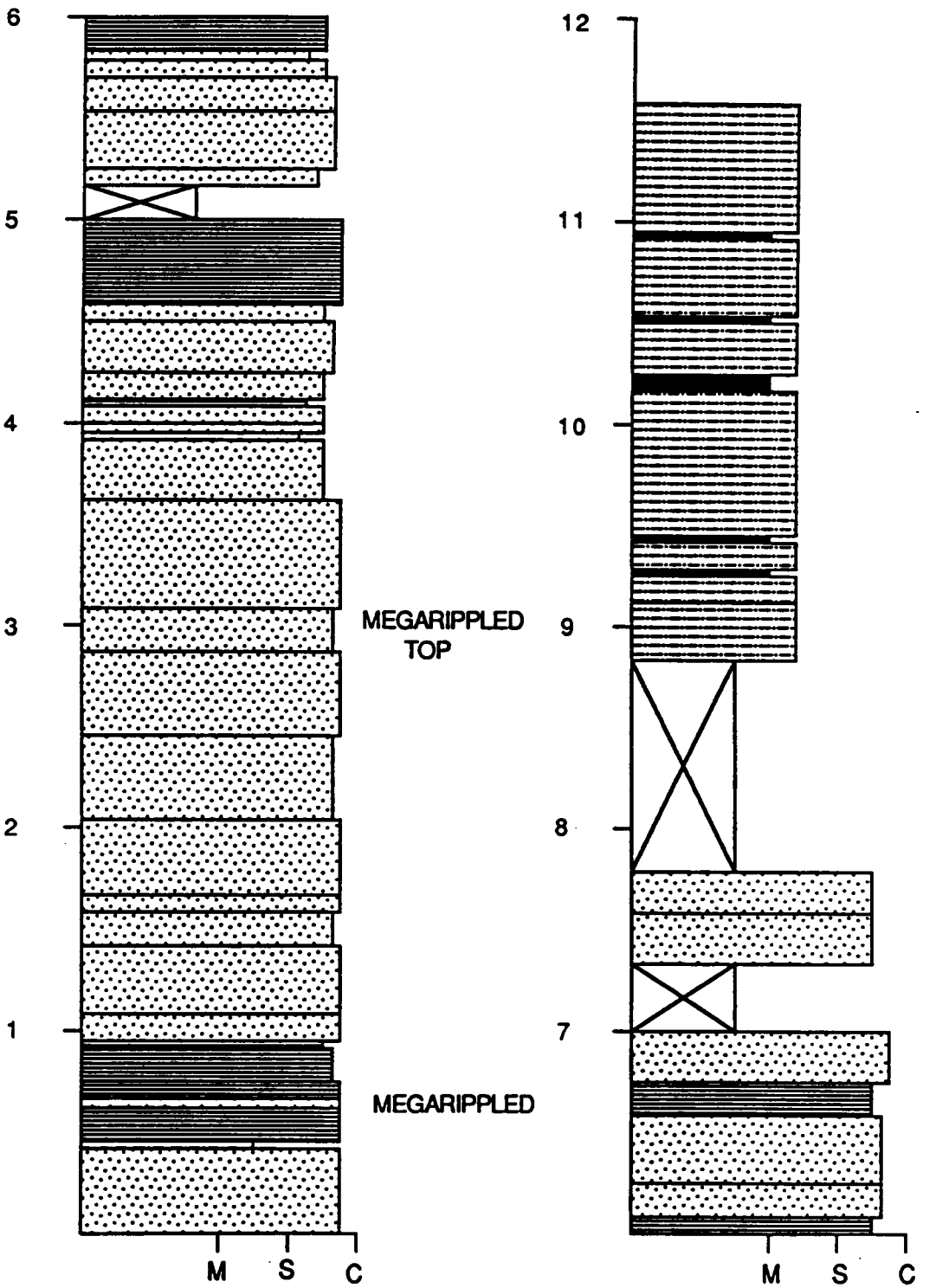

POPLAR CAMP SECTION 2

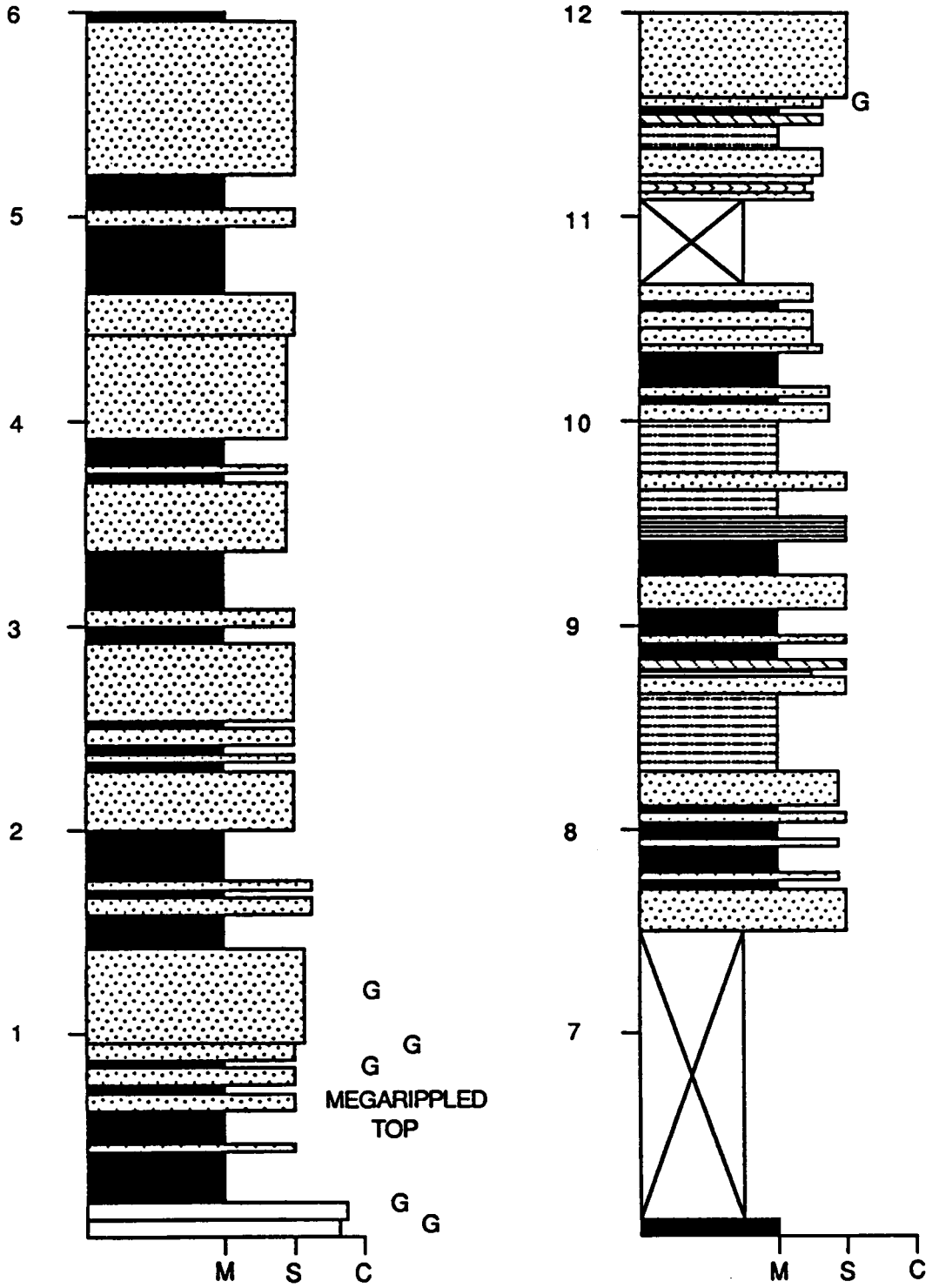

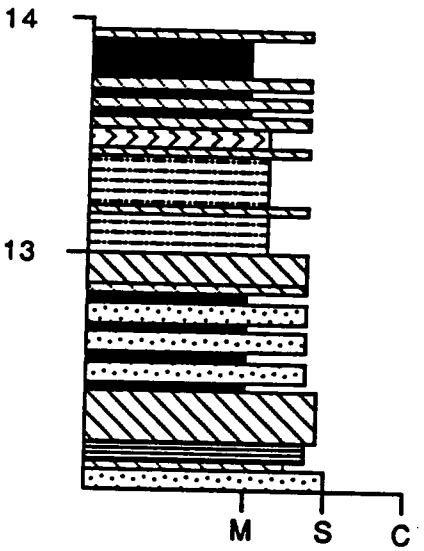
14
13
M
S
C

POPLAR CAMP SECTION 3

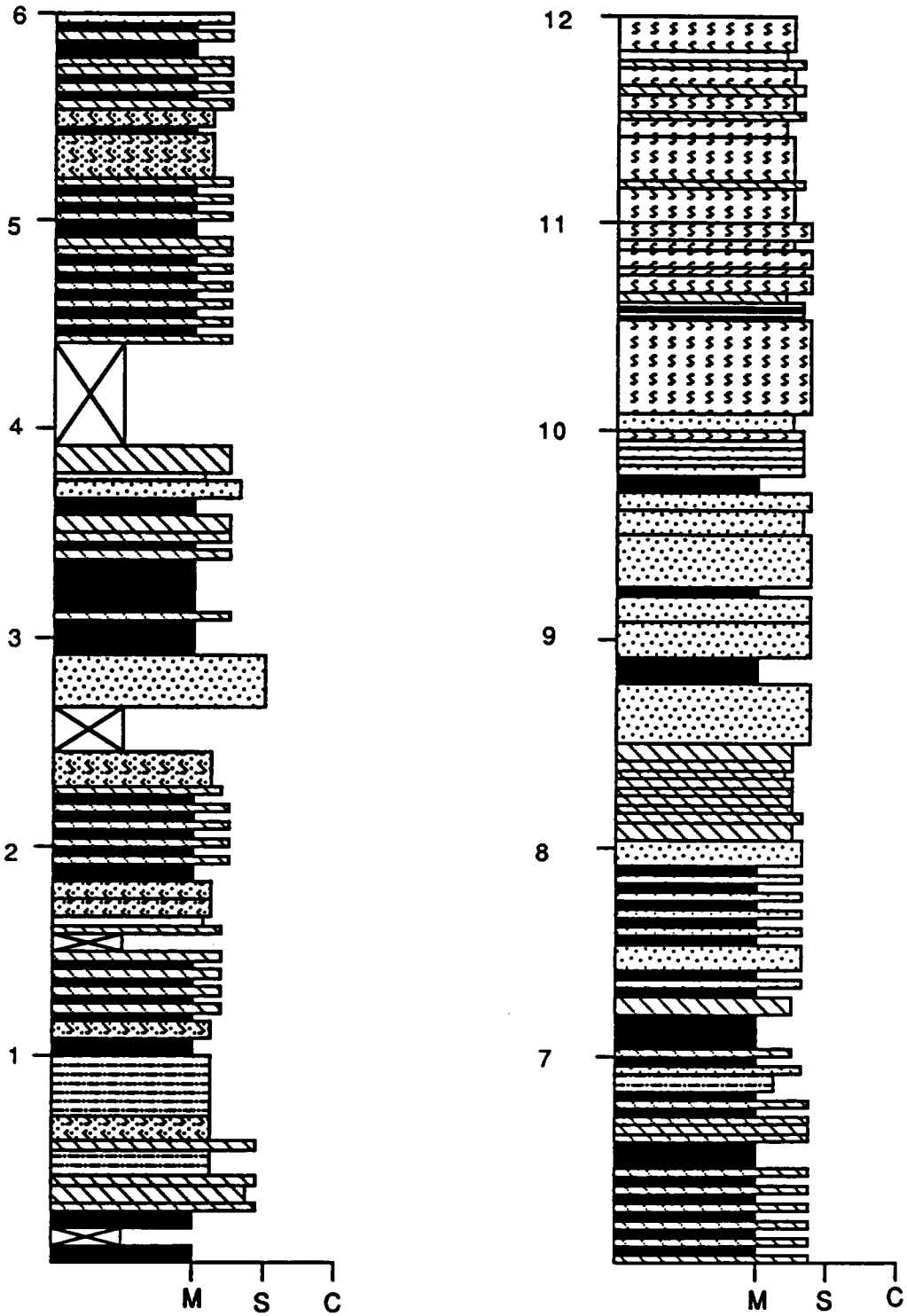

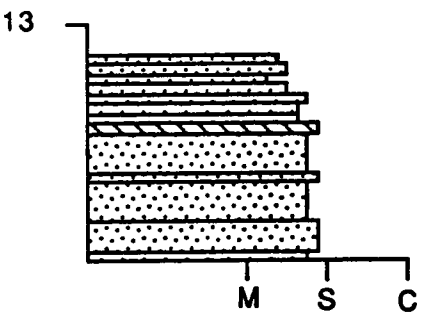
13
M
S
C

POPLAR CAMP SECTION 4

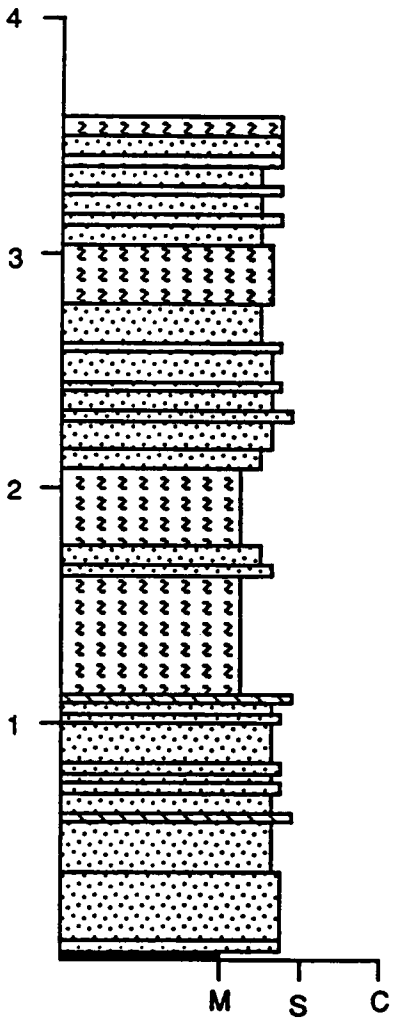

POPLAR CAMP SECTION 5

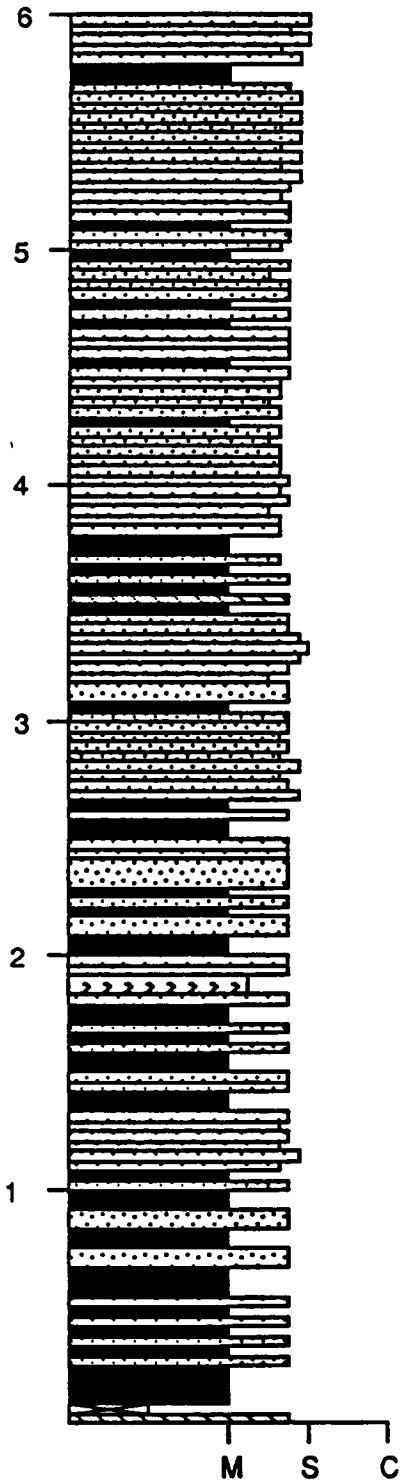

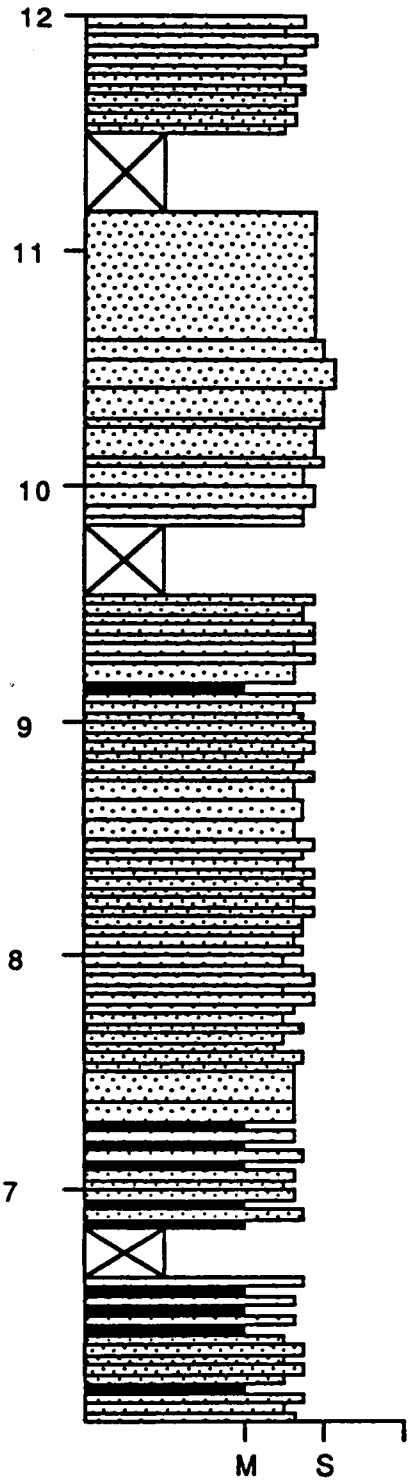

55 METERS TO SHADY DOLOMITE

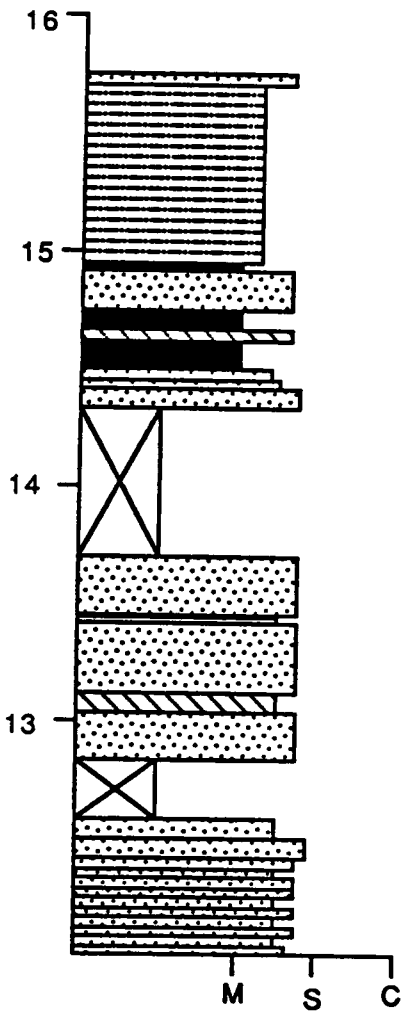

BUCHANAN SECTION (LOCALITY 7)

BUCHANAN QUADRANGLE

ERWIN FORMATION STARTING AT HAMPTON TO ERWIN CONTACT. SHADY DOLOMITE OVERLYING THE ERWIN FORMATION

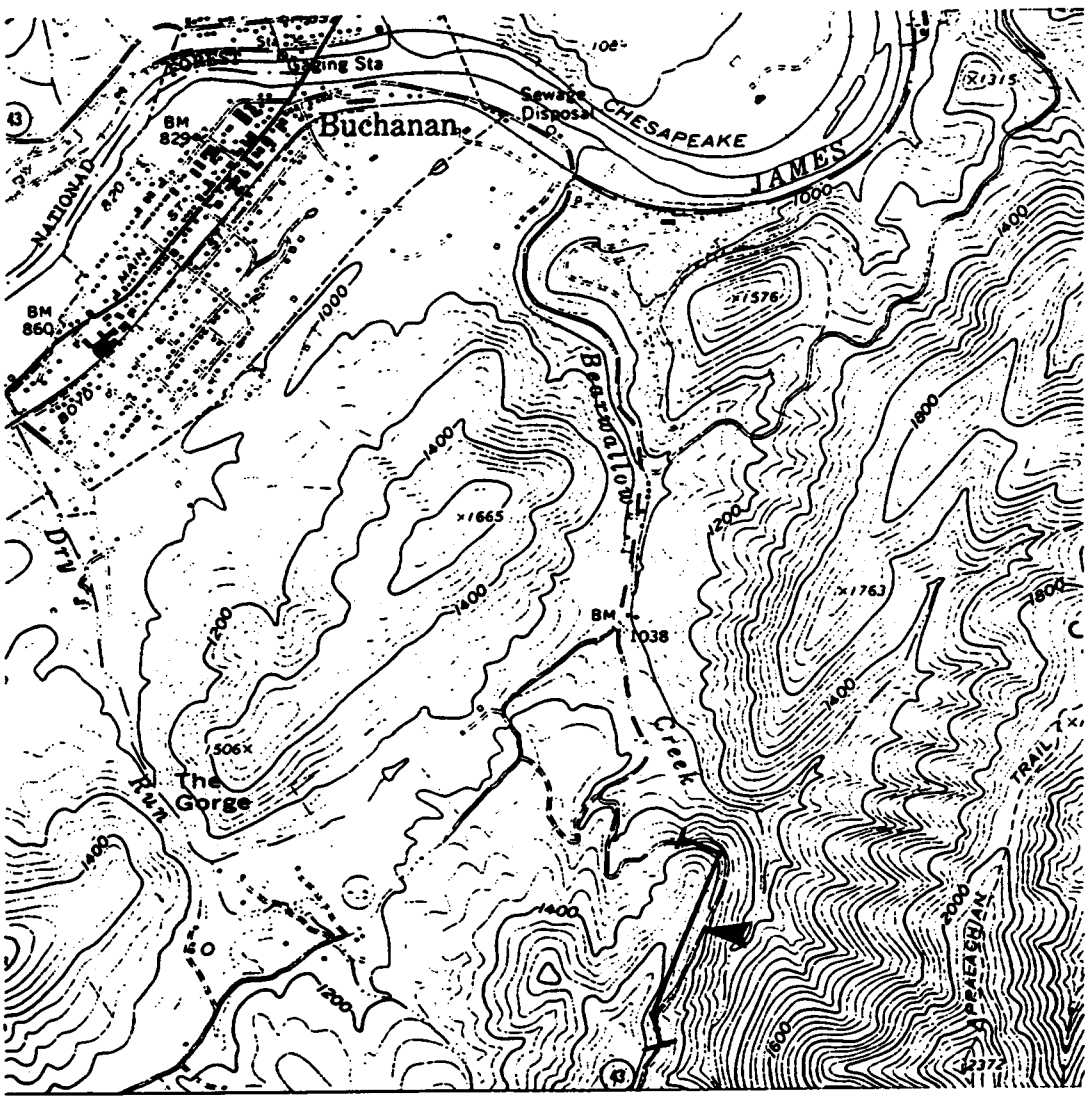

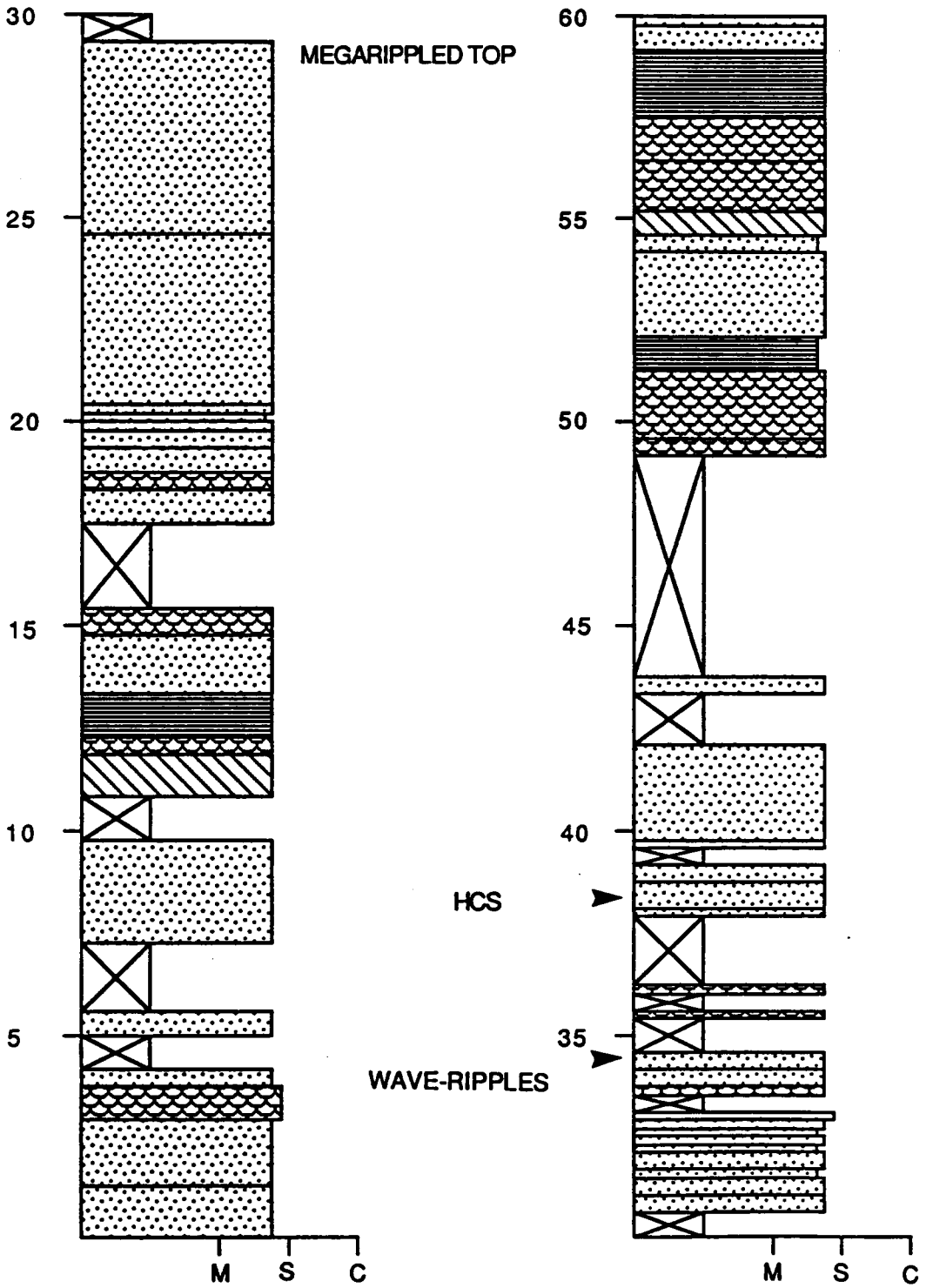
30
25
20
15
10
5
MEGARIPPLED TOP
M
S
C
60
55
50
45
40
35
HCS
WAVE-RIPPLES
M
S
C

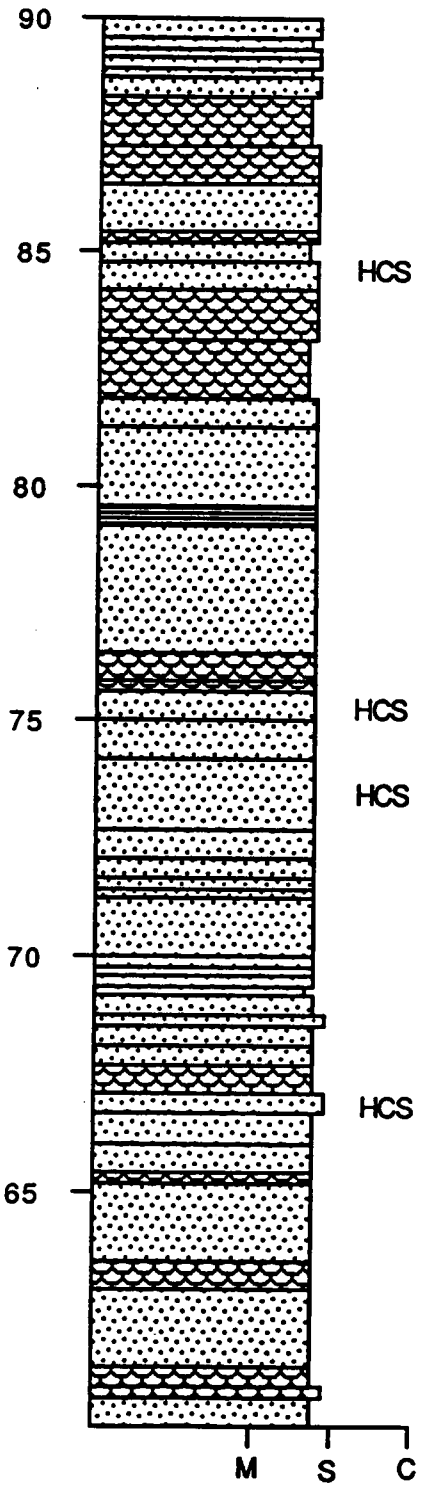
90
85
80
75
70
65
HCS
HCS
HCS
HCS
M
S
C

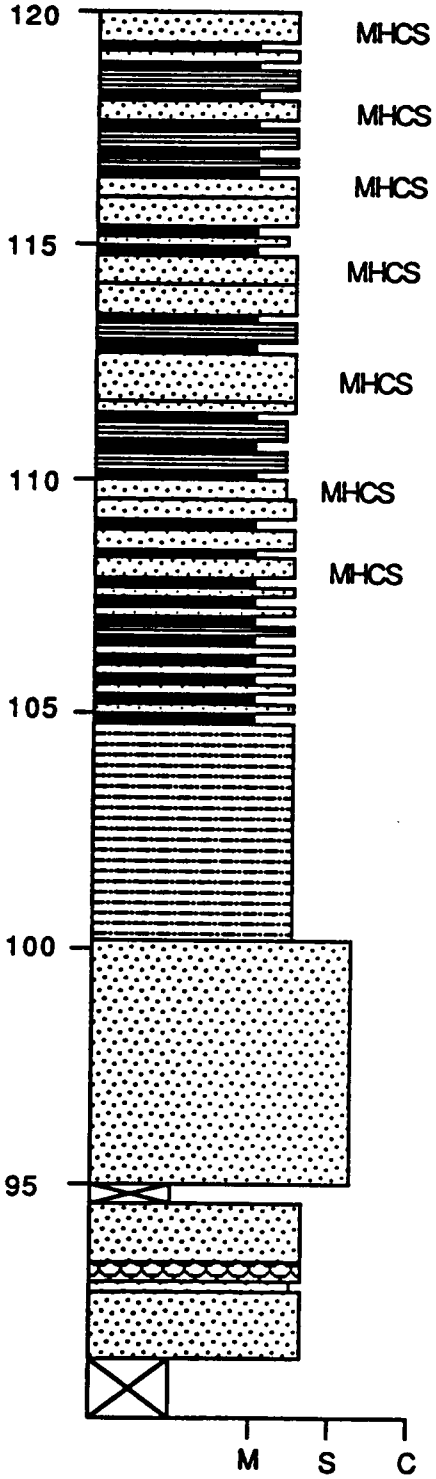
120
115
110
105
100
95
MHCS
MHCS
MHCS
MHCS
MHCS
MHCS
MHCS
M
S
C

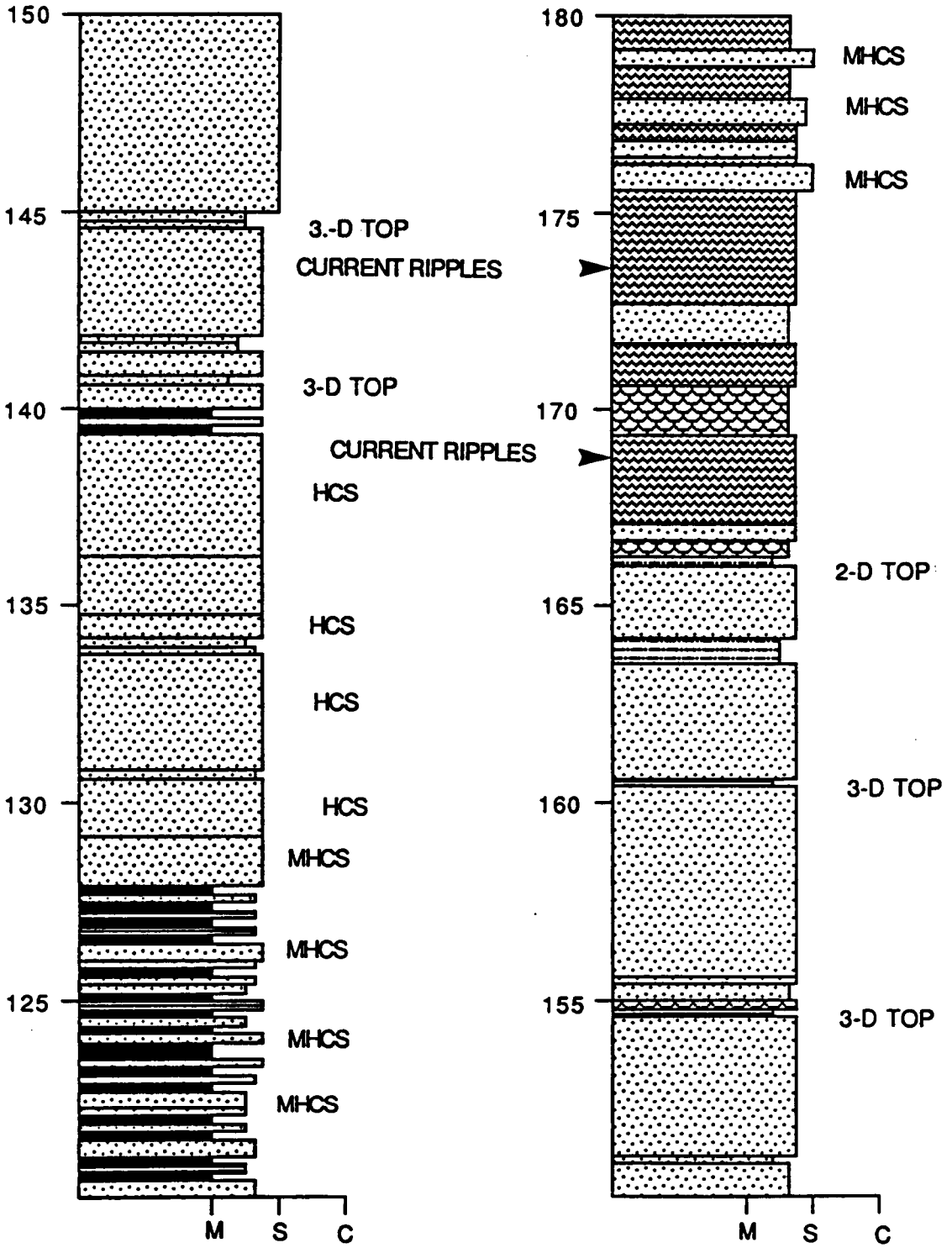
150
145
140
135
130
125
3.-D TOP
CURRENT RIPPLES
3-D TOP
HCS
HCS
HCS
HCS
MHCS
MHCS
MHCS
MHCS
M
S
C
180
175
170
165
160
155
MHCS
MHCS
MHCS
CURRENT RIPPLES
2-D TOP
3-D TOP
3-D TOP
M
S
C

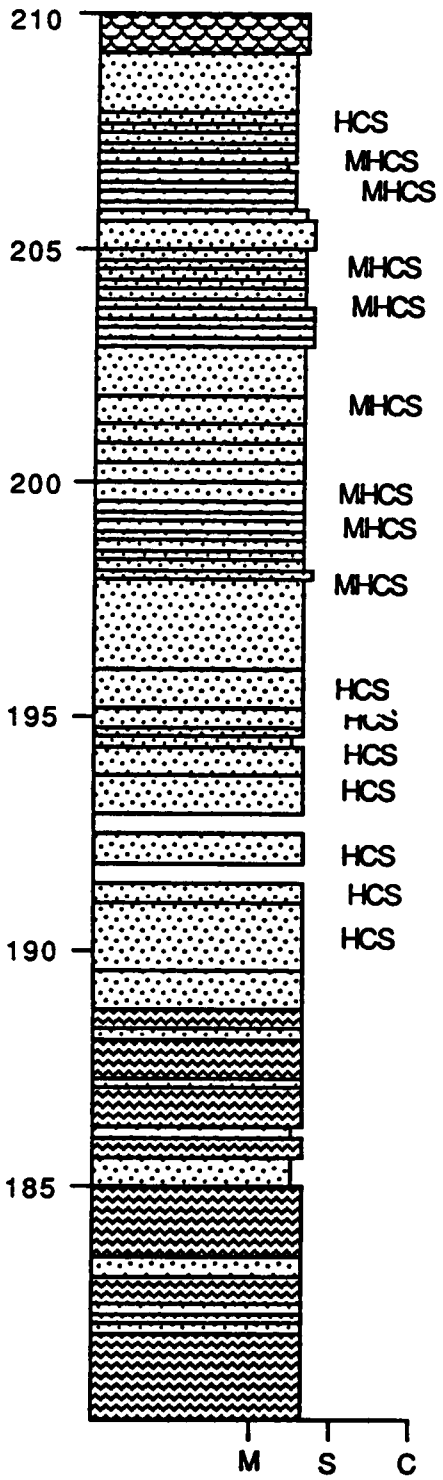
210
205
200
195
190
185
HCS
MHCS
MHCS
MHCS
MHCS
MHCS
MHCS
MHCS
HCS
HCS
HCS
HCS
HCS
HCS
HCS
M
S
C

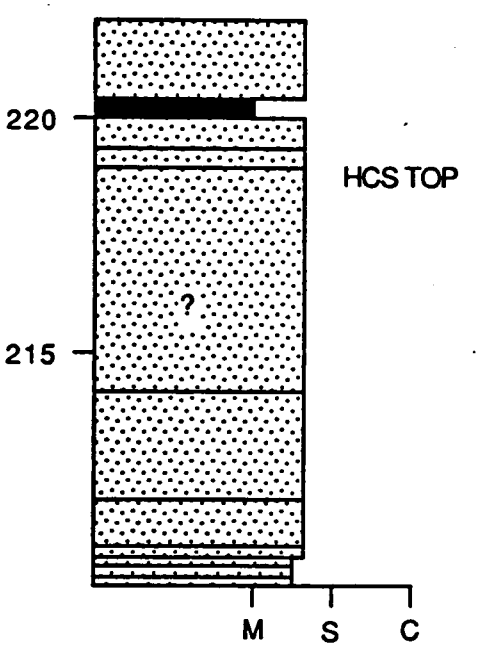
220
215
HCS TOP
?
M
S
C

ARCADIA SECTION (LOCALITY 8)

ARNOLD VALLEY QUADRANGLE

UNICOI FORMATION IN FAULT CONTACT WITH THE HAMPTON FORMATION. SECTION 1 IS IN THE UNICOI FORMATION. SECTION 2 IS IN THE HAMPTON FORMATION. ERWIN OVERLIES THE HAMPTON FORMATION.

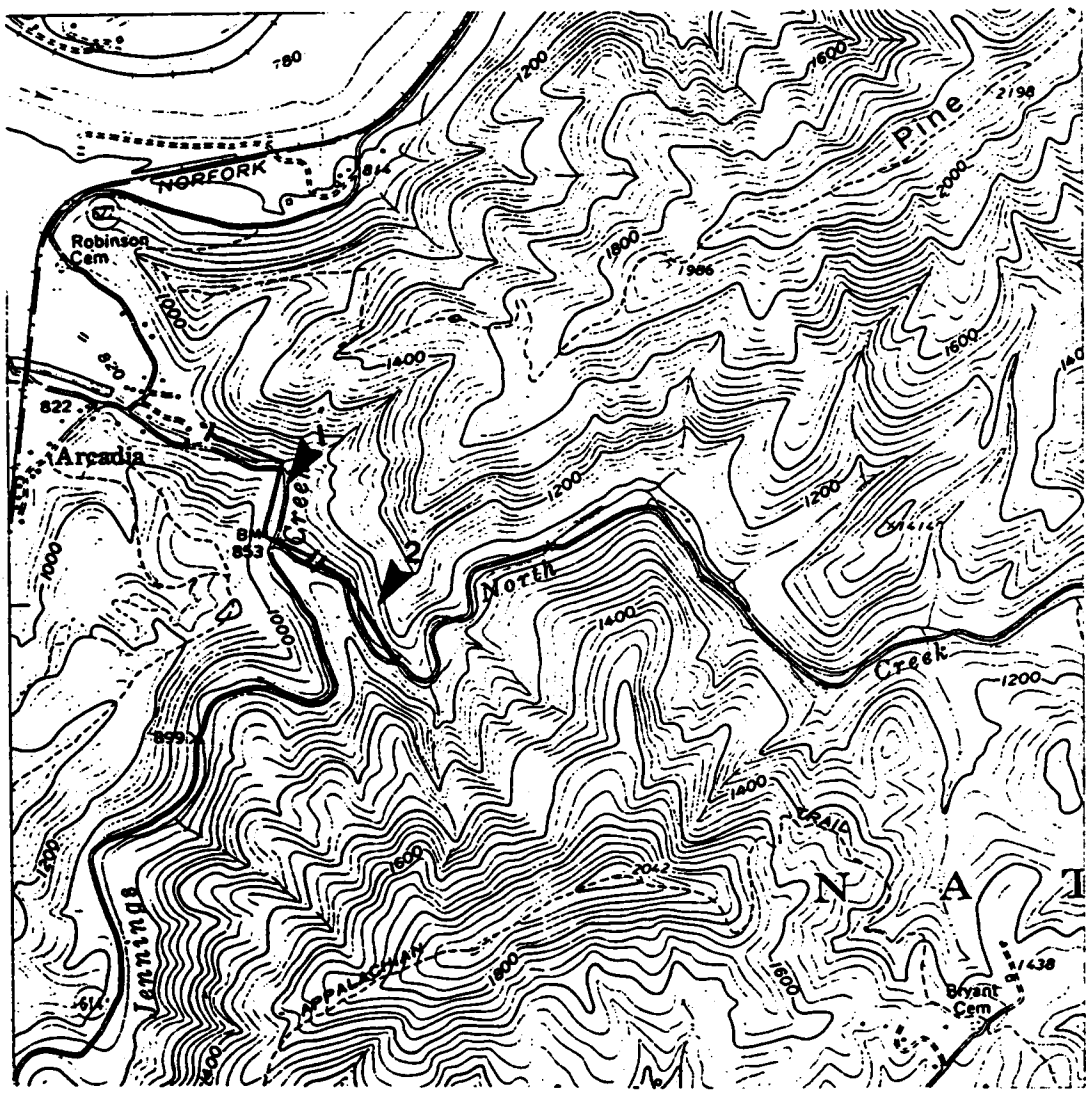

ARCADIA SECTION 1

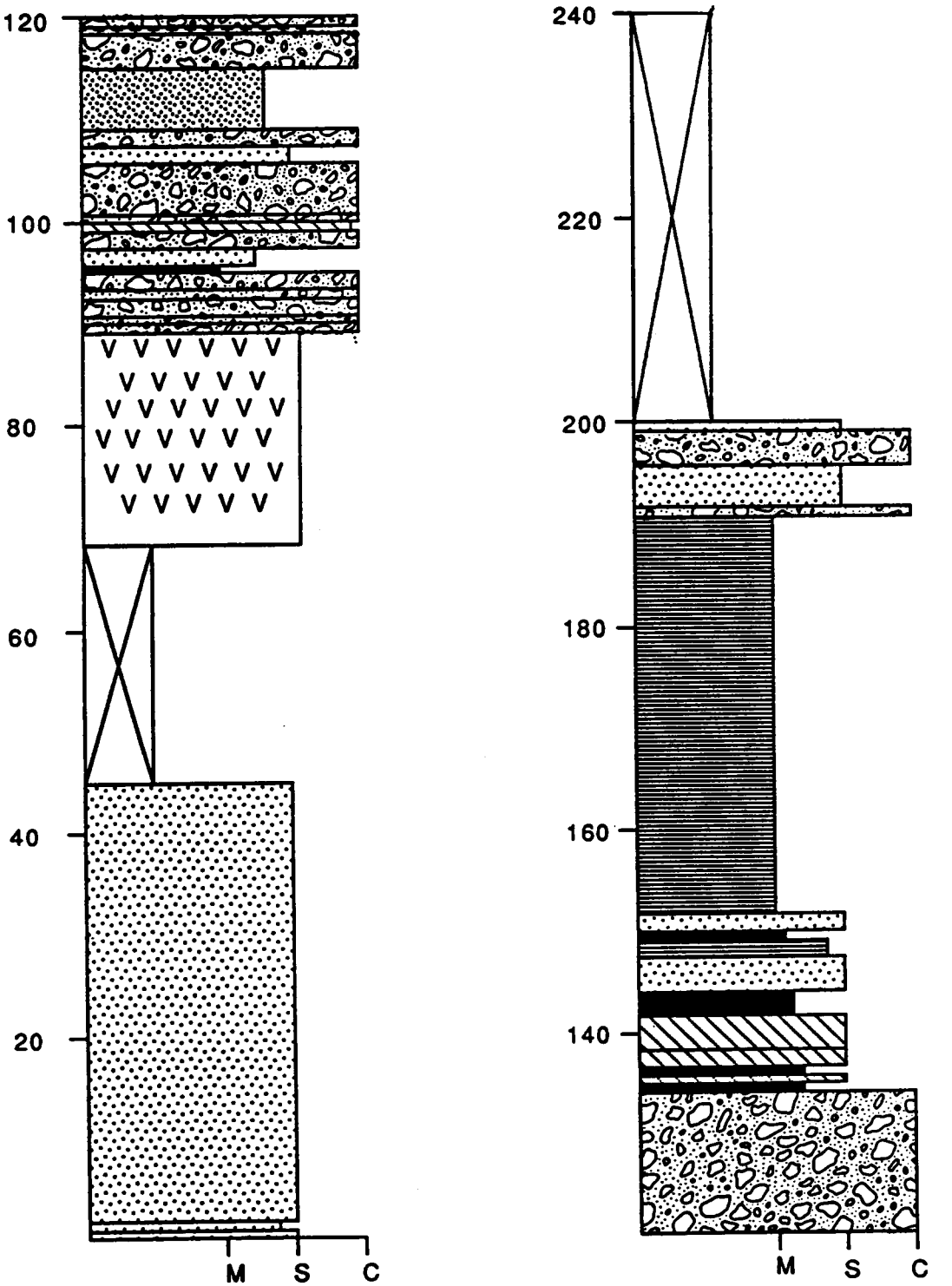

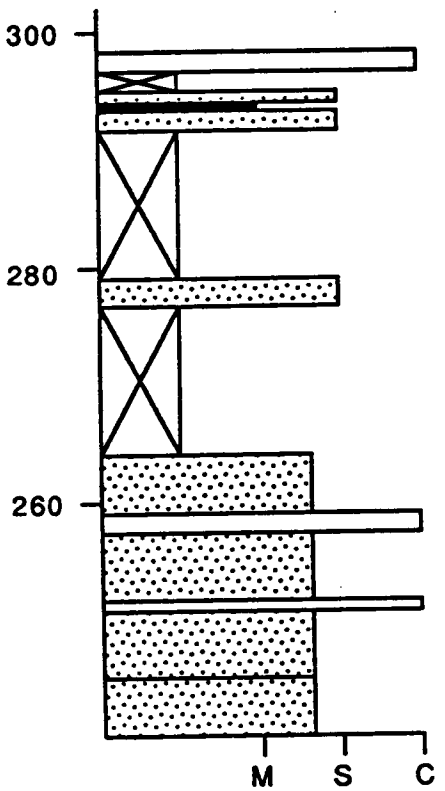
300
280
260
M
S
C

ARCADIA SECTION 2

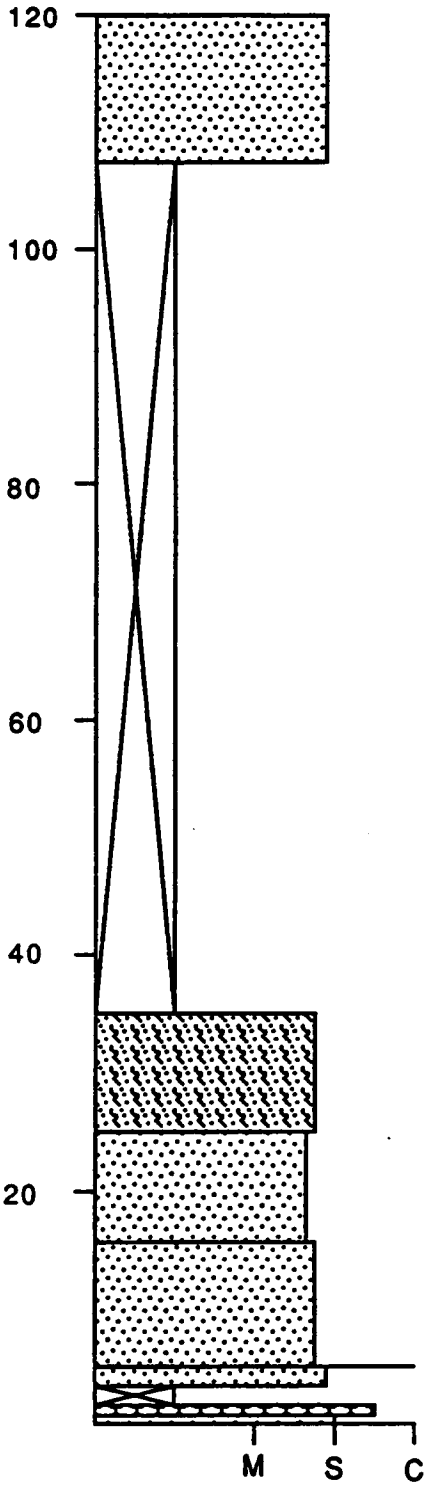

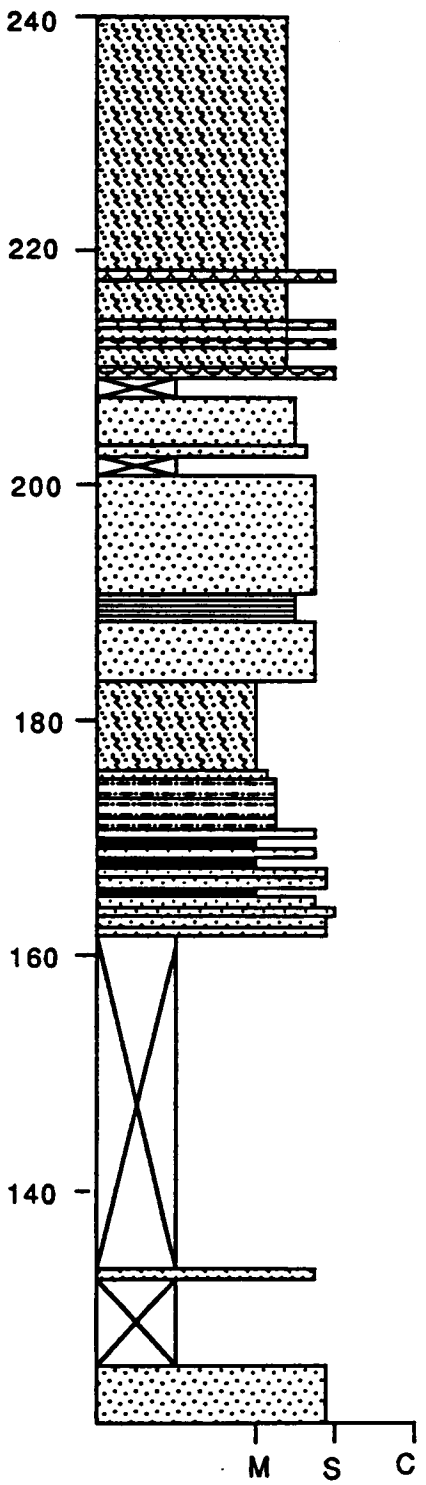

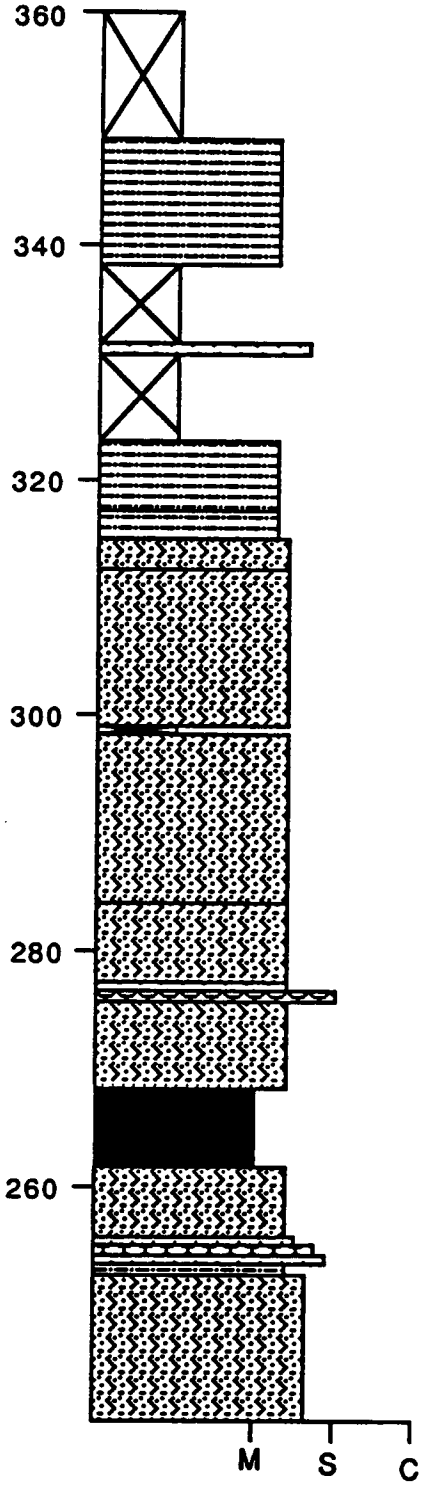
360
340
320
300
280
260
M
S
C

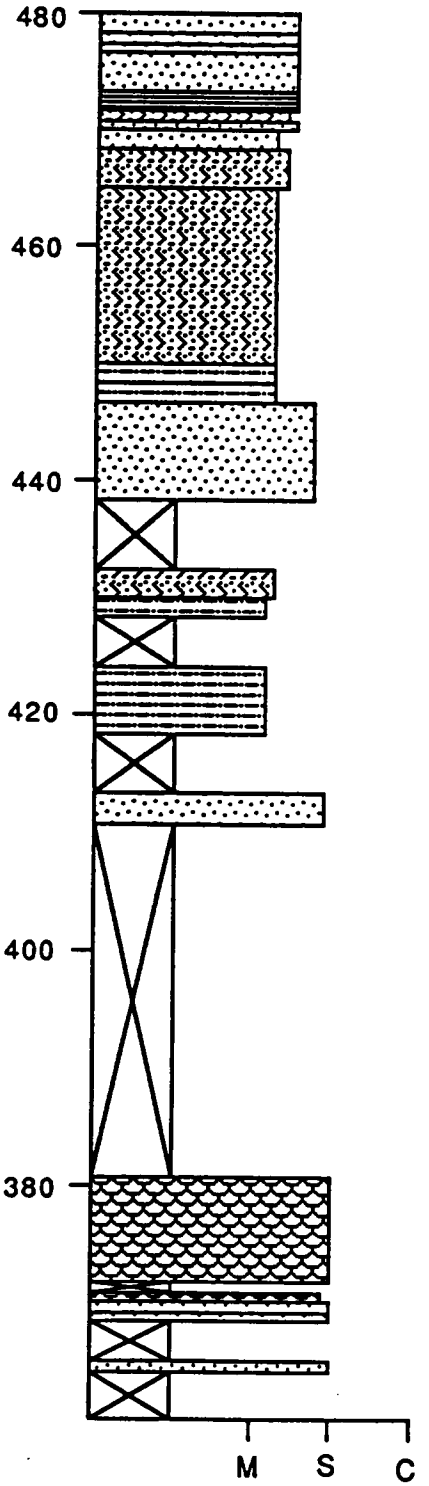
480
460
440
420
400
380
M
S
C

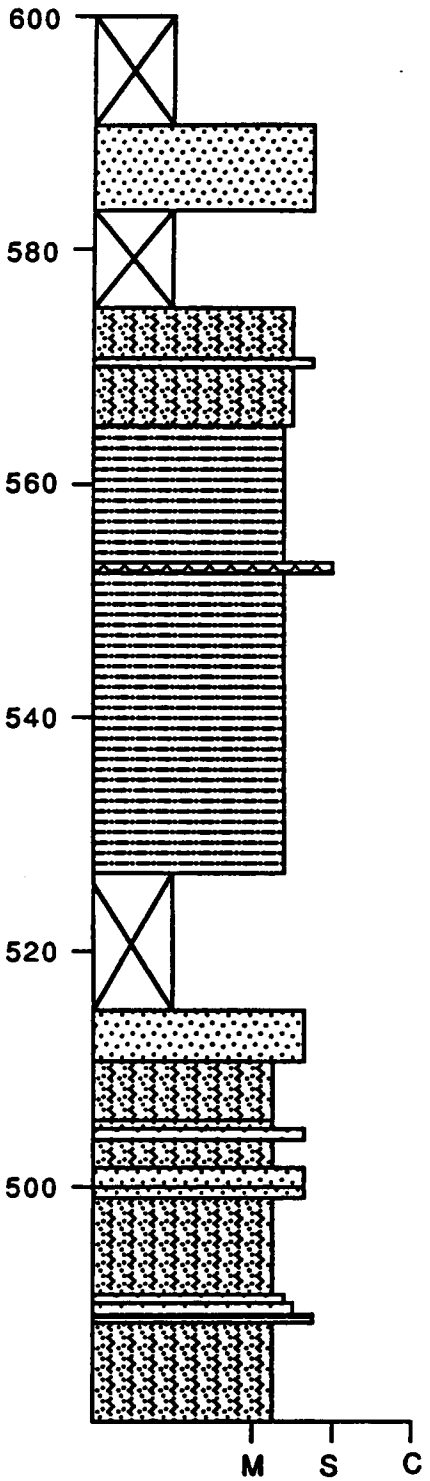
600
580
560
540
520
500
M
S
C

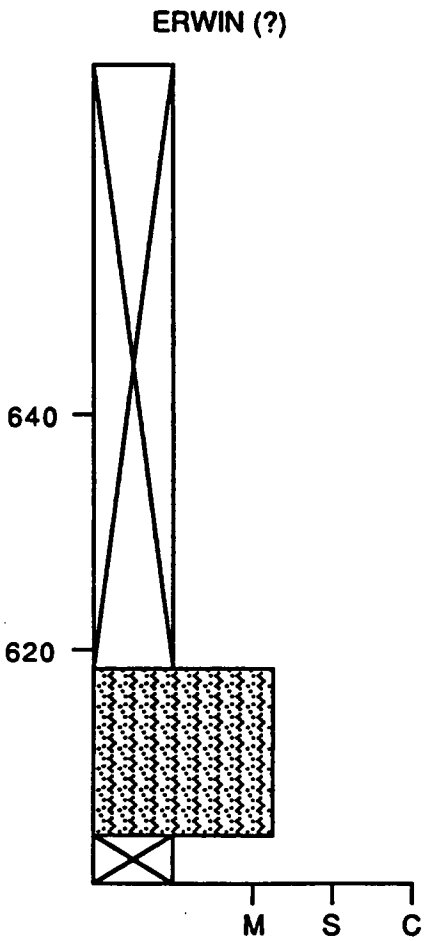
ERWIN (?)
640
620
M
S
C

NATURAL BRIDGE QUARRY SECTION (LOCALITY 9)

SNOWDEN QUADRANGLE

ERWIN FORMATION OVERLAIN BY SHADY DOLOMITE.

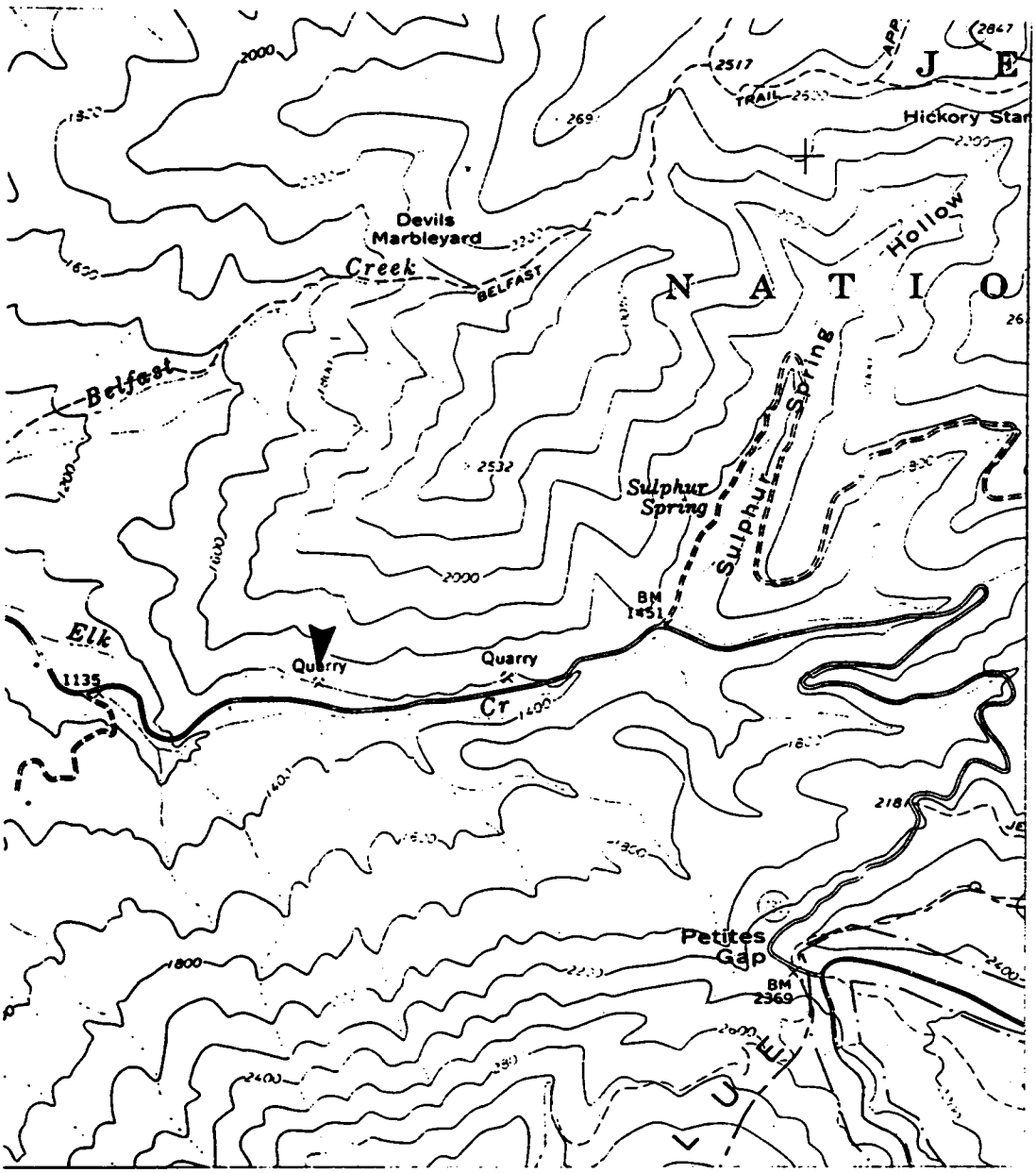

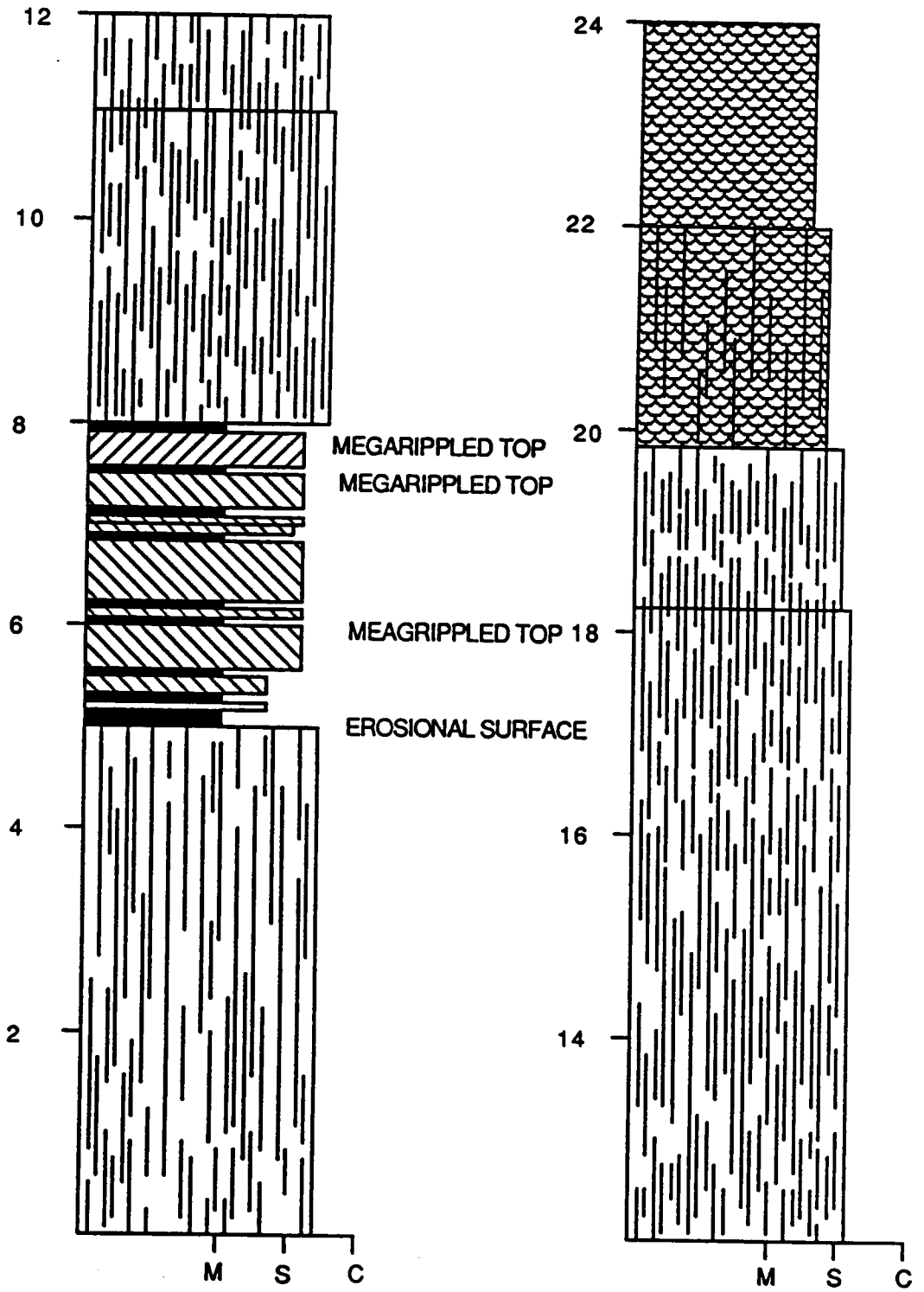
12
10
8
6
4
2
MEGARIPPLED TOP
MEGARIPPLED TOP
MEAGRIPPLED TOP
EROSIONAL SURFACE
M
S
C
24
22
20
18
16
14
M
S
C

BALCONY FALLS UNICOI SECTION (LOCALITY 10)

SNOWDEN QUADRANGLE

GRENVILLE BASEMENT OVERLAIN BY UNICOI FORMATION. TOP OF SECTION CROSSES THE UNICOI TO HAMPTION FORMATION TRANSITION.

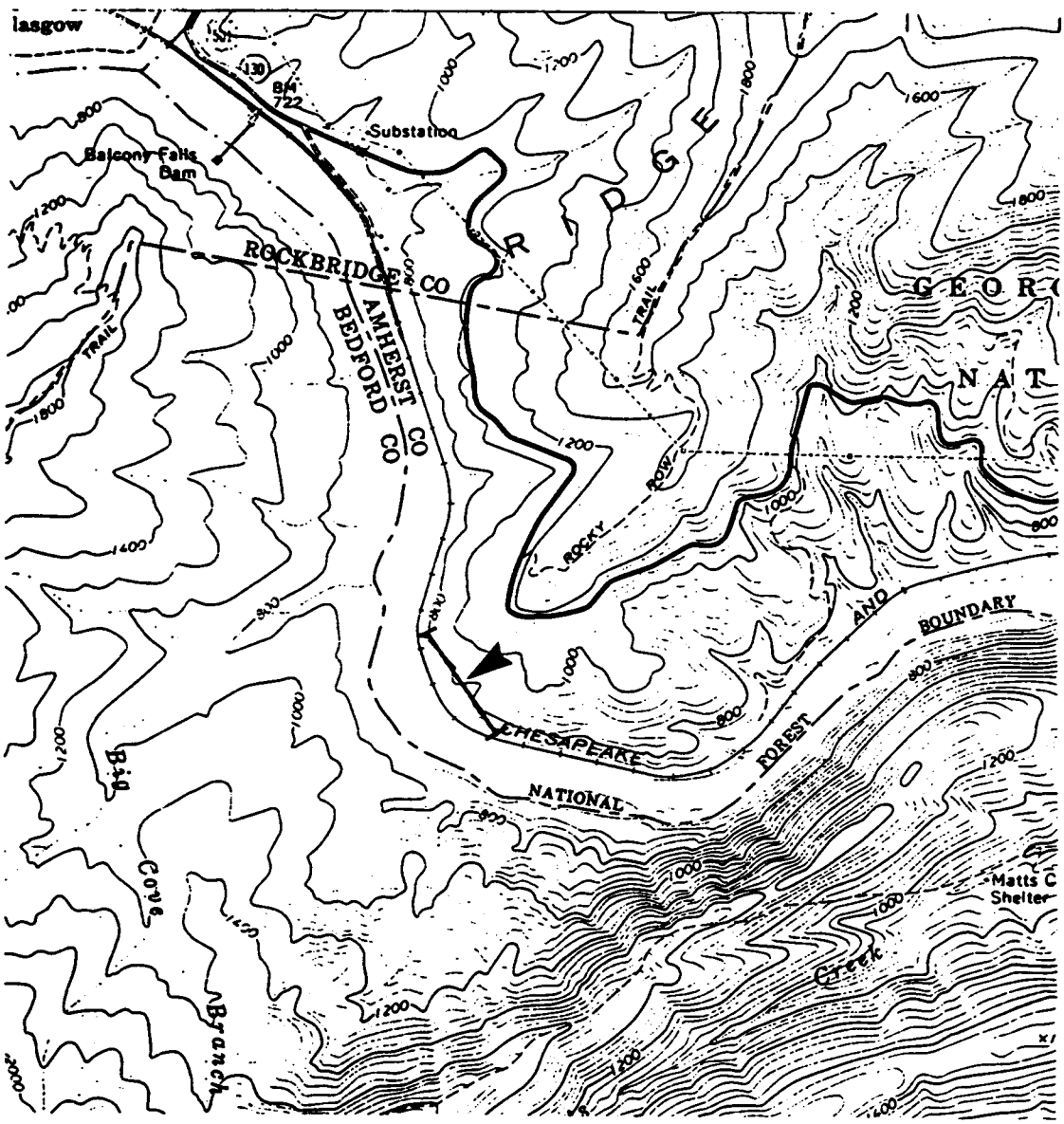

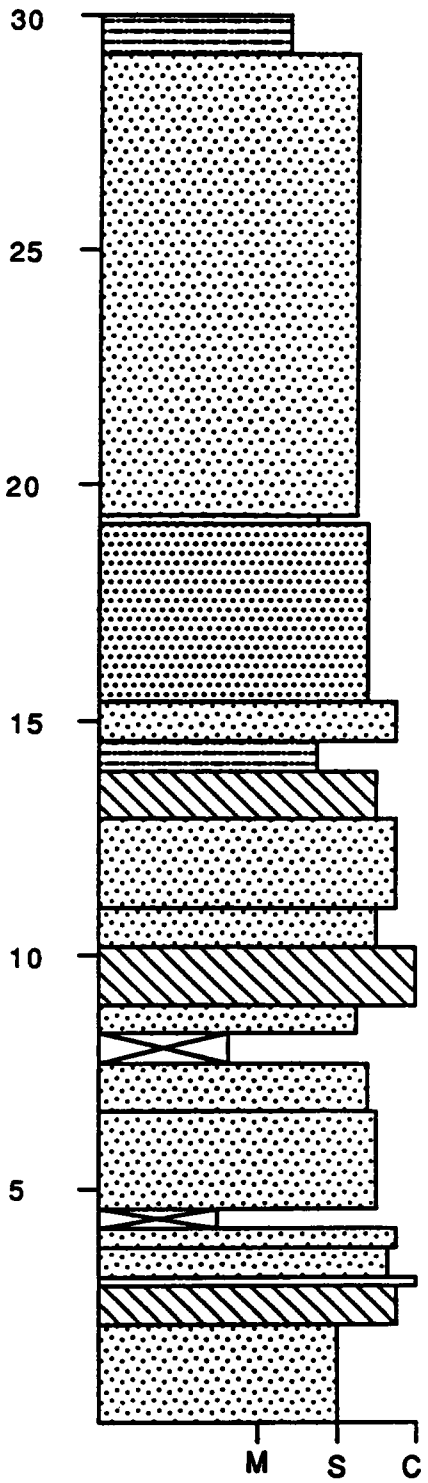
30
25
20
15
10
5
M
S
C

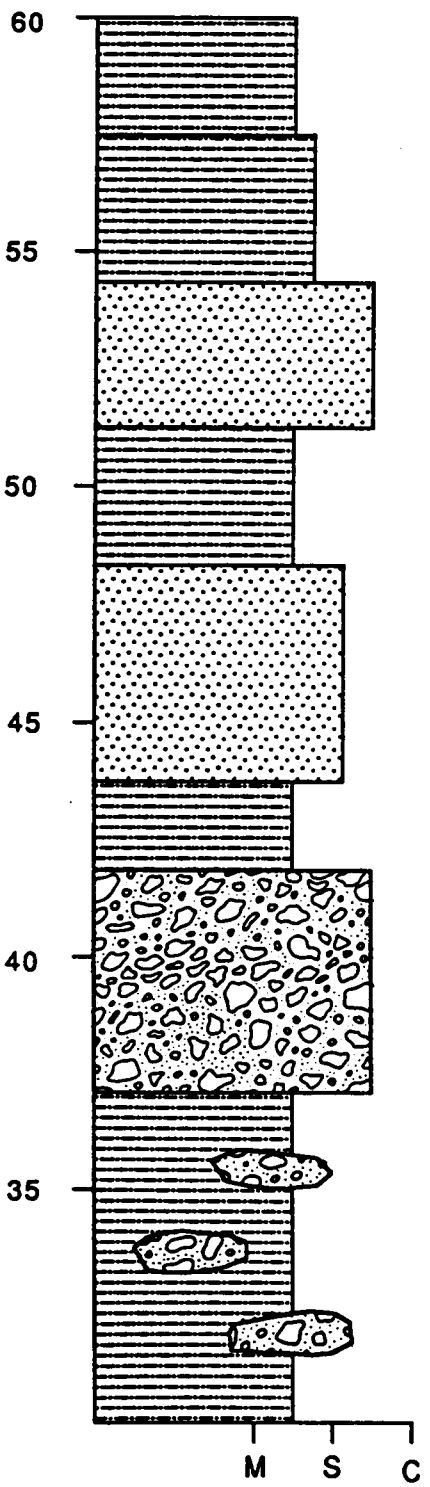
60
55
50
45
40
35
M
S
C

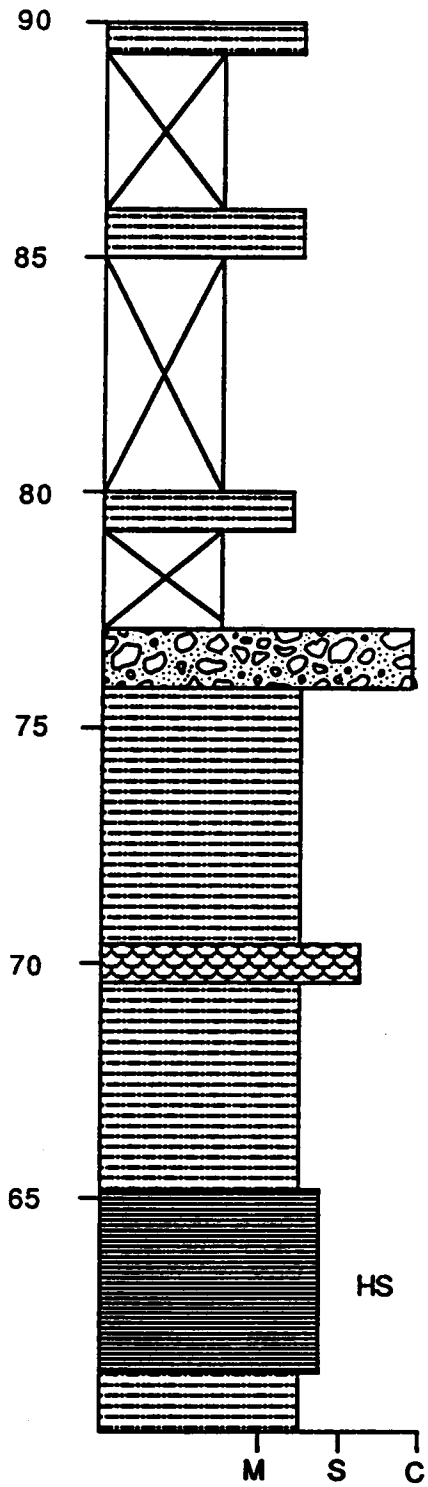
90
85
80
75
70
65
HS
M
S
C

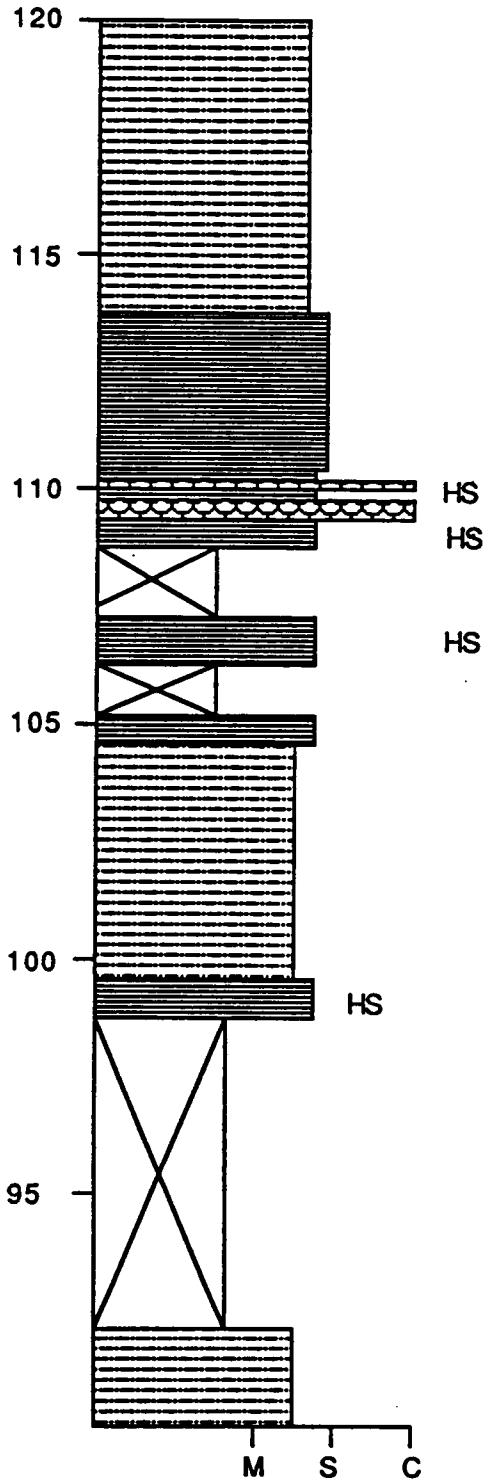
120
115
110
105
100
95
HS
HS
HS
HS
M
S
C

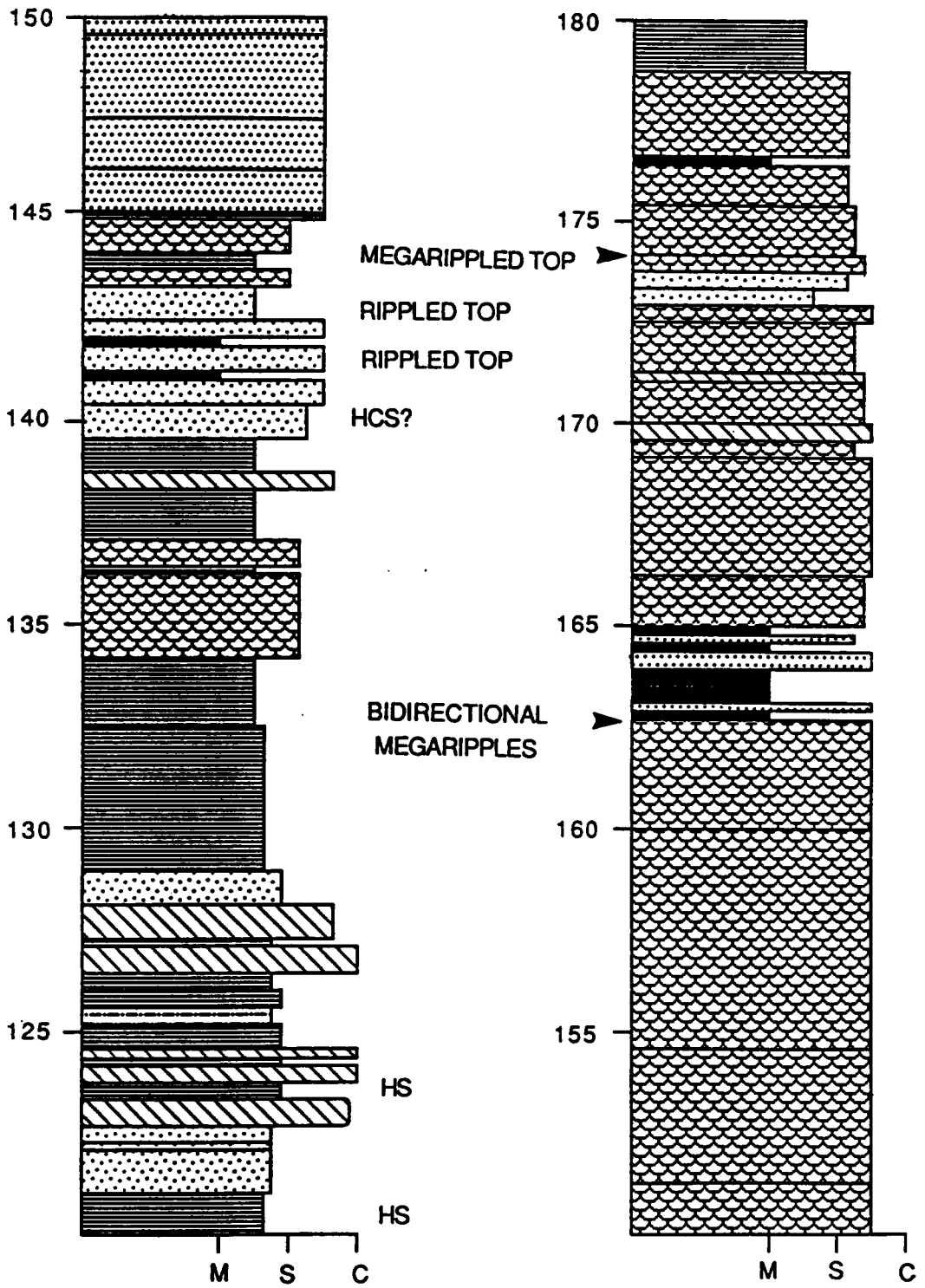
150
145
140
135
130
125
180
175
170
165
160
155
MEGARIPPLED TOP
RIPPLED TOP
RIPPLED TOP
HCS?
BIDIRECTIONAL
MEGARIPPLES
HS
HS
M
S
C
M
S
C

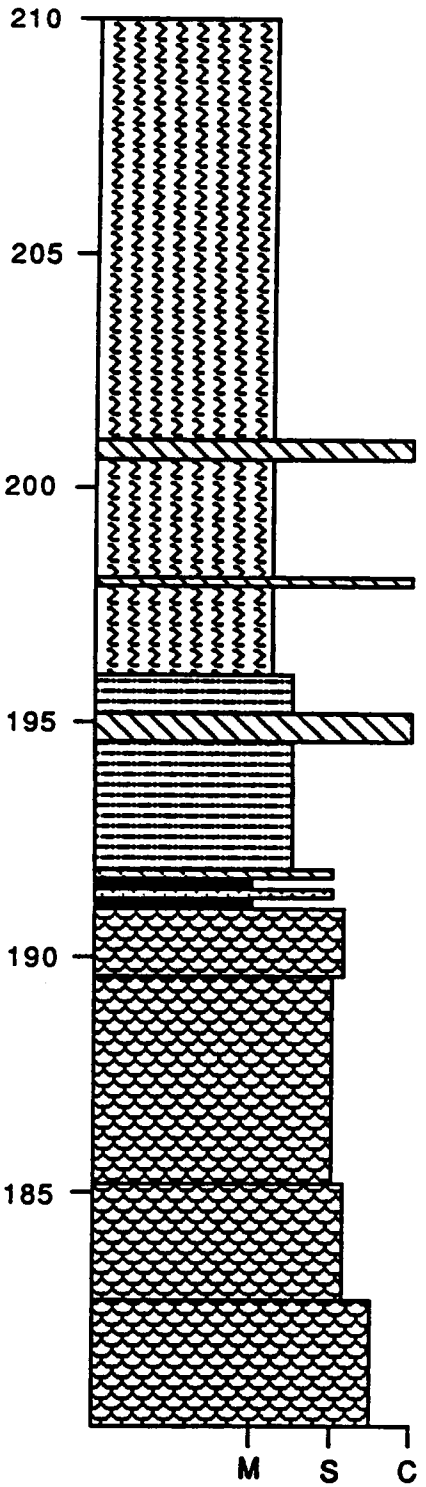
210
205
200
195
190
185
M
S
C

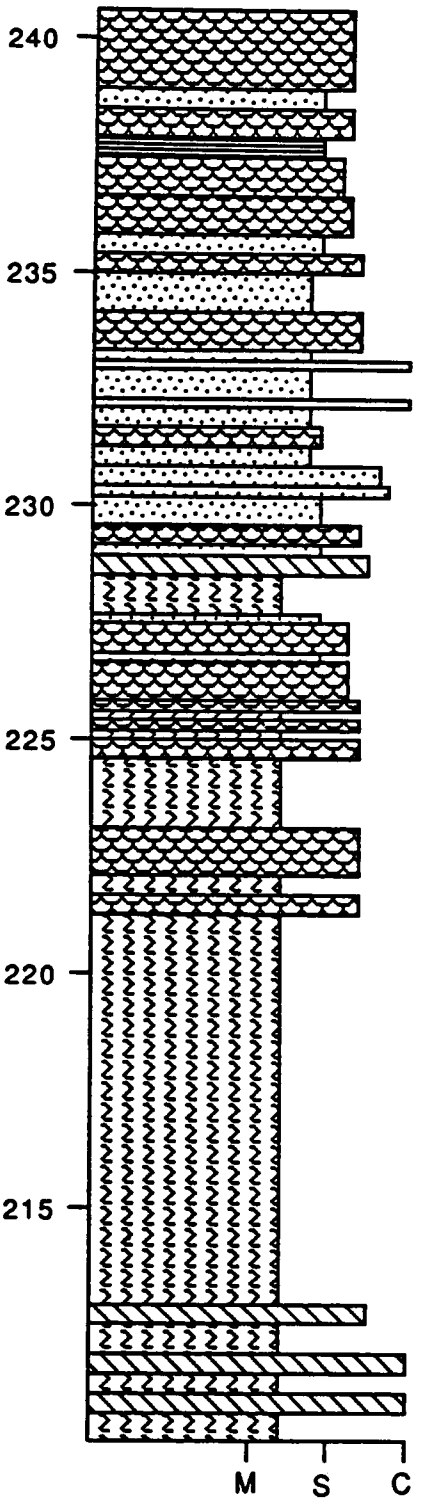
240
235
230
225
220
215
M
S
C

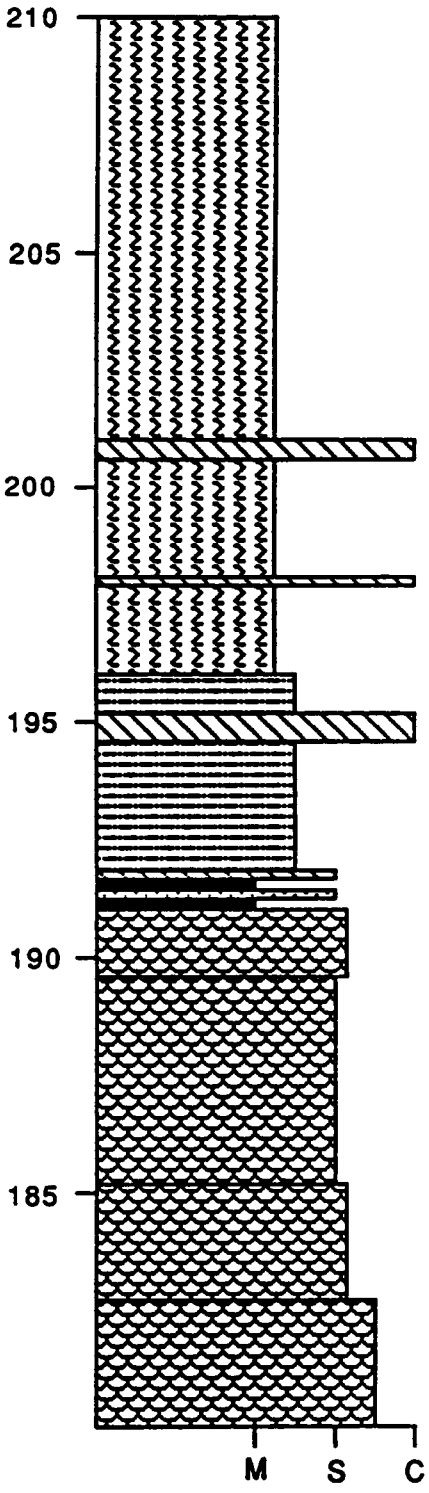
210
205
200
195
190
185
M
S
C

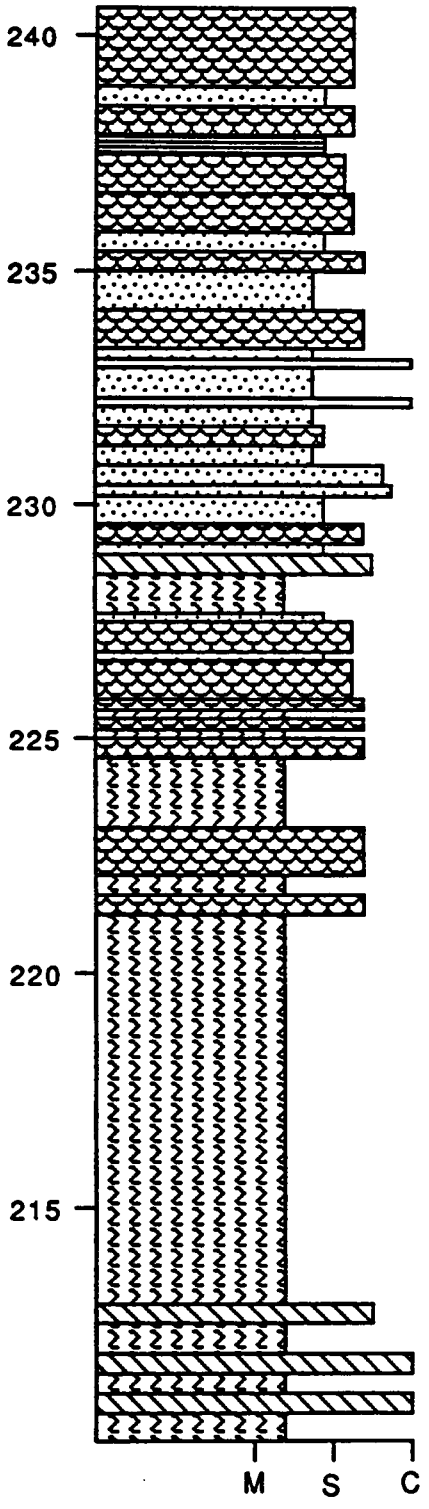
240
235
230
225
220
215
M
S
C

BALCONY FALLS RAILROAD BALCONY FALLS SNOWDEN AND SNOWDEN SECTIONS (LOCALITY 10)

SNOWDEN QUADRANGLE

THREE SECTIONS THROUGH THE SNOWDEN MEMBER OF THE HAMPTON FORMATION.

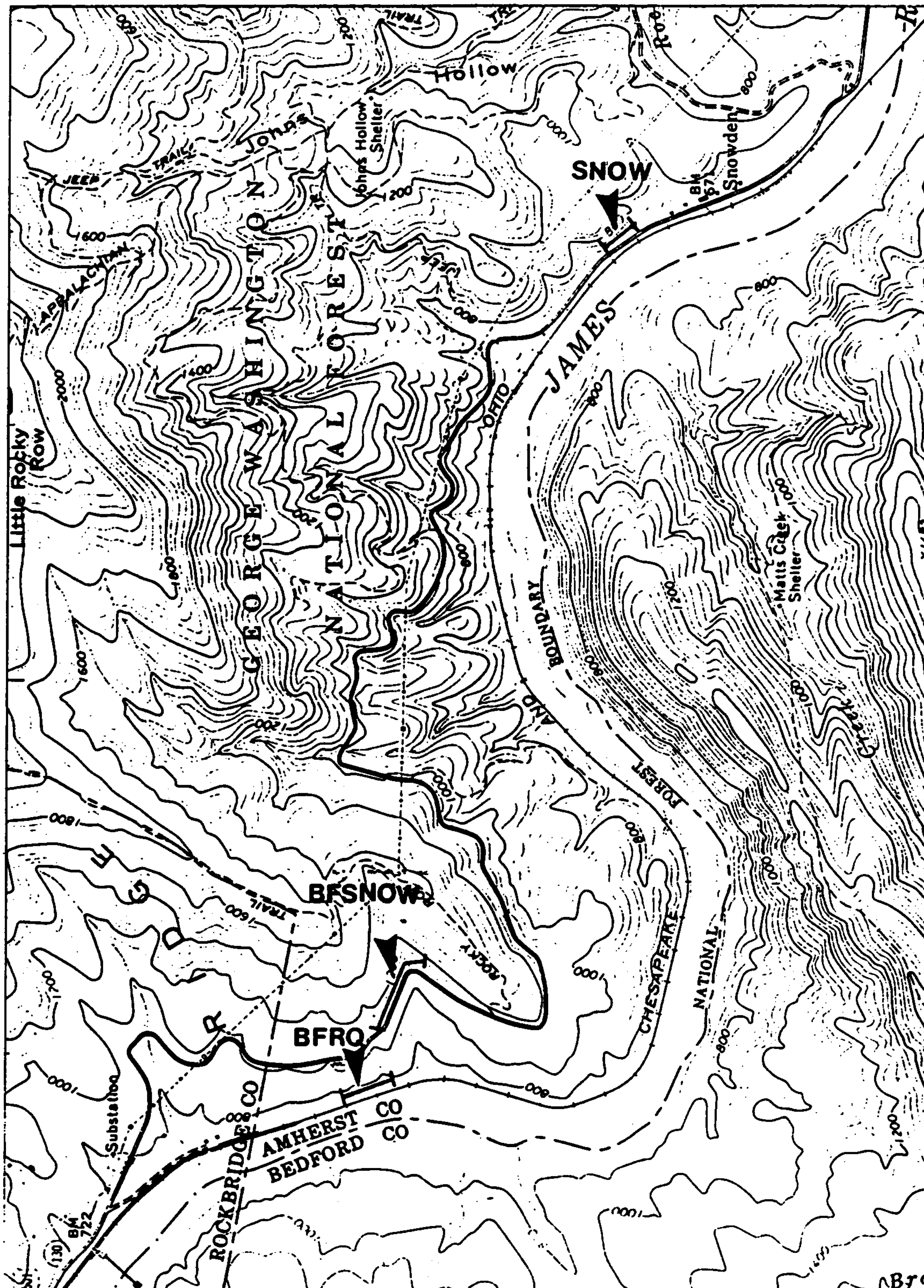
SNOW
BFSNOW
BFRO
GEORGE WASHINGTON
NATIONAL FOREST
JAMES
CHESAPEAKE AND OHIO
NATIONAL FOREST BOUNDARY
AMHERST CO
BEDFORD CO
ROCKBRIDGE CO
Little Rocky Row
Johns Hollow
Johns Hollow Shelter
Matts Creek Shelter
Snowden
APPALACHIAN
TRAIL
JEEP
Substation

SNOWDEN SECTION

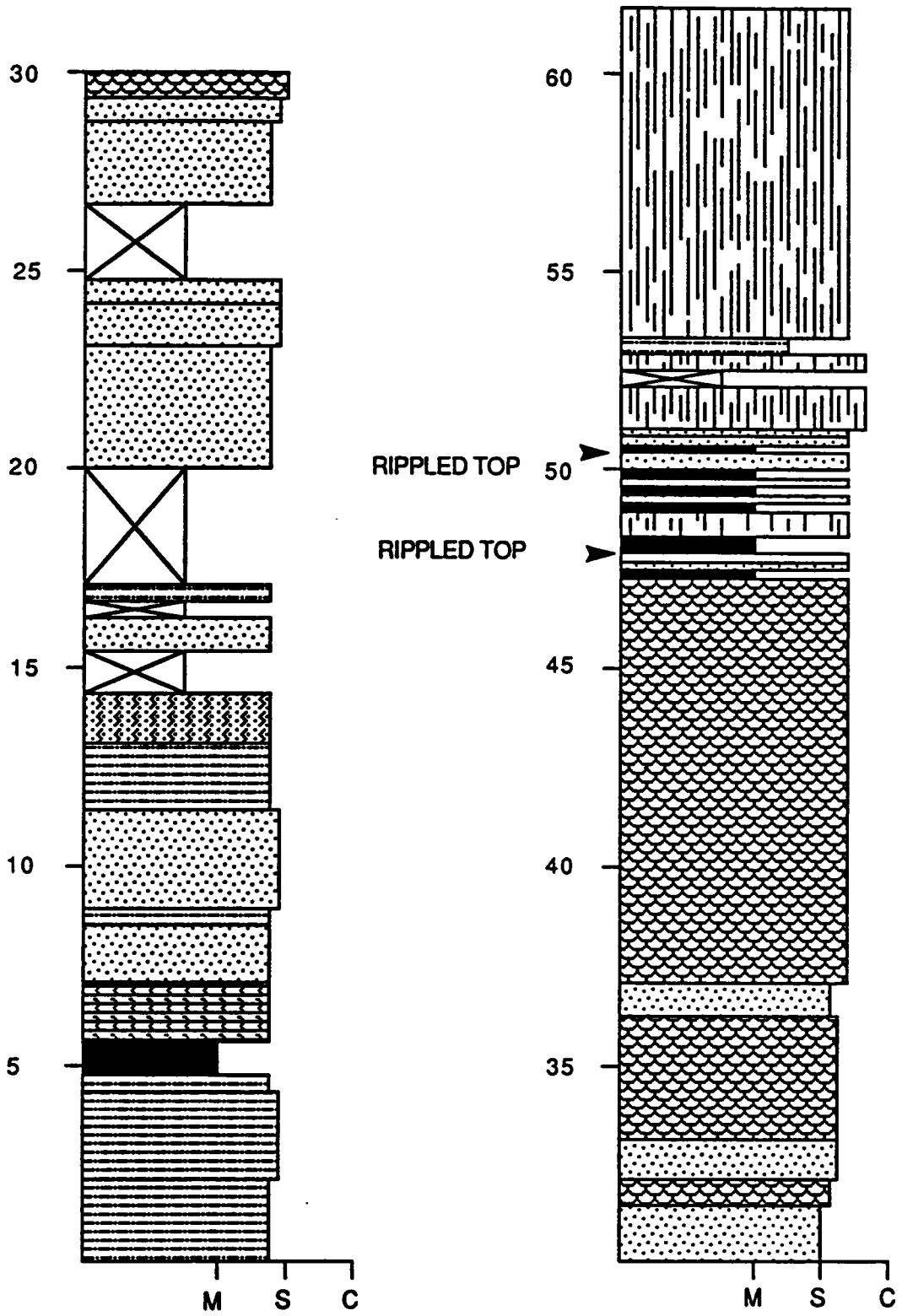

BALCONY FALLS SNOWDEN SECTION

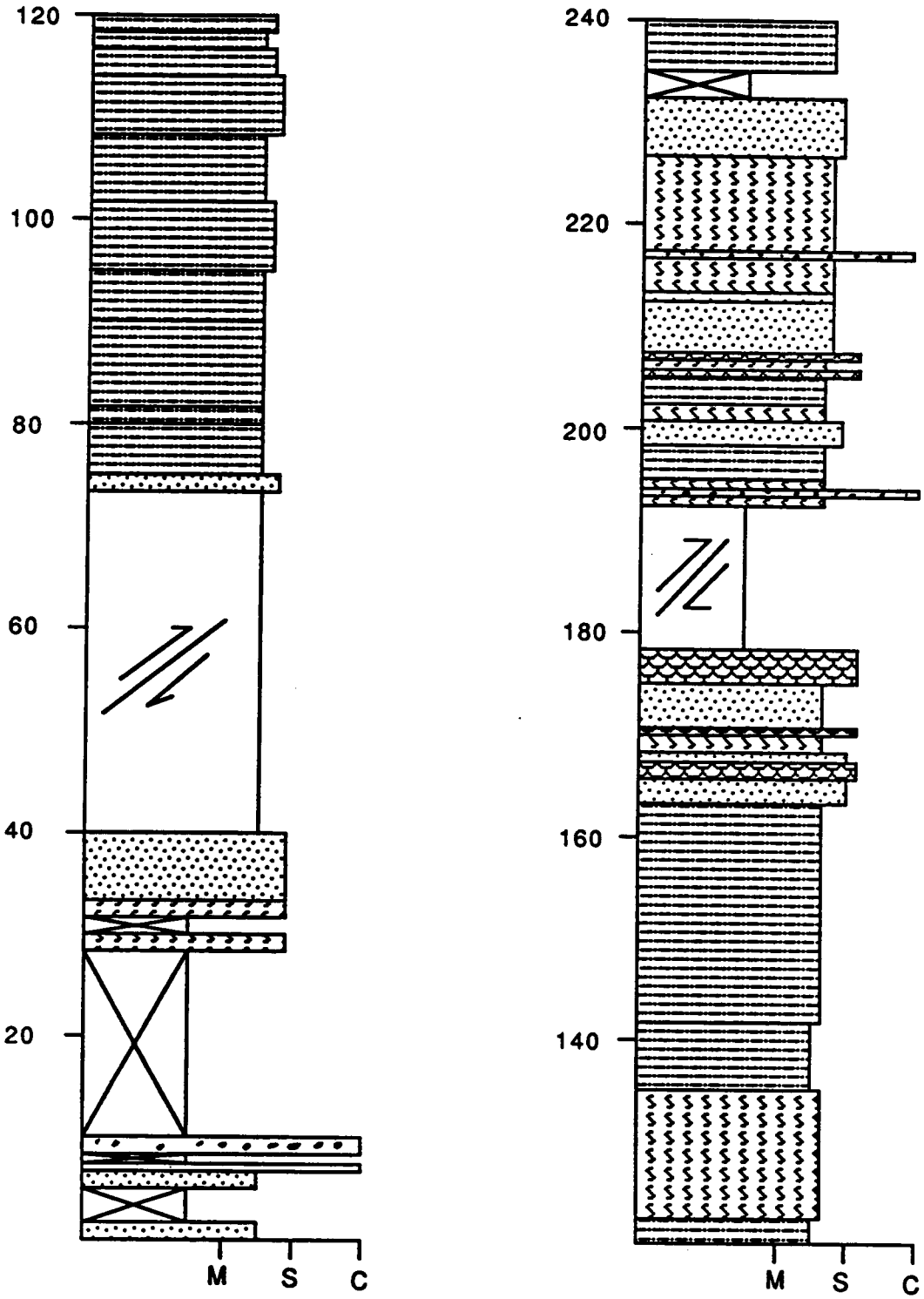

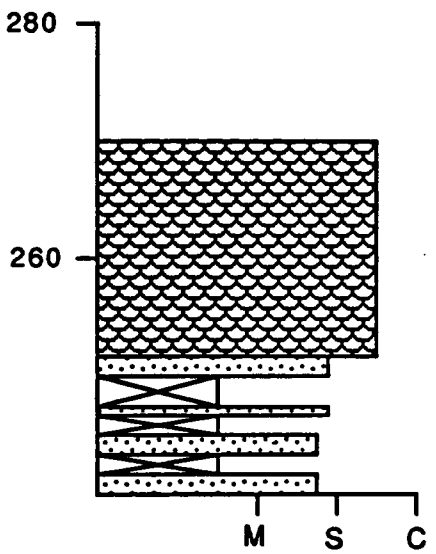
280
260
M
S
C

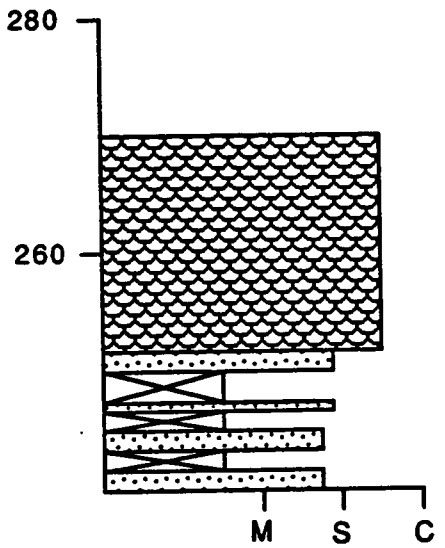
280
260
M
S
C

BALCONY FALLS RAILROAD QUARRY SECTION

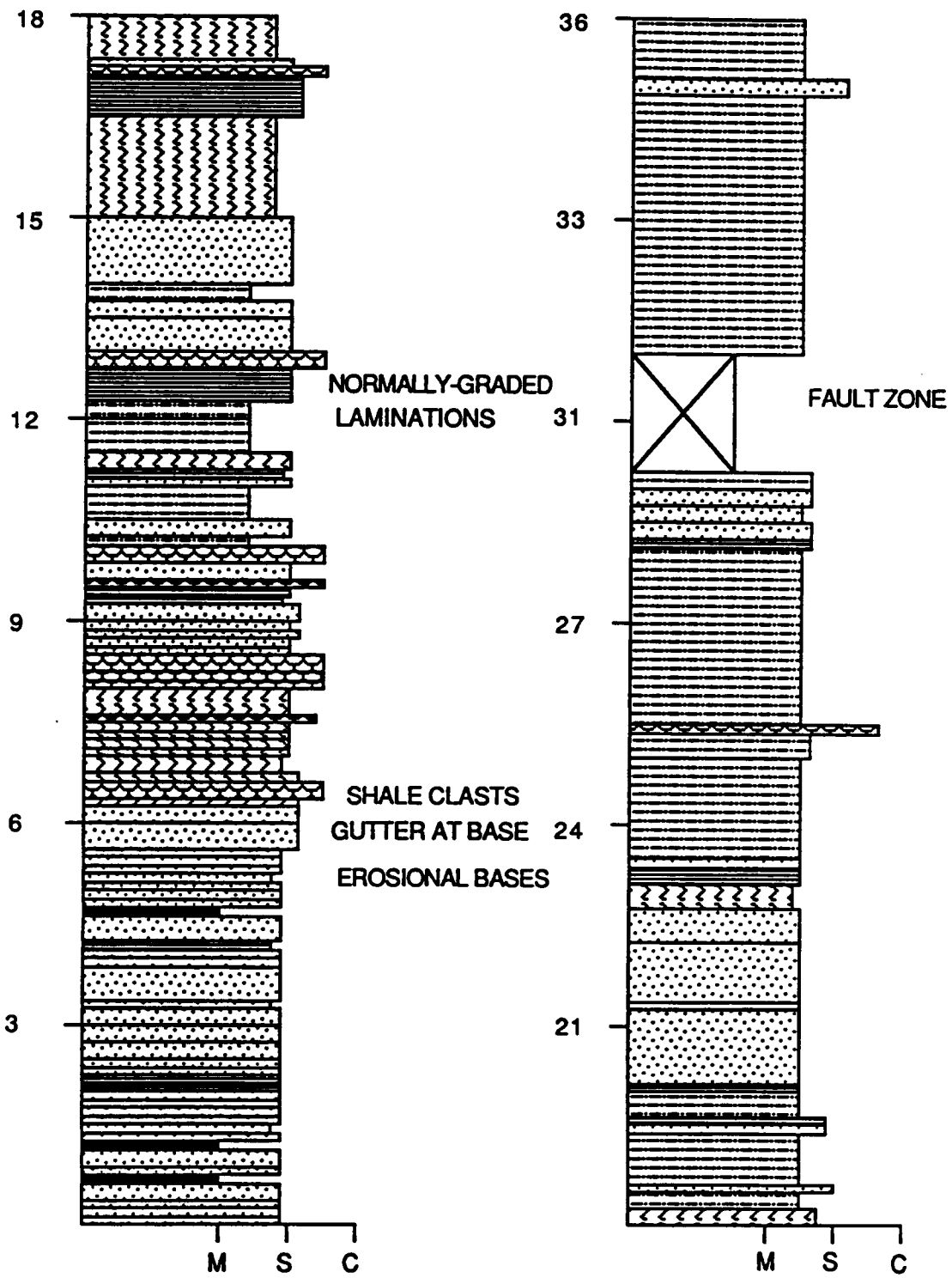

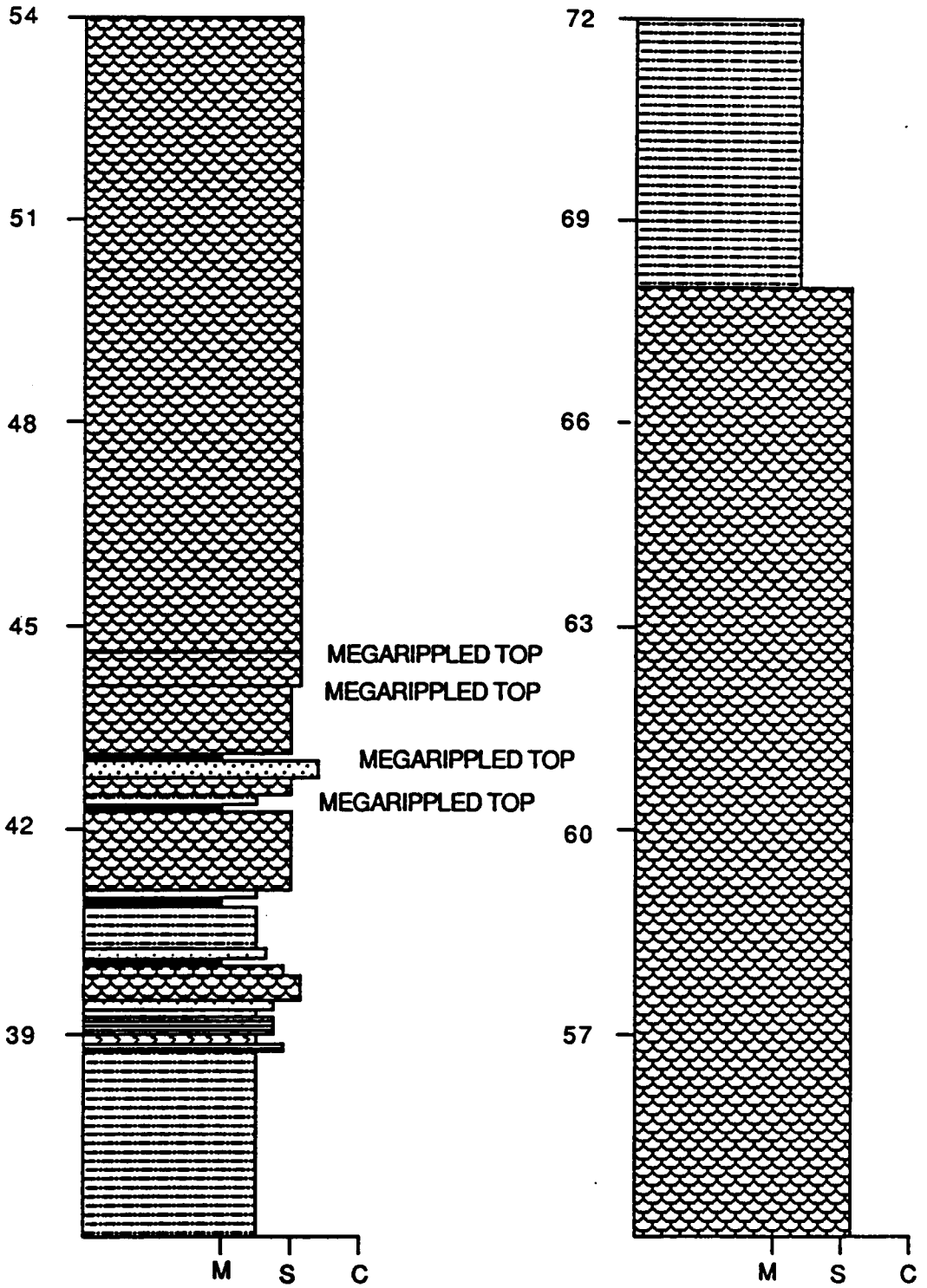
54
51
48
45
42
39
MEGARIPPLED TOP
MEGARIPPLED TOP
MEGARIPPLED TOP
MEGARIPPLED TOP
M
S
C
72
69
66
63
60
57
M
S
C

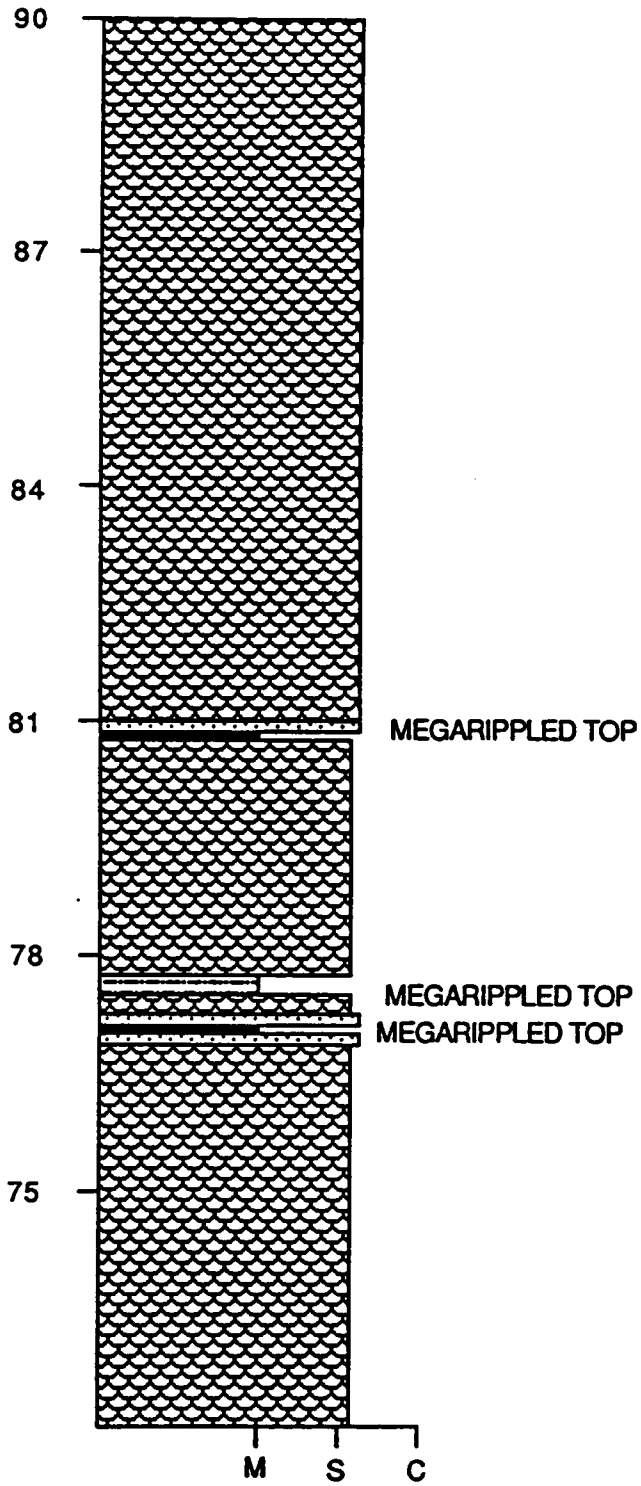
90
87
84
81
MEGARIPPLED TOP
78
MEGARIPPLED TOP
MEGARIPPLED TOP
75
M
S
C

BALCONY FALLS SECTION (LOCALITY 10)

SNOWDEN QUADRANGLE

ERWIN FORMATION OVERLAIN BY SHADY DOLOMITE.

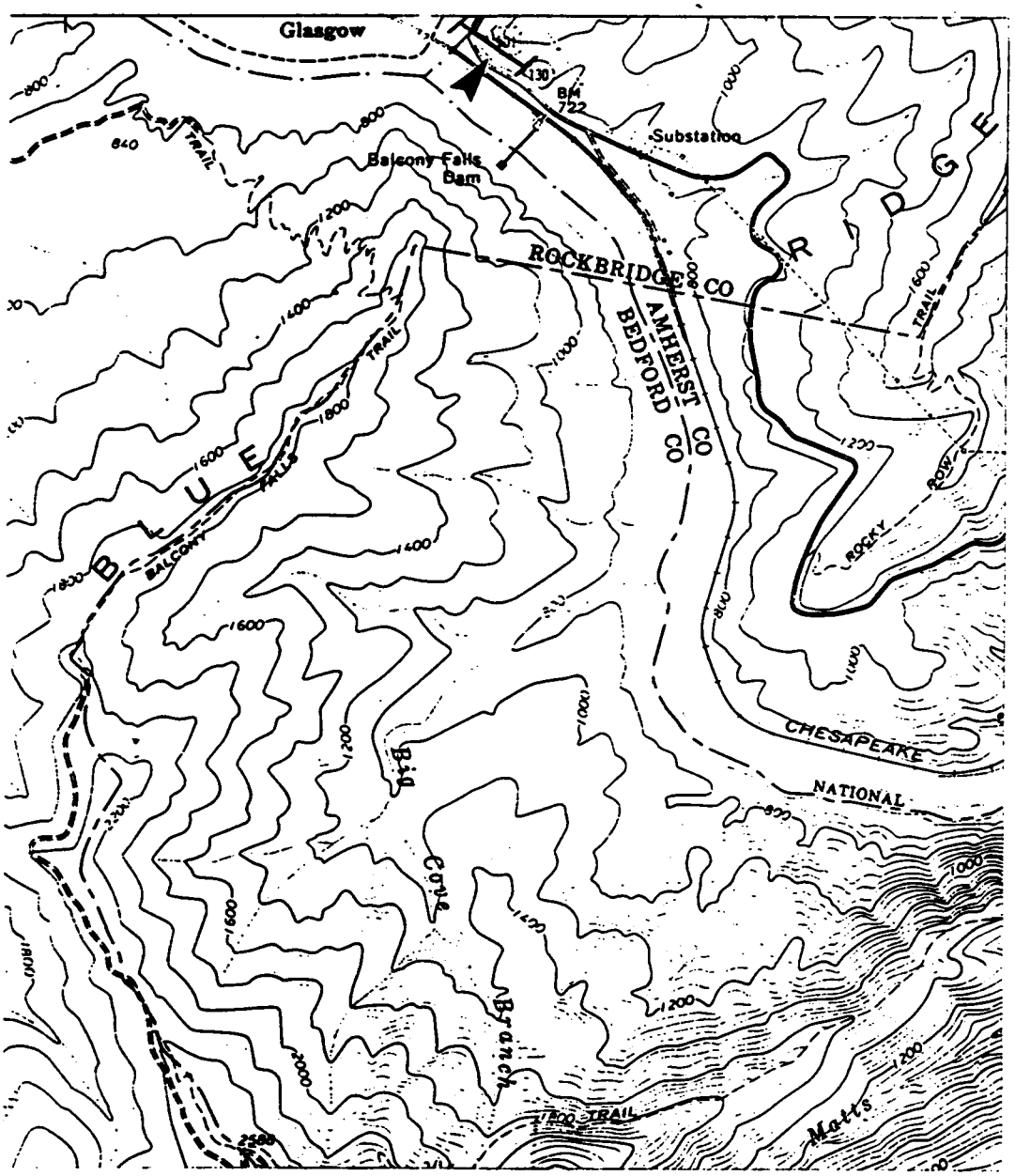

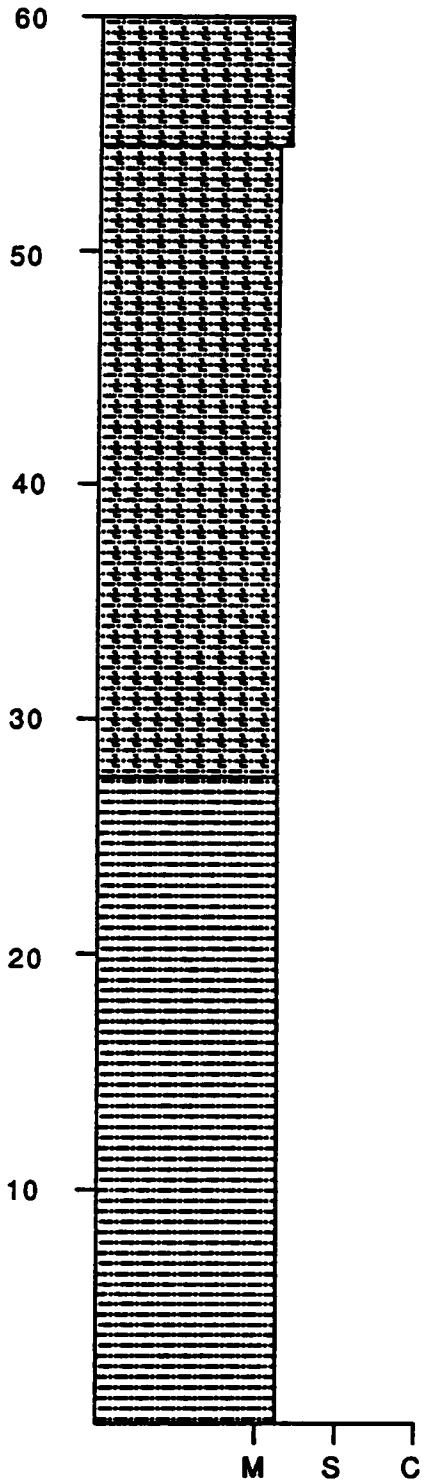
60
50
40
30
20
10
M
S
C

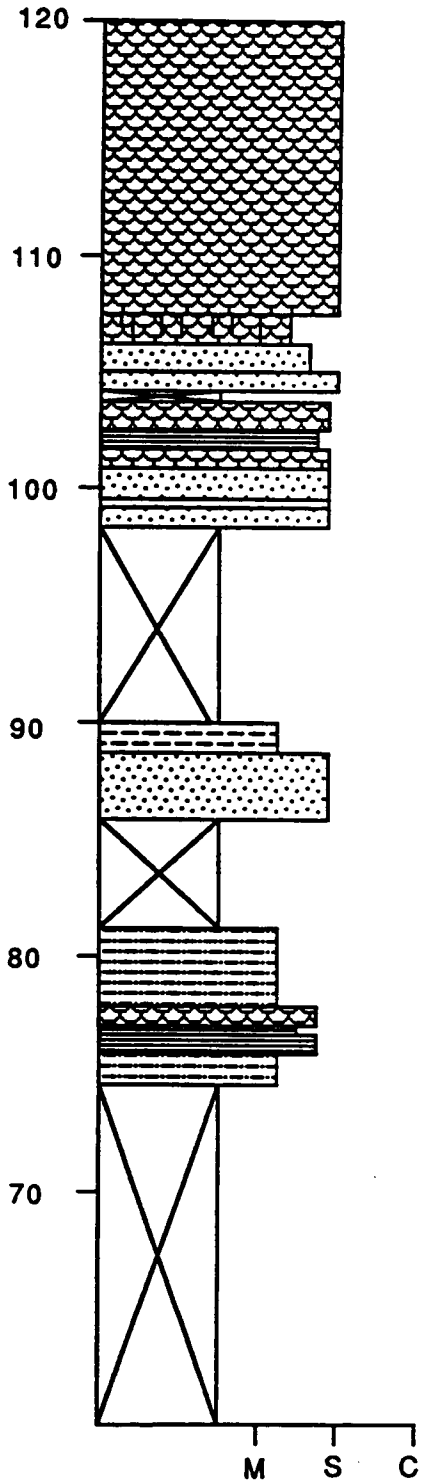
120
110
100
90
80
70
M
S
C

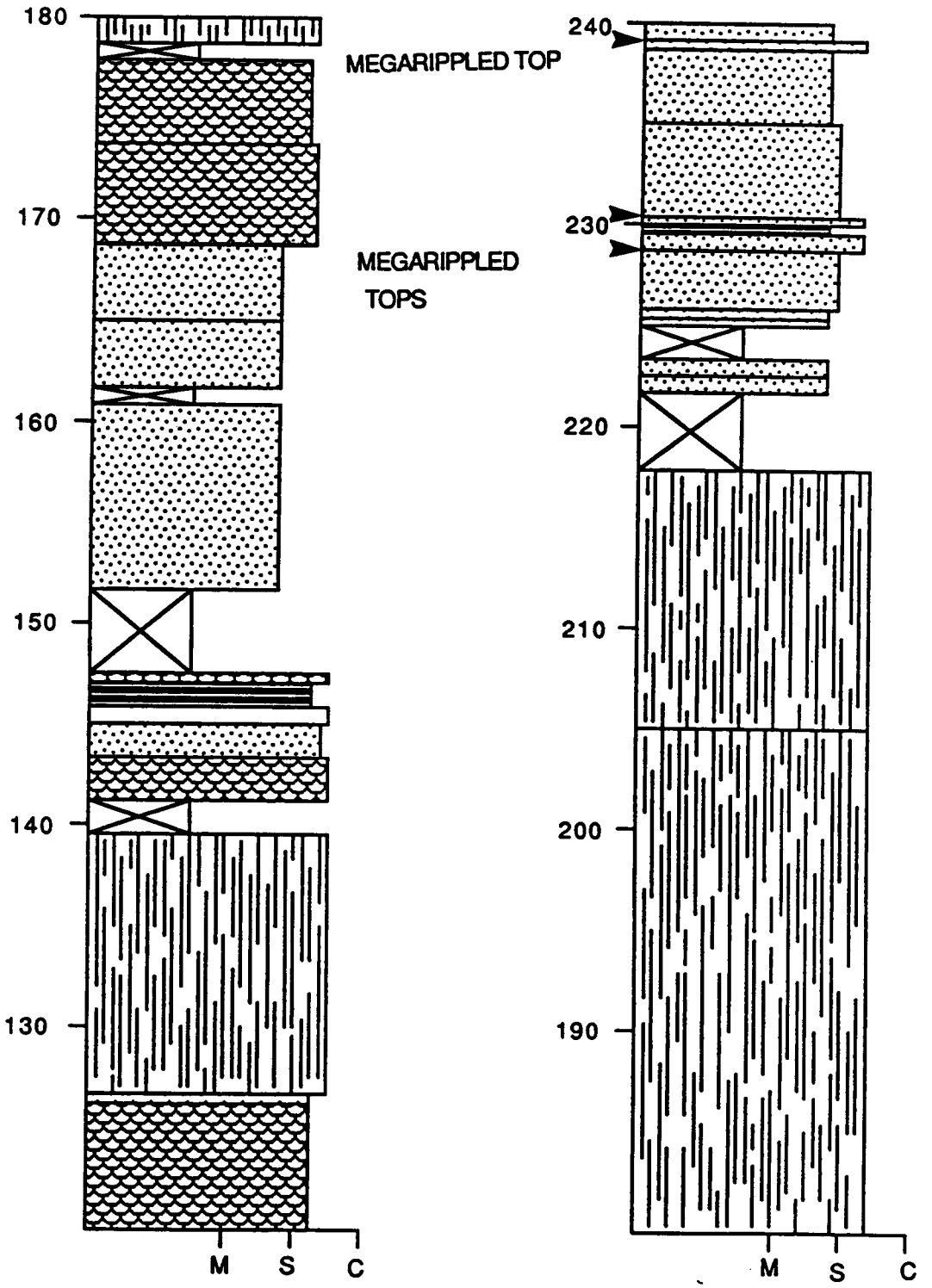
180
170
160
150
140
130
MEGARIPPLED TOP
MEGARIPPLED
TOPS
M
S
C
240
230
220
210
200
190
M
S
C

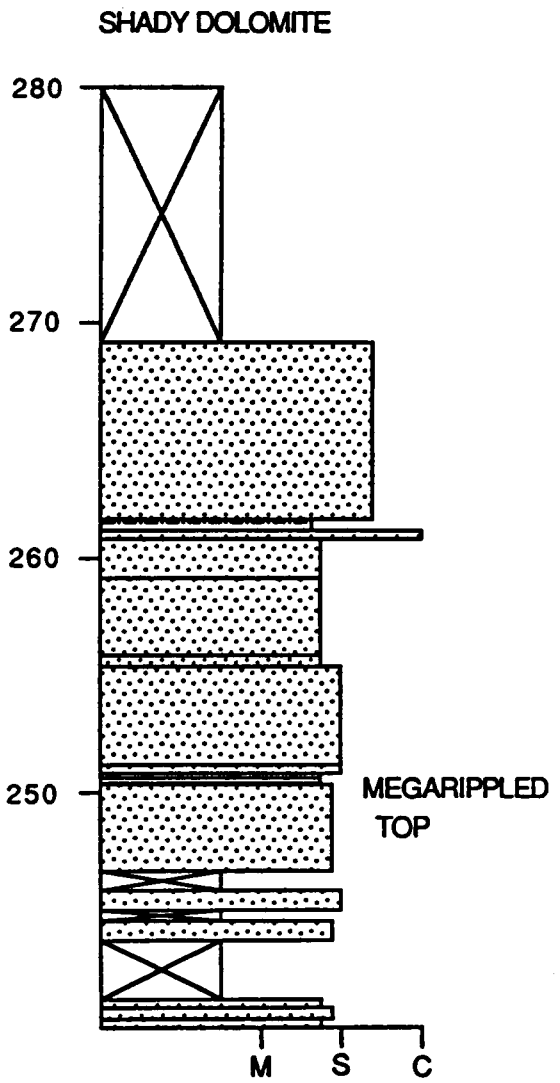
SHADY DOLOMITE
280
270
260
250
MEGARIPPLED
TOP
M
S
C

BUENA VISTA SECTION (LOCALITY 11)

BUENA VISTA QUADRANGLE

ERWIN FORMATION OVERLAIN BY SHADY DOLOMITE.

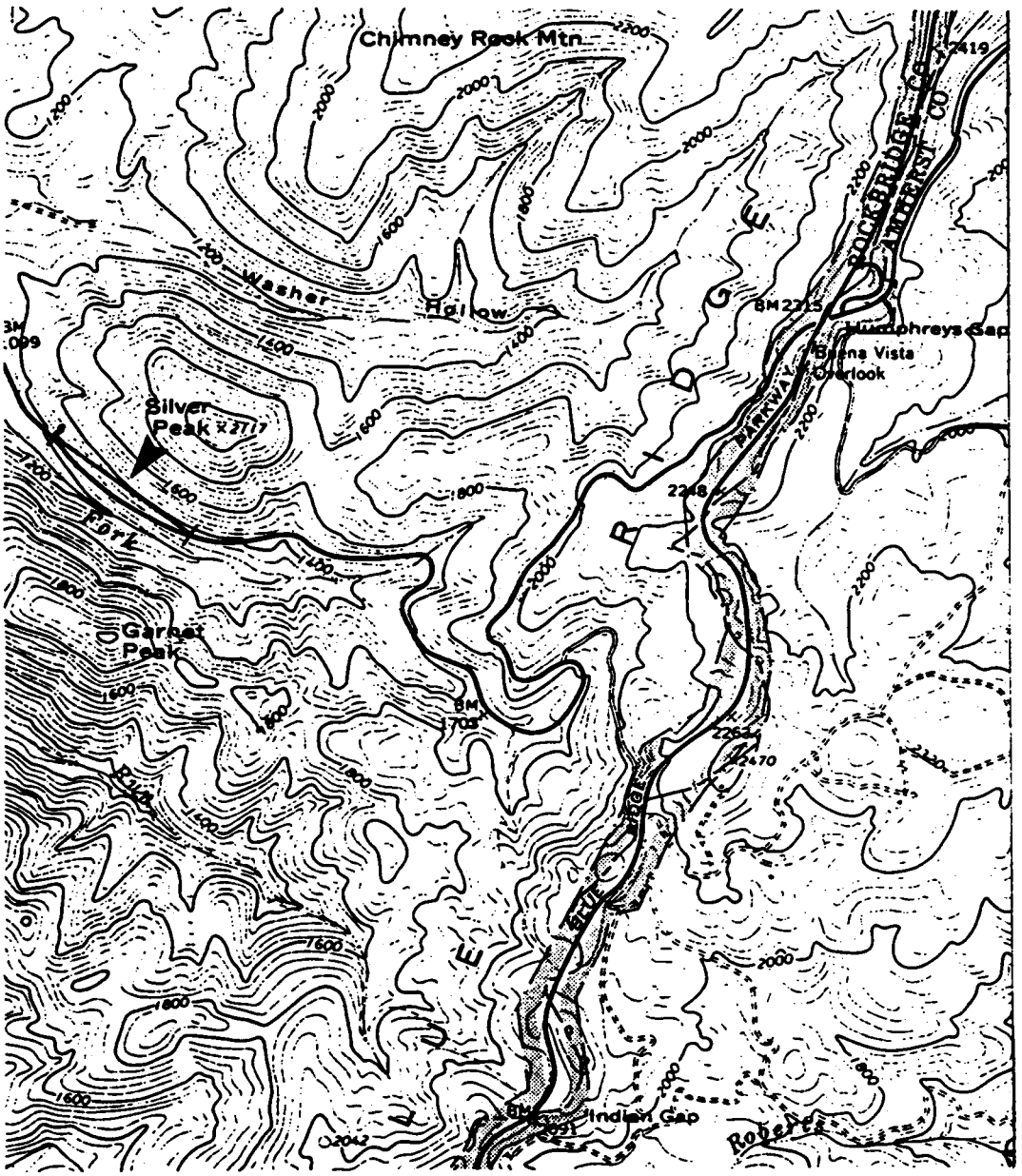

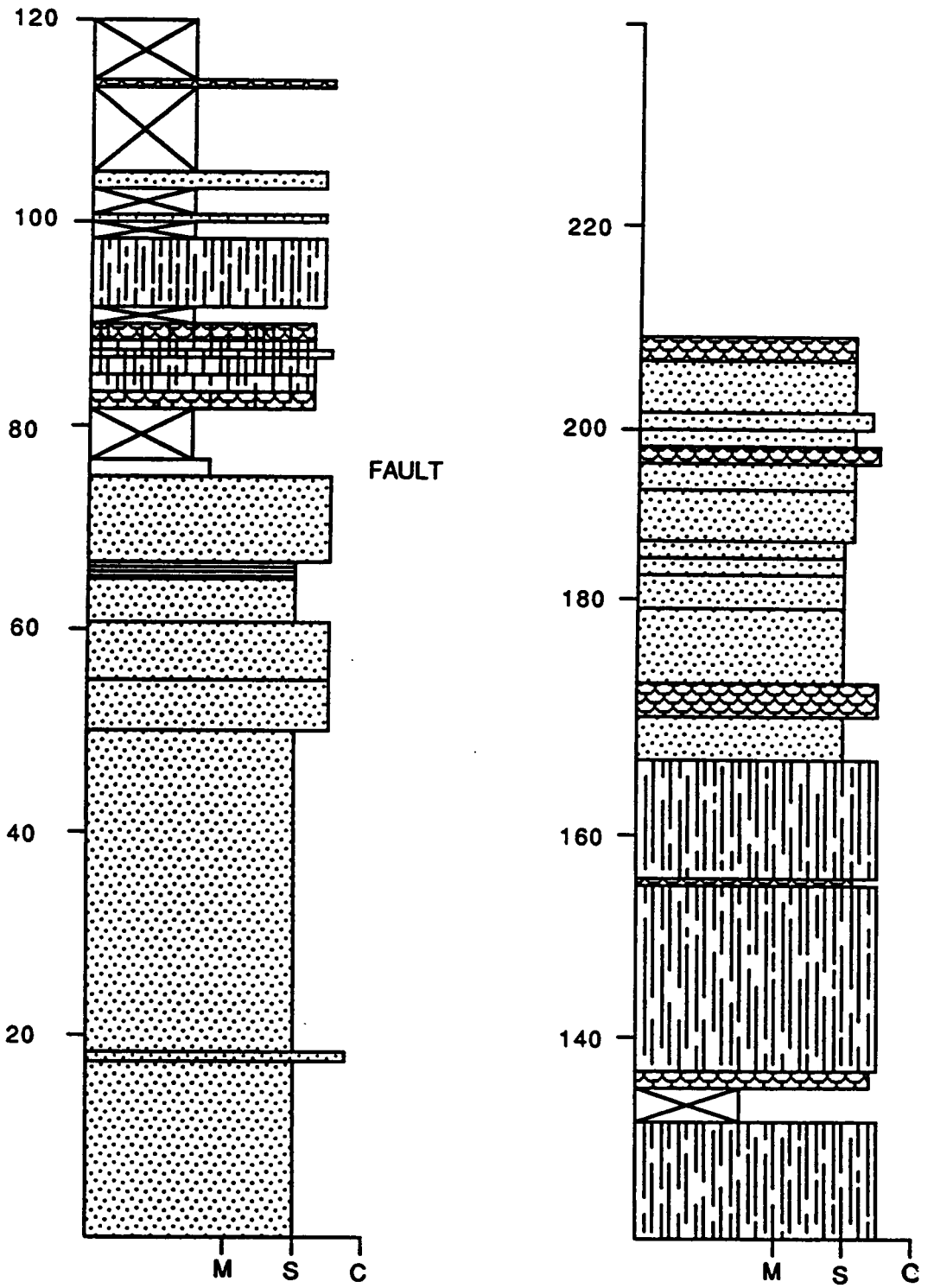
120
100
80
60
40
20
FAULT
M
S
C
220
200
180
160
140
M
S
C

VESUVIUS SECTION (LOCALITY 12)

VESUVIUS QUADRANGLE

ERWIN FORMATION OVERLAIN BY SHADY DOLOMITE.

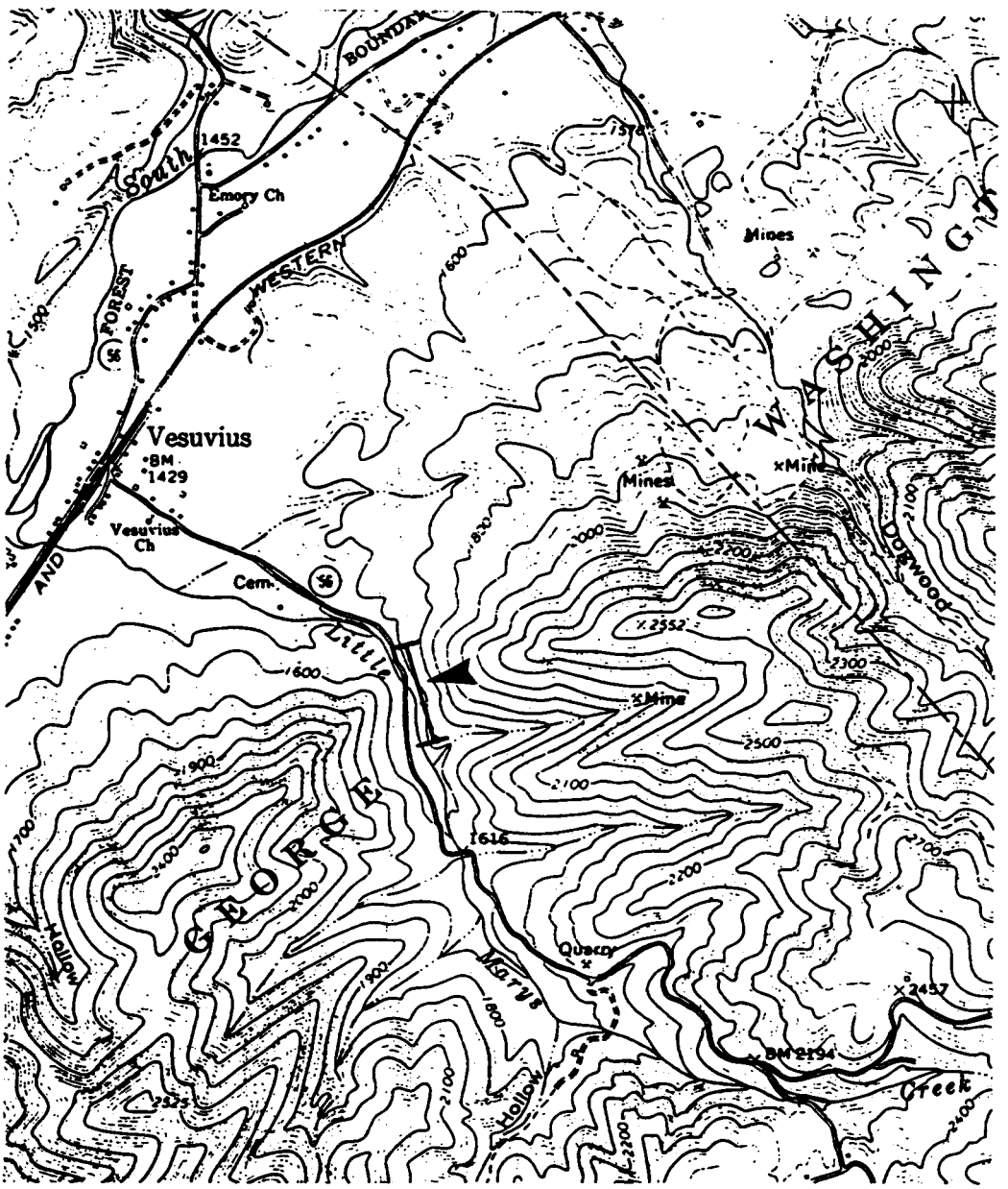

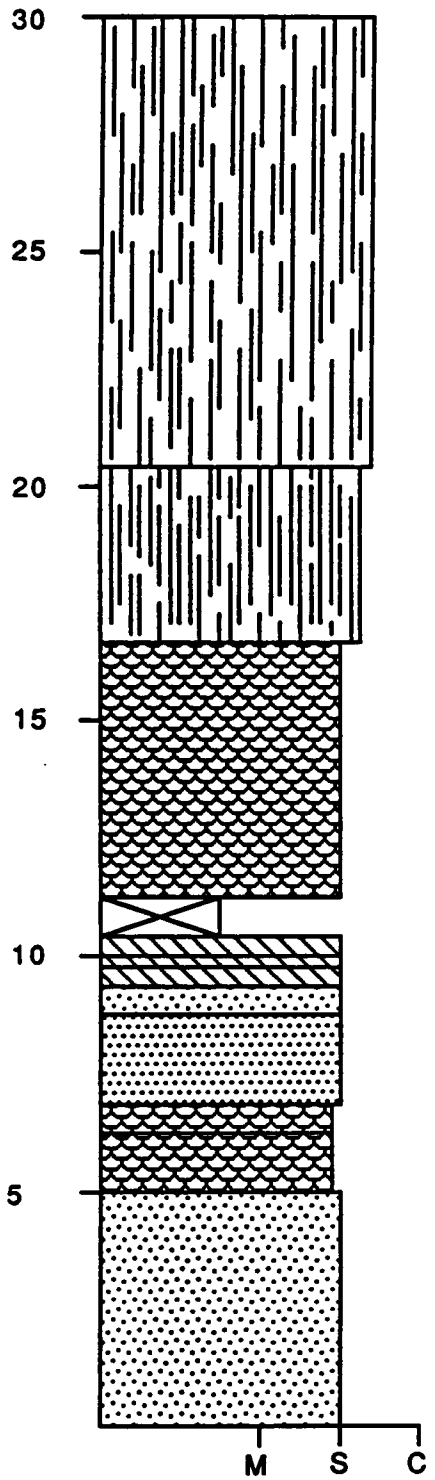
30
25
20
15
10
5
M
S
C

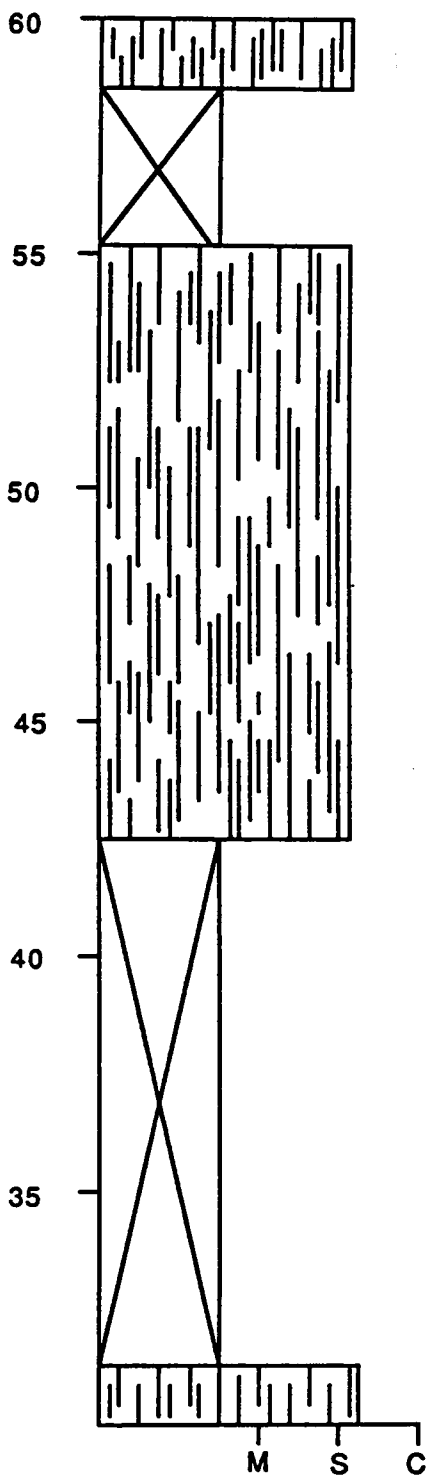
60
55
50
45
40
35
M
S
C

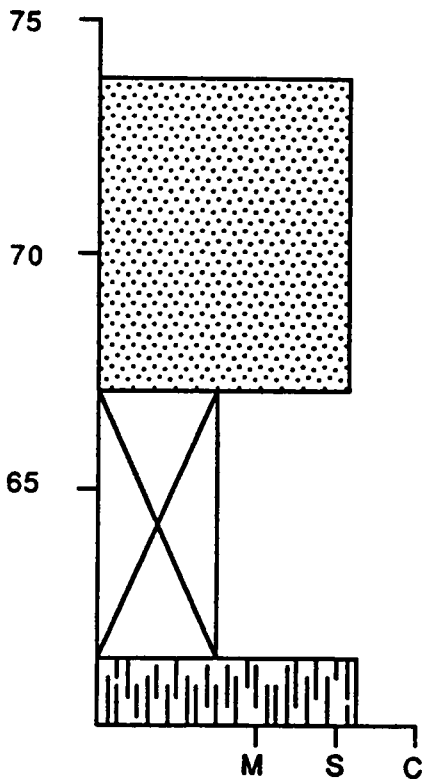
75
70
65
M
S
C

APPENDIX IV: PALEOCURRENT DATA.

VIRGINIA CREEPER TRAIL (LOCALITY 2)
LAURAL CREEK
UNICOI FORMATION

Station Number 89.78-91.63 M
MASTER BEDDING **Strike: 55** **Dip: 78 OT SE**
Paleocurrent Data: foresets

	Unrotated		Rotated		Current Direction	
	Strike	Dip	Strike	Dip	1.	2.
1.	041	81se	125	16sw	215	

Station Number **89.00-89.33 M**
MASTER BEDDING **Strike: 055** **Dip: 78 OT SE**
Paleocurrent Data: Imbricate clasts (AB planes)
Vector Mean: 251.0 **Standard Deviation: 8.49**

	Unrotated		Rotated		Current Direction	
	Strike	Dip	Strike	Dip	1.	2.
1.	005	83w	155	50sw	245	
2.	168	67e	167	52sw	257	

Station Number **89.78-91.63 M**
MASTER BEDDING **Strike: 055** **Dip: 78 OT SE**
Paleocurrent Data: Imbricate clasts (AB Planes)
Vector Mean: 195.97 **Standard Deviation: 65.09**

	Unrotated		Rotated		Current Direction	
	Strike	Dip	Strike	Dip	1.	2.
1.	180	78w	122	62sw	212	
2.	017	65w	104	58s	194	
3.	040	75w	085	31s	175	
4.	004	65e	172	55w	262	
5.	002	42e	190	57w	280	
6.	014	57w	096	60s	186	
7.	165	65e	165	68sw	255	
8.	166	60e	170	66sw	260	
9.	060	45w	051	58se	141	
10.	043	42w	065	61se	155	
11.	035	68e	178	20w	268	
12.	051	55e	050	24nw	320	
13.	105	42n	022	72se	112	
14.	085	30n	040	74se	130	
15.	038	61s	040	41nw	310	
16.	040	60n	074	45se	164	
17.	045	55n	066	49se	156	
18.	070	58n	035	56se	125	
19.	060	61n	050	42se	140	
20.	007	80w	121	55sw	211	

Station Number **98.06-98.51 M**
MASTER BEDDING **Strike: 055** **Dip: 78 OT SE**
Paleocurrent Data: Foresets in gravel

	Unrotated		Rotated		Current Direction	
	Strike	Dip	Strike	Dip	1.	2.
1.	033	62nw	085	45s	175	

Station Number **118.55-119.15 M**

MASTER BEDDING **Strike: 055** **Dip: 78 OT SE**
Paleocurrent Data: Foresets

	Unrotated		Rotated		Current Direction	
	Strike	Dip	Strike	Dip	1.	2.
1.	068	79n	024	26se	114	

Station Number **130.05-130.35 M**
MASTER BEDDING **Strike: 078** **Dip:88 S OT**
Paleocurrent Data: Foreset

	Unrotated		Rotated		Current Direction	
	Strike	Dip	Strike	Dip	1.	2.
1.	065	80n	028	14se	118	

Station Number **141.55-142.27 M**
MASTER BEDDING **Strike: 043** **Dip: 67 S OT**
Paleocurrent Data: Wedge Planar
Vector Mean: 268.3 **Standard Deviation: 11.41**

	Unrotated		Rotated		Current Direction	
	Strike	Dip	Strike	Dip	1.	2.
1.	062	81nw	168	22w	258	
2.	056	85nw	189	24w	279	
3.	056	78nw	177	15w	267	

Station Number **148.78-152.61 M**
MASTER BEDDING **Strike: 043** **Dip: 67 S OT**
Paleocurrent Data: Tabular planar foresets
Vector Mean: 295.0 **Standard Deviation: 45.11**

	Unrotated		Rotated		Current Direction	
	Strike	Dip	Strike	Dip	1.	2.
1.	066	82n	168	22w	258	
2.	049	76nw	015	12w	285	
3.	035	78nw	076	13w	346	

Station Number **297.5-298.1 M**
MASTER BEDDING **Strike: 061** **Dip: 88 SW OT**
Paleocurrent Data: Foresets in interflow units

	Unrotated		Rotated		Current Direction	
	Strike	Dip	Strike	Dip	1.	2.
1.	041	82nw	123	21sw	213	

Station Number **325.18-325.70 M**
MASTER BEDDING **Strike: 061** **Dip: 88 SW OT**
Paleocurrent Data: Tabular planar foresets

	Unrotated		Rotated		Current Direction	
	Strike	Dip	Strike	Dip	1.	2.
1.	075	74e	168	36w	258	

Station Number **327.17 328.09 M**
MASTER BEDDING **Strike: 045** **Dip: 76 SE OT**
Paleocurrent Data: Foresets in channel

	Unrotated		Rotated		Current Direction	
	Strike	Dip	Strike	Dip	1.	2.
1.	022	90	199	28s	109	

Station Number **327.97 328.09 M**
MASTER BEDDING **Strike: 045** **Dip: 78 SE OT**
Paleocurrent Data: Scour lineation on erosion surface

	Unrotated		Rotated	Current Direction	
	Pitch	CD	Azimuth	1.	2.
1.	4sw	—	228	228	048

Station Number **339.39-340.07 M**
MASTER BEDDING **Strike: 048** **Dip: 82 SE OT**
Paleocurrent Data: Trough axes
Vector Mean: 183.0 **Standard Deviation: 4.24**

	Unrotated		Rotated	Current Direction	
	Pitch	CD	Azimuth	1.	2.
1.	42ne	n-s	006	186	
2.	48ne	n-s	000	180	

Station Number **349.72-351.22 M**
MASTER BEDDING **Strike: 046** **Dip: 78 OT SE**
Paleocurrent Data: Current ripples

	Unrotated		Rotated	Current Direction	
	Pitch	CD	Azimuth	1.	2.
1.	26ne	w-e	020	110	

Station Number **411.30-414.59 M**
MASTER BEDDING **Strike: 055** **Dip: 75 SW OT**
Paleocurrent Data: Foresets
Vector Mean: 127.34 **Standard Deviation: 26.32**

	Unrotated		Rotated		Current Direction	
	Strike	Dip	Strike	Dip	1.	2.
1.	069	83n	022	24s	112	
2.	073	83nw	008	23s	098	
3.	055	82nw	060	23s	150	
4.	054	82nw	059	23s	149	

Station Number **414.79-421.59 M**
MASTER BEDDING **Strike: 066** **Dip: 71 SE OT**
Paleocurrent Data: Foresets
Vector Mean: 192.75 **Standard Deviation: 4.862**

	Unrotated		Rotated		Current Direction	
	Strike	Dip	Strike	Dip	1.	2.

1.	061	86nw	098	28s	188
2.	045	79se	100	36s	190
3.	044	86se	109	31s	199
4.	045	84se	104	32s	194

Station Number 430.59-431.14 M
MASTER BEDDING **Strike: 060** **Dip: 75 OT SE**
Paleocurrent Data: Foresets

	Unrotated		Rotated		Current Direction	
	Strike	Dip	Strike	Dip	1.	2.
1.	058	82nw	066	23se	156	

Station Number 433.62-434.07 M
MASTER BEDDING **Strike: 055** **Dip: 76 OT SE**
Paleocurrent Data: Through limbs (Limb technique)

	Unrotated		Rotated		Current Direction	
	Strike	Dip	Strike	Dip	1.	2.
1.	080	86s			163	
2.	055	76s				

Station Number 435.54-435.86 M
MASTER BEDDING **Strike: 065** **Dip: 69 SE OT**
Paleocurrent Data: Foreset in Tabular planar

	Unrotated		Rotated		Current Direction	
	Strike	Dip	Strike	Dip	1.	2.
1.	048	81nw	095	35s	185	

Station Number 445.28-446.40 M
MASTER BEDDING **Strike: 051** **Dip: 78 SE OT**
Paleocurrent Data: Foresets

	Unrotated		Rotated		Current Direction	
	Strike	Dip	Strike	Dip	1.	2.
1.	024	74se	132	27se	222	

Station Number 453.02-453.06 M
MASTER BEDDING **Strike: 060** **Dip: 72 SE OT**
Paleocurrent Data: Foresets

	Unrotated		Rotated		Current Direction	
	Strike	Dip	Strike	Dip	1.	2.
1.	074	86w	028	25se	118	

Station Number 455.75-458.15 M
MASTER BEDDING **Strike: 060** **Dip: 72 SE OT**
Paleocurrent Data: Foresets
Vector Mean: 156.87 **Standard Deviation: 38.24**

	Unrotated		Rotated		Current Direction	
	Strike	Dip	Strike	Dip	1.	2.

1.	067	75nw	048	33se	138
2.	055	85nw	094	27s	184
3.	038	88nw	106	29s	196
4.	041	88nw	102	28s	192
5.	038	86nw	104	31s	194
6.	080	88s	033	21se	123
7.	074	88nw	024	23se	114
8.	077	85nw	022	27se	112

Station Number 458.48-459.95 M
MASTER BEDDING **Strike: 060** Dip: 72 SE OT
Paleocurrent Data: Foresets in coset I
Vector Mean: 132.18 **Standard Deviation: 22.58**

	Unrotated		Rotated		Current Direction	
	Strike	Dip	Strike	Dip	1.	2.
1.	071	84nw	037	27se	127	
2.	069	89nw	037	21se	127	
3.	069	85nw	043	25se	133	
4.	081	66nw	031	39se	121	
5.	058	73nw	065	35se	155	
6.	062	82nw	057	28se	147	
7.	071	80nw	040	30se	130	
8.	055	84nw	074	22se	164	
9.	055	88nw	075	20se	165	
10.	057	87nw	068	21se	158	
11.	075	86nw	026	27se	116	
12.	079	88nw	018	28se	108	
13.	086	85n	014	35se	104	
14.	090	87n	006	37se	096	

Station Number 459.95-460.78 M
MASTER BEDDING **Strike: 060** Dip: 72 SE OT
Paleocurrent Data: Foresets in Coset II
Vector Mean: 135.76 **Standard Deviation: 36.16**

	Unrotated		Rotated		Current Direction	
	Strike	Dip	Strike	Dip	1.	2.
1.	045	82nw	091	30s	181	
2.	047	87nw	091	25s	181	
3.	054	90	075	20se	165	
4.	066	88nw	040	20se	130	
5.	078	90	012	25se	102	
6.	077	74n	032	37se	122	
7.	046	81nw	088	31s	178	
8.	074	89n	020	22e	096	
9.	082	89n	006	27e	098	
10.	084	86n	008	31e	098	

Station Number 461.78-462.48 M
MASTER BEDDING **Strike: 060** Dip: 72 SE OT
Paleocurrent Data: Foresets in Coset III
Vector Mean: 145.55 **Standard Deviation: 28.07**

	Unrotated		Rotated		Current Direction	
	Strike	Dip	Strike	Dip	1.	2.
1.	070	81w	041	29se	131	
2.	078	84nw	025	32s	115	
3.	045	78se	098	32s	188	
4.	050	74n	081	35s	171	
5.	080	72n	037	40se	127	
6.	063	88n	054	21se	144	

Station Number 462.48-464.18 M
MASTER BEDDING **Strike: 060** Dip: 72 SE OT

Paleocurrent Data: Foresets in Coset IV
Vector Mean: 131.80 **Standard Deviation: 7.82**

	Unrotated		Rotated		Current Direction	
	Strike	Dip	Strike	Dip	1.	2.
1.	067	90	040	20se	130	
2.	075	78n	032	36se	122	
3.	074	76n	038	36se	128	
4.	063	88nw	052	20se	142	
5.	068	77nw	047	32se	137	

SHORT MOUNTAIN SECTION (LOCALITY 3)
PALEOCURRENT ROTATION DATA
ERWIN / ANTIETAM FORMATION

Station Number 6.36 M
MASTER BEDDING **Strike: 064** **Dip: 58 S**
Paleocurrent Data: Wave-ripple crests

	Unrotated		Rotated	Current Direction	
	Pitch	CD	Azimuth	1.	2.
1.	11e	—	075	165	345

Station Number 10.90 M
MASTER BEDDING **Strike: 064** **Dip: 58 S**
Paleocurrent Data: Wave-ripple crests

	Unrotated		Rotated	Current Direction	
	Pitch	CD	Azimuth	1.	2.
1.	02w	—	063	153	333

Station Number 11.20 M
MASTER BEDDING **Strike: 064** **Dip: 58 SE**
Paleocurrent Data: Wave-ripple crests
Vector Mean: 160.

	Unrotated		Rotated	Current Direction	
	Pitch	CD	Azimuth	1.	2.
1.	16e	—	081	171	351
2.	05w	—	059	149	329

Station Number 59.98 M
MASTER BEDDING **Strike: 075** **Dip: 51 S**
Paleocurrent Data: Wave-ripple crests

	Unrotated		Rotated	Current Direction	
	Pitch	CD	Azimuth	1.	2.
1	28e	—	103	013	193

ELK CREEK (LOCALITY 4)
PALEOCURRENT ROTATION DATA
UNICOI FORMATION

Station Number 165.99-166.99 M
MASTER BEDDING **Strike: 70** **Dip:81 N OT**
Paleocurrent Data: Tabular foresets

	Unrotated		Rotated		Current Direction	
	Strike	Dip	Strike	Dip	1.	2.
1.	285	77ne	057	30sw	236	

Station Number 187.93-188.43 M
MASTER BEDDING **Strike: 82** **Dip: 80 N OT**
Paleocurrent Data: Tabular planar foresets
Vector Mean: 264.0

	Unrotated		Rotated		Current Direction	
	Strike	Dip	Strike	Dip	1.	2.
1.	260	58n	074	23se	166	
2.	257	56n	070	27se	162	

Station Number 197.52 199.92 M
MASTER BEDDING **Strike: 082** **dip: 80 N OT**
Paleocurrent Data: Large-scale grades foresets

	Unrotated		Rotated		Current Direction	
	Strike	Dip	Strike	Dip	1.	2.
1.	265	78n	120	03sw	210	

Station Number 292.43 M
MASTER BEDDING **Strike: 086** **Dip: 90**
Paleocurrent Data: Scour lineations
Vector Mean: 104.8 **Standard Deviation: 7.30**

	Unrotated		Rotated	Current Direction	
	Pitch	CD	Azimuth	1.	2.
1.	11e	—	098	098	278
2.	13e	—	100	100	280
3.	21e	—	108	108	288
4.	16e	—	103	103	283
5.	13e	—	100	100	280
6.	24e	—	111	111	291
7.	20e	—	107	107	287
8.	13e	—	100	100	280
9.	13e	—	105	105	285
10.	19e	—	106	106	286
11.	36e	—	123	123	303
12.	15e	—	102	102	282
13.	06e	—	093	093	273
14.	18e	—	105	105	285
15.	09e	—	096	096	276
16.	18e	—	105	105	285
17.	26e	—	113	113	293
18.	18e	—	105	105	285
19.	20e	—	107	107	287

20.	19e	—	106	106	286
21.	18e	—	105	105	285
22.	21e	—	108	108	288
23.	19e	—	106	106	286
24.	12e	—	099	099	279
25.	07e	—	094	094	274
26.	08e	—	095	095	275
27.	11e	—	098	098	278
28.	36e	—	123	123	303

Station Number 293.15-294.45 M
MASTER BEDDING **Strike: 086** **Dip: 90**
Paleocurrent Data: Coarse-grained tabular planar foresets
Vector Mean: 205.5

	Unrotated		Rotated		Current Direction	
	Strike	Dip	Strike	Dip	1.	2.
1.	094	60n	100	30s	190	
2.	098	78n	131	16s	221	

Station Number 308.60 319.10 M
MASTER BEDDING **Strike: 079** **Dip:084 N OT**
Paleocurrent Data: Tabular planar foresets
Vector Mean: 123.5

	Unrotated		Rotated		Current Direction	
	Strike	Dip	Strike	Dip	1.	2.
1.	060	63n	041	28se	131	
2.	055	69n	026	27se	116	

Station Number 350.1 M
MASTER BEDDING **Strike: 079** **Dip: 84 N OT**
Paleocurrent Data: Tabular planar foresets

	Unrotated		Rotated		Current Direction	
	Strike	Dip	Strike	Dip	1.	2.
1.	089	70n	117	18sw	207	

Station Number 361.91-362.13 M
MASTER BEDDING **Strike: 079** **Dip: 84 N OT**
Paleocurrent Data: Tabular-planar foresets
Vector Mean: 253.8 **Standard Deviation: 19.66**

	Unrotated		Rotated		Current Direction	
	Strike	Dip	Strike	Dip	1.	2.
1.	095	77n	321	17w	231	
2.	097	85n	356	10w	266	
3.	104	87n	354	26w	264	

Station Number 362.77-363.59 M
MASTER BEDDING **Strike: 079** **Dip: 84 N OT**
Paleocurrent Data: Tabular-planar foresets
Vector Mean: 215.2 **Standard Deviation: 59.77**

	Unrotated		Rotated		Current Direction	
	Strike	Dip	Strike	Dip	1.	2.
1.	074	68n	064	16se	154	

2.	077	67n	069	18se	159
3.	088	76n	130	12sw	220
4.	097	81n	159	17sw	249
5.	088	90n	204	11nw	294

Station Number 363.88 363.99 M
MASTER BEDDING **Strike: 079** **Dip: 84 N OT**
Paleocurrent Data: Tabular-planar foreset

	Unrotated		Rotated		Current Direction	
	Strike	Dip	Strike	Dip	1.	2.
1.	080	62n	080	22s	170	

Station Number 363.99 364.99 M
MASTER BEDDING **Strike: 074** **Dip: 84 N OT**
Paleocurrent Data: Tabular-planar foresets

	Unrotated		Rotated		Current Direction	
	Strike	Dip	Strike	Dip	1.	2.
1.	089	69n	112	18s	202	

Station Number 366.09-366.14 M
MASTER BEDDING **Strike: 079** **Dip: 84 N OT**
Paleocurrent Data: Tabular-planar foresets

	Unrotated		Rotated		Current Direction	
	Strike	Dip	Strike	Dip	1.	2.
1.	091	72n	123	16sw	213	

Station Number 366.14-366.17 M
MASTER BEDDING **Strike: 079** **Dip: 84 N OT**
Paleocurrent Data: Tabular-planar foresets

	Unrotated		Rotated		Current Direction	
	Strike	Dip	Strike	Dip	1.	2.
1.	088	79n	138	10sw	228	

Station Number 368.81-369.34 M
MASTER BEDDING **Strike: 079** **Dip: 84 N OT**
Paleocurrent Data: wedge-planar

	Unrotated		Rotated		Current Direction	
	Strike	Dip	Strike	Dip	1.	2.
1.	058	62n	040	28sw	130	

Station Number 452.66 M
MASTER BEDDING **Strike: 082** **Dip: 82 N**
Paleocurrent Data: Symmetrical wave ripples
Vector Mean: 138.0 **Standard Deviation: 9.65**

	Unrotated		Rotated	Current Direction	
	Pitch	CD	Azimuth	1.	2.
1.	41e	—	041	131	311

2.	46e	—	036	126	306
3.	34e	—	047	137	317
4.	28e	—	052	142	322
5.	33e	—	048	138	318
6.	18e	—	064	154	334

Station Number 453.08 M
MASTER BEDDING **Strike: 082** **Dip: 82 N**
Paleocurrent Data: Symmetrical wave-rippled top
Vector Mean: 131.0

	Unrotated		Rotated	Current Direction	
	Pitch	CD	Azimuth	1.	2.
1.	46e	—	036	126	306
2.	36e	—	046	136	316

Station Number 511.88 M
MASTER BEDDING **Strike: 105** **Dip: 68 N**
Paleocurrent Data: Imbricate clasts
Vector Mean: 320.6 **Standard Deviation: 25.71**

	Unrotated		Rotated		Current Direction	
	Strike	Dip	Strike	Dip	1.	2.
1.	103	69n	050	3nw	321	
2.	062	89n	036	45nw	306	
3.	051	88s	031	56nw	301	
4.	038	84s	027	68nw	297	
5.	102	86n	093	22n	003	
6.	104	74n	088	07n	358	
7.	054	72s	050	63nw	320	
8.	065	85n	045	42nw	304	

Station Number 527.39-528.32 M
MASTER BEDDING **Strike: 106** **Dip: 81 N**
Paleocurrent Data: Grooves
Vector Mean: 70.25 **Standard Deviation: 8.26**

	Unrotated		Rotated	Current Direction	
	Pitch	CD	Azimuth	1.	2.
1.	42e	—	062	062	242
2.	39e	—	065	065	245
3.	24e	—	080	080	260
4.	30e	—	074	074	254

Station Number 530.09 530.61 M
MASTER BEDDING **Strike: 106** **Dip: 81 N**
Paleocurrent Data: Grooves

	Unrotated		Rotated	Current Direction	
	Pitch	CD	Azimuth	1.	2.
1.	19e	—	085	085	265

ELK CREEK SECTION 2 (LOCALITY 4)
PALEOCURRENT ROTATION DATA
ERWIN FORMATION

Station Number 72.14-73.24 M
MASTER BEDDING **Strike: 084** **Dip: 43 N**
Paleocurrent Data: Scour lineations
Vector Mean: 40.4 **Standard Deviation: 24.01**

	Unrotated		Rotated	Current Direction	
	Pitch	CD	Azimuth	1.	2.
1.	60e	—	023	023	203
2.	52e	—	031	031	211
3.	16e	—	068	068	248

Station Number 73.24 M
MASTER BEDDING **Strike: 084** **Dip: 43 N**
Paleocurrent Data: Scour lineations
Vector Mean: 93.5

	Unrotated		Rotated	Current Direction	
	Pitch	CD	Azimuth	1.	2.
1.	11e	—	073	073	253
2.	19w	—	114	114	294

Station Number 82.01-82.61 M
MASTER BEDDING **Strike: 084** **Dip: 43 N**
Paleocurrent Data: Wedge-planar

	Unrotated		Rotated		Current Direction	
	Strike	Dip	Strike	Dip	1.	2.
1.	097	53n	136	15ne	046	

Station Number 84.71-86.24 M
MASTER BEDDING **Strike: 084** **Dip: 43 N**
Paleocurrent Data: Wedge-planar
Vector Mean: 55.5

	Unrotated		Rotated		Current Direction	
	Strike	Dip	Strike	Dip	1.	2.
1.	096	51n	144	16ne	054	
2.	093	48n	147	14ne	057	

Station Number 89.57-90.94 M
MASTER BEDDING **Strike: 084** **Dip: 43 N**
Paleocurrent Data: Wedge-planar

	Unrotated		Rotated		Current Direction	
	Strike	Dip	Strike	Dip	1.	2.
1.	087	48n	125	10ne	035	

Station Number 94.94-95.29 M
MASTER BEDDING **Strike: 084** **Dip: 43 N**

Paleocurrent Data: Wedge-planar

	Unrotated		Rotated			Current Direction	
	Strike	Dip	Strike	Dip		1.	2.
1.	081	65n	077	22n		347	

Station Number 109.42-109.51 M
MASTER BEDDING **Strike: 090** **Dip: 46 N**
Paleocurrent Data: Ripple crests
Vector Mean: 3.5

	Unrotated		Rotated			Current Direction	
	Pitch	CD	Azimuth			1.	2.
1.	02w	—	092			002	182
2.	05w	—	095			005	185

Station Number 148.28-148.34 M
MASTER BEDDING **Strike: 093** **Dip: 43 N**
Paleocurrent Data: Foresets

	Unrotated		Rotated			Current Direction	
	Strike	Dip	Strike	Dip		1.	2.
1.	097	33n	082	10se		172	

Station Number 148.42-149.42 M
MASTER BEDDING **Strike: 093** **Dip: 43 N**
Paleocurrent Data: Foresets

	Unrotated		Rotated			Current Direction	
	Strike	Dip	Strike	Dip		1.	2.
1.	103	41n	034	08se		124	

POPULAR CAMP QUARRY (LOCALITY 5)
PALEOCURRENT ROTATION DATA
ERWIN FORMATION

Station Number 20.27 20.30 M
MASTER BEDDING Strike:096 Dip: 77 S
Paleocurrent Data: Current ripple foresets
Vector Mean: 75.33 Standard Deviation: 47.82

	Unrotated		Rotated		Current Direction	
	Strike	Dip	Strike	Dip	1.	2.
1.	081	73s	018	22s	108	
2.	085	76s	009	25s	099	
3.	084	63s	166	26s	076	
4.	098	58s	093	22n	003	

Station Number 21-30-21.42 M
MASTER BEDDING Strike:102 Dip:70 S
Paleocurrent Data: Current ripple foresets
Vector Mean 26.14 Standard Deviation: 15.38

	Unrotated		Rotated		Current Direction	
	Strike	Dip	Strike	Dip	1.	2.
1.	103	56s	093	13n	003	
2.	081	54s	122	19ne	032	
3.	086	61s	125	11ne	035	
4.	089	64s	124	7ne	034	

Station Number 25.93-27.04 M
MASTER BEDDING Strike:105 Dip:76 S
Paleocurrent Data: ripple crests
Vector Mean: 46.30 Standard Deviation: 31.65

	Unrotated		Rotated	Current Direction	
	Pitch	CD	Azimuth	1.	2.
1.	69e	w-e	174	084	
2.	43e	w-e	148	058	
3.	02e	s-n	116	026	
4.	13w	s-n	093	003	
5.	44e	w-e	149	059	

Station Number 27.19-27.32 M
MASTER BEDDING Strike:104 Dip:77 S
Paleocurrent Data: Current ripple crests

	Unrotated		Rotated	Current Direction	
	Pitch	CD	Azimuth	1.	2.
1.	42e	w-e	152	062	

Station Number 27.19-27.32 M
MASTER BEDDING Strike:104 Dip:77 S
Paleocurrent Data: Current ripple foresets
Vector Mean: 50.30 Standard Deviation: 9.71

	Unrotated	Rotated	Current Direction

	Strike	Dip	Strike	Dip	1.	2.
1.	089	66s	151	18ne	061	
2.	086	57s	132	28ne	042	
3.	088	54s	138	25ne	048	

Station Number 38.78-38.88 M
MASTER BEDDING **Strike:105** **Dip:70 S**
Paleocurrent Data: Current ripple foresets
Vector Mean: 56.8 **Standard Deviation: 23.31**

	Unrotated		Rotated		Current Direction	
	Strike	Dip	Strike	Dip	1.	2.
1.	094	61s	145	13ne	055	
2.	107	57s	104	13n	014	
3.	092	60s	147	15ne	057	
4.	086	48s	136	27ne	046	
5.	087	55s	146	21ne	056	
6.	071	71s	008	32s	098	
7.	091	59s	149	17ne	059	
8.	088	60s	159	17ne	069	

Station Number 45.77-45.85 M
MASTER BEDDING **Strike:108** **Dip:81 S**
Paleocurrent Data: Curret ripple foreset
Vector Mean: 2.60 **Standard Deviation: 20.11**

	Unrotated		Rotated		Current Direction	
	Strike	Dip	Strike	Dip	1.	2.
1.	105	68s	115	14ne	025	
2.	114	65s	087	15n	357	
3.	122	61s	076	23n	346	

Station Number 50.25 50.31 M
MASTER BEDDING **Strike: 112** **Dip:70 S**
Paleocurrent Data: Current ripple foresets

	Unrotated		Rotated		Current Direction	
	Strike	Dip	Strike	Dip	1.	2.
1.	091	73s	024	20e	114	

Station Number 50.45-50.47 M
MASTER BEDDING **Strike:112** **Dip:70 S**
Paleocurrent Data: Current ripple foreset

	Unrotated		Rotated		Current Direction	
	Strike	Dip	Strike	Dip	1.	2.
1.	084	48s	151	32s	061	

Station Number 50.55 50.56 M
MASTER BEDDING **Strike:112** **Dip:70 S**
Paleocurrent Data: Current ripple foresets

	Unrotated		Rotated		Current Direction	
	Strike	Dip	Strike	Dip	1.	2.
1.	098	58s	149	16ne	059	

Station Number 51.06 51.12 M
MASTER BEDDING **Strike:112** **Dip:70 S**
Paleocurrent Data: Current ripple foreset
Vector Mean: 66.50

	Unrotated		Rotated		Current Direction	
	Strike	Dip	Strike	Dip	1.	2.
1.	102	63s	154	10ne	064	
2.	091	56s	159	22ne	069	

Station Number 51.39-51.41 M
MASTER BEDDING **Strike:112** **Dip:70 S**
Paleocurrent Data: Current ripple foreset
Vector Mean: 44.50

	Unrotated		Rotated		Current Direction	
	Strike	Dip	Strike	Dip	1.	2.
1.	100	45s	130	26s	040	
2.	091	42s	139	32ne	049	

Station Number 51.51-51.57 M
MASTER BEDDING **Strike: 112** **Dip:70 S**
Paleocurrent Data: Current ripple foresets

	Unrotated		Rotated		Current Direction	
	Strike	Dip	Strike	Dip	1.	2.
1.	111	51s	113	18n	023	

Station Number 51.64-51.70 M
MASTER BEDDING **Strike: 107** **Dip:78 S**
Paleocurrent Data: Current ripple foresets
Vector Mean: 42.20 **Standard Deviation: 33.14**

	Unrotated		Rotated		Current Direction	
	Strike	Dip	Strike	Dip	1.	2.
1.	108	67s	103	10n	013	
2.	098	68s	143	13ne	053	
3.	095	74s	175	14n	085	
4.	107	63s	110	14n	020	

Station Number 52.22-52.32 M
MASTER BEDDING **Strike:107** **Dip:78 S**
Paleocurrent Data: Current ripple foreset

	Unrotated		Rotated		Current Direction	
	Strike	Dip	Strike	Dip	1.	2.
1.	091	69s	163	18ne	073	

Station Number 52.34-52.44 M
MASTER BEDDING **Strike: 107** **Dip:78 S**
Paleocurrent Data: Current ripple foreset
Vector Mean: 29.00

	Unrotated	Rotated	Current Direction

	Strike	Dip	Strike	Dip	1.	2.
1.	112	53s	098	24n	008	
2.	098	66s	140	15ne	050	

Station Number 52.94-52.95 M
MASTER BEDDING **Strike:107** **Dip:78 S**
Paleocurrent Data: Current ripple foresets

	Unrotated		Rotated		Current Direction	
	Strike	Dip	Strike	Dip	1.	2.
1.	088	62s	150	25ne	060	

Station Number 52.98-52.99 M
MASTER BEDDING **Strike:107** **Dip:78 S**
Paleocurrent Data: Current ripple foreset

	Unrotated		Rotated		Current Direction	
	Strike	Dip	Strike	Dip	1.	2.
1.	097	67s	144	14ne	054	

Station Number 52.99-53.63 M
MASTER BEDDING **Strike:107** **Dip:78 S**
Paleocurrent Data: Current ripple foresets
Vector Mean: 52.00 **Standard Deviation: 7.00**

	Unrotated		Rotated		Current Direction	
	Strike	Dip	Strike	Dip	1.	2.
1.	085	58s	149	28ne	059	
2.	095	59s	135	22ne	045	
3.	096	62s	142	20ne	052	

Station Number 52.99-56.44 M
MASTER BEDDING **Strike:101** **Dip:72 S**
Paleocurrent Data: Current ripple foresets:
Vector Mean: 68.60 **Standard Deviation: 25.29**

	Unrotated		Rotated		Current Direction	
	Strike	Dip	Strike	Dip	1.	2.
1.	094	66s	136	09ne	046	
2.	085	79s	029	16se	119	
3.	076	62s	159	24ne	069	
4.	091	63s	140	12ne	050	
5.	081	79s	025	20se	115	
6.	082	68s	170	17e	080	
7.	081	56s	142	13ne	052	
8.	082	51s	130	28ne	040	
9.	093	65s	144	10ne	054	
10.	091	68s	159	10e	069	
11.	083	66s	164	18ne	074	
12.	065	56s	154	35ne	064	

Station Number 56.44-56.49 M
MASTER BEDDING **Strike: 101** **Dip:72 S**
Paleocurrent Data: Current Ripple Foresets
Vector Mean: 23.50 **Standard Deviation: 19.66**

	Unrotated	Rotated	Current

					Direction	
	Strike	Dip	Strike	Dip	1.	2.
1.	091	63s	140	13ne	050	
2.	093	675s	137	10ne	047	
3.	088	48s	121	26n	031	
4.	103	62s	095	10n	005	
5.	101	60s	107	12n	017	
6.	100	50s	105	21n	015	
7.	106	56s	090	15n	000	

Station Number 56.49-64.89 M
MASTER BEDDING **Strike:107** **Dip:70 S**
Paleocurrent Data: Current ripple foresets
Vector Mean: 49.90 **Standard Deviation: 41.27**

	Unrotated		Rotated		Current Direction	
	Strike	Dip	Strike	Dip	1.	2.
1.	095	73s	024	12se	114	
2.	077	56s	162	30ne	072	
3.	087	63s	171	19n	081	
4.	092	53s	142	21ne	052	
5.	100	65s	154	19ne	064	
6.	090	60s	160	19ne	070	
7.	112	52s	096	18n	006	
8.	102	61s	133	11ne	043	
9.	090	63s	137	10ne	047	
10.	114	60s	041	16nw	311	
11.	090	63s	137	10ne	047	
12.	088	72s	008	11e	098	
13.	092	66s	141	7ne	051	
14	099	58s	088	11n	358	
15	106	66s	110	04ne	020	

Station Number 64.99-65.02 M
MASTER BEDDING **Strike: 105** **Dip: 70 S**
Paleocurrent Data: Current ripple foresets
Vector Mean: 95.00

	Unrotated		Rotated		Current Direction	
	Strike	Dip	Strike	Dip	1.	2.
1.	075	68s	006	28e	096	
2.	085	68s	004	118e	094	

Station Number 65.05-65.08 M
MASTER BEDDING **Strike: 105** **Dip: 70 S**
Paleocurrent Data: Current ripple foresets
Vector Mean: 64.00 **Standard Deviation: 13.00**

	Unrotated		Rotated		Current Direction	
	Strike	Dip	Strike	Dip	1.	2.
1.	099	67s	112	11e	072	
2.	097	60s	139	12ne	049	
3.	090	62s	161	16ne	071	

Station Number 65.14-65.16 M
MASTER BEDDING **Strike:105** **Dip:70 S**
Paleocurrent Data: Current ripple foresets
Vector Mean: 42.90 **Standard Deviation: 20.22**

	Unrotated		Rotated		Current Direction	
	Strike	Dip	Strike	Dip	1.	2.

1.	100	58s	125	12ne	035
2.	093	62s	156	13ne	066
3.	103	58s	118	11ne	028

Station Number 65.22 65.24 M
MASTER BEDDING **Strike: 105** **Dip: 70 S**
Paleocurrent Data: Current ripple foresets

	Unrotated		Rotated		Current Direction	
	Strike	Dip	Strike	Dip	1.	2.
1.	095	60s	150	10ne	060	

Station Number 65.30-65.33 M
MASTER BEDDING **Strike: 105** **Dip: 70 S**
Paleocurrent Data: Current ripple foresets
Vector Mean: 56.20 **Standard Deviation: 28.03**

	Unrotated		Rotated		Current Direction	
	Strike	Dip	Strike	Dip	1.	2.
1.	082	66s	178	21e	088	
2.	103	62s	118	08n	028	
3.	097	55s	128	16ne	038	
4.	097	66s	161	08e	071	

Station Number 65.34-65.38 M
MASTER BEDDING **Strike:105** **Dip:70 S**
Paleocurrent Data: Current ripple foresets
Vector Mean: 62.5

	Unrotated		Rotated		Current Direction	
	Strike	Dip	Strike	Dip	1.	2.
1.	096	63s	146	13ne	056	
2.	091	62s	159	15e	069	

Station Number 65.98-66.03 M
MASTER BEDDING **Strike: 106** **Dip:73 S**
Paleocurrent Data: Current ripple foresets
Vector Mean: 62.50

	Unrotated		Rotated		Current Direction	
	Strike	Dip	Strike	Dip	1.	2.
1.	118	54s	079	20nw	349	
2.	100	61s	126	12ne	136	

Station Number 66.11-66.14 M
MASTER BEDDING **Strike: 106** **Dip:73 S**
Paleocurrent Data: Current ripple foresets
Vector Mean: 39.50

	Unrotated		Rotated		Current Direction	
	Strike	Dip	Strike	Dip	1.	2.
1.	092	51s	130	24ne	040	
2.	098	58s	129	15ne	039	

Station Number 66.39-66.40 M

MASTER BEDDING **Strike: 106** **Dip: 73 S**
Paleocurrent Data: Current ripple foresets

	Unrotated		Rotated		Current Direction	
	Strike	Dip	Strike	Dip	1.	2.
1.	087	67s	168	16e	078	

Station Number 66.57-66.67 M
MASTER BEDDING **Strike: 106** **Dip:73 S**
Paleocurrent Data: Current ripple foresets
Vector Mean: 66.90 **Standard Deviation: 12.83**

	Unrotated		Rotated		Current Direction	
	Strike	Dip	Strike	Dip	1.	2.
1.	072	66s	176	31e	086	
2.	084	55s	151	25ne	061	
3.	092	65s	148	16ne	058	
4.	091	62s	153	17ne	063	

Station Number 67.76-67.78 M
MASTER BEDDING **Strike: 106** **Dip: 73 S**
Paleocurrent Data: Current ripple foresets
Vector Mean: 38.5

	Unrotated		Rotated		Current Direction	
	Strike	Dip	Strike	Dip	1.	2.
1.	091	64s	129	09ne	039	
2.	084	57s	128	19ne	038	

Station Number 67.87-67.92 M
MASTER BEDDING **Strike: 106** **Dip: 73 S**
Paleocurrent Data: Current ripple foresets
Vector Mean: 67.5

	Unrotated		Rotated		Current Direction	
	Strike	Dip	Strike	Dip	1.	2.
1.	084	50s	117	14ne	027	
2.	083	76s	018	14se	108	

Station Number 69.48-70.93 M
MASTER BEDDING **Strike: 106** **Dip: 73 S**
Paleocurrent Data: Current ripple foresets
Vector Mean: 60.5

	Unrotated		Rotated		Current Direction	
	Strike	Dip	Strike	Dip	1.	2.
1.	072	71s	176	23e	086	
2.	094	68s	125	05ne	035	

Station Number 68.20-68.26 M
MASTER BEDDING **Strike: 106** **Dip: 73 S**
Paleocurrent Data: Pitch of ripple crests

Unrotated	Rotated	Current Direction

	Pitch	CD	Azimuth	1.	2.
1.	45e	n-s	151	061	

Station Number 68.40-68.47 M
MASTER BEDDING **Strike: 106** **Dip: 73 S**
Paleocurrent Data: Pitch of ripple crests

	Unrotated		Rotated	Current Direction	
	Pitch	CD	Azimuth	1.	2.
1.	49e	n-s	155	065	

Station Number 70.93-70.99 M
MASTER BEDDING **Strike: 103** **Dip: 74 S**
Paleocurrent Data: Pitch of ripple crests
Vector Mean: 55.90 **Standard Deviation: 13.20**

	Unrotated		Rotated	Current Direction	
	Pitch	CD	Azimuth	1.	2.
1.	42e	w-e	145	055	
2.	22e	w-e	125	035	
3.	34e	w-e	137	047	
4.	42e	w-e	145	055	
5.	54e	w-e	157	067	
6.	43e	w-e	146	056	
7.	63e	w-e	166	076	

Station Number 71.25-71.28 M
MASTER BEDDING **Strike: 103** **Dip: 74 S**
Paleocurrent Data: Current ripple foresets
Vector Mean: 33.50

	Unrotated		Rotated		Current Direction	
	Strike	Dip	Strike	Dip	1.	2.
1.	092	51s	121	24n	031	
2.	093	54s	126	20n	036	

Station Number 71.46-71.49 M
MASTER BEDDING **Strike: 103** **Dip: 74 S**
Paleocurrent Data: Current ripple foresets
Vector Mean: 27.5

	Unrotated		Rotated		Current Direction	
	Strike	Dip	Strike	Dip	1.	2.
1.	099	49s	114	26n	021	
2.	093	51s	124	24n	034	

Station Number 71.59-71.63 M
MASTER BEDDING **Strike: 103** **Dip: 74 S**
Paleocurrent Data: Current ripple foresets

	Unrotated		Rotated		Current Direction	
	Strike	Dip	Strike	Dip	1.	2.
1.	093	66s	152	12ne	062	

Station Number 71.65-71.76 M
MASTER BEDDING **Strike: 103** **Dip: 74 S**

Paleocurrent Data: Current ripple foresets
Vector Mean: 50.50

	Unrotated		Rotated		Current Direction	
	Strike	Dip	Strike	Dip	1.	2.
1.	103	52s	105	20n	015	
2.	088	72s	176	16n	086	

Station Number 71.76-72.57 M
MASTER BEDDING **Strike: 103** **Dip: 74 S**
Paleocurrent Data: Current ripple foresets
Vector Mean: 33.10 **Standard Deviation: 44.66**

	Unrotated		Rotated		Current Direction	
	Strike	Dip	Strike	Dip	1.	2.
1.	108	55s	067	20nw	337	
2.	092	72s	138	04ne	048	
3.	089	60s	112	14ne	022	
4.	072	71s	173	20e	083	

Station Number 72.57-72.64 M
MASTER BEDDING **Strike: 103** **Dip: 73 S**
Paleocurrent Data: Current ripple foresets
Vector Mean: 34.00

	Unrotated		Rotated		Current Direction	
	Strike	Dip	Strike	Dip	1.	2.
1.	094	74s	141	02e	051	
2.	093	69s	107	05ne	017	

Station Number 72.64-75.64 M
MASTER BEDDING **Strike: 103** **Dip: 74 S**
Paleocurrent Data: Current ripple foresets
Vector Mean: 15.00 **Standard Deviation: 20.22**

	Unrotated		Rotated		Current Direction	
	Strike	Dip	Strike	Dip	1.	2.
1.	096	55s	090	18n	000	
2.	080	55s	128	22ne	038	
3.	093	55s	097	17ne	007	

Station Number 77.26-77.34 M
MASTER BEDDING **Strike: 103** **Dip: 79 S**
Paleocurrent Data: Coarse-sand ripple foresets
Vector Mean: 111.0

	Unrotated		Rotated		Current Direction	
	Strike	Dip	Strike	Dip	1.	2.
1.	076	82s	016	27se	106	
2.	083	85s	026	21se	116	

Station Number 78.23-78.35 M
MASTER BEDDING **Strike: 103** **Dip: 79 S**
Paleocurrent Data: Coarse-sand ripple foresets
Vector Mean: 45.5

	Unrotated		Rotated		Current Direction	
	Strike	Dip	Strike	Dip	1.	2.
1.	094	63s	131	17ne	041	
2.	092	67s	140	15ne	050	

Station Number 78.74 78.86 M
MASTER BEDDING Strike: 103 Dip: 79 S
Paleocurrent Data: Coarse-sand ripple foresets
Vector Mean: 98.00 Standard Deviation: 17.22

	Unrotated		Rotated		Current Direction	
	Strike	Dip	Strike	Dip	1.	2.
1.	078	81s	015	24se	105	
2.	076	84s	020	27se	110	
3.	079	69s	168	24e	078	

Station Number 78.97-79.03 M
MASTER BEDDING Strike: 103 Dip:79 S
Paleocurrent Data: Coarse-sand ripple foresets

	Unrotated		Rotated		Current Direction	
	Strike	Dip	Strike	Dip	1.	2.
1.	092	65s	138	17ne	048	

Station Number 79.05-79.37 M
MASTER BEDDING Strike: 103 Dip: 79 S
Paleocurrent Data: Coarse-sand ripple foresets
Vector Mean: 66.00

	Unrotated		Rotated		Current Direction	
	Strike	Dip	Strike	Dip	1.	2.
1.	088	65s	149	19ne	059	
2.	071	65s	163	32e	073	

Station Number 79.42-79.70 M
MASTER BEDDING Strike: 103 Dip: 79 S
Paleocurrent Data: Coarse-sand ripple foreset

	Unrotated		Rotated		Current Direction	
	Strike	Dip	Strike	Dip	1.	2.
1.	081	74s	178	22e	088	

Station Number 79.71-80.73 M
MASTER BEDDING Strike: 103 Dip: 79 S
Paleocurrent Data: Coarse-sand ripple foresets
Vector Mean: 68.50

	Unrotated		Rotated		Current Direction	
	Strike	Dip	Strike	Dip	1.	2.
1.	074	78s	006	28e	096	
2.	094	63e	131	17ne	041	

Station Number 86.96-87.00 M

MASTER BEDDING **Strike: 103** **Dip: 79 S**
Palaeocurrent Data: Coarse-sand ripple foresets

	Unrotated		Rotated		Current Direction	
	Strike	Dip	Strike	Dip	1.	2.
1.	069	64s	163	34e	073	

Station Number **Additional data from quarry-floor**
MASTER BEDDING **Strike: 110** **Dip: 81 S**
Palaeocurrent Data: Coarse-sand ripple foresets
Vector Mean: 97.40 **Standard Deviation: 59.69**

	Unrotated		Rotated		Current Direction	
	Strike	Dip	Strike	Dip	1.	2.
1.	094	72s	167	18e	077	
2.	128	83s	013	28nw	283	
3.	084	85s	025	26se	115	
4.	085	80s	015	24se	105	
5.	082	76s	005	28e	095	
6.	073	86s	026	36se	116	
7.	077	75s	005	32e	095	
8.	081	76s	005	29e	095	
9.	083	81s	017	28se	107	
10.	098	74s	167	12e	077	

POPLAR CAMP SECTION 2 (LOCALITY 6)
PALEOCURRENT ROTATION DATA
ERWIN / ANTIETAM FORMATION

Station Number 0.64-0.72 M
MASTER BEDDING **Strike: 065** **Dip: 20 SE**
Paleocurrent Data: Ripple crests

	Unrotated		Rotated	Current Direction	
	Pitch	CD	Azimuth	1.	2.
1.	35w	nw-se	210	120	

Station Number 1.72-1.76 M
MASTER BEDDING **Strike: 065** **Dip: 21 SE**
Paleocurrent Data: Ripple crest
Vector Mean: 175.0

	Unrotated		Rotated	Current Direction	
	Pitch	CD	Azimuth	1.	2.
1.	06e	nw-se	071	161	
2.	32e	nw-se	099	189	

Station Number 2.35 2.44 M
MASTER BEDDING **Strike: 088** **Dip: 22 SE**
Paleocurrent Data: Wave-rippled top

	Unrotated		Rotated	Current Direction	
	Pitch	CD	Azimuth	1.	2.
1.	69e	—	158	068	248

Station Number 12.41 M
MASTER BEDDING **Strike: 081** **Dip: 16 S**
Paleocurrent Data: Wedge-planar
Vector Mean: 60.7 **Standard Deviation: 33.30**

	Unrotated		Rotated		Current Direction	
	Strike	Dip	Strike	Dip	1.	2.
1.	011	09e	354	14e	084	
2.	035	21se	344	15se	074	
3.	039	22se	292	16e	022	

Station Number 12.98 M
MASTER BEDDING **Strike: 081** **Dip: 17 S**
Paleocurrent Data: Ripple cross-lamination
Vector Mean: 80.5

	Unrotated		Rotated		Current Direction	
	Strike	Dip	Strike	Dip	1.	2.
1.	022	27e	348	25e	078	
2.	022	30e	352	25e	083	

Station Number 12.51-12.55 M
MASTER BEDDING **Strike: 081** **Dip: 16 S**

Paleocurrent Data: Ripple-cross laminations
Vector Mean: 80.7 **Standard Deviation: 8.08**

	Unrotated		Rotated		Current Direction	
	Strike	Dip	Strike	Dip	1.	2.
1.	033	19se	342	14e	072	
2.	035	21se	352	15e	082	
3.	038	22se	358	16e	088	

Station Number 12.98-13.19 M
MASTER BEDDING **Strike: 081** **Dip: 16 S**
Paleocurrent Data: Ripple cross-lamination
Vector Mean: 85.7 **Standard Deviation: 9.45**

	Unrotated		Rotated		Current Direction	
	Strike	Dip	Strike	Dip	1.	2.
1.	032	27se	003	20se	093	
2.	037	26se	359	18e	089	
3.	022	24se	345	22e	075	

Station Number 13.89-13.96 M
MASTER BEDDING **Strike: 082** **Dip: 16 S**
Paleocurrent Data: Ripple cross-lamination
Vector Mean: 99.5

	Unrotated		Rotated		Current Direction	
	Strike	Dip	Strike	Dip	1.	2.
1.	038	21se	353	15e	083	
2.	043	28se	016	18se	116	

POPLAR CAMP SECTION 3
PALEOCURRENT ROTATION DATA
ERWIN / ANTIETAM FORMATION

Station Number 0.57-0.72 M
MASTER BEDDING **Strike: 064** **Dip: 32 SE**
Paleocurrent Data: Ripple cross-lamination

	Unrotated		Rotated		Current Direction	
	Strike	Dip	Strike	Dip	1.	2.
1.	029	36e	333	19se	063	

Station Number 1.32-1.37 M
MASTER BEDDING **Strike: 064** **Dip: 32 SE**
Paleocurrent Data: Ripple cross-lamination

	Unrotated		Rotated		Current Direction	
	Strike	Dip	Strike	Dip	1.	2.
1.	040	30e	317	12ne	047	

Station Number 1.42-1.44 M
MASTER BEDDING **Strike: 064** **Dip: 32 SE**
Paleocurrent Data: Ripple cross-lamination

	Unrotated		Rotated		Current Direction	
	Strike	Dip	Strike	Dip	1.	2.
1.	055	33se	332	05ne	062	

Station Number 1.42-1.44 M
MASTER BEDDING **Strike: 064** **Dip: 32 SE**
Paleocurrent Data: Ripple crest
Vector Mean: 12.0

	Unrotated		Rotated	Current Direction	
	Pitch	CD	Azimuth	1.	2.
1.	36ne	sw-ne	092	002	
2.	26ne	sw-ne	112	022	

POPLAR CAMP SECTION 5
PALEOCURRENT ROTATION DATA
ERWIN / ANTIETAM FORMATION

Station Number 1.21-1.69 M
MASTER BEDDING **Strike: 070** **Dip: 21 SE**
Paleocurrent Data: Ripple crest
Vector Mean: 164.2 **Standard Deviation: 9.55**

	Unrotated		Rotated	Current Direction	
	Pitch	CD	Azimuth	1.	2.
1.	11e	nw-se	081	171	
2.	09w	nw-se	241	152	
3.	02e	nw-se	072	162	
4.	10e	nw-se	080	170	
5.	12e	nw-se	082	172	
6.	14w	nw-se	237	147	
7.	15e	nw-se	086	176	
8.	08e	nw-se	078	164	
9.	04e	nw-se	074	164	

Station Number 7.68-7.78 M
MASTER BEDDING **Strike: 065** **Dip: 23 SW**
Paleocurrent Data: Ripple crests
Vector Mean: 153 **Standard Deviation: 5.00**

	Unrotated		Rotated	Current Direction	
	Pitch	CD	Azimuth	1.	2.
1.	02w	nw-se	243	153	
2.	07w	nw-se	238	148	
3.	03e	nw-se	068	158	

POPLAR CAMP SECTION 6
PALEOCURRENT ROTATION DATA
ERWIN / ANTIETAM FORMATION

Station Number 0.39-0.41 M
MASTER BEDDING **Strike: 045** **Dip: 08 SE**
Paleocurrent Data: Current ripple crests

	Unrotated		Rotated	Current Direction	
	Pitch	CD	Azimuth	1.	2.
1.	14sw	nw-se	212	122	

BUCHANAN SECTION (LOCALITY 7)
PALEOCURRENT ROTATION DATA
ERWIN FORMATION
FACIES ASSOCIATION

Station Number 148.8 M
MASTER BEDDING **Strike:016** **Dip: 78 W**
Paleocurrent Data: Wave-ripple crests
Vector Mean: 134.2 **Standard Deviation: 14.75**

	Unrotated		Rotated	Current Direction	
	Pitch	CD	Azimuth	1.	2.
set 1					
1.	37s	—	233	143	323
2.	32s	—	228	138	318
3.	35s	—	231	141	321
4.	29s	—	225	135	325
5.	18s	—	214	124	304
set 2					
1.	23s	—	219	129	309
2.	42s	—	238	148	328
3.	40s	—	236	146	326
4.	45s	—	241	151	331
5.	35s	—	231	321	141
set 3					
1.	04s	—	200	110	290
2.	02s	—	198	108	288
3.	01n	—	015	105	285
set 4					
1.	22s	—	218	128	308
2.	31s	—	227	137	137
3.	41s	—	237	147	327
4.	43s	—	239	149	329

Station Number 161.46
MASTER BEDDING **Strike: 018** Dip: 77 W
Paleocurrent Data: Rippled tops
Vector Mean: 129.8 **Standard Deviation: 10.64**

	Unrotated		Rotated	Current Direction	
	Pitch	CD	Azimuth	1.	2.
1.	18sw	se	216	126	306
2.	07sw	se	205	115	295
3.	20sw	se	218	128	308
4.	30sw	se	228	138	318
5.	34sw	se	232	142	322

Station Number 157.74 M
MASTER BEDDING **Strike: 020** Dip: 79 W
Paleocurrent Data: Rippled tops
Vector Mean; 115.0 **Standard Deviation: 3.56**

	Unrotated		Rotated	Current Direction	
	Pitch	CD	Azimuth	1.	2.
1.	11sw	—	210	120	300
2.	04sw	—	203	113	293

3.	03sw	—	202	112	292
4.	06sw	—	205	115	295

Station Number 169.27 M
MASTER BEDDING **Strike: 023** **Dip: 75 W**
Paleocurrent Data: Ripple tops
Vector Mean: 125.6 **Standard Deviation: 7.50**

	Unrotated		Rotated	Current Direction	
	Pitch	CD	Azimuth	1.	2.
1.	17sw	—	219	129	309
2.	24sw	—	226	136	316
3.	14sw	—	216	126	306
4.	09sw	—	210	120	300
5.	05sw	—	207	117	297

Station Number 179.25
MASTER BEDDING **Strike: 021** **Dip: 81 W**
Paleocurrent Data: Rippled tops
Vector Mean: 116.1 **Standard Deviation: 8.25**

	Unrotated		Rotated	Current Direction	
	Pitch	CD	Azimuth	1.	2.
1.	04ne	—	017	107	287
2.	11se	—	211	121	301
3.	04ne	—	017	107	287
4.	04se	—	205	115	295
5.	05ne	—	016	106	286
6.	22sw	—	222	132	312
7.	13sw	—	213	123	303
8.	03sw	—	204	114	294
9.	10sw	—	210	120	300
10.	05sw	—	206	116	296

Station Number 152.80 M
MASTER BEDDING **Strike: 016** **Dip: 78 W**
Paleocurrent Data: Rippled top
Vector Mean: 113.4 **Standard Deviation: 2.99**

	Unrotated		Rotated	Current Direction	
	Pitch	CD	Azimuth	1.	2.
1.	06s	—	202	112	292
2.	08s	—	204	114	294
3.	09s	—	205	115	295
4.	14s	—	210	120	300
5.	05s	—	210	111	291
6.	04s	—	201	110	290
7.	07s	—	203	113	293
8.	10s	—	206	116	296
9.	06s	—	202	112	292
10.	05s	—	210	111	291

Station Number 202.30 M
MASTER BEDDING **Strike: 024** **Dip: 75 SW**
Paleocurrent Data: Large-scale wave-ripples
Vector Mean: 323.0 **Standard Deviation: 9.17**

	Unrotated		Rotated	Current Direction	
	Pitch	CD	Azimuth	1.	2.
1.	30s	s-n	235	325	
2.	18s	s-n	223	313	

3.	36s	s-n	241	331	

Station Number 82.1-87.46 M
MASTER BEDDING **Strike: 035** **Dip: 74 W**
Paleocurrent Data: Trough axis

	Unrotated		Rotated	Current Direction	
	Pitch	CD	Azimuth	1.	2.
1.	05ne	—	030	030	210

Station Number 137.99-138.31
MASTER BEDDING **Strike: 030** **Dip: 73 W**
Paleocurrent Data: Rippled-top

	Unrotated		Rotated	Current Direction	
	Pitch	CD	Azimuth	1.	2.
1.	12w	—	222	132	312

Station Number 187.25-187.77 M
MASTER BEDDING **Strike: 024** **Dip: 74 W**
Paleocurrent Data: Rippled top
Vector Mean: 128.8 **Standard Deviation: 2.90**

	Unrotated		Rotated	Current Direction	
	Pitch	CD	Azimuth	1.	2.
1.	16w	—	220	130	310
2.	16w	—	220	130	310
3.	17w	—	221	131	311
4.	12w	—	216	126	306
5.	11w	—	215	125	305
6.	18w	—	222	132	312
7.	19w	—	223	133	313
8.	15w	—	219	129	209
9.	13w	—	217	127	307
10.	11w	—	215	125	305

BUCHANAN SECTION (2)

Station Number 66.0-66.02 M
MASTER BEDDING **Strike: 038** **Dip: 68 W**
Paleocurrent Data: Large-scale wave-ripples
Vector Mean: 160.3 **Standard Deviation: 2.52**

	Unrotated		Rotated	Current Direction	
	Pitch	CD	Azimuth	1.	2.
1.	32w	—	250	160	340
2.	30w	—	248	158	338
3.	35w	—	253	163	343

BUCHANAN SECTION (5)
FACIES ASSOCIATION 2

Station Number 106.40-106.54
MASTER BEDDING **Strike: 212** **Dip: 72 SE**
Paleocurrent Data: Large-scale wave-ripples
Vector Mean: 95.7 **Standard Deviation: 1.53**

	Unrotated		Rotated	Current Direction	
	Pitch	CD	Azimuth	1.	2.
1.	28sw	—	184	094	274
2.	26sw	—	186	096	276
3.	25sw	—	187	097	277

ARCADIA SECTION (2) (LOCALITY 8)
PALEOCURRENT ROTATION DATA
HARPERS / HAMPTON FORMATION
FACIES ASSOCIATION 4

Station Number 206.90-206.92 M
MASTER BEDDING **Strike: 054** **Dip: 54 SE OT**
Paleocurrent Data: Trough axis

	Unrotated		Rotated	Current Direction	
	Pitch	CD	Azimuth	1.	2.
1.	79ne	—	335	155	335

Station Number 207.11-207.14 M
MASTER BEDDING **Strike: 054** **Dip: 54 SE OT**
Paleocurrent Data: Trough-axis

	Unrotated		Rotated	Current Direction	
	Pitch	CD	Azimuth	1.	2.
1.	72ne	—	342	162	342

Station Number 207.20-207.36 M
MASTER BEDDING **Strike: 054** **Dip: 54 SE OT**
Paleocurrent Data: Trough Axis
Vector Mean: 154.0 **Standard Deviation: 5.48**

	Unrotated		Rotated	Current Direction	
	Pitch	CD	Azimuth	1.	2.
1.	72ne	—	342	162	342
2.	84ne	—	330	150	330
3.	81ne	—	333	153	333
4.	83ne	—	331	151	331

Station Number 207.93-207.29 M
MASTER BEDDING **Strike: 054** **Dip: 54 SE OT**
Paleocurrent Data: Trough axis
Vector Mean: 154.5 **Standard Deviation: 3.11**

	Unrotated		Rotated	Current Direction	
	Pitch	CD	Azimuth	1.	2.
1.	78ne	—	336	156	336
2.	83ne	—	331	151	331
3.	76ne	—	338	158	338
4.	81ne	—	333	153	333

Station Number 369.96-371.00 M
MASTER BEDDING **Strike: 054** **Dip: 46 SE**
Paleocurrent Data: Trough-axis:
Vector Mean: 121.8 **Standard Deviation: 13.07**

	Unrotated		Rotated	Current Direction	
	Pitch	CD	Azimuth	1.	2.
1.	54nw	—	288	108	288
2.	74nw	—	308	128	308
3.	87nw	—	321	141	321
4.	59nw	—	293	113	293
5.	65nw	—	299	119	299

NATURAL BRIDGE QUARRY (LOCALITY 9)
PALEOCURRENT ROTATION DATA
ERWIN / ANTIETAM FORMATION

Station Number 5.00 m FACE 1
MASTER BEDDING **Strike: 114** **Dip: 31 S**
Paleocurrent Data: current ripple crests

	Unrotated		Rotated	Current Direction	
	Pitch	CD	Azimuth	1.	2.
1.	36e	e-w	150	240	
2.	21e	e-w	135	225	
3.	23e	e-w	137	227	
4.	11e	e-w	125	215	
5.	08e	e-w	122	212	
6.	12e	e-w	126	216	
7.	11e	e-w	125	215	
8.	15e	e-w	129	219	
9.	26e	e-w	140	230	
10.	18e	e-w	132	222	
11.	48e	e-w	162	252	
12.	16e	e-w	130	220	
13.	15e	e-w	129	219	
14.	27e	e-w	141	231	
15.	12e	e-w	126	216	
16.	19e	e-w	133	223	
17.	18e	e-w	132	222	
18.	24e	e-w	138	228	
19.	33e	e-w	147	237	
20.	24e	e-w	138	228	
21.	12e	e-w	126	216	
22.	16e	e-w	130	220	
23.	16e	e-w	130	220	
24.	57e	e-w	171	261	
25.	42e	e-w	156	246	
26.	69w	n-s	225	135	
27.	78w	n-s	216	126	
28.	75w	n-s	219	129	
29.	60w	n-s	234	144	
30.	63w	n-s	231	141	
31.	66w	n-s	228	138	
32.	13w	n-s	281	191	
33.	32w	n-s	262	172	
34.	52w	n-s	242	152	
35.	41w	n-s	253	163	
36.	22w	n-s	272	182	
37.	13w	n-s	281	191	
38.	19w	n-s	275	185	
39.	36e	e-w	148	238	
40.	57e	e-w	169	259	
41.	56e	e-w	168	258	
42.	73e	e-w	185	275	
43.	58e	e-w	170	260	
44.	62e	e-w	174	264	
45.	45e	e-w	157	247	
46.	57e	e-w	169	259	
47.	60e	e-w	172	262	
48.	36e	e-w	148	238	
49.	65e	e-w	177	267	
50.	88e	e-w	200	290	
51.	68e	e-w	180	270	
52.	57e	e-w	169	259	
53.	34e	e-w	146	236	
54.	48e	e-w	160	250	
55.	41e	e-w	153	243	
56.	44e	e-w	156	246	
57.	02e	n-s	114	204	
58.	00e	n-s	112	202	
59.	04e	n-s	116	206	
60.	46e	e-w	158	248	
61.	49e	e-w	161	251	

62.	47e	e-w	159	249
63.	52e	e-w	164	254
64.	31e	e-w	143	233
65.	33e	e-w	145	235
66.	45e	e-w	157	247
67.	33e	e-w	145	235
68.	53e	e-w	165	255
69.	27e	e-w	139	229
70.	25e	e-w	137	227
71.	47e	e-w	159	249
72.	24e	e-w	136	226
73.	16e	e-w	128	218
74.	38e	e-w	150	240
75.	37e	e-w	149	239
76.	28e	e-w	140	230
77.	53e	e-w	165	255
78.	42e	e-w	154	244
79.	24e	e-w	136	226
80.	55e	e-w	167	257
81.	58e	e-w	170	260
82.	60e	e-w	172	262
83.	42e	e-w	154	244
84.	43e	e-w	155	245
85.	11w	n-s	281	191
86.	59e	e-w	171	261
87.	64e	e-w	176	266
88.	27e	e-w	139	229
89.	23e	e-w	135	225
90.	19e	e-w	131	221
91.	26e	e-w	138	228
92.	21e	e-w	133	223
93.	22e	e-w	134	224
94.	24e	e-w	136	226
95.	16e	e-w	128	228
96.	15e	n-s	127	217
97.	07e	n-s	119	209
98.	77w	s-n	215	305
99.	75w	s-n	217	307
100.	71w	s-n	221	311
101.	21e	n-s	133	223
102.	22e	n-s	134	224
103.	26e	n-s	138	228
104.	25e	n-s	137	227
105.	76e	e-w	188	278
106.	63e	e-w	175	265
107.	32e	e-w	144	234
108.	16e	e-w	128	218
109.	10e	n-s	122	212
110.	19e	e-w	131	221
111.	11e	n-s	123	213
112.	24e	e-w	136	226
113.	34e	e-w	146	236
114.	42e	e-w	154	244
115.	63e	e-w	175	265
116.	48e	e-w	160	250
117.	43e	e-w	155	245
118.	53e	e-w	165	255
119.	37e	e-w	149	239
120.	45e	e-w	157	247
121.	44e	e-w	156	246
122.	37e	e-w	149	239
123.	02e	n-s	114	204
124.	43e	e-w	155	245
125.	37e	e-w	149	239
126.	35e	e-w	147	239
127.	38e	e-w	150	240
128.	00e	n-s	112	202
129.	16e	n-s	128	218
130.	29e	e-w	141	213
131.	16e	n-s	128	218
132.	16e	n-s	128	218
133.	63e	e-w	175	265
134.	32e	e-w	144	234
135.	61e	e-w	173	263
136.	34e	e-w	146	236
137.	51e	e-w	163	253
138.	32e	e-w	144	234

139.	52e	e-w	164	254
140.	43e	e-w	155	245
141.	30e	e-w	142	232
142.	16e	n-s	128	218
143.	00	n-s	112	202
144.	01e	n-s	113	203
145.	03w	n-s	289	199
146.	08e	n-s	120	210
147.	21e	n-s	133	223

Station Number 5.00 M FACE 1
MASTER BEDDING **Strike: 114** **Dip: 31 S**
Paleocurrent Data: Drain direction from modified current ripples in scour depressions
Vector Mean: 176 **Standard Deviation: 30.3**

	Unrotated		Rotated	Current Direction	
	Pitch	CD	Azimuth	1.	2.
1.	67e	n-s	179	179	
2.	88e	n-s	200	200	
3.	83e	n-s	195	195	
4.	87w	n-s	205	205	
5.	30e	n-s	142	142	
6.	24e	n-s	136	136	
7.	18e	n-s	130	130	
8.	42e	n-s	154	154	
9.	18e	n-s	130	130	
10.	35e	n-s	147	147	
11.	83e	n-s	195	195	
12.	85w	n-s	207	207	
13.	87w	n-s	205	205	
14.	90	n-s	202	202	
15.	78e	n-s	190	190	
16.	89e	n-s	201	201	
17.	84w	n-s	208	208	

Station Number 5.00 m face 2
MASTER BEDDING **Strike: 108** **Dip:33 s**
Palcocurrent Data: Crests of current ripples

	Unrotated		Rotated	Current Direction	
	Pitch	CD	Azimuth	1.	2.
1.	04w	n-s	284	194	
2.	03w	n-s	285	195	
3.	14e	n-s	122	212	
4.	00e	n-s	108	198	
5.	13w	n-s	275	185	
6.	33w	n-s	255	165	
7.	46w	n-s	242	152	
8.	53w	n-s	235	145	
9.	55w	n-s	233	143	
10.	59w	n-s	229	139	
11.	46w	n-s	242	152	
12.	58w	n-s	230	140	
13.	36w	n-s	252	142	
14.	33w	n-s	255	145	
15.	54e	e-w	162	252	
16.	49e	e-w	157	247	
17.	52e	e-w	160	250	
18.	61e	e-w	169	259	
19.	63e	e-w	171	261	
20.	49e	e-w	157	247	
21.	42e	e-w	150	240	
22.	38e	e-w	146	236	
23.	33e	e-w	141	231	
24.	34e	e-w	142	232	
25.	35e	e-w	143	233	
26.	42e	e-w	150	240	
27.	62e	e-w	170	260	

28.	53e	e-w	161	251
29.	21e	e-w	129	219
30.	25e	e-w	133	223
31.	26e	e-w	134	224
32.	36e	e-w	144	234
33.	44e	e-w	152	242
34.	42e	e-w	150	240
35.	08e	n-s	116	206
36.	12e	n-s	120	210
37.	21e	n-s	129	219
38.	67e	e-w	175	265
39.	33w	e-w	141	231
40.	24w	e-w	132	222
41.	02e	n-s	110	200
42.	16e	n-s	124	214
43.	18e	n-s	126	216
44.	31e	n-s	139	229
45.	42e	n-s	150	240
46.	39e	e-w	147	237
47.	40e	e-w	148	238
48.	24e	e-w	132	222
49.	22e	e-w	130	220
50.	35e	e-w	143	233
51.	36e	e-w	144	234
52.	21e	n-s	129	219
53.	14e	n-s	122	211
54.	36e	e-w	144	234
55.	37e	e-w	145	235
56.	36e	e-w	144	234
57.	53e	e-w	161	251
58.	51e	e-w	159	249
59.	48e	e-w	156	246
60.	42e	e-w	150	240
61.	41e	e-w	149	239
62.	57e	e-w	165	255
63.	46e	e-w	154	244
64.	13e	n-s	121	211
65.	06e	n-s	114	204
66.	28e	n-s	136	226
67.	27e	n-s	135	225
68.	37e	n-s	145	235
69.	29e	e-w	137	227
70.	59e	e-w	167	257
71.	41e	e-w	149	239
72.	28w	n-s	256	166
73.	47w	n-s	241	151
74.	56w	n-s	232	142
75.	34w	n-s	254	164
76.	44w	n-s	244	154
77.	50w	n-s	238	148
78.	43w	n-s	245	155
79.	42w	n-s	246	156
80.	18e	n-s	126	216
81.	27e	n-s	135	225
82.	20e	n-s	128	218
83.	82w	e-w	206	296
84.	77w	e-w	211	301
85.	86w	e-w	202	292
86.	84w	e-w	204	294
87.	31e	e-w	139	229
88.	36e	e-w	144	234
89.	38e	e-w	146	236
90.	08e	n-s	116	206
91.	04e	n-s	112	202
92.	08e	n-s	116	206
93.	76e	e-w	184	274
94.	56e	e-w	164	254
95.	63e	e-w	171	261
96.	52e	e-w	160	250
97.	53e	e-w	161	251
98.	52e	e-w	160	250
99.	58e	e-w	166	256
100.	72e	e-w	180	270
101.	07e	n-s	115	205
102.	06e	n-s	114	204
103.	07e	n-s	115	205
104.	11e	n-s	119	209

105.	18e	n-s	126	216
106.	28e	n-s	136	226
107.	34e	n-s	142	232
108.	31e	n-s	139	229
109.	30e	n-s	138	228
110.	27e	n-s	135	225
111.	22e	n-s	130	220
112.	22e	n-s	130	220
113.	21e	n-s	129	219
114.	22e	n-s	130	220
115.	32e	e-w	140	230
116.	31e	e-w	139	229
117.	58e	e-w	166	256
118.	56e	e-w	164	254
119.	59e	e-w	167	257
120.	66e	e-w	174	264

Station Number 5.00 m surface 1
MASTER BEDDING **Strike: 114** **Dip: 31 S**
Paleocurrent Data: current ripple crests
Vector Mean: 48.67 **Standard Deviation: 19.68**

	Unrotated		Rotated	Current Direction	
	Pitch	CD	Azimuth	1.	2.
1.	35e	w-e	143	053	
2.	51e	w-e	159	069	
3.	46e	w-e	154	064	
4.	28w	s-n	256	346	
5.	50w	w-e	238	328	
6.	38e	w-e	146	056	
7.	38e	w-e	146	056	
8.	35e	w-e	143	053	
9.	25e	w-e	133	043	
10.	27e	w-e	135	045	
11.	52e	w-e	160	070	
12.	55e	w-e	163	073	
13.	16e	w-e	124	034	
14.	31e	w-e	139	049	
15.	10e	w-e	118	028	
16.	09e	w-e	117	027	
17.	20e	w-e	128	038	
18.	21e	w-e	129	039	
19.	25e	w-e	133	043	
20.	35e	w-e	143	053	
21.	42e	w-e	150	060	
22.	47e	w-e	155	065	
23.	53e	w-e	161	071	
24.	49e	w-e	157	067	
25.	39e	w-e	147	057	
26.	40e	w-e	148	058	
27.	16e	w-e	124	034	
28.	25e	w-e	133	043	
29.	50e	w-e	158	068	
30.	47e	w-e	155	065	
31.	27e	w-e	135	045	
32.	32e	w-e	141	051	
33.	35e	w-e	143	053	
34.	26e	w-e	134	044	
35.	25e	w-e	133	043	
36.	45e	w-e	153	063	
37.	16e	w-e	124	034	
38.	18e	w-e	126	036	
39.	42e	w-e	150	060	
40.	47e	w-e	155	065	
41.	21e	w-e	129	039	
42.	23e	w-e	131	041	
43.	35e	w-e	143	053	
44.	30e	w-e	138	048	
45.	22e	w-e	130	040	
46.	18e	w-e	126	036	
47.	50e	w-e	158	068	

Station Number 5.00 m Face 3

MASTER BEDDING **Strike: 120** **Dip: 32 S**
Paleocurrent Data: Pitch of current ripple crests

	Unrotated		Rotated	Current Direction	
	Pitch	CD	Azimuth	1.	2.
1.	26e	n-s	146	236	
2.	28e	e-w	148	238	
3.	38e	e-w	158	248	
4.	43e	e-w	163	253	
5.	38e	e-w	158	248	
6.	12e	e-w	132	222	
7.	41e	e-w	161	251	
8.	38e	e-w	158	248	
9.	31e	e-w	151	241	
10.	46e	e-w	166	256	
11.	21e	e-w	141	231	
12.	33e	e-w	153	243	
13.	14e	e-w	134	224	
14.	28e	e-w	148	238	
15.	26e	e-w	146	236	
16.	16e	e-w	136	226	
17.	06e	e-w	126	216	
18.	16e	e-w	136	226	
19.	18e	e-w	138	228	
20.	31e	e-w	151	241	
21.	27e	e-w	147	237	
22.	44e	e-w	164	254	
23.	34e	e-w	154	244	
24.	24e	e-w	144	234	
25.	26e	e-w	146	236	
26.	29e	e-w	149	239	
27.	19e	e-w	139	229	
28.	34e	e-w	154	244	
29.	38e	e-w	158	248	
30.	33e	e-w	153	243	
31.	27e	e-w	147	237	
32.	23e	e-w	143	233	
33.	18e	e-w	138	228	
34.	31e	e-w	151	241	
35.	34e	e-w	154	244	
36.	71e	e-w	191	281	
37.	71e	e-w	191	281	
38.	43e	e-w	163	253	
39.	48e	e-w	168	258	
40.	40e	e-w	160	250	
41.	34e	e-w	154	244	
42.	31e	e-w	151	241	
43.	14e	e-w	134	224	
44.	11e	n-s	131	221	
45.	20e	n-s	140	230	
46.	17e	n-s	137	227	
47.	07e	n-s	127	217	

Station Number 5.00 m FACE 3
MASTER BEDDING **Strike: 120** **Dip: 32 S**
Paleocurrent Data: Drain direction from ripple troughs
Vector Mean: 207 **Standard Deviation: 6.78**

	Unrotated		Rotated	Current Direction	
	Pitch	CD	Azimuth	1.	2.
1.	87e	n-s	207	207	
2.	88e	n-s	208	208	
3.	89e	n-s	209	209	
4.	85w	n-s	215	215	
5.	89w	n-s	211	211	
6.	79w	n-s	221	221	
7.	88w	n-s	212	212	
8.	78e	n-s	198	198	
9.	90	n-s	210	210	

10.	90	n-s	210	210
11.	86w	n-s	204	204
12.	80w	n-s	200	200
13.	86w	n-s	204	204
14.	88w	n-s	202	202
15.	85w	n-s	205	205
16.	86e	n-s	206	206
17.	83e	n-s	203	203
18.	90	n-s	210	210
19.	86w	n-s	214	214
20.	87w	n-s	213	213
21.	86w	n-s	214	214
22.	82w	n-s	218	218
23.	87w	n-s	213	213
24.	85w	n-s	215	215
25.	89e	n-s	209	209
26.	77e	n-s	197	197
27.	74e	n-s	197	194
28.	76e	n-s	196	196
29.	84e	n-s	204	204
30.	86e	n-s	206	206
31.	88e	n-s	208	208
32.	69e	n-s	189	189
33.	84e	n-s	204	204
34.	88e	n-s	208	208
35.	86e	n-s	206	206

Station Number 5.00 m FACE 1
MASTER BEDDING **Strike: 114** **Dip: 31 S**
Paleocurrent Data: ripple crests in troughs of megaripples

	Unrotated		Rotated	Current Direction	
	Pitch	CD	Azimuth	1.	2.
1.	13w	n-s	281	191	
2.	06w	n-s	288	198	
3.	09w	n-s	285	195	
4.	06w	n-s	288	198	
5.	10w	n-s	284	194	
6.	14w	n-s	280	190	
7.	08w	n-s	286	196	
8.	11e	n-s	125	215	
9.	12e	n-s	126	216	
10.	08e	n-s	122	212	
11.	06e	n-s	120	212	
12.	11e	n-s	125	215	
13.	21e	n-s	135	225	
14.	22e	n-s	136	226	
15.	31w	n-s	145	235	
16.	21w	n-s	273	183	
17.	06e	n-s	120	210	
18.	01w	n-s	293	203	
19.	04w	n-s	290	200	
20.	09e	n-s	123	213	
21.	02e	n-s	116	206	
22.	12w	n-s	282	192	
23.	04e	n-s	118	208	
24.	02e	n-s	116	206	
25.	08w	n-s	286	196	
26.	10w	n-s	284	194	
27.	07w	n-s	287	197	
28.	00w	n-s	114	204	
29.	04w	n-s	290	200	
30.	12e	n-s	126	216	
31.	01e	n-s	115	205	
32.	02w	n-s	292	202	
33.	22e	n-s	136	226	
34.	03e	n-s	117	207	
35.	18e	n-s	132	222	
36.	14e	n-s	128	218	
37.	23e	n-s	137	227	
38.	02w	n-s	292	202	
39.	00e	n-s	114	204	
40.	13e	n-s	127	217	

41.	12e	n-s	126	216
42.	08w	n-s	286	196
43.	02w	n-s	118	208
44.	04e	n-s	118	208
45.	02w	n-s	292	202
46.	07e	n-s	121	211
47.	06e	n-s	120	210
48.	02e	n-s	116	206
49.	25e	n-s	139	229
50.	21e	n-s	135	225
51.	11e	n-s	125	215
52.	05w	n-s	289	199
53.	03e	n-s	117	207

Station Number 5.00 M
MASTER BEDDING **Strike: 114** **Dip: 31 S**
Paleocurrent Data: current ripple on stoss-side of sandwaves

	Unrotated		Rotated	Current Direction	
	Pitch	CD	Azimuth	1.	2.
1.	72w	e-w	222	312	
2.	81w	e-w	213	303	
3.	78w	e-w	216	306	
4.	78e	e-w	192	282	
5.	87w	e-w	207	297	
6.	86w	e-w	208	298	
7.	88w	e-w	206	296	
8.	81w	e-w	213	303	
9.	88w	e-w	206	296	
10.	81w	e-w	213	303	
11.	84w	e-w	210	300	
12.	77w	e-w	217	307	
13.	88w	e-w	206	296	
14.	84e	e-w	198	288	
15.	79w	e-w	215	305	
16.	78e	e-w	192	282	
17.	76e	e-w	190	280	
18.	77e	e-w	191	281	
19.	84e	e-w	198	288	
20.	83e	e-w	197	287	
21.	86e	e-w	200	290	
22.	82e	e-w	196	286	
23.	85e	e-w	199	289	
24.	83w	e-w	211	301	
25.	82w	e-w	212	302	
26.	77w	e-w	217	307	

Station Number 5.67 M
MASTER BEDDING **Strike: 118** **Dip: 33 S**
Paleocurrent Data: Current ripple crests
Vector Mean: 289.00

	Unrotated		Rotated	Current Direction	
	Pitch	CD	Azimuth	1.	2.
1.	84w	e-w	214	304	
2.	88w	e-w	210	300	
3.	87w	e-w	211	301	
4.	84w	e-w	214	304	
5.	86w	e-w	212	302	
6.	85w	e-w	213	303	
7.	22e	e-w	140	230	
8.	47e	e-w	165	255	
9.	65e	e-w	183	273	
10.	86e	e-w	204	294	
11.	88e	e-w	206	296	
12.	90e	e-w	208	298	
13.	90e	e-w	208	298	
14.	78e	e-w	196	286	
15.	83e	e-w	201	291	

Station Number 5.70 M
MASTER BEDDING **Strike: 118** **Dip: 33 S**
Paleocurrent Data: Drain direction from modified ripples
Vector Mean: 187.12 **Standard Deviation 18.36**

	Unrotated		Rotated	Current Direction	
	Pitch	CD	Azimuth	1.	2.
1.	88e	e-w	206	206	
2.	84e	e-w	202	202	
3.	82e	e-w	200	200	
4.	62e	e-w	180	180	
5.	68e	e-w	186	186	
6.	76e	e-w	194	194	
7.	88e	e-w	206	206	
8.	88e	e-w	206	206	
9.	50e	e-w	168	168	
10.	42e	e-w	160	160	
11.	32e	e-w	150	150	
12.	66e	e-w	184	184	
13.	70e	e-w	188	188	

Station Number 5.67 M
MASTER BEDDING **Strike: 118** **Dip: 33 S**
Paleocurrent Data: Sandwave crests
Vector Mean: 247.1 **Standard Deviation: 34.12**

	Unrotated		Rotated	Current Direction	
	Pitch	CD	Azimuth	1.	2.
1.	55e	e-w	173	263	
2.	53e	e-w	171	261	
3.	79e	e-w	197	287	
4.	10e	e-w	128	218	
5.	05w	e-w	293	203	

Station Number 6.38-6.88 M
MASTER BEDDING **Strike: 118** **Dip: 33 S**
Paleocurrent Data: Foresets
Vector Mean: 261.0

	Unrotated		Rotated		Current Direction	
	Strike	Dip	Strike	Dip	1.	2.
1.	146	54sw	166	27w	256	
2.	152	53sw	176	28w	266	

Station Number 7.20 M
MASTER BEDDING **Strike: 118** **Dip: 33 S**
Paleocurrent Data: Sandwave crests
Vector Mean: 72.70 **Standard Deviation: 19.18**

	Unrotated		Rotated	Current Direction	
	Pitch	CD	Azimuth	1.	2.
1.	48e	s-n	166	76	
2.	63e	s-n	181	91	
3.	30e	s-n	148	58	
4.	20e	s-n	138	48	
5.	62e	s-n	180	90	

Station Number 7.20 M
MASTER BEDDING **Strike: 118** **Dip: 33 S**

Paleocurrent Data: Opposed ripples
Vector Mean: 248.4

Standard Deviation: 3.6

	Unrotated		Rotated	Current Direction	
	Pitch	CD	Azimuth	1.	2.
1.	36e	e-w	154	244	
2.	45e	e-w	163	254	
3.	40e	e-w	158	248	
4.	38e	e-w	156	246	
5.	43e	e-w	161	251	

Station Number 7.00 M
MASTER BEDDING **Strike: 118** Dip: 33 S
Paleocurrent Data: Sandwave crests
Vector Mean: 255.6

Standard Deviation: 39.49

	Unrotated		Rotated	Current Direction	
	Pitch	CD	Azimuth	1.	2.
1.	16w	n-s	282	192	
2.	60e	n-s	178	268	
3.	30e	n-s	148	238	
4.	78e	n-s	196	286	
5.	76e	n-s	194	284	

Station Number 22.00 M +
MASTER BEDDING **Strike: 118** Dip: 33 S
Paleocurrent Data: tabular-tangential
Vector Mean: 327.1

Standard Deviation: 34.12

	Unrotated		Rotated		Current Direction	
	Strike	Dip	Strike	Dip	1.	2.
1.	163	36w	216	23nw	306	
2.	168	33w	225	25nw	315	
3.	158	44w	196	25nw	286	
4.	175	25w	243	26nw	333	
5.	158	34w	217	20nw	307	
6.	002	15w	265	27n	355	
7.	004	20w	255	29n	345	
8.	012	17w	263	30n	353	
9.	002	27w	242	29n	332	
10.	006	25w	247	30n	337	

BALCONY FALLS (LOCALITY 10)
UNICOI FORMATION

Station Number 2.10-3.20 M
MASTER BEDDING **Strike: 040** Dip: 31 NE
Paleocurrent Data: Forsets

	Unrotated		Rotated		Current Direction	
	Strike	Dip	Strike	Dip	1.	2.
1.	105	50n	316	38ne	046	

Station Number 8.70-10.20 M
MASTER BEDDING **Strike: 050** Dip: 55 NW
Paleocurrent Data: Foresets

	Unrotated		Rotated		Current Direction	
	Strike	Dip	Strike	Dip	1.	2.
1.	080	50nw	344	23ne	074	

Station Number 13.20-14.00 M
MASTER BEDDING **Strike: 050** Dip: 47 SE
Paleocurrent Data: Foresets

	Unrotated		Rotated		Current Direction	
	Strike	Dip	Strike	Dip	1.	2.
1.	035	47ne	318	13sw	228	

Station Number 14.50-15.65 M
MASTER BEDDING **Strike:096** Dip:77 S
Paleocurrent Data: Foresets

	Unrotated		Rotated		Current Direction	
	Strike	Dip	Strike	Dip	1.	2.
1.	210	46ne	304	16nw	214	

Station Number 29.31-35.70 M
MASTER BEDDING **Strike: 050** Dip: 47 NW
Paleocurrent Data: Small channel orientation
Vector Mean: 201.5 **Standard Deviation: 9.19**

	Unrotated		Rotated	Current Direction	
	Pitch	CD	Azimuth	1.	2.
1.	22ne	s	028	208	
2.	35ne	s	015	195	

Station Number 112.52-128.18 M
MASTER BEDDING **Strike: 041** Dip: 42 NW
Paleocurrent Data: Foresets
Vector Mean: 133.0 **Standard Deviation: 49.50**

	Unrotated		Rotated		Current Direction	
	Strike	Dip	Strike	Dip	1.	2.
1.	041	42ne	028	21w	298	

2.	070	64n	107	22n	017
3.	036	61n	005	18w	275
4.	085	57w	132	28ne	042
5.	062	40n	188	09e	098
6.	040	35n	078	14e	168

Station Number 130.58-131.18 M
MASTER BEDDING **Strike: 065** **Dip: 43 NW**
Paleocurrent Data: Symmetrical ripple crests
Vector Mean: 137.75 **Standard Deviation: 4.19**

	Unrotated		Rotated	Current Direction	
	Pitch	CD	Azimuth	1.	2.
1.	16e	—	049	139	319
2.	17e	—	048	138	318
3.	23e	—	042	132	312
4.	13e	—	052	142	322

Station Number **135.20-136.52 M**
MASTER BEDDING **Strike: 065** **Dip: 43 NW**
Paleocurrent Data: Tabular Planar foresets

	Unrotated		Rotated		Current Direction	
	Strike	Dip	Strike	Dip	1.	2.
1.	085	14n	055	30sw	145	

Station Number 135.20-136.52 M
MASTER BEDDING **Strike: 065** **Dip: 43 NW**
Paleocurrent Data: Trough axes
Vector Mean: 204.5 **Standard Deviation: 6.36**

	Unrotated		Rotated	Current Direction	
	Pitch	CD	Azimuth	1.	2.
1.	45ne	s	020	200	
2.	36ne	s	029	209	

Station Number 153.0 M
MASTER BEDDING **Strike: 065** **Dip: 43 NE**
Paleocurrent Data: Asymmetrical ripples
Vector Mean: 329.25 **Standard Deviation: 5.28**

	Unrotated		Rotated	Current Direction	
	Pitch	CD	Azimuth	1.	2.
1.	12e	nw	053	323	
2.	06w	nw	249	339	
3.	09e	nw	056	326	
4.	05e	nw	060	330	
5.	04e	nw	061	331	
6.	03e	nw	062	332	
7.	05e	nw	060	330	
8.	12e	nw	053	323	

Station Number 153.20 M
MASTER BEDDING **Strike: 065** **Dip: 43 NE**
Paleocurrent Data: Asymmetrical ripples
Vector Mean: 165.11 **Standard Deviation: 8.18**

Unrotated	Rotated	Current Direction

	Pitch	CD	Azimuth	1.	2.
1.	20w	s	265	175	
2.	00	s	245	155	
3.	05w	s	250	160	
4.	06w	s	251	161	
5.	01e	s	244	154	
6.	13w	s	258	168	
7.	14w	s	259	169	
8.	22w	s	267	177	
9.	12w	s	257	167	

Station Number 150.50-153.20 M
MASTER BEDDING **Strike: 042** Dip: 31 NW
Paleocurrent Data: Foresets
Vector Mean: 105.66 **Standard Deviation: 5.64**

	Unrotated		Rotated		Current Direction	
	Strike	Dip	Strike	Dip	1.	2.
1.	124	14s	013	30e	103	
2.	100	11s	014	25e	104	
3.	135	11e	023	32e	113	

Station Number 153.69-153.73 M
MASTER BEDDING **Strike: 042** Dip: 31 NW
Paleocurrent Data: Asymmetrical ripple crest.

	Unrotated		Rotated	Current Direction	
	Pitch	CD	Azimuth	1.	2.
1.	23e	w	019	289	

Station Number 153.82-154.04 M
MASTER BEDDING **Strike: 042** Dip: 31 NW
Paleocurrent Data: Megarippled top
Vector Mean: 307.0 **Standard Deviation: 7.07**

	Unrotated		Rotated	Current Direction	
	Pitch	CD	Azimuth	1.	2.
1.	00	n	042	312	
2.	10e	n	032	302	

Station Number 154.48-154.63 M
MASTER BEDDING **Strike: 042** Dip: 31 NW
Paleocurrent Data: Megarippled top
Vector Mean: 308.8 **Standard Deviation: 5.66**

	Unrotated		Rotated	Current Direction	
	Pitch	CD	Azimuth	1.	2.
1.	08e	nw	034	304	
2.	00e	nw	042	312	

Station Number 154.63-156.43 M
MASTER BEDDING **Strike: 042** Dip: 31 NW
Paleocurrent Data: Foresets
Vector Mean: 130.79 **Standard Deviation: 20.89**

	Unrotated		Rotated		Current Direction	
	Strike	Dip	Strike	Dip	1.	2.

1.	068	11n	210	21se	120
2.	093	18n	184	25se	094
3.	082	15n	195	21se	105
4.	035	19n	226	13se	136
5.	006	14n	244	32se	154
6.	059	08n	216	24se	126
7.	032	25n	254	08se	164
8.	010	11se	057	22se	147
9.	013	10se	054	22se	144
10.	110	05s	032	29s	122
11.	117	07s	036	30s	126

Station Number 161.96-162.4 M
MASTER BEDDING
Paleocurrent Data: Symmetrical ripples
Vector Mean: 112.34

Strike: 042 **Dip: 38 NW**

Standard Deviation: 5.69

	Unrotated		Rotated	Current Direction	
	Pitch	CD	Azimuth	1.	2.
1.	15e	—	027	117	297
2.	26e	—	016	106	286
3.	18e	—	024	114	294

Station Number 162.40-162.55 M
MASTER BEDDING
Paleocurrent Data: Rippled tops
Vector Mean: 104.5

Strike: 042 **Dip: 38 NW**

Standard Deviation: 6.36

	Unrotated		Rotated	Current Direction	
	Pitch	CD	Azimuth	1.	2.
1.	23e	—	019	109	289
2.	32e	—	010	100	280

Station Number **162.55-162.70 M**
MASTER BEDDING **Dip: 38 NW**
Paleocurrent Data: Tabular planar foresets

Strike: 042

	Unrotated		Rotated		Current Direction	
	Strike	Dip	Strike	Dip	1.	2.
1.	110	30s	174	36s	084	

Station Number 162.55-162.70 M
MASTER BEDDING
Paleocurrent Data: Trough axis

Strike: 042 **Dip: 38 N**

	Unrotated		Rotated	Current Direction	
	Pitch	CD	Azimuth	1.	2.
1.	55w	se	274	094	

Station Number 165.37-166.73 M
MASTER BEDDING
Paleocurrent Data: Asymmetrical ripple crests
Vector Mean: 314.0

Strike: 049 **Dip: 45 NW**

Standard Deviation: 2.83

	Unrotated		Rotated	Current Direction	
	Pitch	CD	Azimuth	1.	2.

1.	07e	nw	042	312
2.	03e	nw	046	316

Station Number 166.74-168.1 M
MASTER BEDDING Strike: 049 Dip: 45 NW
Paleocurrent Data: Megaripples and trough axes
Vector Mean: 297.13 Standard Deviation: 47.21

	Unrotated		Rotated	Current Direction	
	Pitch	CD	Azimuth	1.	2.
1.	01w	nw	230	320	
2.	09w	nw	238	328	
3.	15e	w	030	300	
4.	06w	w	235	225	

Station Number 166.74-168.19 M
MASTER BEDDING Strike: 049 Dip: 45 NW
Paleocurrent Data: Foresets
Vector Mean: 00.00 Standard Deviation: 00.00

	Unrotated		Rotated		Current Direction	
	Strike	Dip	Strike	Dip	1.	2.
1.	060	78nw				
2.	051	67nw				

108 2s 9

Station Number 169.45-170.09 M
MASTER BEDDING Strike: 049 Dip: 45 NW
Paleocurrent Data: Current rippled tops
Vector Mean: 328.0 Standard Deviation: 2.00

	Unrotated		Rotated	Current Direction	
	Pitch	CD	Azimuth	1.	2.
1.	07w	nw	236	326	
2.	09w	nw	238	328	
3.	11w	nw	240	330	

Station Number 175.09-179.39 M
MASTER BEDDING Strike: 049 Dip: 45 NW
Paleocurrent Data: Trough axes
Vector Mean: 236.06 Standard Deviation: 21.44

	Unrotated		Rotated	Current Direction	
	Pitch	CD	Azimuth	1.	2.
1.	04w	w	233	233	
2.	67w	w	305	305	
3.	00w	w	229	229	
4.	13w	w	242	242	
5.	07w	sw	236	236	
6.	09w	w	238	238	
7.	28w	s	257	257	
8.	07w	w	236	236	
9.	03e	w	226	226	
10.	08w	w	237	237	
11.	55w	w	284	284	
12.	07w	w	236	236	
13.	09w	w	238	238	
14.	18w	w	247	247	
15.	03e	w	226	226	
16.	14e	w	035	215	
17.	09e	w	040	220	

18.	06e	w	043	223
19.	33e	w	016	196
20.	08w	w	237	237
21.	02e	w	047	227
22.	18e	w	031	211
23.	07w	w	236	236
24.	16w	w	245	245
25.	09w	w	238	238

Station Number 179.39-181.02 M
MASTER BEDDING **Strike: 049** **Dip: 45 NW**
Paleocurrent Data: Trough axis

	Unrotated		Rotated	Current Direction	
	Pitch	CD	Azimuth	1.	2.
1.	10e	w	039	219	0

Station Number 181.17 M
MASTER BEDDING **Strike: 052** **Dip: 47 NW**
Paleocurrent Data: Current-rippled top
Vector Mean: 226.5 **Standard Deviation: 6.36**

	Unrotated		Rotated	Current Direction	
	Pitch	CD	Azimuth	1.	2.
1.	01w	w	231	231	
2.	10e	w	042	222	

Station Number 184.52-185.32 M
MASTER BEDDING **Strike: 052** **Dip: 47 NW**
Paleocurrent Data: Foresets

	Unrotated		Rotated		Current Direction	
	Strike	Dip	Strike	Dip	1.	2.
1.	074-78N-092-35N-002					

Station Number 185.32-186.60 M
MASTER BEDDING **Strike: 052** **Dip: 47 NE**
Paleocurrent Data: Wave-rippled tops
Vector Mean: 312.0 **Standard Deviation: 1.00**

	Unrotated		Rotated	Current Direction	
	Pitch	CD	Azimuth	1.	2.
1.	11e	—	041	131	311
2.	10e	—	042	132	312
3.	09e	—	043	133	313

Station Number 187.73-187.91 M
MASTER BEDDING **Strike: 052** **Dip: 47 NW**
Paleocurrent Data: Symmetrical Megaripples
Vector Mean: 129.5 **Standard Deviation: 3.54**

	Unrotated		Rotated	Current Direction	
	Pitch	CD	Azimuth	1.	2.
1.	15e	—	037	127	307
2.	10e	—	042	132	312

Station Number 191.29-191.51 M

MASTER BEDDING **Strike: 052** **Dip: 47 NW**
Paleocurrent Data: Symmetrical ripples
Vector Mean: 131.0 **Standard Deviation: 1.41**

	Unrotated		Rotated	Current Direction	
	Pitch	CD	Azimuth	1.	2.
1.	10e	—	042	132	312
2.	12e	—	040	130	310

Station Number 200.63-200.84 M
MASTER BEDDING **Strike: 052** **Dip: 47 NW**
Paleocurrent Data: Symmetrical Ripples
Vector Mean: 128.0 **Standard Deviation: 9.17**

	Unrotated		Rotated	Current Direction	
	Pitch	CD	Azimuth	1.	2.
1.	22e	—	030	120	300
2.	16e	—	036	126	306
3.	40e	—	048	138	318

Station Number 201.28-201.40 M
MASTER BEDDING **Strike: 052** **Dip: 47 NW**
Paleocurrent Data: Symmetrical ripple top

	Unrotated		Rotated	Current Direction	
	Pitch	CD	Azimuth	1.	2.
1.	08e	—	044	134	314

Station Number 217.63-218.5 M
MASTER BEDDING **Strike: 060** **Dip: 60 N**
Paleocurrent Data: Symmetrical rippled top
Vector Mean: 168.5 **Standard Deviation: 9.19**

	Unrotated		Rotated	Current Direction	
	Pitch	CD	Azimuth	1.	2.
1.	12w	—	252	162	342
2.	25w	—	265	175	355

Station Number 217.63-218.15 M
MASTER BEDDING **Strike: 060** Dip: 80 N
Paleocurrent Data: Foresets

	Unrotated		Rotated		Current Direction	
	Strike	Dip	Strike	Dip	1.	2.
1.	060	74se	241	26nw	331	

BALCONY FALLS (LOCALITY 10)
PALEOCURRENT ROTATION DATA
ERWIN / ANTIETAM FORMATION

Station Number 105.1-107.65 M
MASTER BEDDING **Strike: 002** **Dip: 29 W**
Paleocurrent Data: Trough axis
Vector Mean: 242.6 **Standard Deviation: 16.23**

	Unrotated		Rotated	Current Direction	
	Pitch	CD	Azimuth	1.	2.
1.	51sw	e-w	231	231	
2.	83sw	e-w	263	263	
3.	72sw	e-w	252	252	
4.	55sw	e-w	235	235	
5.	26sw	e-w	206	206	
6.	58sw	e-w	238	238	
7.	75sw	e-w	255	255	
8.	68sw	e-w	248	248	
9.	74sw	e-w	254	254	
10.	62sw	e-w	242	242	

Station Number 107.65-122.65 M
MASTER BEDDING **Strike: 002** **Dip: 29 W**
Paleocurrent Data: Trough Axis
Vector Mean: 225.0 **Standard Deviation: 12.08**

	Unrotated		Rotated	Current Direction	
	Pitch	CD	Azimuth	1.	2.
1.	39sw	e-w	218	218	
2.	36sw	e-w	215	215	
3.	45sw	e-w	225	225	
4.	62sw	e-w	242	242	

Station Number 229.5 M
MASTER BEDDING **Strike: 043** **Dip: 50 W**
Paleocurrent Data: Large-scale wave ripples
Vector Mean: 138.7 **Standard Deviation: 18.27**

	Unrotated		Rotated	Current Direction	
	Pitch	CD	Azimuth	1.	2.
Set 1					
1.	07ne	—	036	127	307
2.	14ne	—	029	119	299
3.	03ne	—	040	130	310
4.	17ne	—	026	116	296
5.	05ne	—	038	128	308
6.	08w	—	231	141	321
7.	09ne	—	034	142	322
Set 2					
1.	37sw	—	260	170	350
2.	24sw	—	247	157	337
3.	20sw	—	243	153	333
4.	33sw	—	256	166	346
5.	27sw	—	250	160	340
6.	23sw	—	246	156	336
7.	24sw	—	247	157	337
Set 3					
1.	07ne	—	036	126	306
2.	16ne	—	027	117	297
3.	07ne	—	036	127	307

4.	03ne	—	040	130	310
5.	18ne	—	025	115	295

Station Number 238.98-240.25 M
MASTER BEDDING **Strike: 047** **Dip: 52 NW**
Paleocurrent Data: Large-scale wave-ripples
Vector Mean: 81.0

	Unrotated		Rotated	Current Direction	
	Pitch	CD	Azimuth	1.	2.
1.	60e	—	347	077	257
2.	52e	—	355	085	265

Station Number 240.25-240.65 M
MASTER BEDDING **Strike: 047** **Dip: 52 NW**
Paleocurrent Data: Large-scale wave-ripples

	Unrotated		Rotated	Current Direction	
	Pitch	CD	Azimuth	1.	2.
1.	045e	—	002	092	272

BALCONY FALLS RAILROAD QUARRY (LOCALITY 10)
PALEOCURRENT ROTATION DATA
HARPERS / HAMPTON FORMATION
SNOWDEN MEMBER

Station Number 6.43-6.63 M
MASTER BEDDING **Strike: 105** **Dip: 57 NE**
Paleocurrent Data: Foresets

	Unrotated		Rotated		Current Direction	
	Strike	Dip	Strike	Dip	1.	2.
1.	130	e	358	088		

Station Number 6.43-6.63 M
MASTER BEDDING **Strike: 105** **Dip: 57 NE**
Paleocurrent Data: Trough axes
Vector Mean: 183.5

	Unrotated		Rotated	Current Direction	
	Pitch	CD	Azimuth	1.	2.
1.	73sw	n-s	358	178	
2.	84sw	n-s	009	189	

Station Number 9.92-10.28 M
MASTER BEDDING **Strike: 105** **Dip: 57 NE**
Paleocurrent Data: Trough axes
Vector Mean: 59.5

	Unrotated		Rotated	Current Direction	
	Pitch	CD	Azimuth	1.	2.
1.	26sw	w-e	065	065	
2.	15sw	w-e	054	054	

Station Number 45.53-45.85 M
MASTER BEDDING **Strike: 081** **Dip: 58 N**
Paleocurrent Data: Mega-ripple top

	Unrotated		Rotated	Current Direction	
	Pitch	CD	Azimuth	1.	2.
1.	88sw	—	343	072	252

Station Number 48.56-46.95 M
MASTER BEDDING **Strike: 059** **Dip: 43 N**
Paleocurrent Data: Mega-rippled top
Vector Mean: 147.0 **Standard Deviation: 5.00**

	Unrotated		Rotated	Current Direction	
	Pitch	CD	Azimuth	1.	2.
1.	07e	—	052	142	322
2.	02e	—	057	147	327
3.	02w	—	242	152	332

Station Number 49.19-49.22 M

MASTER BEDDING **Strike: 059** **Dip: 43 N**
Paleocurrent Data: Mega-rippled top
Vector Mean: 136.7 **Standard Deviation: 4.73**

	Unrotated		Rotated	Current Direction	
	Pitch	CD	Azimuth	1.	2.
1.	16e	—	043	133	313
2.	14e	—	045	135	315
3.	07e	—	052	142	322

Station Number 49.23-50.13 M
MASTER BEDDING **Strike: 059** **Dip: 43 N**
Paleocurrent Data: Mega-rippled tops
Vector Mean: 163.0 **Standard Deviation: 5.29**

	Unrotated		Rotated	Current Direction	
	Pitch	CD	Azimuth	1.	2.
1.	10w	—	251	161	341
2.	08w	—	249	159	339
3.	18w	—	259	169	349

BALCONY FALLS RAILROAD QUARRY SECTION 2
PALEOCURRENT ROTATION DATA
HARPERS / HAMPTON FORMATION
FACIES ASSOCIATION 2

Station Number 4.91-5.48 M
MASTER BEDDING **Strike: 064** **Dip: 27 NW**
Paleocurrent Data: Mega-rippled top
Vector Mean: 127.0

	Unrotated		Rotated	Current Direction	
	Pitch	CD	Azimuth	1.	2.
1.	26e	—	038	128	308
2.	28e	—	036	126	306

Station Number 6.86-7.92 M
MASTER BEDDING **Strike: 064** **Dip: 27 NW**
Paleocurrent Data: Mega-rippled top
Vector Mean: 147.0

	Unrotated		Rotated	Current Direction	
	Pitch	CD	Azimuth	1.	2.
1.	11e	—	053	143	323
2.	03e	—	061	151	331

VESUVIUS SECTION (LOCALITY 12)
PALEOCURRENT ROTATION DATA
ERWIN / ANTIETAM FORMATION

Station Number 9.09-10.20 M
MASTER BEDDING **Strike: 084** **Dip: 78 N**
Paleocurrent Data: Tabular-planar
Vector Mean: 181.0

	Unrotated		Rotated		Current Direction	
	Strike	Dip	Strike	Dip	1.	2.
1.	075	51nw	082	27s	173	
2.	085	57n	099	21se	189	

Station Number 73.00 M
MASTER BEDDING **Strike: 084** **Dip: 78 N**
Paleocurrent Data: Tabular-planar

	Unrotated		Rotated		Current Direction	
	Strike	Dip	Strike	Dip	1.	2.
1.	074	67n	129	15s	219	

The vita has been removed from the scanned document